Semiactive Friction Connections for Seismic Control of Multi-Storey Buildings

by

Humberto Caudana Quintana

A thesis submitted in partial fulfilment for the
degree of Doctor of Philosophy

in the
Faculty of Engineering
Department of Civil and Structural Engineering

December 2013

Declaration of Authorship

I, Humberto Caudana, declare that this thesis titled "Semiactive Friction Connections for Seismic Control of Multi-Storey Buildings" and the work presented herein are my own. I confirm that:

- This work was done wholly or mainly while in candidature for a research degree at this University.

- Where any part of this thesis has previously been submitted for a degree or any other qualification at this University or any other institution, this has been clearly stated.

- Where I have consulted the published work of others, this is always clearly attributed.

- Where I have quoted from the work of others, the source is always given.

- I have acknowledged all main sources of help.

- Where the thesis is based on work done by myself jointly with others, I have made clear exactly what was done by others and what I have contributed myself.

Signed:

Date: 11/NOV/2013

THE UNIVERSITY OF SHEFFIELD

Abstract

Faculty of Engineering

Department of Civil and Structural Engineering

Doctor of Philosophy

by Humberto Caudana Quintana

This document describes an investigation of the efficiency of friction-based passive and semiactive systems for control of the seismic response of multi-storey buildings, and the mechanisms behind their performance. Passive and semiactive systems are novel strategies used to reduce the seismic demand in structural systems by increasing the energy dissipation capacity and altering the dynamic properties of the building. The investigation is conducted by the means of simulations of the non-linear response of low- and medium-rise frames to a variety of seismic excitations with different frequency content, using a computer program especially designed for this purpose. The efficiency of existing passive and four semiactive control systems, as it was demonstrated by the simulations, is closely related to pre-defined control parameters, which limit their effectiveness.

In order to investigate the possibility of improving the performance of the existing control systems, two new algorithms are also developed in this research, exploring *decentralised* and *partially decentralised* architectures. The novelty of these new algorithms is the use of variable gain factors that determine the required control forces either: (i) based on the relation between the real-time response of the structure and pre-defined values of *target deformation*, which in this investigation are related to the elastic limits of deformation in the frame (*decentralised* system); or (ii) by proportionally determining the control forces into a novel strategy of maintaining a constant inter-storey drift along the height of the building (*partially decentralised* system). The performance of the new control systems on four multi-storey frames is compared to that of existing passive and semiactive systems. The results indicate an improved performance in the two new systems, in comparison to existing strategies, in terms of enhanced adaptability, by not compromising the levels of response reduction, but using lower levels of control forces.

Acknowledgements

Sincere acknowledgement is due to my research supervisor, Dr Mihail Petkovski, whose pertinent advice led me to the achievement of the objectives of this research project.

My deepest gratitude to my parents, brother and sister, because their unconditional support has been my reliable source of encouragement through every situation.

All my gratitude to Nicole, my life partner, who became the additional term for completeness of my life matrix. Her company and support played no passive part on me during this stage.

I sincerely acknowledge Profr T Boothby, from Pennsylvania State University, whose advice helped me to have a different perspective of the academic life.

Contents

List of Figures

List of Tables

Chapter 1

Introduction

1.1   The need of structural control

Seismic design of multi-storey buildings is a field within civil engineering submerged in a constant evolutionary process. On one hand, densely populated urban centres located in earthquake prone areas require buildings with more reliability and higher safety levels. On the other, economical restrictions strain the necessity to optimise resources and craftsmanship.

A current design methodology, which utilises a ductility-based criterion, may not be a unique, optimal solution. Such a design approach takes advantage of the non-linear properties of the structural system. Thus, the structural response is attenuated by allowing dissipation of seismic energy through damage at specific zones of the structure. Although a more efficient use of materials is achieved (resulting in smaller, lighter structures), allowing damage in the structure implies further repairs and additional costs, as well as aesthetic distortion.

Structural control is a possible solution that is currently under broad investigation. Its main advantage is the reduction of the seismic response, which could preclude any structural damage, without the need to modifying the original design of the building.

Control systems can be classified in three types: active, passive and semiactive. Attending each type, the systems allow reduction of the seismic response by counteracting the seismic forces directly, or by dissipating the seismic energy through special mechanisms. As it will be detailed later, there are several advantages and disadvantages associated with each type, but one important aspect is the complexity for practical implementations. Depending on each type, structural control systems may imply the use of advanced

technological resources, including those of other engineering fields like electronics and control.

The seismic response of the building and the damage in the structural elements can be reduced or even avoided by using relatively simple passive control systems. In such systems, the seismic energy is dissipated by using dampers, i.e. devices with special mechanisms designed for that purpose. Passive systems utilising frictional mechanisms have shown high efficiency in some cases, as it was demonstrated by the studies of several researchers (e.g. Aiken et al. 1988; Martinez-Rueda and Elnashai 1995; Pall and Marsh 1982), but the best performance for a given structure and earthquake has been associated with a narrow range of capacities of the passive friction connections.

As a possible solution, semiactive control is an approach in which the capacity (slip-load) of the friction connections (or dampers) can be adjusted in real time during the earthquake. This can be considered as a self-adaptive passive system, with an enhanced performance, without increasing the complexity of application or the resources required.

1.2   Scope of the research

This research is focused on the performance of control systems in which seismic energy is dissipated through hysteretic frictional mechanisms. These friction-based control systems include both passive and semiactive strategies.

The efficiency of passive systems within a broad range of damper capacities and the parameters affecting their performance are within the interests of this investigation. Moreover, the performance of semiactive control systems based on *decentralised* implementations (i.e. systems with local autonomous controllers) is considered in this research.

Development of a computational tool for simulations of the seismic response of a variety of non-linear frame structures under different ground excitations, in order to investigate the efficiency of passive and semiactive control systems, is also within the scope of this study.

1.3   Aim of the research

The aim of the research is to examine the efficiency of existing friction-based passive and semiactive seismic control of multi-storey buildings. Along with this, the mechanisms behind the performance of each system will also be investigated.

The research also aims at developing an efficient and simple friction-based semiactive algorithm, as a possible solution to the limitations of existing semiactive systems.

1.4 Objectives of the research

For the investigation of the efficiency of existing friction-based passive and semiactive control systems, and development of new algorithms, this research has the following objectives:

1.4.1 Objective 1

Assessment of the performance of passive control systems for a broad range of dampers' capacities, aiming at identification of the optimum system, and examination of its mechanism.

1.4.2 Objective 2

Assessment of the performance of a selection of existing decentralised, friction-based, semiactive control systems, including the modulated homogeneous control (Inaudi, 1997), linear and smooth boundary layer controllers (He et al., 2003) and Tri-D control (Chen and Chen, 2004c), and examination of its mechanism.

1.4.3 Objective 3

Development of new semiactive control algorithms, as possible solution to the limitations of passive and existing semiactive controllers, and investigation of their performance.

1.5 Organisation of the thesis

This thesis is organised in 11 chapters and 2 appendices. Definitions of structural control and literature review of friction-based semiactive control systems, including examples of practical applications, description of existing semiactive algorithms and friction-based semiactive devices are presented in Chapter 2. The methodology approached for the fulfilment of the aim and objectives of this research is presented in Chapter 3.

In Chapter 4, a description of the computer program *ConStruc*© for non-linear simulations of seismic response of frame structures with control systems, developed as part of

this research, is presented. The program *ConStruc* was utilised to simulate the response of a set of four multi-storey frames, subjected to the action of six historic ground excitations. Details of those reference structures and the seismic inputs are presented in Chapter 5.

Investigation of existing control systems was also within the scope of this work. The study on the efficiency of friction-based passive control and the mechanisms behind the optimum performance of those systems is presented in Chapter 6, whereas the study on the efficiency of a selection of existing semiactive control algorithms is presented in Chapter 7.

Two new semiactive algorithms were developed as part of this research. The study of the *decentralised* target deformation with variable gain factors (TδVG) algorithm, is presented in Chapter 8. The study corresponding to the second control algorithm, the *partially decentralised*, average deformation with variable gain factors (AδVG) algorithm, is presented in Chapter 9.

In Chapter 10, a summary of results from the simulations of the response of all frames is presented, along with comparisons of performance between passive and semiactive control systems. The general conclusions of this project and recommendations for future research are given in Chapter 11.

Two appendices have also been included in this document. In Appendix A, a user guide of the computer program *ConStruc* is presented. In Appendix B, selected examples for verification of results obtained with *ConStruc* and another popular academic software for non-linear dynamic analysis, Drain-2DX, are presented.

Chapter 2

Literature review of friction-based semiactive control

2.1 Introduction

Structural control, as an alternative approach to reduce the seismic response of buildings, is a relatively new field within civil engineering. However, over the past decades there has been a rapid and broad investigation on control systems, which has led to many practical applications nowadays. Among the outcomes of the research on structural control, there are several semiactive control algorithms, which have been investigated theoretically and/or experimentally.

General definitions of the concept of structural control, along with the findings from a literature review focused on control systems with frictional hysteretic devices, are presented in this Chapter, including existing semiactive algorithms, practical applications and friction-based devices.

2.2 Definition of structural control

Structural control is a concept allowing for the dissipation of seismic energy (exerted in a structure) by means of special mechanical devices. Its principal objective is to reduce the seismic damage and structural demand of the main framing system. Additional objectives include reduction of the structural response due to excessive vibration caused by earthquakes and wind loads (Arfiadi and Hadi, 2000).

In general terms, *structural control is a concept that refers to a secondary system installed within a structure, aiming at improving the structural response by means of mechanical work, without affecting the design resistance of the main structure, but enhancing structural properties, such as stiffness or damping.*

Extensive research on structural control has taken place mainly during the last 30 years (Spencer and Nagarajaiah, 2003), but the idea is much older. The earliest notion of structural control is due to John Milne, who built a house standing on ball bearings in Japan, more than one hundred years ago (Housner et al., 1997). Recent evidence of the concept can be traced back to the 1950s, when an initial concept of seismic-response-controlled structures was proposed (Kobori, 1996). As Kobori defined, "*a seismic-response control means providing the characteristics and/or devices to a structure that are capable of controlling earthquake responses*". The same author proposed five ways to achieve that control, as follows:

- Cut off the energy transmission from the ground motion to the structure.

- Isolate the natural period of the building from the predominant frequency domain of the ground motion.

- Achieve the non-stationary and non-resonant state by providing non-linear characteristics to the system.

- Apply control force such as a mass damper/driver or tendon.

- Utilize an energy absorption mechanism.

Another early definition of the concept of structural control was given by Yao (1972), stating that a structural system with control was such whose behaviour "*varies automatically in accordance with unpredictable variations in the loading as well as environmental conditions and thereby produces desirable responses under all possible loading conditions*".

2.3 Classification of control systems

Control systems consist in the placement of special devices at specific locations of the structure. According to the type of devices and the mechanism used to modify the structural response of the building, control systems can be classified in three major groups (Symans and Constantinou, 1999):

- **Active controllers**, which are effective in a broad range of seismic frequencies, as they adapt to the structural response in real time, by using *feedback* information and control algorithms. However, these systems exert forces into the building, in order to control the response, and their application is limited by large amounts of energy required during the earthquake.

- **Passive controllers** utilise dissipative mechanisms to reduce the response. Special devices for such dissipation get activated using only the motion of the building. The main drawback of passive systems is the lack of adaptability, which limits their efficiency to a narrow range of frequencies.

- **Semiactive controllers** minimise the limitations of passive systems by including mechanical regulators, i.e. implements to modify the capacity of the control devices, such as valves, piezoelectric stacks or electric motors. Similar to passive, semiactive systems are reactive, i.e. they do not require external energy (apart from a battery to operate the regulator), and use the motion of the structure to trigger activation. Similar to active systems, the regulation of devices is based on the structural response feedback and a control algorithm, which improves their adaptability.

2.3.1 Active control systems

Active control systems modify the seismic response by exerting forces directly into the building, counter-acting the seismic action. In active systems, the magnitude of control forces is determined by an algorithm. A computer utilises the feedback information of the structural response and/or feedforward information of the ground motion (collected by sensors). With that information, the control signals are generated and sent to the actuators. An schematic representation of active systems is shown in Fig. 2.1. A *feedback* algorithm is *fed* with information about the structural response, whereas a *feedforward* algorithm utilises information about the excitation. This makes active systems highly adaptable, as they are capable of modifying its properties according to the characteristics of the structural response and/or the seismic excitation.

The control forces are generated through electro-mechanical or electro-hydraulic actuators, i.e. devices with capacity to generate and exert forces into the buildings, such as active tendons or mass dampers. Due to the nature of earthquakes, large amounts of energy are required by the actuators during the ground motion. Active systems may also compromise the stability due to large forces exerted into the building (Housner et al., 1997).
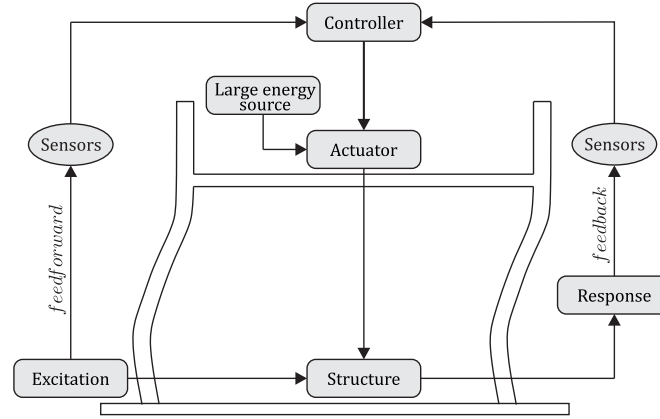
FIGURE 2.1:   Schematic implementation of active control systems (adapted from Symans and Constantinou, 1999).

2.3.2   Passive control

Passive controllers are reactive systems that dissipate seismic energy by means of mechanical work. These systems do not require external power to operate, but are activated using only the motion of the building. However, their reactive nature results in lack of adaptability, limiting their efficiency to a narrow range of frequencies. As it can be observed in Fig. 2.2, passive systems do not require *feedback* or *feedforward* information, thus their performance depends on the characteristics of the ground motion and the structural response at the location of each damper. Different devices based on viscous fluids, viscoelastic materials, mild metallic plates, friction and addition of masses have been used in passive systems. Detailed reviews and descriptions of these devices are out of the scope of this investigation, but can be consulted in several references, e.g. Aiken (1996), Housner et al. (1997), Constantinou et al. (1998), Parulekar and Reddy (2009) and Rai et al. (2009).

Passive devices can be classified as rate-dependent and rate-independent (Symans et al., 2008). The first classification includes those devices whose output force depends on their rate of deformation (e.g. viscous and viscoelastic dampers). The second classification include those dampers whose output force depends on the amount of deformation across them, but without an influence of its rate (e.g. metallic and friction dampers). An advantage of rate-independent devices is their larger hysteretic area, which indicates higher dissipative capacity (Fig. 2.3). This type of hysteretic behaviour, however, makes these devices highly non-linear. A review of rate-independent devices, specifically metallic yield and friction devices, is given by Martinez-Rueda (2002).

The inclusion of passive dampers into the main structure does not compromise its design resistance. It rather enhances the damping capacity and modifies the vibration properties, hence altering the dynamic response. It has been reported that the increase of damping may be in the order of 20% to 30% of critical, which is higher that 1% to 5% due to inherent damping (Pall and Pall, 2004). Since passive systems do not exert any energy into the system, they are considered inherently stable (Housner et al., 1997).
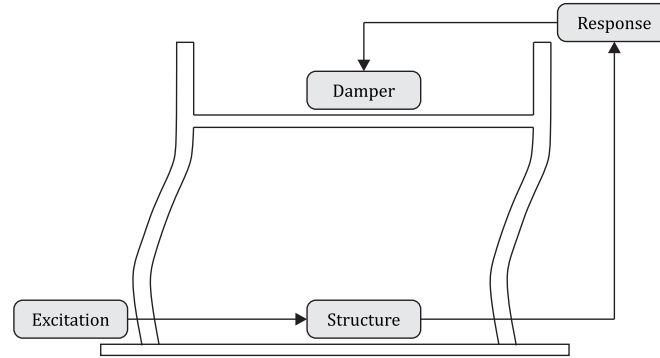
FIGURE 2.2: Schematic implementation of passive control (adapted from Symans and Constantinou, 1999).
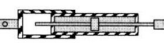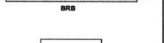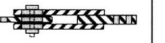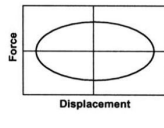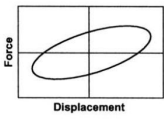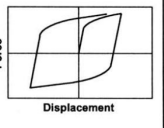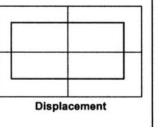
FIGURE 2.3: Characteristics of passive devices (after Symans et al., 2008).

2.3.3 Semiactive control

Semiactive systems combine the simplicity of passive control, but increasing their degree of adaptability. These systems consist of passive devices enhanced with mechanical regulators (e.g. valves, motors, piezoelectric materials) to modify their capacity. Semiactive systems are inherently stable due to their dissipative nature, and cannot destabilise the structure by exerting additional energy, unlike active systems. Also, they can operate

using small amounts of external power, in the order of a few watts or a small battery (Datta, 2003; Spencer and Nagarajaiah, 2003).

Although simpler than active, the implementation of semiactive control is more complicated than passive (Fig. 2.4). A semiactive system requires the use of sensors to acquire *feedback* information and computers to process data and generate control signals. Thus, their performance depends on the control algorithm implemented.
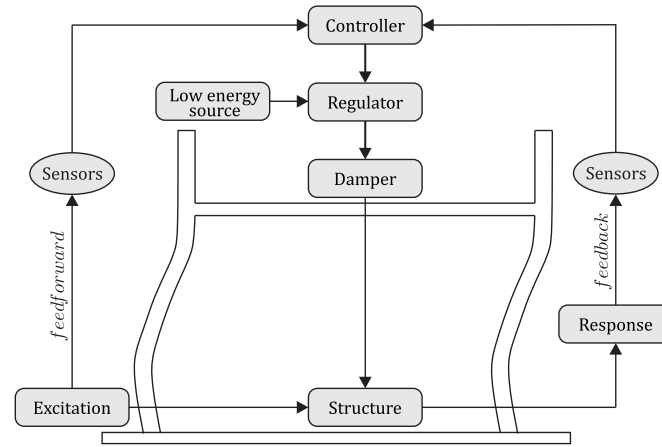
FIGURE 2.4: Schematic implementation of semiactive control systems (adapted from Symans and Constantinou, 1999).

Depending on how they modify the vibrational properties of the main structure, two groups of semiactive systems can be divided in (Datta, 2003):

- *Stiffness control devices*, which modify the stiffness of the main structure, hence modifying the frequency of vibration to avoid resonant conditions. They generally work by locking or unlocking a mechanism within the device, thus switching between braced or unbraced states. An example of this type of devices is the active variable stiffness system, which consists of a cylindrical oil container installed between a set of chevron braces and the beams of the frame. The braces are engaged or released from the main structure by using a regulator valve, which locks or unlocks the flow of the oil within the cylinder (Kobori et al., 1993). Another example is the device invented by Nagarajaiah (2000), which consists of four spring elements arranged in a variable rhombus configuration, adjusted by means of a piston rod controlled by a motor. According to Nagarajaiah, the device modifies continuously the stiffness of the main frame, unlike the active variable stiffness device.

- *Friction control devices*, which also alter the frequency of vibration of the structure by modifying the clamping force in the friction connections, hence increasing or reducing the frictional force required to start slippage (Section 2.6).

2.4 Advantages and disadvantages of control systems

Control systems have been implemented in a number of buildings, and have proven to be efficient. However, there are still some disadvantages that prevent a generalized application to civil structures.

In the case of active control systems, the main disadvantage is the large amount of energy required for operation. Datta (2003) has identified another real-time application issues:

- The idealization of the models, which may not represent accurately the actual structure, thus introducing errors in the control algorithm.

- The time delay in the generation of the control force, which can cause ineffective control and instability.

- The impracticality of installing sensors and controllers at every point of the structure to get *feedback* information. This raises the need for optimisation of the placement of sensors and controllers.

- Uncertainties in the online identification of the characteristics of the system and time-dependent degradation.

- The reliability, which might be debatable due to infrequent operation, maintenance, availability of power source when the earthquake occurs.

- The high cost of the equipment and implementation.

Additionally, Dyke et al. (1995) reported that the interaction between the active system and the structure may also affect the performance of the controller, specially in systems utilising hydraulic actuators, due to secondary vibrations exerted by the actuators into the building.

On the other hand, advantages of passive systems include economy, inherent stability and dissipative capacity even during major earthquakes (Housner et al., 1997). However, the main disadvantage is their lack of adaptability, which may limit their efficiency for

broad range of excitation frequencies. There is some research about the optimal distribution of passive dampers in the structure (e.g. Agrawal and Yang, 1998; Apostolakis and Dargush, 2010; Aydin et al., 2007; Ciampi et al., 1995). However, even in that case, the capacity of the dampers is pre-set to one value. This condition may result in performance variations for different earthquakes. Even for the same excitation, passive systems show a narrow range of dampers' slip-loads with maximum response reductions (Cherry and Filiatrault, 1993; Martinez-Rueda and Elnashai, 1995; Pall and Pall, 2004), hence requiring tuning in order to find the *optimum slip-load*. Passive control may also result in residual deformations, due to the inability of the main structure to produce restoring forces larger than the dampers' slip-load, especially when the structure's stiffness is reduced due to inelastic deformations.

Semiactive systems are a possible solution for the limitations of passive and active systems. Several points leading to enhancement of these systems may be listed as:

- Simplicity, reliability and durability of the control device.

- Simplicity and performance of the control algorithm.

- Avoidance of problems associated with active control, e.g. delays in the control signals or large energy requirements.

2.5 Practical applications of control systems

An exhaustive investigation of control systems installed in actual buildings is out of the scope of this study. Instead, several references can be suggested to the reader, such as Kobori (1996), Housner et al. (1997), Spencer and Nagarajaiah (2003), Symans et al. (2008), Ikeda (2009), and Casciati et al. (2012).

The conceptual and theoretical stage of active structural control saw its first modern full-scale implementation in 1989, when a control system was installed in Japan, in the Kyobashi Seiwa Building (Kobori et al., 1991), a 10-storey, slender, steel structure, likely to have important transverse and torsional demands. The control system consisted of two active mass drivers (AMD) installed at the top floor of the building. One AMD introduced forces counter-acting the transversal movement of the structure, whereas the other counter-acted the torsional moments.

Also in Japan, the first application of a semiactive system was developed in 1990. An active variable stiffness (AVS) system was installed in a test 3-storey steel building with the purpose of avoiding resonance by altering the structural stiffness during the seismic

excitation (Kobori et al., 1993). The control system consisted of a hydraulic device connecting steel braces to the beams. A valve included in the device made it possible to engage or disengage the braces to the beams, hence switching between braced/unbraced frame.

Starting with those two applications, there has been a growing acceptance of control technologies, as demonstrated by the increase from 32 active and 3 semiactive applications in 2001 (Nishitani and Inoue, 2001) to 52 active and 17 semiactive in 2009 (Ikeda, 2009).

In the United States, there has been a considerable amount of research on structural control, but a limited number of active and semiactive applications. Only one semiactive application in the Walnut Creek Bridge on interstate highway I-35, in Oklahoma, was found in the literature (Nagarajaiah et al., 2008; Spencer and Nagarajaiah, 2003; Spencer and Soong, 1999). Reasons that impede the application of control systems are attributed to the conservative character of the construction industry in that country (Spencer and Nagarajaiah, 2003).

In contrast to active and semiactive, there is a wide spread use of passive systems, accounting about 5000 applications worldwide (Martelli and Forni, 2008). The character of such applications is diverse, ranging from retrofitting of historical buildings to inclusion in new constructions and bridges. Detailed reviews of passive control applications can be found in Martelli and Forni (2008); Mazzolani (2001); Symans et al. (2008).

In Mexico, a country with high seismicity, several applications of passive control systems have been documented (Martinez-Romero, 1993; Symans et al., 2008). The iconic Torre Mayor building in Mexico City is a high-rise steel and reinforced concrete structure, with a rate-dependent, viscous fluid-based passive system. In this case, the dampers are installed within diagonal mega-braces across several storeys.

Passive friction dampers have been applied in a variety of buildings, including the 18-storey, steel frame, La Gardenia Towers (Chandra et al., 2000), in India; the 9-storey, dual concrete and steel frame Eaton building in Canada (Pasquin et al., 2002); and several other structures described in Pall and Pall (2004). Slip-load capacities up to 700kN were reached for the Eaton Building. Friction dampers have also been installed in the 3-storey, Monterey County Government Center, in California, with maximum slip-load of 1113kN (Symans et al., 2008).

2.6   Mechanism of a friction-based damper

Two considerations for the use of friction devices are important: (i) the simplicity of the design, and (ii) the durability. Generally, the design of friction dampers is rather simplistic, consisting of steel plates bolted together, where dissipation of energy occurs due to their relative slippage, as shown in Fig. 2.5. Several dampers using this principle have been proposed by Pall and Marsh (1982), FitzGerald et al. (1989), Grigorian et al. (1993), Martinez-Rueda and Elnashai (1995), Cho and Kwon (2004). The second consideration, i.e. durability, is related to the materials used, specially in the frictional interface of the moving plates. Experimental investigations carried out by Pall and Marsh (1982) and Grigorian et al. (1993) showed stability in the hysteretic behaviour when heavy duty brake lining or brass were used.

Accounting to such stability, the mechanical behaviour of friction dampers can be modelled using a Coulomb friction model, as:

$$f_{p,i} = \mu N_i sgn(\dot{\delta}_i(t)) \tag{2.1}$$

where $f_{p,i}$ represents the passive slip-load of the ith damper, μ is the friction coefficient of the sliding interface, and N_i is the clamping force. The direction of the friction force (and motion in the damper) is determined by the sign of the deformation rate across the damper, given by $sgn(\dot{\delta}_i(t))$.

A representation of the mechanical model of passive friction dampers is shown in Fig. 2.6. The force f_p (with the sub-index i removed, for simplicity of notation), is determined with Eq. 2.1. This force represents the slip-load that initiates relative slippage of the connections. The initial stiffness of the damper, k_d, is usually very high, hence slippage
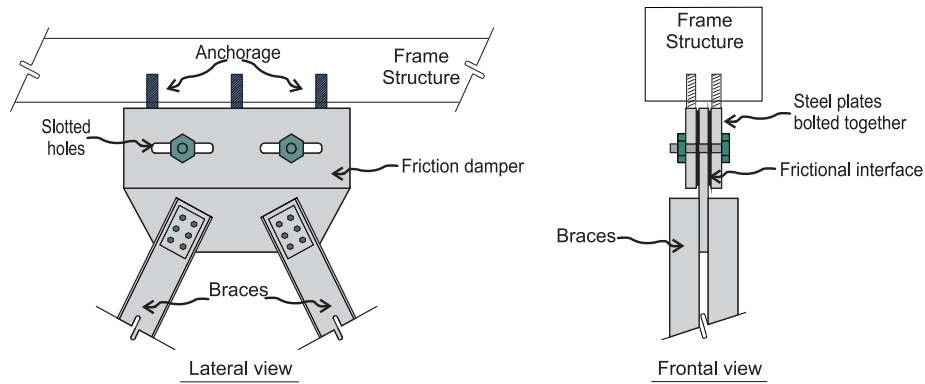
FIGURE 2.5: Schematic view of a friction damper.
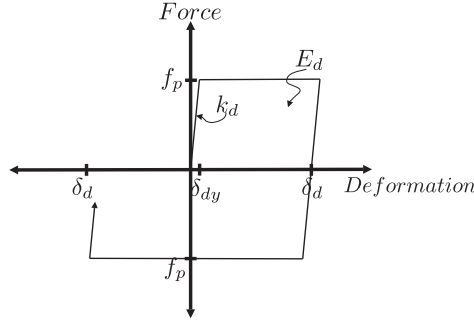
FIGURE 2.6: Mechanical model of passive friction dampers.

occurs at small deformations, $\delta_{d,y}$. Being rate-independent devices, the amount of energy dissipated by friction dampers, E_d, is not related to the velocity across the interface, but rather is given by the product of the frictional force and the amount of deformation. The energy dissipated, then, is represented by the area enclosed in the hysteretic curve of Fig. 2.6.

When a friction damper is installed within a structure, the stiffness of the system structure-damper increases as a result of the combination of the higher stiffness of the friction connection, k_d, and the stiffness of the storey where the damper is installed, k_f. This is illustrated in Fig. 2.7, where $k_d >> k_f$ and F_v represents the inter-storey shear force. In general, F_v increases as a result of higher stiffness in the system, given by $k_d + k_f$ (Fig. 2.7a). However, for combinations where $f_p < f_y$ and $\delta < \delta_{fy}$, it is also possible a reduction of the shear force (Fig. 2.7b). Here, f_y and δ_{fy} represent the yield strength and yield deformation of the structure, respectively.

a) Slip-load > Frame's yield load   b) Slip-load < Frame's yield load
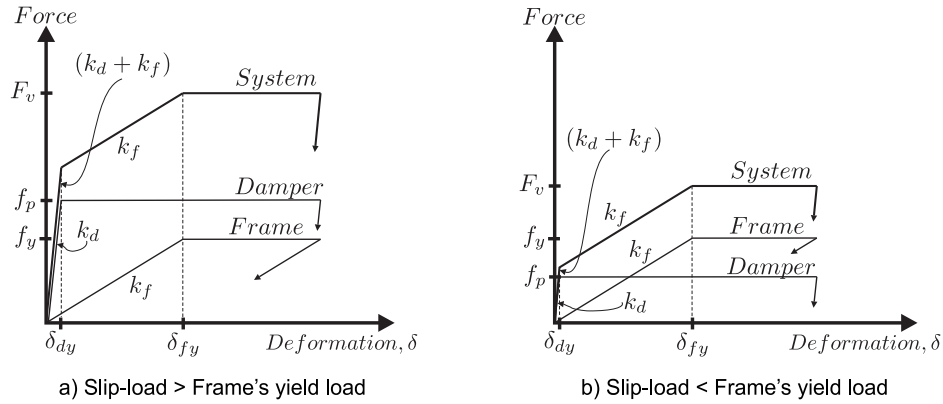
FIGURE 2.7: Structure-damper combined stiffness model.

Although passive friction dampers have proved to be effective, both analytically and experimentally (e.g. Aiken, 1996; Cherry and Filiatrault, 1993; Filiatrault and Cherry,

1987; Rao et al., 1995), there are still some issues of concern. Passive friction dampers have pre-set capacities which limit their application. This characteristic makes them optimum for certain excitations but less efficient for wider frequency ranges, due to higher or lower inter-story forces in the main structure. This may lead to structural behaviour comparable to either bare frame (activation during the whole excitation) or braced frame (lack of activation), for which additional cost generated by the dampers is not justified. Some authors have indicated that optimum reductions are achieved for a small range of slip loads, outside of which the structural response increases (Pall and Pall, 2004).

The main feature of semiactive friction dampers is their adaptability. They are able to modify the slip-loads in real time, according to the signal of the control algorithm implemented. Generally, the clamping force is variable in time as a function of response *feedback*. Considering this variation of the slip-load, Eq. 2.1 may be modified as:

$$f_{s,i}(t) = \mu N_i(u) sgn(\dot{\delta}_i(t)) \qquad (2.2)$$

In Eq. 2.2, the control force $f_{s,i}(t)$ of the i*th* damper varies in time. Its value depends on the likewise variable clamping force $N_i(u)$, which is a function of the response parameter u (e.g. displacement, velocity and so on).

2.7 Algorithms for friction-based semiactive control

2.7.1 Architectures of control

Control systems can be installed using different architectures, i.e. the network of communication between sensors and computers. Thus, control systems can be *centralised* or *decentralised* (Casciati et al., 2006).

The term *centralisation* refers to those systems in which the control signals are generated by one central computer. This central controller determines control signals based on the global *feedback* from all sensors, and sends it to the control devices. A *centralised* system (Fig. 2.8a) requires *a priori* information, i.e. definition of the characteristics of the controlled structure, and *a posteriori* information, i.e. the state of the system (Lynch and Law, 2002).

In a *decentralised* system, a number of local computers generate control signals using only *a posteriori* local information provided by local sensors. Due to the large-scale, non-linear nature of civil structures, *decentralised* systems are advantageous as smaller

quantities of information can be processed by each local controller in parallel. This may lead to reductions in the transmission and computational costs, as well as increases in the reliability of the controller (Casciati et al., 2012).

Decentralisation can be total or partial (Lynch and Law, 2002). In a (*totally*) *decentralised* system (Fig. 2.8b), the local controllers do not exchange any information, whereas in a *partially decentralised* system (Fig. 2.8c), there is a transference of information between local computers, ensuring a partial knowledge of how the local control is affecting the overall response of the building.

In this investigation, emphasis is put on the simplicity of the control systems. Features of simple systems imply *decentralisation* and determination of control forces based on a few physical parameters (e.g. deformation or velocity). Systems with such characteristics are those proposed by Inaudi (1997), He et al. (2003) and Chen and Chen (2004c).

2.7.2 Modulated homogeneous friction control

The modulated homogeneous friction (MHF) control algorithm was developed by Inaudi (1997). In this (*totally*) *decentralised* algorithm, the dampers' slip-loads were adjusted
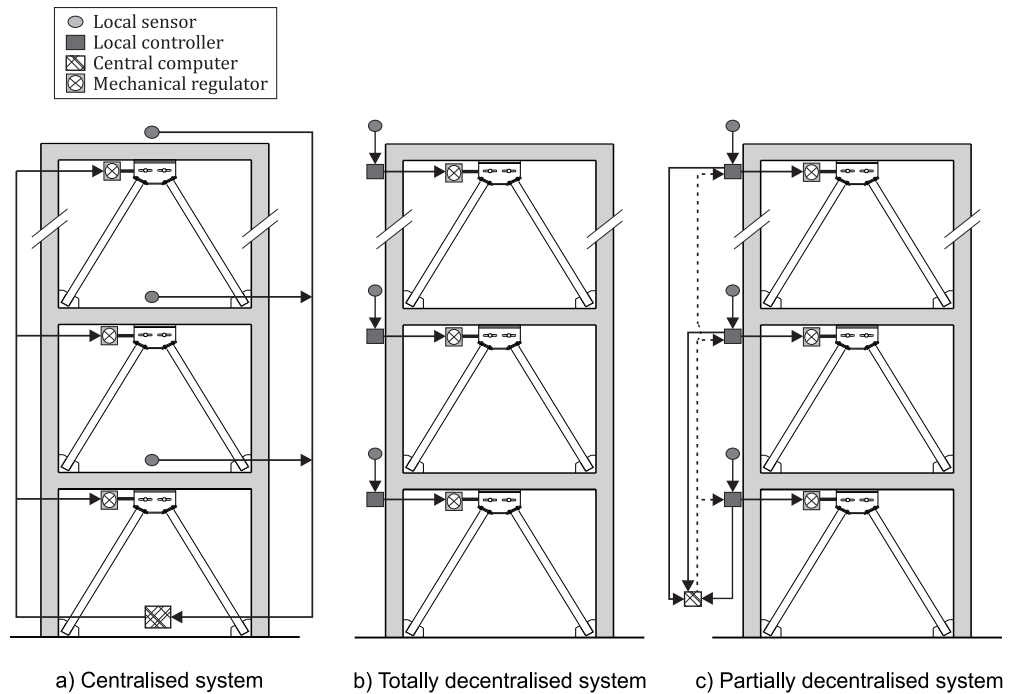
FIGURE 2.8: Different architectures of control.

based on the local *feedback* of deformation, and their magnitude was proportional to the deformation's prior local peak (or trough).

In the MHF algorithm, the control force $f_{s,i}(t)$ of the damper i was given by:

$$
\begin{aligned}
f_{s,i}(t) = g_i \mu |P[\delta_i(t)]| sgn(\dot{\delta}_i(t)) &\qquad \text{if } \dot{\delta}_i(t) \neq 0, \\
-g_i \mu |P[\delta_i(t)]| \leq f_{s,i}(t) \leq g\mu|P[\delta(t)]| &\quad \text{if } \dot{\delta}(t) = 0
\end{aligned}
\tag{2.3}
$$

where g_i is a pre-defined, constant gain factor (with units of stiffness), and $P[\delta_i(t)]$ is an operator that made the control force proportional to the "prior-local-peak" of deformation. For each damper i, this operator was defined as:

$$
P[\delta_i(t)] = \delta_i(t-s) \quad \text{where } s = \left\{ \min x \geq 0 : \frac{d\delta}{dt}(t-x) = 0 \right\}
\tag{2.4}
$$

Since the MHF control required adjustment of slip-load at every local peak (or trough), the original controller of Eq. 2.3 can be expressed as:

$$
f_{s,i}(t) = g_i \mu |P[\delta_i(t)]| sgn(\dot{\delta}_i(t))
\tag{2.5}
$$

where:

$$
P[\delta_i(t)] = \begin{cases} \delta_i(t) & \text{if } \dot{\delta}_i(t) = 0, \\ \delta_i(t-s) & \text{if } \dot{\delta}(t) \neq 0 \end{cases}
\tag{2.6}
$$

where s represents the time of occurrence of the prior-local-peak, (i.e. zero velocity, as in Eq. 2.4).

The possibility of a null force determined by using the sign of the velocity at the instant of peak (or trough) deformation (i.e. $sgn(\dot{\delta}_i(t)) = 0$), is eliminated in a digital implementation, such as the one used in this investigation. The occurrence of peak deformations is determined by comparing the signs of the velocity at consecutive time steps. Whenever there is change in the sign, the value of the peak deformation is acquired by the controller and the sign of the current velocity is used to determine the direction of the motion.

2.7.3   Linear and smooth boundary layer control

According to He et al. (2003), the MHF algorithm had some limitations: continuous slippage in the friction dampers was not guaranteed, resulting in locking of the device, and amounts of energy dissipation were not maximised. Also, since the slip-loads were proportional only to the extremes (peaks and troughs) of deformation, the transition between sticky (locking) and sliding (activation) phases in the friction connections would generate spikes in the acceleration response.

As a solution, He et al. (2003) proposed the use of boundary layers related to the velocity across the dampers, i.e. close to the time of extremes of deformation, when the slip-load was adjusted. The authors proposed two *decentralised* algorithms using different boundary layers.

The first control algorithm, referred to as the linear boundary layer (LBL) semiactive friction control, utilised a pre-defined linear layer in the vicinity of zero velocity. The control force in the damper i was determined as:

$$f_{s,i}(t) = \begin{cases} g_i\mu|P[\delta_i(t)]|sgn(\dot{\delta}_i(t)) & \text{if } |\dot{\delta}_i(t)| > \lambda_{a,i}, \\ g_i\mu|P[\delta_i(t)]|\left(\dfrac{|\dot{\delta}_i(t)|}{\lambda_{a,i}}\right)sgn(\dot{\delta}_i(t)), & \text{if } |\dot{\delta}_i(t)| \leq \lambda_{a,i}, \end{cases} \tag{2.7}$$

where the term $\lambda_{a,i}$ represents the *thickness* of the linear boundary layer in the vicinity of zero velocity. According to He et al., a drawback of the LBL algorithm was its sensitivity to the *thickness* of the boundary layer for a particular earthquake.

The second control algorithm was referred to as smooth boundary layer (SBL) control, with the control force of the damper i given as:

$$f_{s,i}(t) = g_i\mu|P[\delta_i(t)]|tanh(\lambda_{b,i}\,\dot{\delta}_i(t)). \tag{2.8}$$

where the boundary layer was determined by:

$$tanh(\lambda_{b,i}\,\dot{\delta}_i(t)) \tag{2.9}$$

and the parameter $\lambda_{b,i}$ represents the *thickness* of the smooth boundary layer. According to the authors, this smooth boundary layer alleviated the sensitivity of the LBL algorithm.

2.7.4 Tri-D control algorithm

Another *decentralised* friction-based control system, reportedly including viscous and Reid damping, was developed by Chen and Chen (2001, 2000). In the algorithm, the control force in the damper i was determined by:

$$
f_{s,i}(t) = \begin{cases} \mu g \dot{\delta}_i(t) + \mu e \delta_i(t), & \text{if } \delta_i \dot{\delta}_i > 0, \\ \mu g \dot{\delta}_i(t) - \mu e \delta_i(t), & \text{if } \delta_i \dot{\delta}_i < 0, \\ -\mu e |\delta_i(t)| \le f_{s,i}(t) \le \mu e |\delta_i(t)|, & \text{if } \delta_i = 0 \end{cases} \tag{2.10}
$$

where e and g are pre-defined, constant gain factors, and $\delta_i(t)$ and $\dot{\delta}_i(t)$ are the local deformation and its rate, respectively. According to the authors, by using this algorithm the rectangular hysteretic curve of the friction damper (Fig. 2.6 on page 15) changes for one of the shape shown in Fig. 2.9c, due to the inclusion of the elliptic viscous damping (Fig. 2.9a) and triangular Reid damping (Fig. 2.9b).

Later on, Chen and Chen (2004c) proposed a simplified algorithm to account for small amplitudes of motion passively. The so-called Tri-D algorithm included a pre-defined clamping force $N_{p,i}$, and the control force in the damper i was adjusted only when such force was surpassed, as:

$$
f_{s,i}(t) = \begin{cases} \mu N_{p,i}\, sgn(\dot{\delta}_i(t)), & \text{if } e|\delta_i(t)| + g|\dot{\delta}_i(t)| \le N_{p,i}, \\ \mu \left(e|\delta_i(t)| + g|\dot{\delta}_i(t)| \right) sgn(\dot{\delta}_i(t)), & \text{if } e|\delta_i(t)| + g|\dot{\delta}_i(t)| > N_{p,i} \end{cases} \tag{2.11}
$$

thus, for small displacements, the system acted passively, whereas if the motion increased, the semiactive phase was activated. In their study, the authors reported an optimum relation of the gain factors e and g similar to the circular frequency of the structure, f_f, such that $e = 2\pi f_f g$.
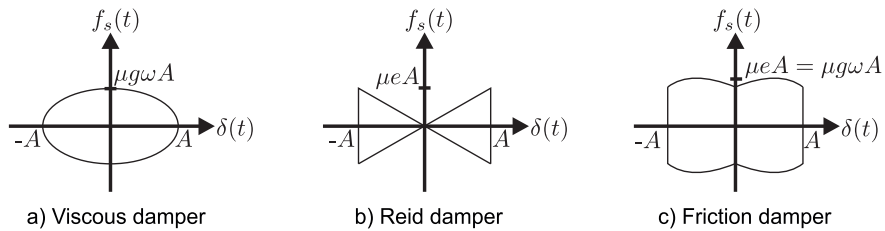
FIGURE 2.9: Hysteretic behaviour of dampers with Tri-D control (after Chen and Chen, 2000).

2.7.5 Other semiactive control algorithms

Bang-Bang control of slip bracing device

Early in the 1990s, Akbay and Aktan (1990) and Kannan et al. (1995) proposed a semiactive algorithm to modify the slip-load of a so-called "active slip bracing device (ASBD)". The control algorithm, based on Bang-Bang control, consisted in increasing or reducing the clamping force in fixed increments, at fixed time intervals, aiming at reversing the stationary (locking) or sliding status of the ASBD. In order to do this, the controller monitored the status of the damper and determined two possible actions: (i) increase the force when deformation and velocity acted in the same direction (i.e. sliding), or (ii) reduce the force if they acted in opposite directions (i.e. locking).

The ASBD was tested analytically by simulating the response of a 6-storey shear building, subjected to an impulsive and a harmonic base excitations (Akbay and Aktan, 1990). In both cases, when compared to slip-braces with constant slip-loads, the response of the ASBD was smaller. In the case of the impulsive loading, the top floor displacement with the semiactive control was approximately 50% smaller. In the case of harmonic loading with varying amplitude, the ASBD demonstrated changes in the system's stiffness for smaller levels of deformations, which was attributed to the earlier activation of the semiactive connections.

Xu et al. (2001) also applied this algorithm to reduce the response of a truss tower including piezoelectric friction dampers. The authors showed that the performance of the algorithm depends on the size of the fixed force increment (for one single value of time step that they used). In their study, maximum reductions of deformation of about 46% were achieved using the largest fixed increment. However, they also showed that for increments larger than a certain value (approximately 0.01% of the maximum axial force acting on the corresponding truss element), there was no significant improvement.

Off-On friction damper and centralised friction damper control

Dowdell and Cherry (1996) developed two semiactive controllers: a *decentralised* "Off-On" friction damper and a *centralised* "semiactive friction damper".

The "Off-On" algorithm used the local feedback of the velocity. In the algorithm, the control force was modified from a pre-set value ("On" state) to a near-zero value ("Off" state), every time there was an extreme of deformation, i.e. unloading at zero velocity. After this brief moment of zero velocity, the control force was again modified to its "On"

state. One possible drawback of this controller are the spikes in acceleration, likely to occur due to abrupt variations of the slip-load.

The second controller, referred to as continuously variable "semiactive friction damper", required *feedback* from the entire structure to construct a state vector of deformations and their rate, which indicates a *centralisation* of the algorithm. Once the state vector of the structure was constructed, at every sampling time, the control forces were proportional to pre-defined, constant gain factors.

Constant ductility factor algorithm

Nishitani et al. (2003) proposed a decentralised algorithm in which, according to the authors, the damper maintained a constant ductility factor of two, regardless of the level of seismic excitation. The dissipation of energy would be maximised by using this factor, as it was showed previously by Tajimi (1965), for structures subjected to steady-state sinusoidal excitations.

In the control algorithm, the dampers' slip-loads were adjusted based on the feedback of local drift velocity. According to Nishitani et al. (2003) and Nishitani et al. (2000), by making the damper slip at the time of maximum velocity (i.e. the time when the reversal deformation crossed the origin, or zero deformation, for sinusoidal excitations), a ductility factor close to two was guaranteed, even for non-sinusoidal excitations, such as earthquakes.

The authors simulated the response of a high-rise (20-storey) building using the proposed algorithm, with different distributions of the dampers along the height of the structure. From the results, the system with dampers at every storey was more efficient in reducing inter-storey deformation, according to the authors. The system was not very efficient in reducing the accelerations.

Non-sticking friction control

The so-called non-sticking friction (NSF) control was proposed by Ng and Xu (2007). This *decentralised* control algorithm was based on the smooth layer $tanh(\lambda_{b,i}\dot{\delta}_i(t))$ previously proposed by He et al. (2003). One advantage of the NSF algorithm is that the variable control force was limited by a maximum, pre-defined clamping force (setting realistic control forces), as: $N_{max,i}tanh(\lambda_{b,i}\dot{\delta}_i(t))$, in which $N_{max,i}$ represented the maximum clamping force capacity of the ith friction damper. The rationale behind the controller was to achieve realistic maximum control forces, whilst allowing the damper to slip back. However, possible limitations of this algorithm are: (i) the control force

was adjusted using only the local velocity as *feedback*, which, depending on the value of the parameter $\lambda_{b,i}$ and the ground excitation, may lead to behaviours similar to "on-off" controllers due to rapid variations between low and high slip-loads, and also saturating the friction damper to its maximum capacity. Nonetheless, another clear advantage of this algorithm is a potential continuous slippage in the connections.

The efficiency of the NSF algorithm was investigated analytically by applying it to a 20-storey benchmark building with an attached 3-storey podium, subjected to different earthquakes (El Centro, Hachinohe, Northridge and Kobe). In the simulations, the authors used different levels of $N_{max,i}$ and $\lambda_{b,i}$. From their results, the authors noted efficiency in reducing the norm inter-storey deformation and norm acceleration, in average, with little influence of the parameter $\lambda_{b,i}$, for either building. The response reductions, on the other hand, varied significantly with the value of $N_{max,i}$. Higher capacities of the clamping force leaded to better levels of deformation reduction but slightly increased accelerations, in the case of the high-rise building, and lower accelerations but slightly increased deformations, in the case of the podium structure.

Lin et al. (2010, 2012) tested the controller experimentally, by applying it to control a tuned mass damper installed in a single-DOF structure subject to the action of different earthquakes, including Mexico 1985, Hachinohe 1968, El Centro 1940 and Kobe 1995, scaled to different peak ground accelerations. From the results, those authors concluded that the system is efficient in reducing both the displacement and the norm acceleration.

2.8 Performance of MHF, LBL, SBL and Tri-D controllers

The MHF, LBL, SBL and Tri-D algorithms seem convenient for implementation on frame structures, since the magnitude of control forces depends on the structural response (inter-storey deformation and/or velocity, in this case). Therefore, these four controllers are selected for further investigation in this study.

Inaudi (1997) applied the MHF algorithm to control the simulated seismic response of a steel moment resistant frame. The structure comprised 6-storeys, 6-bays, and was lightly damped, with damping ratios of 0.5%. In the simulations, only the ground excitation of the El Centro 1940 earthquake (PGA=0.35g), with a predominant frequency similar to the frame's fundamental frequency (i.e. 0.67Hz), was used. Two gains of 98.1kN/cm and 490kN/cm were used in the algorithm. The response reductions depended on the gain factor, but better levels of reductions were achieved by using the higher gain. In the case of the top floor displacement, the controller with lower gain resulted in approximately 20% of reduction, in comparison to the bare frame ($d_{top} = 20$cm), whereas the reduction

achieved by the system with higher gain was approximately 35%. In the case of the first floor deformations, the system using lower gain produced 40% reduction, in comparison to the bare frame (with $\delta = 5.24$cm), whereas the system with higher gain achieved 48%. However, the performance of the algorithm should also consider the level of control forces. For these two gain factors, there was an increase of almost 4 times (i.e. 49.9kN vs 194.7kN) in the maximum control force when the higher gain was used, in comparison to the low gain factor.

Jansen and Dyke (2000) applied the MHF algorithm to control the forces of magneto-rheological (MR) dampers installed in a simulated, small-scale 6-storey building. To adapt the controller from frictional forces to MR forces (which depend on the velocity), the product $\mu g_i |P[\delta_i(t)]|$ in Eq. 2.3 was substituted with a factor $g_{n,i} |P[\delta_i(t)]|$, hence allowing the damper to develop the same magnitude of forces than the frictional counterpart. The simulated frame represented a laboratory scale-model with total height of 1.80m and weight of 1.34kN. In the simulations, the frame was subject to the action of the El Centro 1940 earthquake, scaled to 10% of its full-scale amplitude, and one single gain $g_{n,i} = 0.47$kN/cm was used in the algorithm. From the results, the MHF control produced reductions of 58% and 44% of the bare frame's peak displacement ($d_b = 1.31$cm) and drift ($\delta_b = 0.0098$), respectively. However, the algorithm resulted in a slight increase of 6% in the bare frame's peak acceleration ($a_b = 146.95$cm/s^2). The maximum control force required by the controller was 2.38kN, corresponding to 1.78% of the weight of the building.

He et al. (2003) numerically tested the LBL and SBL controllers on a base isolation system and a supplemental energy dissipation system. The isolation system was installed in a 5-storey frame subjected to a series of ground excitations, including resonant sinusoidal waves and the El Centro 1940 earthquake (0.35g). Gain factors of 3, 6 and 9kN/cm and a layer $\lambda_{a,i} = 10$cm/s were used in the LBL when the sinusoidal excitations were exerted. In the case of the SBL, the same three gains were used, along with a smooth layer $\lambda_{b,i} = 10$. According to those authors, the LBL and SBL systems under the sinusoidal excitations showed better levels of response reduction (normalised rubber drift and acceleration) than those of a passive system. Under the El Centro excitation, layers $\lambda_{a,i} = 20$cm/s and $\lambda_{b,i} = 5$ and 50 were used, respectively. The smaller layer $\lambda_{b,i} = 5$ produced a smoother variation of the slip-load, hence avoiding higher acceleration spikes. This is indicated by the control law of Eq. 2.7, which also suggest that tuning of the layer is required, as discontinuity may be produced when $\lambda_{a,i}$ is too small (LBL algorithm) or $\lambda_{b,i}$ is too high (SBL algorithm). The efficiency of the controllers was also investigated by those authors for a set of earthquakes (El Centro, Kobe, Takatori, Northridge and Chi-Chi). In these simulations, a gain factor of $g_i = 12$kN/cm,

$\lambda_{a,i} = 10$cm/s and $\lambda_{b,i} = 20$ were used in the algorithms. From the results, the maximum response of the bare frame with fixed base, for any of the earthquakes, was caused by Takatori (0.65g), with maximum inter-storey drift and acceleration of 2.28cm and 3.5g, respectively. For this frame, the LBL and SBL performed comparatively well, achieving reductions of 85%, for the drift. In the case of the maximum acceleration, the LBL resulted in slightly better reductions of 81% versus 79% of the SBL. This denotes sensitivity of the controllers to the layer parameter. In the case of friction-based passive system, the reductions were 82% and 85% (for maximum drift and acceleration, respectively). However, the control forces required by the semiactive algorithms were more than 5 times higher than those of the passive system (79kN vs 14kN). The same authors applied both semiactive algorithms to a 3-storey, single bay frame, including one damper in each storey. The frame was subjected to the same set of earthquakes than the base-isolated building. The LBL algorithm was used with gain of 200kN/cm and $\lambda_{a,i} = 20$cm/s, and the SBL with gain of 400kN/cm and $\lambda_{a,i} = 2.2$. According to those authors, the bare frame's maximum inter-storey deformation ($\delta_b = 11.6$cm) and acceleration ($a_b = 5.17$g) were caused by Chi-Chi earthquake (1.01g). The introduction of the LBL and SBL resulted in smaller levels of drift (1.26cm and 1.33cm, respectively) and acceleration (1.10g and 1.12g, respectively).

The SBL algorithm was applied to a building complex by Ng and Xu (2007). The complex consisted on a 20-storey main building with a 3-storey podium attached, and was subjected to a set of earthquakes (El Centro, Hachinohe, Northridge and Kobe). The control system was applied by installing different deployments of dampers: damper in third storey, and dampers in second and third storeys. The algorithm was examined using three values of the gain factors, determined as 10, 20 and 30 times the average weight of the building, and three values of the layer $\lambda_{b,i}$, as 5, 10 and 15. According to the authors, there was no difference in results by using either damper configuration. From the results, there was an influence of the gain factor in the performance of the controller, with smaller levels of response for higher values of the gain (maximum reductions of average norm drift around 60% and 65% for average norm acceleration, for the low-rise frame, and 50% and 30%, respectively, for the high-rise building). On the other hand, the layer $\lambda_{b,i}$ showed less influence in the response, most notably for the high-rise building, but without a significant effect (i.e. differences of around 10%). The efficiency of the systems also varied from earthquake to earthquake. For the main building, there were reductions of 30% in the peak drift for El Centro and Hachinohe excitations, but for Northridge and Kobe, the reductions were only 3% and 17%, respectively. Furthermore, in the case of the peak acceleration, the controller was less efficient, producing reductions of only 8% and 1% for El Centro and Hachinohe, respectively, and even increasing the acceleration for Northridge and Kobe (30% and 3%, respectively).

Ng and Xu (2007) also applied the Tri-D control (without including any pre-defined, initial passive load) to the same building complex. Two different gains e determined as 5 and 10 times the average weight of the building were used in the simulations. Similar to the SBL algorithm, there was a significant reduction of norm drift and acceleration for both frames (approximately 50% and 22%, respectively, for the high-rise building, and 60% and 65%, respectively, for the low-rise frame), with no significant differences by using the low or high gains. Again, the algorithm was more efficient for the El Centro and Hachinohe earthquakes, with reductions of peak drift of 31% and 28%, respectively, and 8% and 2% reduction of peak accelerations. For the Northridge and Kobe excitations, drift reductions were only 14% and 16%, respectively, but peak accelerations increased 37% and 6%, for each earthquake.

Chen and Chen (2004a) performed numerical simulations of an 1/4 scale structure, applying the MHF and Tri-D algorithms. The frame had 3-storeys and one single bay, with one friction damper in the first storey only. A set of far-field (El Centro and Taft) and near-fault (Northridge and Kobe) earthquakes with scaled peak ground accelerations of up to 0.191g were used in the numerical simulations. For both types of excitations, the two algorithms showed comparable levels of peak drift, acceleration and control force for most of the earthquakes. In average, however, the Tri-D algorithm resulted in better levels of peak drift ratio (0.399 vs 0.416), for almost the same levels of peak acceleration (58.4cm/s^2) and control forces. In that study, the response of the structure appears to be very small, in the order of 3.5mm for the first storey, which is likely to be due to elastic deformations of the structural components.

The same 1/4 scale structure was experimentally tested by Chen and Chen (2004b), using the Tri-D algorithm. In the experiments, one stack actuator with a pre-load of 1.78kN required 1000V to produce a friction force of about 3kN. Four stack actuators were included in the damper, hence it was suitable to produce a force of about 12kN. The same set of earthquakes was applied, scaling the time to create resonant conditions. The results demonstrated the efficiency of reducing the seismic response, although similarly to the numerical simulations, the controlled deformations were very small, in the order of 10mm or less, and it is not clear if there was slippage in the damper or it only accounted for elastic deformations of the components.

Chen and Chen (2004c) investigated the efficiency of the Tri-D algorithm to control the seismic response of a 20-storey benchmark steel building proposed by Ohtori et al. (2004), and utilised the near-fault and far-field excitations described therein. In the investigation, 80 dampers were distributed throughout the building, such that some levels included dampers and other levels did not. The bottom storey accounted for the maximum number of devices, with 26, whereas 9 were installed at the top floor.

According to Chen and Chen, the semiactive strategy is more efficient than a passive control in terms of response reduction (specially peak acceleration) and control force required. However, their results suggest only slight improvements of the semiactive control in reducing the peak deformation for the majority of the excitations, apart from El Centro excitation (which requires control power of about 2kW). Furthermore, according to those results, drift reductions were achieved only in the upper levels (17 to 20), under Kobe excitation.

2.9 Summary and conclusion on decentralised controllers

Several algorithms existing in the literature were examined. In general, the following conclusions can be made:

- *Decentralised* systems allow for simpler control algorithms, with associated avoidance of control delays, lower costs and reliability in case of failure of one local controller.

- In general, the *decentralised* controllers existing in the literature use pre-defined, constant gain factors.

- The control forces (and, inherently, the response reductions) are proportional to the gain factors.

- The inclusion of the velocity term has been reported as adequate to reduce the control forces at the moment of motion reversal, hence avoiding locking of the friction connections.

From the literature review, a variety of structures and parameters have been used to investigate the performance of *decentralised* algorithms (MHF, LBL, SBL and Tri-D), as summarised in Table 2.1. It was noticed that each report concluded on the efficiency of the corresponding algorithm, but in many cases there was no uniform evaluation criteria. Furthermore, the algorithms were applied to different structures using different control parameters, distribution of dampers along the height of the buildings and ground excitations. Only in a few cases the performance of the algorithms was compared.

The structures to which the selected control algorithms have been applied are, mainly, low-rise structures, with two cases of high-rise buildings. There was no exhaustive investigation of frame models representative of large-scale building, including low-rise and medium-rise.

TABLE 2.1: Summary of application of decentralised controllers.

Structure	Algorithm	Earthquakes
6-storey, 6-bay	MHF	El Centro (0.35g)
6-storey, 1-bay (small-scale)	MHF	El Centro (0.03g)
5-storey, 1-bay (base-isolated) 3-storey, 1-bay	LBL & SBL	El Centro, Kobe, Takatori, Northridge, Chi-Chi (up to 1.01g)
20-storey 3-storey	SBL & Tri-D	El Centro, Hachinohe, Northridge, Kobe (up to 0.82g)
3-storey, 1-bay (1/4 scale)	MHF & Tri-D	El Centro, Taft, Northridge, Kobe (up to 0.191g)

2.10 Friction-based devices

The materials and mechanisms used in semiactive dampers are different, ranging from magneto- and electro-rheological devices, viscous fluid-based devices, variable stiffness devices, friction devices and shape memory alloys (Casciati et al., 2006; Cheng et al., 2008; Datta, 2003). Friction-based devices are advantageous due to its relative simplicity, economy and long durability. Different mechanisms have been proposed to adjust the damper's slip-load.

Xu and Ng (2008) experimented on a laboratory-scale building complex using piezo-electric actuators to control the normal force in the damper. This piezo-driven variable friction damper (PVFD), was integrated by a steel housing with attached friction pads and a piezoelectric actuator, which adjusted the clamping force. The dissipative mechanism consisted in longitudinal slippage of a plate of steel collocated between the pads. The slip-load capacity of this damper ranged between 5 and 340N at input voltage of 0 to 150V, respectively.

Another device was developed by He et al. (2003), in which the clamping forces were regulated through an electromagnetic field. The device consisted of solenoids located at the external sides of metallic plates slotted-bolted together, with frictional pads in between them. A regulated electrical current across the solenoids generated a magnetic field, thus letting adjustment of the normal force.

Another semiactive friction damper was developed by Unsal et al. (2003). This damper was integrated by a fixed circular shaft to which a flex-tensional mechanical amplifier was mounted. For regulation of the normal force, the mechanical amplifier consisted of a piezoelectric stack whose longitudinal expansion allowed for normal deformation of the amplifier's stainless steel housing, and a shape memory alloy preload wire was incorporated for bidirectional motion. Two frictional pads were placed in outer plates

of the amplifier to provide a frictional surface. The moving components of the damper consist of the outer housing (in contact with the amplifier's outer plates) and the air bearing. This device was tested experimentally by exerting harmonic excitations through a shaker, developing maximum friction forces of 85N when 150 V were applied to the piezoelectric actuator.

For enhancement of truss towers, Xu et al. (2001) developed a device consisting of an inner frame with low transversal stiffness to allow deformation in that direction. The inner frame was installed within an outer circular tube of larger transversal stiffness. In the interface between the inner frame and the outer tube, a friction layer was collocated. To produce transversal deformation in the inner frame, columns of piezoelectric material were installed transversely, together with the sensor.

In the early 1990s, an actively regulated friction slip brace was proposed and tested as an alternative to passive slip braces (Akbay and Aktan, 1990; Kannan et al., 1995). This damper consisted on a shaft rigidly connected to the braces of the structure. A pre-load friction in the shaft was modified by using hydraulic forces which drove a piston, either increasing or reducing the compression force in the frictional interface. The device was tested experimentally, using a maximum slip-load of 270kN, with a stroke of ±50mm.

Another device utilising piezoelectric actuators was developed by Durmaz et al. (2002). The device consisted on two sets of parallel shims, moving relatively to each other. One set was allowed to move, whereas the other was fixed to a steel housing and the structure. The clamping force in the fixed set of shims was adjusted by the piezoelectric stack actuator. The device was tested experimentally under a range of electric currents, to produce different forces in the actuators. The maximum force developed was 11kN, for a demand of less that 0.5W.

Laflamme et al. (2012) developed a prototype damper incorporating a viscous, stiffness and variable friction elements in parallel. Both the viscous and stiffness elements provided minimal damping and acted as fail-safe mechanism of the frictional component. The variable frictional mechanism consisted of a rotating drum in which pressure on *braking shoes* was applied and regulated by a hydraulic actuator. Based on analytical work, those authors concluded that high frictional forces in the order of 1200kN are possible to develop using this device, by applying a pressure of 20kN on the *braking shoes*.

2.11 Concluding remarks

Control systems are an alternative to reduce the seismic demand on frame structures. According to the mechanism used to modify the structural response, control systems are classified in active, passive and semiactive. Active systems are highly adaptable, but they can also introduce instability in the structure, as control forces are exerted into the building. Passive control is a simpler solution that has proven to be effective, but with limited adaptability. The introduction of mechanical regulators into passive devices is an alternative to increase the adaptability of passive control, which is also the main potential advantage of semiactive control systems.

The performance of semiactive systems depends on the control algorithm implemented. There are several algorithms existing in the literature, four of which seem convenient for implementation into practical applications and are, therefore, selected for further investigation in this project. They are the modulated homogeneous control (MHF), linear boundary layer (LBL), smooth boundary layer (SBL) and Tri-D control. The performance of these controllers has been reported in the literature, where different control parameters were used in the corresponding investigations. In general, the performance of each control algorithm is greatly dependent on the value of pre-defined, constant gain factors. This characteristic of semiactive control algorithms may result in limitation of their performance, due to random nature of ground excitations and possible generation of inappropriate control forces.

Different mechanisms have been used to adjust the clamping force in semiactive friction damper, varying from piezoelectric stack actuators to hydraulic mechanisms. Experimental testing of several devices demonstrated the effectiveness of the mechanisms employed to produce a large range of control forces. Among the mechanisms tested, the hydraulic device employed in the actively regulated friction slip brace resulted in the largest control forces, in the order of 270kN.

Chapter 3

Methodology

3.1 Introduction

The investigation of the performance of the passive and semiactive control systems was conducted by simulating inelastic dynamic response of multi-storey buildings subjected to a variety of seismic excitations. The assessment of the efficiency of each control system was made in terms of building response, building damage and required control forces.

3.2 Development of computer program

Although there is availability of different computer programs for non-linear analysis of frame structures, there were no programs which included equipment for semiactive control and the corresponding control algorithms.

For this reason, a computer program for simulations of the non-linear response of multi-storey frames equipped with control systems was developed as part of this project. The program was based on the stiffness method for determination of forces acting in structural elements. The step-by-step, Newmark-β's average acceleration method was implemented in the program to determine nodal displacements, velocities and accelerations in time history analysis.

3.3 Reference structures and seismic excitations

A set of four multi-storey frame structures representative of low- and medium-rise buildings were used for studying the efficiency of control systems. These reference structures

included two steel frames (6-storey and 9-storey), selected from the literature (Inaudi, 1997; Ohtori et al., 2004), and two concrete frames (6-storey and 10-storey), designed as part of this research project. All four (bare) structures were modelled in *ConStruc* as planar, moment-resistant frames, with rigid beam-column connections and fully-restrained supports at the base.

The control systems were introduced in the bare frames by installing sets of concentric chevron braces in each storey, as recommended in the literature (Symans et al., 2008). The dampers were modelled as zero-length, friction connections between the braces and the beams.

The efficiency of the controllers was investigated for a variety of seismic excitations with different frequency content. Three historical earthquake records recommended in a benchmark problem (Ohtori et al., 2004) were used, with different peak ground acceleration: El Centro (0.35g and 0.55g), Northridge (0.35g and 0.55g) and Kobe (0.35g, 0.55g and 0.82g). In addition, another three records with different frequency content were used: Loma Prieta (0.35g, 0.55g and 0.65g), Imperial Valley (0.35g, 0.55g and 0.70g) and Taft (0.22g, 0.35g and 0.55g). The Taft record was used as an extreme, rare, earthquake with very broad frequency content. A total of 16 seismic inputs were used in the dynamic simulations.

3.4 Modelling assumptions

In the frame structures used for the seismic simulations, it was assumed that column elements behaved elastically during the ground excitations. It was also assumed that the rigid beam-column connections included adequate reinforcement and appropriate detailing, hence providing sufficient capacity of rotation, i.e. the ductility demand in the frames was not greater then the available ductility. The non-linearity effects were included only in beam elements, by utilising a bi-linear hysteretic model, which included plasticity due to rotations at either one or both ends of the beams. The bi-linear model did not included degradation of stiffness. Also, the non-linearities associated with shear deformations in the beam elements were not included in the hysteretic model.

The diagonal braces used in the retrofit (damper-bracing) systems were also assumed with an elastic behaviour, regardless of the level of axial force transmitted by the control devices, and no buckling effects were considered.

In the control systems, it was also assumed that all dampers behaved correctly during the ground excitations, and no failures (of either dampers or computers, in case of the semiactive systems) occurred during the simulations.

3.5   Examination of passive control

The passive control system was introduced in the frame structures, and a methodology to determine the dampers' capacity was initially proposed. In this methodology, the capacity (i.e. stiffness and slip-load) of each damper was determined as a function of the structural properties of the main frame, i.e. inter-storey stiffness and lateral force resistance prior to yielding in the corresponding storey.

The efficiency of the passive system and its mechanism was investigated for a broad range of dampers' capacities, varying from low values (in order to simulate responses resembling those of a bare frame) to high values (in order to simulate responses resembling those of a fully braced frame).

3.6   Examination of existing semiactive control

Four semiactive control algorithms existing in the literature were selected for this research. The modulated homogeneous friction control, linear and smooth boundary layer controllers and the Tri-D control were convenient for implementation in frame structures due to their *decentralised* control architecture and relatively simple algorithms. Their efficiency was also reported in the literature, where they were applied to different structures (either low- or high-rise buildings), e.g. low-rise steel frame with 3-storeys and 1-bay (He et al., 2003), low-rise steel frame with 6-storeys and 6-bays (Inaudi, 1997) and a high-rise steel frame, with 20-storeys and 5-bays (Ohtori et al., 2004).

In this study, the efficiency of the algorithms was investigated using different control parameters, and applying them to the set of four reference frames.

3.6.1   Modulated homogeneous friction control

The modulated homogeneous friction control (Inaudi, 1997) required control forces proportional to the inter-storey deformation, by using a pre-defined, constant gain factor. In this research, a parametric study of this controller was performed by using two gain factors originally proposed by Inaudi. In addition, a third, higher gain factor was used. Thus, each pre-defined factor corresponded to low, medium and high gain, respectively.

3.6.2 Linear and smooth boundary layer controllers

The linear boundary layer and the smooth boundary layer controllers (He et al., 2003) were proposed as a modification of the modulated homogeneous friction control. These two controllers adjusted the control forces proportionally to the inter-storey deformation (using pre-defined gain factors), but also gradually reduced and/or increased the forces in the vicinity of zero velocity, using boundary layers. A parametric study of these controllers was performed by using low, medium and high gain factors (with same values as those used in the modulated homogeneous control) and six boundary layers (three linear layers and three smooth layers).

3.6.3 Tri-D control

The Tri-D control algorithm was proposed by (Chen and Chen, 2004c). In the algorithm, the control forces were adjusted by using an initial passive slip-load and a set of two pre-defined, constant gain factors. In order to investigate its efficiency, a parametric study was performed: two different values of the initial passive load were defined. As for the gain factors, a methodology for determining their value based on the average of the bare frame's maximum deformation under different earthquakes, was initially proposed. By using this methodology, three gain factors (low, medium and high) were determined.

3.7 Development of new semiactive algorithms

As a possible solution to the limitations of existing control systems, new control algorithms were devised by correcting some of the observed limitations. It was noticed that passive control is suitable to produce the best response reductions, within a narrow range of damper capacities. Therefore, it was convenient to make the new controllers self-adaptable only for such range of passive capacities.

Also, both (*totally*) *decentralised* and *partially decentralised* strategies were examined.

3.8 Indices for assessment of control performance

In order to evaluate the performance of each control system, a series of six indices (J_1 to J_6) was used in this research. The performance of each system was evaluated by the indices in three categories: building response (maximum drift, acceleration and base

shear), building damage (expressed as energy dissipated through plastic hinges in the beams and/or through friction connections) and control forces required by the algorithm.

In the case of the *partially decentralised* control system, its efficiency was also evaluated by using two additional indices that measured the deformation distribution along the height of the buildings.

Chapter 4

Computational framework for non-linear simulations: *ConStruc*©

4.1 Introduction

For the purposes of this research, a computational framework (*ConStruc* software) for structural dynamic simulations has been developed. With *ConStruc*, it is possible to perform linear and non-linear analysis of planar frame structures including friction-based control systems. The programming platform of MATLAB® (The MathWorks Inc., 2012) was chosen for developing *ConStruc* due to its fast matrix manipulation and graphical output capabilities. It was necessary to develop this new code from scratch because, apart from providing full programming flexibility, there were no programs available with the features required due to the nature of this investigation: a combination of non-linear seismic analysis of frame structures equipped with friction-based devices, and algorithms for semiactive control of the dampers.

The analytical core of the program is based on the stiffness method for determining the structural forces, and the step-by-step Newmark-β's average acceleration method for determining the displacements, velocities and accelerations of the planar frame model. Currently, the software incorporates three types of elements that can be used for modelling beams/columns, bars and friction dampers.

The novel feature of this software is a module for control of the friction dampers' slip-load, using several semiactive algorithms. Furthermore, the program is structured in a way that allows implementation of new controllers.

Details of the theory behind the analytical engine of *ConStruc* are presented in this Chapter, whereas a user guide with details for the operation of the program can be found in Appendix A. Verification examples of structures analysed with this program using seismic loading conditions can be found in Appendix B.

4.2 Modelling frame structures

In *ConStruc*, frame structures are modelled through an assemblage of individual structural elements, which are described by nodes and their associated coordinates and degrees of freedom (DOFs). As shown in Fig. 4.1, each element is defined by two nodes i and j, and its length l, orientation θ and DOF-indices are determined automatically by the software. There is a fixed global coordinate system (GCS) for the frame model, but each structural element has its own local coordinate system (LCS), which is oriented with respect to the X axis of the GCS. The LCS is important for its relation to the element's internal forces, i.e. axial force in the longitudinal axis x, shear force in the transversal axis y and bending moment around the axis z, normal to the plane. The nodes have 3-DOFs, but for bar and damper elements the transversal and rotational degrees are free. In the Fig. 4.1, the DOF-indices are shown inside round brackets. The LCS is also necessary for correct *transformation* of internal forces from local to global coordinates, as it will be detailed later.

Every element has a local stiffness matrix, whose size and non-zero terms are determined by the restrained degrees of freedom. The number of restrictions depends on the element type. In the current version of *ConStruc*, three types of elements are available: (i) type 1, for modelling beams and columns; (ii) type 2, for modelling bars; and (iii) type 3, for modelling friction dampers. For correct assemblage of the frame model, the nodes and elements must be defined in the input file in a sequential order (Appendix A). The elements' local stiffness matrices are then *transformed* to global coordinates by means of transformation matrices. This is necessary to correctly relate the stiffness of the element to the global stiffness of the frame.

Finally, for completeness of the characteristics of the elements, the area A of their cross-section, second moment of area I, and modulus of elasticity E, must be entered in the input file (see Appendix A).
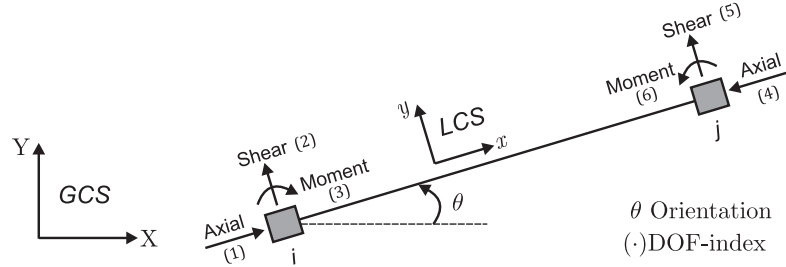
FIGURE 4.1: Definition of a structural element with 3-DOFs, in *ConStruc*.

4.2.1 Element types

Element type 1: Beam-column

Element type 1 is used to model beam-column elements with rigid connections, where two translational and one rotational DOFs per node are restrained. Hence, this element has both axial and flexural stiffness, with a 6x6 local stiffness matrix $\mathbf{k}_e$ given by:

$$
\mathbf{k}_e =
\begin{bmatrix}
\frac{EA}{l} & 0 & 0 & -\frac{EA}{l} & 0 & 0 \\
 & \frac{12EI}{l^3} & \frac{6EI}{l^2} & 0 & -\frac{12EI}{l^3} & \frac{6EI}{l^2} \\
 & & \frac{4EI}{l} & 0 & -\frac{6EI}{l^2} & \frac{2EI}{l} \\
 & & & \frac{EA}{l} & 0 & 0 \\
 & symmetric & & & \frac{12EI}{l^3} & -\frac{6EI}{l^2} \\
 & & & & & \frac{4EI}{l}
\end{bmatrix}.
$$

ConStruc offers the option to perform analysis considering linear-elastic beams and columns, regardless of the level of internal forces. However, when this option is not selected, non-linearity due to rotation at the ends of the beams is included. Then, the beams can be modelled assuming elasto-plastic, bi-linear stiffness by means of the coefficient κ, which indicates the ratio between post-yield and initial stiffness, as shown in Fig. 4.2.
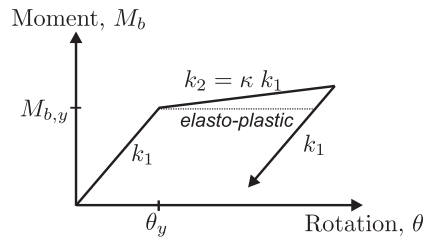
FIGURE 4.2: Non-linear model of element type 1, for beam elements.

To determine if the beam element is in either a linear or non-linear state, the software compares the acting bending moment M_b and the yielding moment $M_{b,y}$, whose value is pre-set in the input file. When M_b is equal to the value of $M_{b,y}$, the stiffness matrix $\mathbf{k}_e$ is modified. In this hysteretic model, however, kinematic or isotropic hardening effects are neglected, thus the value of the yielding moment $M_{b,y}$ is not modified after each non-linear cycle.

Three scenarios including non-linearity may occur, and the stiffness matrix of the element is modified accordingly, as follows:

- **Yielding at node i**

$$
\mathbf{k}_e = \begin{bmatrix}
\frac{EA}{l} & 0 & 0 & -\frac{EA}{l} & 0 & 0 \\
 & \frac{(3+9\kappa)EI}{l^3} & \frac{6\kappa EI}{l^2} & 0 & -\frac{(3+9\kappa)EI}{l^3} & \frac{(3+3\kappa)EI}{l^2} \\
 & & \frac{4\kappa EI}{l} & 0 & -\frac{6\kappa EI}{l^2} & \frac{2\kappa EI}{l} \\
 & & & \frac{EA}{l} & 0 & 0 \\
 & symmetric & & & \frac{(3+9\kappa)EI}{l^3} & -\frac{(3+3\kappa)EI}{l^2} \\
 & & & & & \frac{(3+\kappa)EI}{l}
\end{bmatrix}
$$

- **Yielding at node j**

$$
\mathbf{k}_e = \begin{bmatrix}
\frac{EA}{l} & 0 & 0 & -\frac{EA}{l} & 0 & 0 \\
 & \frac{(3+9\kappa)EI}{l^3} & \frac{(3+3\kappa)EI}{l^2} & 0 & -\frac{(3+9\kappa)EI}{l^3} & \frac{6\kappa EI}{l^2} \\
 & & \frac{(3+\kappa)EI}{l} & 0 & -\frac{(3+3\kappa)EI}{l^2} & \frac{2\kappa EI}{l} \\
 & & & \frac{EA}{l} & 0 & 0 \\
 & symmetric & & & \frac{(3+9\kappa)EI}{l^3} & -\frac{6\kappa EI}{l^2} \\
 & & & & & \frac{(4\kappa)EI}{l}
\end{bmatrix}
$$

- **Yielding at nodes i and j**

$$
\mathbf{k}_e = \begin{bmatrix}
\frac{EA}{l} & 0 & 0 & -\frac{EA}{l} & 0 & 0 \\
 & \frac{12\kappa EI}{l^3} & \frac{6\kappa EI}{l^2} & 0 & -\frac{12\kappa EI}{l^3} & \frac{6\kappa EI}{l^2} \\
 & & \frac{4\kappa EI}{l} & 0 & -\frac{6\kappa EI}{l^2} & \frac{2\kappa EI}{l} \\
 & & & \frac{EA}{l} & 0 & 0 \\
 & symmetric & & & \frac{12\kappa EI}{l^3} & -\frac{6\kappa EI}{l^2} \\
 & & & & & \frac{4\kappa EI}{l}
\end{bmatrix} .
$$

Once the element's local stiffness matrix has been determined, its global stiffness matrix $\mathbf{K}_e$ is determined with the following expression:

$$
\mathbf{K}_e = \mathbf{T}_e \mathbf{k}_e \mathbf{T}_e^T,
$$

where $\mathbf{T}_e$ is a transformation matrix given by

$$
\mathbf{T}_e = \begin{bmatrix}
\cos\theta & -\sin\theta & 0 & 0 & 0 & 0 \\
\sin\theta & \cos\theta & 0 & 0 & 0 & 0 \\
0 & 0 & 1 & 0 & 0 & 0 \\
0 & 0 & 0 & \cos\theta & -\sin\theta & 0 \\
0 & 0 & 0 & \sin\theta & \cos\theta & 0 \\
0 & 0 & 0 & 0 & 0 & 1
\end{bmatrix}.
\tag{4.1}
$$

Element type 2: Bar

Element type 2 is used to model diagonal braces with pinned connections. Bar elements have only axial stiffness, with 2-DOF restrained in the global coordinate system (due to displacements in X and Y). Their local stiffness matrix $\mathbf{k}_b$ is given by:

$$
\mathbf{k}_b = \begin{bmatrix}
\frac{EA}{l} & -\frac{EA}{l} \\
-\frac{EA}{l} & \frac{EA}{l}
\end{bmatrix}.
$$

For the purposes of this investigation, a linear-elastic behaviour is assumed for element type 2, regardless of the level of axial force demand.

Similarly to element type 1, the global stiffness matrix of a bar element is determined by multiplying the local matrix and the transformation matrix, as follows:

$$
\mathbf{K}_b = \mathbf{T}_b \mathbf{k}_b \mathbf{T}_b^T
\tag{4.2}
$$

In this case, however, the transformation matrix is a 4x2 matrix given by

$$
\mathbf{T}_b = \begin{bmatrix}
\cos\theta & 0 \\
\sin\theta & 0 \\
0 & \cos\theta \\
0 & \sin\theta
\end{bmatrix}.
$$

Thus, $\mathbf{K}_b$ is a 4x4 matrix, due to horizontal and vertical translations in the global coordinate system GCS.

Element type 3: Friction damper

Friction dampers are modelled using element type 3. The element has zero length and is described by two nodes with the same coordinates. Similar to bar elements, friction dampers have only local deformations along the longitudinal axis, but may have horizontal and vertical displacements in the global system due to transformation [1] . The axial stiffness k_d of damper elements is a constant scalar pre-defined in the input file, and their local stiffness matrix $\mathbf{k}_d$ is given by:

$$\mathbf{k}_d = \left[\begin{array}{cc} k_d & -k_d \\ -k_d & k_d \end{array} \right].$$

Due to their frictional mechanism, damper elements are strongly non-linear. The software utilises a perfectly elasto-plastic model, which has been found to be adequate through experimental investigation (e.g. Grigorian et al. 1993; Pall and Marsh 1982). The modified stiffness matrix $\mathbf{k}_d$ is thus formed by changing all the terms k_d to zero. As shown in Fig. 4.3, the stiffness is updated when the friction force acting in the damper reaches the passive or semiactive slip-load (f_p and $f_s(t)$, respectively), i.e. damper activation.
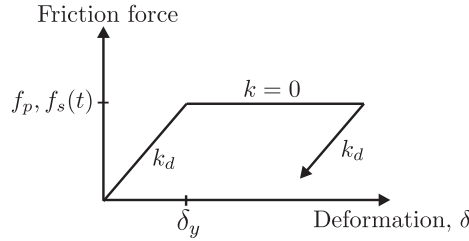
FIGURE 4.3: Non-linear model of element type 3.

4.2.2 Global stiffness matrix

The frame model's global stiffness matrix $\mathbf{K}$ is assembled from the individual matrices $\mathbf{K}_e$, $\mathbf{K}_b$ and $\mathbf{K}_d$. To speed up the process of assemblage, *ConStruc* utilises an indexing system which allows storage and combination of non-zero terms only into a sparse matrix in MATLAB. To do this, the nodes of the frame model must be numbered in sequence starting with elements type 1, elements type 2 and elements type 3 in the input file. The DOFs per node are indexed using the following expressions:

---
[1]The current version of *ConStruc* allows only horizontal orientation of dampers.

- **For elements type 1**

$$\mathbf{ix}_n = n \cdot 3 - 3 + \begin{bmatrix} 1 & 2 & 3 \end{bmatrix}$$

- **For elements type 2 and 3**

$$\mathbf{ix}_n = \begin{cases} n \cdot 3 - 3 + \begin{bmatrix} 1 & 2 \end{bmatrix} & \text{if } n \leq n_{max} \\ n \cdot 2 - 2 + n_{max} + \begin{bmatrix} 1 & 2 \end{bmatrix} & \text{if } n > n_{max}, \end{cases}$$

where n is the node number and n_{max} is the last node connecting elements type 1 only. The numbers in square brackets represent the number of DOFs, and $\mathbf{ix}_n$ is a vector containing the indices of node n.

For each element, the terms of $\mathbf{ix}$ corresponding to its two nodes are combined, resulting in 36 indices for elements type 1 and 16 for elements type 2 and 3. The indices corresponding to its two nodes are then stored in index matrices $\mathbf{IX}_e$, for each element. An example of the indexing process is shown in Fig. 4.4, for a type 1 and a type 2 elements. The numbers inside squares and circles indicate the element number and node number, respectively. The node 4 is n_{max} because it is the last node connecting only beams and columns. The index matrices corresponding to the element 3 (type 1) and the element 5 (type 2) are indicated by $\mathbf{IX_3}$ and $\mathbf{IX_5}$, respectively. In the figure, an additional matrix $\mathbf{IX_K}$ has been included only to indicate the indices of the frame model, i.e. the indices of the global matrix $\mathbf{K}$.

The assemblage of the global stiffness is then performed by adding the stiffness of the elements linked to each index into the matrix $\mathbf{K}$, whose size is given by the total quantity of DOFs.

4.2.3   Mass matrix

In addition to the stiffness matrix, a mass matrix is also required for dynamic analysis. Currently, only horizontal translational masses lumped at the nodes are considered in the analysis with *ConStruc*. The software assembles a diagonal matrix $\mathbf{M}$ with the same size as $\mathbf{K}$, as follows:

$$\mathbf{M} = \begin{bmatrix} m_n & & & zeros \\ & m_{n+1} & & \\ & & \ddots & \\ zeros & & & m_j \end{bmatrix},$$

FIGURE 4.4: Indexing of degrees of freedom.

where m_n represents the mass lumped at node n, and j indicates the last node.

4.2.4 Damping matrix

Inherent viscous damping in the structure is modelled by using Rayleigh coefficients. The software assembles a damping matrix $\mathbf{C}$ with the following expression:

$$\mathbf{C} = \alpha_r \mathbf{M} + \beta_r \mathbf{K}, \tag{4.3}$$

where α_r and β_r are the damping coefficients, whose values can be determined using the ratio of critical damping in the structure (Chopra, 1995).

Although uncommon, the software allows for different values of α_r to be specified for each mass, as well as different β_r coefficients to be assigned in each element.

4.2.5 External loads

External static loads acting on the nodes can be pre-specified in the input file. The loads can be horizontal, vertical or bending moments, and are assembled automatically into a vector of global loads, $\mathbf{F}$.

For dynamic analysis, ground accelerations can be declared through an input file containing acceleration points only, arranged either in rows or columns. The arrangement, along with the sampling time and the scale factor must be also specified in the input file (see Appendix A). With this information, the software constructs the vector of ground excitations, $\ddot{\mathbf{x}}_g$.

It should be noted here that, at its current stage, the program *ConStruc* uses the vector $\mathbf{F}$ to perform static analysis only. However, for dynamic analysis, it assumes initial conditions of displacements as zero, as it will be detailed in the following section.

4.3 Method of analysis used in *ConStruc*

Linear static and linear and non-linear dynamic analysis can be performed in *ConStruc*. In the case of static analysis, the global displacements $\mathbf{x}$ in the structure are calculated from the relation of stiffness and force, using the following equation:

$$\mathbf{F} = \mathbf{K}\,\mathbf{x} \tag{4.4}$$

The local deformations δ_i and internal forces $\mathbf{f}_i$ in the structural element i are then determined with the following two expressions:

$$\delta_i = \mathbf{T}_i \mathbf{x}_i \tag{4.5}$$

and

$$\mathbf{f}_i = \mathbf{k}_i \delta_i \tag{4.6}$$

In Eqs. 4.5 and 4.6, the sub-indices e, b, and d have been removed from $\mathbf{k}$ and $\mathbf{T}$ because the process is the same regardless of the type of element. Instead, the sub-index i indicates the corresponding element in the frame model.

Dynamic analyses, on the other hand, are performed by applying a step-by-step method. The Newmark-β's average acceleration method with $\gamma = 1/2$ and $\beta = 1/4$ has been found to be accurate and unconditionally stable for dynamic analysis including non-linearity

1. Assume values for γ and β as $1/2$ and $1/4$, respectively, and define the size of the time step Δt.

2. Calculate the constant matrices $\mathbf{A}$ and $\mathbf{B}$ with the following expressions:
$\mathbf{A} = \dfrac{1}{\beta \Delta t}\mathbf{M} + \dfrac{\gamma}{\beta}\mathbf{C}$ and $\mathbf{B} = \dfrac{1}{2\beta}\mathbf{M} + \Delta t \left(\dfrac{\gamma}{2\beta} - 1 \right)\mathbf{C}$.

3. Determine the vector of initial conditions for global displacements $\mathbf{x}_0$ and velocities $\dot{\mathbf{x}}_0$. In *ConStruc*, they are assumed as zero.

4. Determine the initial external excitation, $\mathbf{p}_0 = \mathbf{M}\,\ddot{\mathbf{x}}_g$.

5. Based on the initial conditions, calculate the initial acceleration $\ddot{\mathbf{x}}_0$, from the equation of motion:
$\mathbf{M}\ddot{\mathbf{x}}_0 + \mathbf{C}\dot{\mathbf{x}}_0 + \mathbf{K}\mathbf{x}_0 = -\mathbf{p}_0$.

6. For each time step j:

   (a) Calculate the effective incremental external force,
   $\Delta \hat{\mathbf{p}}_j = \Delta \mathbf{p}_j + \mathbf{A}\dot{\mathbf{x}}_j + \mathbf{B}\ddot{\mathbf{x}}_j$.

   (b) Calculate the effective stiffness, $\hat{\mathbf{K}}_j = \mathbf{K}_j + \dfrac{1}{\beta (\Delta t)^2}\mathbf{M} + \dfrac{\gamma}{\beta \Delta t}\mathbf{C}$.

   (c) Calculate the increment of displacement, from $\Delta \hat{\mathbf{p}}_j = \hat{\mathbf{K}}_j\,\Delta \mathbf{x}_j$.

   (d) Calculate the increment of velocity as
   $\Delta \dot{\mathbf{x}}_j = \dfrac{\gamma}{\beta \Delta t}\Delta \mathbf{x}_j - \dfrac{\gamma}{\beta}\dot{\mathbf{x}}_j + \Delta t \left(1 - \dfrac{\gamma}{2\beta} \right)\ddot{\mathbf{x}}_j$.

   (e) Determine the displacement and velocity for the next step, as
   $\mathbf{x}_{j+1} = \mathbf{x}_j + \Delta \mathbf{x}_j$ and $\dot{\mathbf{x}}_{j+1} = \dot{\mathbf{x}}_j + \Delta \dot{\mathbf{x}}_j$.

   (f) Determine the acceleration $\ddot{\mathbf{x}}_{j+1}$, from the equation of motion.

7. Increase the time step $j + 1$, and repeat the calculations of point 6.

(Subbaraj and Dokainish, 1989), and has been used in popular computer programs, (e.g. Paz 1997; Prakash et al. 1993). A detailed description of the method can be found in several references, such as Chopra (1995), Paz (1997) and Clough and Penzien (2003). A summary of the method, as programmed in *ConStruc*, is presented in Table 4.1. It is worth noticing that the effective incremental external force $\Delta \hat{p}_j$ and effective stiffness $\hat{\mathbf{K}}_j$ are used in the method as a correction of the errors generated by the use of the tangent stiffness, instead of the actual secant stiffness (Chopra, 1995).

A flow chart of the general engine to execute dynamic simulations in *ConStruc* is shown in Fig. 4.5. The program starts by reading the input files for definition of model, seismic parameters and ground excitation (see Appendix A), and generates all the elements' stiffness matrices in local and global coordinates, $\mathbf{k}_i$ and $\mathbf{K}_i$, respectively. The global

matrices are then used to assemble the frame's global stiffness matrix $\mathbf{K}$. For completeness of the model, the mass matrix $\mathbf{M}$ and the damping matrix $\mathbf{C}$ are also assembled. With this information, the procedure described in Table 4.1 is applied to determine the global displacement, velocity and acceleration at the current time step j. [2] After this, the local deformations and forces of every element are calculated with Eqs. 4.5 and 4.6. However, if a control system has been specified in the model, then the sub-routine **Control Strategy** is called, where the dampers' slip-loads are determined. This is an interactive process, i.e. whereas the main system provides the *feedback* information, the control module returns the required slip-load.
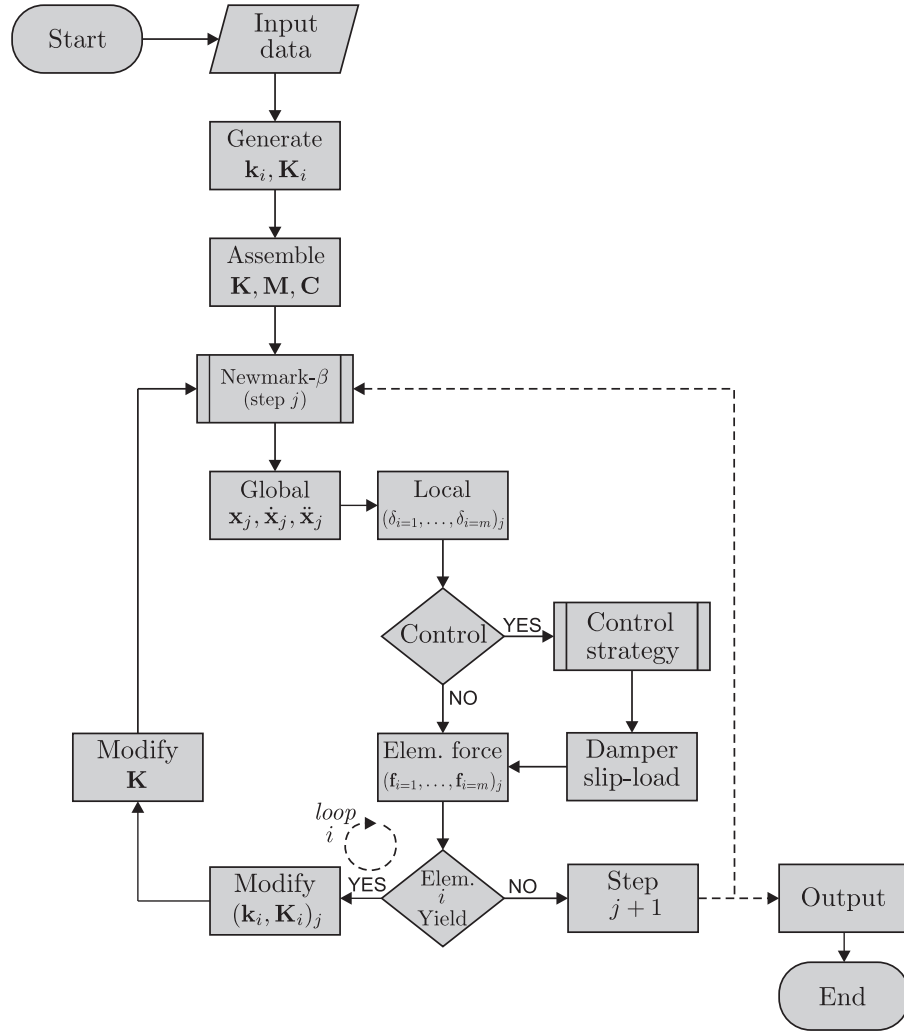
FIGURE 4.5: Flow chart for execution of dynamic simulations in *ConStruc*.

---

[2]The current version of *ConStruc* assumes initial conditions of displacement as zero. As a future improvement, the actual deformed configuration due to static loading should be used.

Once the full state of forces has been determined, the resistance of non-linear elements (i.e. beams and dampers) is checked. If yielding occurs at any beam or if any damper is activated, the corresponding local and global stiffness matrices are modified, and a new matrix $\mathbf{K}$ is assembled. The Newmark-β method is re-applied at the same time step j, but using the new stiffness. Otherwise, if all the elements remain elastic, the method is applied for the next time step, $j + 1$. The program continues until the total time of analysis is completed, thus generating output files and plots of the frame's response.

4.4   Quantification of energy and work performance

During strong ground motions, there is energy dissipated by different mechanisms in the structure. As such, the performance of structural systems can be understood by means of the work done and energy dissipated during the earthquake. The equation of motion given by:

$$\mathbf{M}\ddot{\mathbf{x}}(t) + \mathbf{C}\dot{\mathbf{x}}(t) + \mathbf{K}\mathbf{x}(t) = -\mathbf{M}\ddot{\mathbf{x}}_g(t), \tag{4.7}$$

can be modified as:

$$\mathbf{M}\ddot{\mathbf{x}}(t) + \mathbf{C}\dot{\mathbf{x}}(t) + \mathbf{K}_s\mathbf{x}(t) + \mathbf{K}_c\mathbf{x}(t) = -\mathbf{M}\ddot{\mathbf{x}}_g(t), \tag{4.8}$$

when a friction control system is included in the structure.

The terms of Eq. 4.7 have been defined previously. However, in Eq. 4.8 the global matrix $\mathbf{K}$ has been separated in two matrices, $\mathbf{K}_s$ and $\mathbf{K}_c$, that contain the stiffness due to structural elements and control devices, respectively. Integrating Eq. 4.8, it can be expressed in terms of energy (Chopra, 1995; Uang and Bertero, 1990), as follows:

$$\int \mathbf{M}\ddot{\mathbf{x}}\,dx + \int \mathbf{C}\dot{\mathbf{x}}\,dx + \int \mathbf{f}_s\,dx + \int \mathbf{f}_c\,dx = -\int \mathbf{M}\ddot{\mathbf{x}}_g\,dx, \tag{4.9}$$

where $\mathbf{f}_s = \mathbf{K}_s\mathbf{x}$ and $\mathbf{f}_c = \mathbf{K}_c\mathbf{x}$, and include elastic and inelastic forces.

In the Eq. 4.9, the term in the right side indicates the total energy exerted into the structure by the earthquake, E_i. The terms in the left side of the equation represent the energy distribution in the system: kinetic energy E_k, viscous damping E_ζ, restoring energy E_s and supplemental energy provided by the control devices, E_c. According to this, the Eq. 4.9 can be re-written as a balance of energy in the following form:

$$E_i = E_k + E_\zeta + E_s + E_c, \tag{4.10}$$

where the terms E_s and E_c include both the elastic (recoverable) and hysteretic (irrecoverable) energy of structural elements and dampers.

In the software *ConStruc*, an approach considering the level of forces and deformations done in the structure has been used to quantify the seismic energy and the dissipative mechanism of the system. The Eq. 4.7 can also be expressed as a balance of forces generated by each term, as follows:

$$\mathbf{f}_i = \mathbf{f}_k + \mathbf{f}_\zeta + \mathbf{f}_s + \mathbf{f}_c \tag{4.11}$$

where $\mathbf{f}_i$ is the force produced by the ground acceleration on the nodal masses, $\mathbf{f}_k$ and $\mathbf{f}_\zeta$ are the inertia and damping forces, respectively, and $\mathbf{f}_s$ and $\mathbf{f}_c$ are the structural and control forces, respectively. The set of forces are determined by $\mathbf{f}_i = \mathbf{M}\ddot{\mathbf{x}}_g$, $\mathbf{f}_k = \mathbf{M}\ddot{\mathbf{x}}$, $\mathbf{f}_\zeta = \mathbf{C}\dot{\mathbf{x}}$ and $\mathbf{f}_s$ and $\mathbf{f}_c$ as defined previously.

Considering that the step-by-step method adopted for dynamic analysis provides increments of global displacement and local deformation ($\Delta\mathbf{x}$ and $\Delta\delta$, respectively), it is possible to evaluate the energy in the structure at the end of each time step by applying the following expressions:

$$E_i = \Delta\mathbf{x}^T \left(\mathbf{f}_i + \frac{\Delta\mathbf{f}_i}{2} \right),$$

$$E_k = \Delta\mathbf{x}^T \left(\mathbf{f}_k + \frac{\Delta\mathbf{f}_k}{2} \right),$$

$$E_\zeta = \Delta\mathbf{x}^T \left(\mathbf{f}_\zeta + \frac{\Delta\mathbf{f}_\zeta}{2} \right), \tag{4.12}$$

$$E_s = \Delta\delta^T \left(\mathbf{f}_s + \frac{\Delta\mathbf{f}_s}{2} \right), \text{ and}$$

$$E_c = \Delta\delta^T \left(\mathbf{f}_c + \frac{\Delta\mathbf{f}_c}{2} \right).$$

Hence, the total energy in the structure-earthquake system at the end of the excitation is given as an scalar produced by adding up each term at every time step.

4.5 Concluding remarks

In this Chapter, a computer program developed as part of this research was described. The software *ConStruc* is capable of performing linear-elastic static analysis and linear-elastic and non-linear dynamic analysis of planar frame structures.

In the program, an assemblage of individual stiffness matrices allowed for the modelling of planar frames. The individual matrices corresponded to three types of elements to model columns, beams, bars and friction dampers. Columns and bars are linear-elastic elements, but beams and dampers can be modelled as bi-linear or perfectly elasto-plastic elements, respectively.

The Newmark-β's average acceleration was programmed in *ConStruc*. This step-by-step method was used to calculate the displacements, velocities and accelerations of the frame. The stiffness method, on the other hand, was used to determine the local deformations and forces of each element.

A module for control of friction damper's slip-load was included in the software. Such module was implemented using a *feedback* algorithm in which the damper's local deformation was sent to the controller from the main program. The damper's slip-load should then be determined within the control module, and its value returned to the main program.

Finally, the seismic energy in the structure was quantified by considering the work done in the frame during each incremental time step.

Chapter 5

Reference frame structures and seismic excitations

5.1 Introduction

In the review presented in Chapter 2, it was noticed that there was a large variability in the studied parameters of friction-based *decentralised* systems, including ground excitations and frame structures. In most of the references presented therein, the efficiency of the controllers was demonstrated for a number of specific structures specially designed for their purposes, some of which were scaled models that required low levels of control forces.

An exhaustive investigation of the efficiency of existing decentralised control systems is one of the objectives of this study. For this reason, a variety of frame structures representative of low- and medium-rise buildings were analysed using the software *ConStruc*, which was developed as part of this research (Chapter 4). The set of structures included a low-rise steel frame (Inaudi, 1997) and a benchmark medium-rise steel frame (Ohtori et al., 2004). It also included a low- and a medium-rise reinforced concrete structures, which were designed as part of this project.

The efficiency of the control systems was investigated for a variety of ground excitations. Six historical earthquakes were exerted in dynamic non-linear simulations. The excitations included three earthquakes proposed by Ohtori et al. (2004) in their benchmark problem, and three additional earthquakes to provide a wider range of excitation frequencies.

A description of the four reference frame structures and the set of historical earthquake excitations used in the simulations is presented in this Chapter, as a prelude to the

following four Chapters, which show the analyses of performance of different control systems.

5.2 Steel frames

5.2.1 Low-rise steel frame

A low-rise, moment resistant steel frame was previously analysed by Inaudi (1997). The bare frame consisted of six storeys and six bays, as illustrated in Fig. 5.1. The total height and width of the structure were 28.20 and 36.60m, respectively. As shown in the same figure, different wide flange sections were used for the beams and columns.

The information about the elastic limits of the frame was not available in the litera-ture. For this reason, a pushover analysis using DRAIN-2DX (Prakash et al., 1993) was performed to determine the inter-storey stiffness and yield load of the structure. In the analysis, an incremental lateral load was applied at each level, whilst restraining the horizontal translation of the lower storeys. The results showing the structural proper-ties of the frame (i.e. inter-storey stiffness $k_{s,i}$, yield deformation $\delta_{y,i}$, yield load $f_{y,i}$ and weight W_i per level i), are presented in Table 5.1. Before the analysis, the resistance of beams and columns was calculated as the product of the section's plastic modulus and the yield strength of steel grade S275, without including any reduction factor.
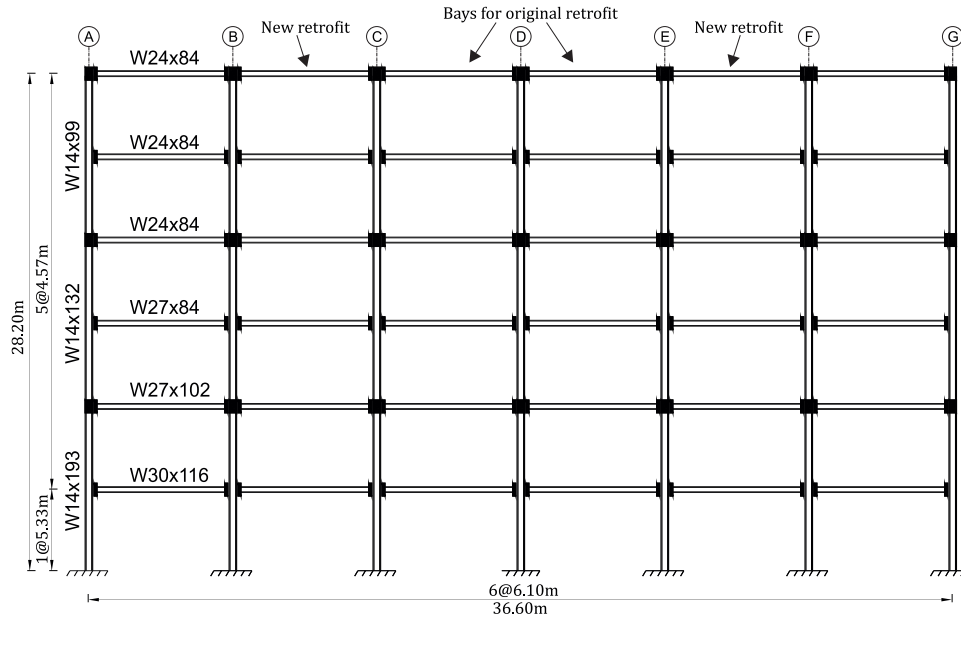
FIGURE 5.1: Low-rise steel frame structure (Inaudi, 1997)

TABLE 5.1: Structural properties of low-rise steel frame.

Level i	$k_{s,i}$ [kN/cm]	$\delta_{y,i}$ [cm]	$f_{y,i}$ [kN]	W_i [kN]
1	870	4.51	3920	2232
2	1076	4.10	4410	2232
3	753	4.00	3010	2232
4	700	4.25	2975	2232
5	546	4.07	2240	2232
6	538	4.13	2205	2232

The frame analysed by Inaudi included low levels of viscous damping, with ratios in the order of 0.5% of the critical. To create similar conditions, in this investigation the damping was included by means of Rayleigh coefficients, which were calculated using the following simultaneous equations (Chopra, 1995):

$$\zeta_1 = \frac{\alpha_r}{2\omega_1} + \frac{1}{2}\beta_r\omega_1,$$

$$\zeta_3 = \frac{\alpha_r}{2\omega_3} + \frac{1}{2}\beta_r\omega_3 \tag{5.1}$$

from where:

$$\alpha_r = \zeta\frac{2\omega_1\omega_3}{\omega_1 + \omega_3},$$

$$\beta_r = \zeta\frac{2}{\omega_1 + \omega_3} \tag{5.2}$$

where ω_1 and ω_3 are the circular frequency of the corresponding mode. After applying Eqs. 5.2, the values of α_r and β_r were 0.0331 and 0.0004, respectively. The damping ratios of the first three modes resulted in 0.50, 0.40 and 0.52%, respectively, which are in good agreement with the original ratios. The natural frequencies of the frame were 0.67, 1.88 and 3.16Hz for the first, second and third mode of vibration, respectively.

In Inaudi's work, the bare frame was retrofitted by installing a diagonal bracing-damper system in the two middle bays (C-D and D-E, in Fig. 5.1), in every storey. The retrofit system included one friction damper in each brace. In this investigation, however, the retrofit system was installed using a different array, as a solution to the possible slenderness and buckling of the brace. The new system included a chevron bracing in the bays B-C and E-F. The dampers were then installed in the connections between the braces

and the beams, as shown in Fig. 5.2. A possible advantage of this system is that, by including two concentric braces, it is possible to sustain higher control forces, due to the reduced axial load and slenderness.

The braces were designed to remain linear-elastic and to avoid buckling during the seismic excitations. A very stiff bracing system was also convenient for reducing the elastic deformations that could affect the efficiency of the control system. For these reasons, two upper limits of axial loads corresponding to the dampers' maximum slip-loads of $1.0f_{y,i}$ and $2.50f_{y,i}$ were used as design loads (see Chapter 6). The cross sections resulting from the first upper limit were used for all the cases of analysis with slip-loads of up to $1.0f_{y,i}$. Thus, Celsius$^{©}$ CHS244.5x16 sections were used in the first and second storeys, and CHS244.5x10 sections were used in the third to sixth storeys. The second upper limit was used for cases of analysis with slip-loads greater that $1.0f_{y,i}$. The cross sections used for this upper limit were CHS355.6x16 sections for the first and second storeys, and CHS273.0x16 for all other storeys.
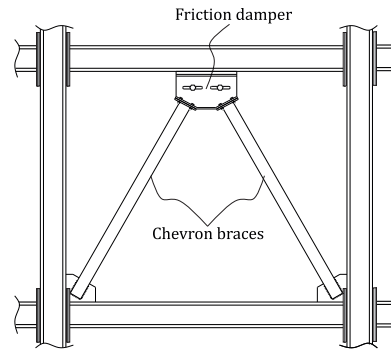
FIGURE 5.2: Detail of friction connections used for retrofit.

The introduction of the retrofit system increased the stiffness and modified the vibrational properties of the structure. Depending on the state of the dampers, the frequencies of the controlled structures may vary between those of a bare frame (i.e. all dampers slipping), a fully braced frame (i.e. all dampers locked), or as intermediate, partially braced frames. In the case of a fully braced condition, the frequencies of the three first modes resulted in 1.14, 3.48 and 6.14Hz, respectively.

5.2.2 Medium-rise steel frame

Ohtori et al. (2004) proposed a set of three benchmark structures, which included a high-rise, a medium-rise and a low-rise steel buildings. The medium-rise building was utilised for the purposes of this investigation. It consisted of four moment resistant frames arranged in orthogonal directions, each with nine storeys above ground level and

one basement, as shown in Fig. 5.3. The total height of the frames was 37.37m and the total width, which comprised five equally spaced bays, was 45.75m.

In this investigation, some modifications were made to the original frame proposed by Ohtori et al. The geometry, dimensions and cross sections of the benchmark frame were maintained, but the model adopted in this research (Fig. 5.4) included the following changes:

- Only floors above ground level were considered.

- Supports at the base were fully restrained.

- All beam-column connections were assumed as rigid.

These modifications, however, were not expected to have a significant influence on the dynamic properties of the structure.
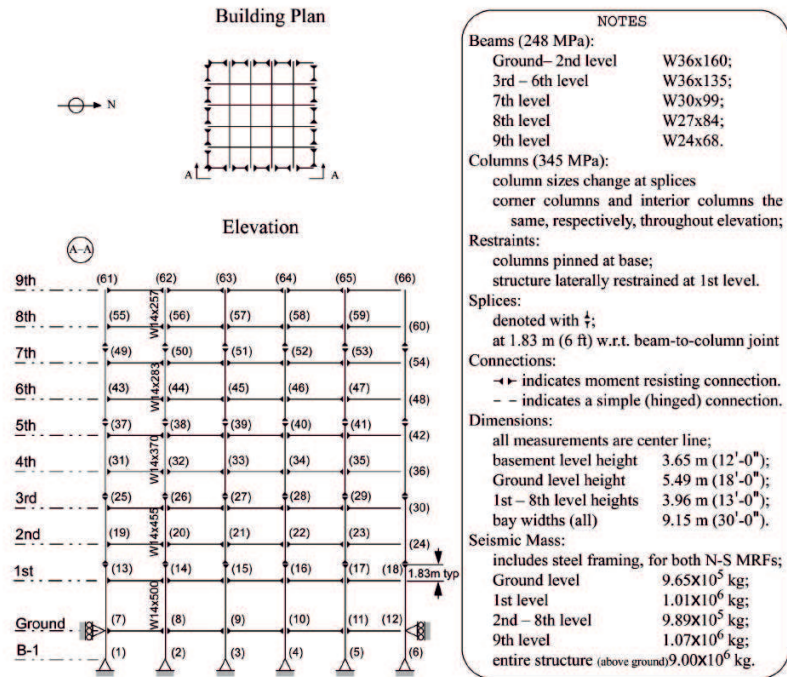
FIGURE 5.3: Medium-rise steel frame model, proposed by Ohtori et al. (2004).

In the benchmark model, the damping ratios of the first and fifth modes of vibration were specified as $\zeta_1 = \zeta_5 = 0.02$. Based on those ratios, the Rayleigh coefficients α_r and β_r of the modified frame were calculated as 0.1008 and 0.00135 with Eqs. 5.2. The damping ratios of the frame resulted in $\zeta_1 = 0.018$ and $\zeta_5 = 0.021$, which agreed with the benchmark model.
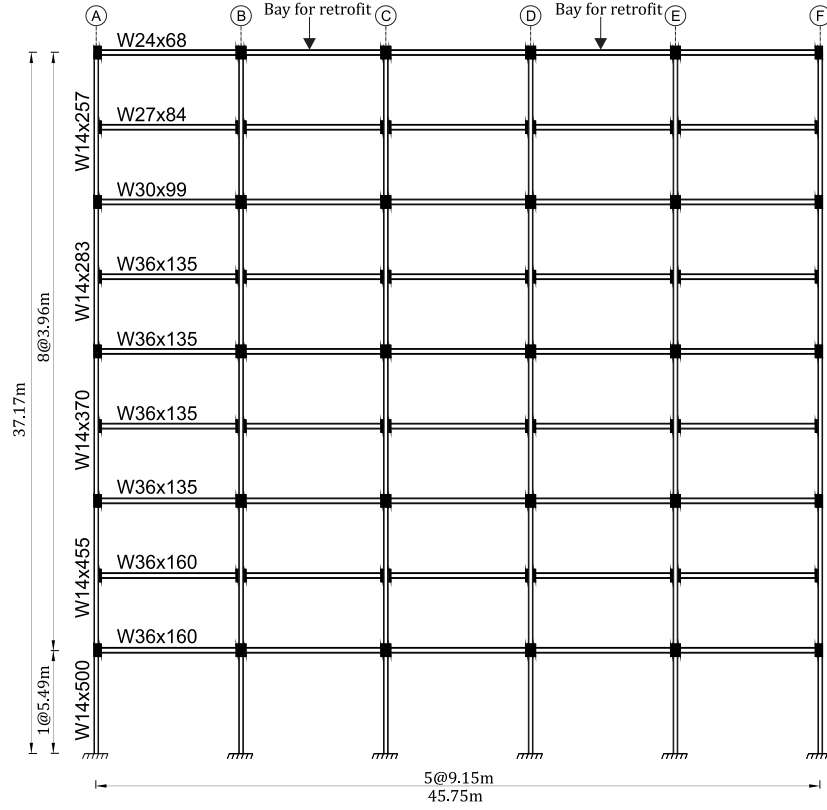
FIGURE 5.4: Modified medium-rise steel frame model.

The frequencies of vibration of both frames were also in good agreement. The first five natural frequencies of the modified frame were 0.49, 1.29, 2.23, 3.33 and 4.56Hz, whereas those of the benchmark model were 0.44, 1.18, 2.05, 3.09 and 4.27Hz.

The structural properties of the bare frame were determined by means of pushover analysis using DRAIN-2DX (Prakash et al., 1993). In those analyses, lateral loads were applied at each floor, whilst restraining the lower levels in the horizontal direction. The properties resulting from the analysis are shown in Table 5.2.

The bare frame model was retrofitted by introducing a system similar to that described in Section 5.2.1. In this case, the concentric chevron bracing-damper system was installed in the bays B-C and D-E (Fig. 5.4), in every storey. Using a similar approach, the braces were designed to sustain the dampers' maximum slip-loads of $1.0f_{y,i}$ and $2.50f_{y,i}$. From the first design load limit, CHS406.4x16 sections were used for the braces in the first three storeys, CHS323.9x16 sections for the braces in the fourth and fifth storeys, CHS323.9x12.5 sections for braces in the sixth and seventh storeys, CHS323.9x10 sections for braces in the eighth storey and finally CHS273x10 sections for the braces in the top storey. From the second design limit, SHS400x400x20 sections were used in the first

TABLE 5.2: Structural properties of medium-rise steel frame.

Level i	$k_{s,i}$ [kN/cm]	$\delta_{y,i}$ [cm]	$f_{y,i}$ [kN]	W_i [kN]
1	2176	5.10	11100	4954
2	3840	3.75	14400	4856
3	3583	3.60	12900	4856
4	3083	3.60	11100	4856
5	2921	3.80	11100	4856
6	2400	3.50	8400	4856
7	2053	3.80	7800	4856
8	1610	4.10	6600	4856
9	1250	3.60	4500	5249

five floors, CHS406.4x16 sections for the braces in floors sixth, seventh and eighth, and CHS323.9x12.5 sections for the braces in the ninth floor.

The inclusion of the retrofit system resulted in the variability of frequencies between bare and fully braced frame, depending on the state of the dampers. In the fully braced condition, the frequencies of the first five modes were 1.09, 3.15, 5.61, 7.97 and 10.31Hz, respectively.

5.3 Reinforced concrete frames

5.3.1 Low- and medium-rise RC frames

Two moment resistant, reinforced concrete frames were designed according to guidelines provided in the Eurocodes 2 and 8 (European Committee for Standardization, 1992, 1998). The bare frames corresponded to the interior bays of low- and medium-rise hypothetical office buildings. The low-rise frame consisted of six storeys and three bays. The total height and width were 22.80 and 18.0m, respectively. The medium-rise frame consisted of ten storeys and three bays. In this case, the total height was 37.20m, and the width was 18.0m. As a characteristic of both frames, the two lower levels were 4.20m in height, whereas the rest of the storeys were 3.60m. A slice of the typical plan and the elevation of the bare frame models are shown in Figs. 5.5 and 5.6.

Due to the occupancy of the hypothetical buildings, the frames were designed for ductility class high and importance class III. A concrete with compressive strength of 30MPa and reinforcement steel with yield strength of 460MPa were used as materials of construction. The seismic behaviour factor corresponding to those structural characteristics
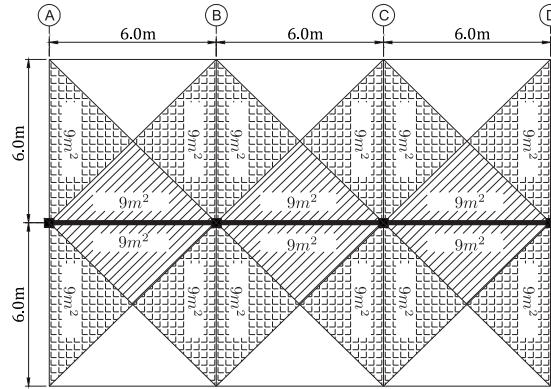
FIGURE 5.5: Typical plan of low- and medium-rise RC frames.

c) Beams and columns cross-section

a) 6-storey frame model

b)10-storey frame model
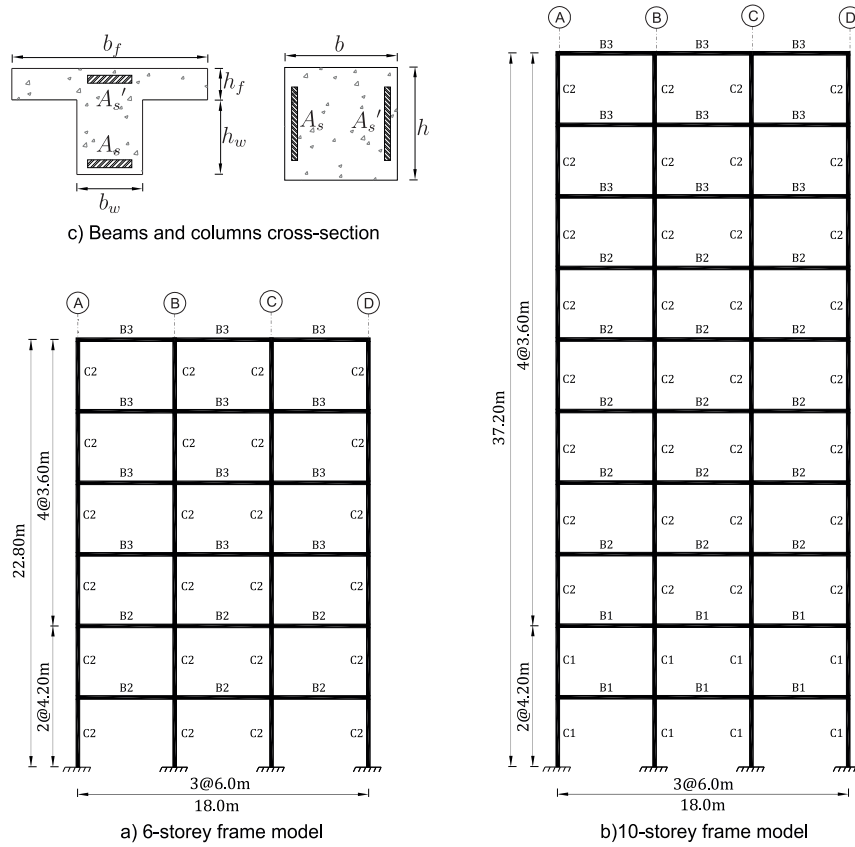
FIGURE 5.6: Elevation and cross-sections of low- and medium-rise RC frames.

TABLE 5.3: Elastic Response Spectra for ground type C.

Soil	S	$T_B(S)$	$T_C S$	$T_D(S)$	a_g
C	1.15	0.20	0.60	2	0.53

TABLE 5.4: Dimensions of columns.

Section	b [cm]	h [cm]	Area [cm^2]	Inertia [cm^4]
C1	45	45	2025	341719
C2	40	40	1600	213333

TABLE 5.5: Dimensions of beams.

Section	b_f [cm]	b_w [cm]	h [cm]	h_f [cm]	h_w [cm]	Area [cm^2]	Inertia [cm^4]
B1 exterior	122	35	45	18	27	3141	451174
B1 interior	194	35	45	18	27	4437	528207
B2 exterior	117	35	45	18	27	3051	444498
B2 interior	189	35	45	18	27	4347	523668
B3 exterior	112	30	40	18	22	2586	275244
B3 interior	184	30	40	18	22	3882	332730

was 5.85. An elastic design spectrum corresponding to ground type C was used for the seismic design. The parameters used to construct the elastic spectrum are indicated in Table 5.3. The seismic behaviour factor of 5.85 was used as a reduction factor of such spectrum, as specified in the Eurocode 8.

The dimensions of the cross sections of beams and columns are indicated in Tables 5.4 and 5.5, respectively. Square cross sections were adopted for the columns, and T-sections for the beams. The flange was included to account for the additional stiffness of a concrete slab. A detail of the cross sections and the corresponding structural elements using each cross section can be observed in the Fig. 5.6.

The vibrational properties of the bare frames were determined for inelastic conditions by using a reduced modulus of elasticity to simulate a state of cracked sections. The first three frequencies of the low-rise frame resulted in 0.65, 1.99 and 3.50Hz. The first three damping ratios for the same structure were 4.96, 3.96 and 5.37%. For the medium-rise frame, the first five frequencies were 0.50, 1.46, 2.49, 3.68 and 4.94Hz. In this case, the damping ratios were 6.03, 3.70, 4.40, 5.60 and 7.10%.

Pushover analysis using DRAIN-2DX (Prakash et al., 1993) were performed to determine the structural properties of the bare frames. The results showing the stiffness, yield deformation and yield load of the inter-storey i are indicated in Tables 5.6 and 5.7, for each frame. In those tables, the weight per storey is also indicated.

TABLE 5.6: Structural properties of low-rise RC frame.

Level	$k_{s,i}$	$\delta_{y,i}$	$f_{y,i}$	W_i
i	[kN/cm]	[cm]	[kN]	[kN]
1	210	3.50	680	609
2	177	3.90	660	609
3	255	2.90	740	578
4	240	3.00	720	578
5	243	2.80	680	578
6	210	1.80	420	525

TABLE 5.7: Structural properties of medium-rise RC frame.

Level	$k_{s,i}$	$\delta_{y,i}$	$f_{y,i}$	W_i
i	[kN/cm]	[cm]	[kN]	[kN]
1	303	2.90	880	609
2	250	3.60	900	609
3	264	3.26	860	578
4	264	3.26	860	578
5	264	2.93	773	578
6	264	2.93	773	578
7	264	2.93	773	578
8	250	2.80	700	546
9	227	3.00	680	546
10	207	2.32	480	525

The bare frames were retrofitted by including a concentric bracing-damper system, with the friction dampers installed between the braces and the beams, similar to that shown in Fig. 5.2. Since it was assumed that the frames were sufficiently ductile, the retrofit systems were included with the purpose of reducing the inter-storey deformations. The retrofit system was installed in the middle bay of each storey. In this system, the braces were designed to remain linear-elastic during the earthquake, but also sufficiently stiff to undergo small deformations. The two levels of axial loads corresponding to the dampers' maximum slip-loads of $1.0 f_{y,i}$ and $2.50 f_{y,i}$ were used as design loads. In the case of $1.0 f_{y,i}$, CHS219.10x12.5 sections were used in the braces of the first and second floor and CHS193.7x10 sections were used in the rest of the floors of the low-rise frame. In the case of $2.50 f_{y,i}$, CHS219.10x12.5 sections were used in all the floors. The braces in the medium-rise frame were CHS193.7x6.3 sections in floors one to ninth, and CHS168.3x6.3 sections in the top floor, for the design load limit of $1.0 f_{y,i}$. For the higher design load, CHS219.1x16 sections were used in all the floors.

Due to the characteristics of the retrofit system, there was a variability in the frequencies of vibration of the frames. Frequencies similar to those of the bare frame occur when all dampers are activated. On the other hand, a fully braced condition occurs when all the dampers are locked. In this state, the first three frequencies of the low-rise frame were

1.79, 5.63 and 10.29Hz, whereas the same frequencies for the medium-rise frame were 1.0, 3.03 and 5.78Hz. A third condition in which only some dampers are activated is also possible. Then, the frames may vibrate with frequencies corresponding to intermediate, partially braced frames.

5.4   Ground excitations

The six historical earthquakes used in this investigation are indicated in Table 5.8. The first three earthquakes (i.e. El Centro, Northridge and Kobe) were specified in the benchmark problem proposed by Ohtori et al. (2004). The last three records (i.e. Loma Prieta, Imperial Valley and Taft) were specially utilised in this study to set up a wider range of excitation frequencies.

The excitations exerted in the simulations were composed of 30 seconds of the original earthquake accelerograms and additional 10 seconds with zero acceleration to allow for decay of the response. However, in the case of Northridge, only 25 seconds of accelerations and 10 seconds for response decay were included. To study the adaptability of the control systems, all the excitations were scaled to peak ground accelerations (PGA) of 0.35 and 0.55g. Additional PGAs were also used for Kobe (0.82g), Taft (0.22g), Loma Prieta (0.65g) and Imperial Valley (0.70g). Thus, a total of 16 excitations were used in this project. The earthquake's accelerograms scaled to the PGA of 0.35g are shown in Fig. 5.7. Note that the amplitudes of the Taft record were scaled to 0.22, 0.35 and also 0.55g, in order to create an extreme event.

The frequency content of each earthquake was determined by means of Fourier spectra, as shown in Fig. 5.8. As it can be observed, the records selected are useful because they provide a broad band of excitation frequencies. The Taft record, however, represents an extreme excitation with broad frequency content and high amplitude.

TABLE 5.8: Historical earthquakes used in non-linear simulations.

Name	Year	ID	Station (USGS)	NAG record
El Centro	1940	cn40	IVI District Array #9	180
Northridge	1994	nr94	Fletcher	234
Kobe	1995	ko95	JMA	1106
Loma Prieta	1989	lo89	SF Bay-Dumberton B	757
Imperial Valley	1979	iv79	Calipatria FS	163
Taft	1952	tf52	Hollywood	012

Note. The accelerograms corresponding to the NAG records were obtained from the PEER Strong Motion Database (PEER, 2011).

Finally, the response spectra of each earthquake excitation are shown in Fig. 5.9. Those spectra include 5% damping.
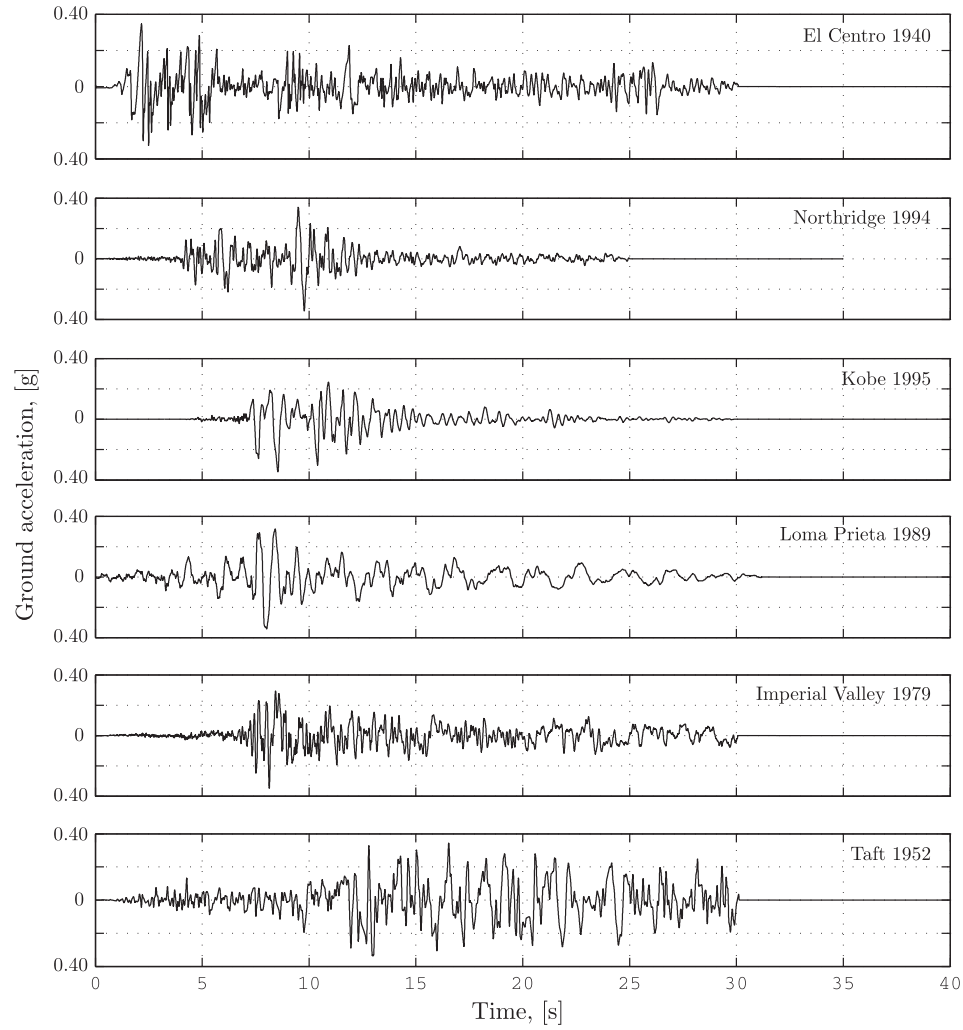
FIGURE 5.7: Earthquake excitations used in simulations.

5.5   Concluding remarks

In this Chapter, four bare frame structures were described. These moment resistant structures are representative of low- and medium-rise buildings, and included a 6- and 9-storey steel and a 6- and 10-storey RC frames.

The low-rise steel structure was utilised in a previous study by Inaudi (1997). A low damping ratio of 0.5% was specified in Inaudi's work, thus Rayleigh coefficients were calculated to create similar conditions in this research. The resulting damping of the
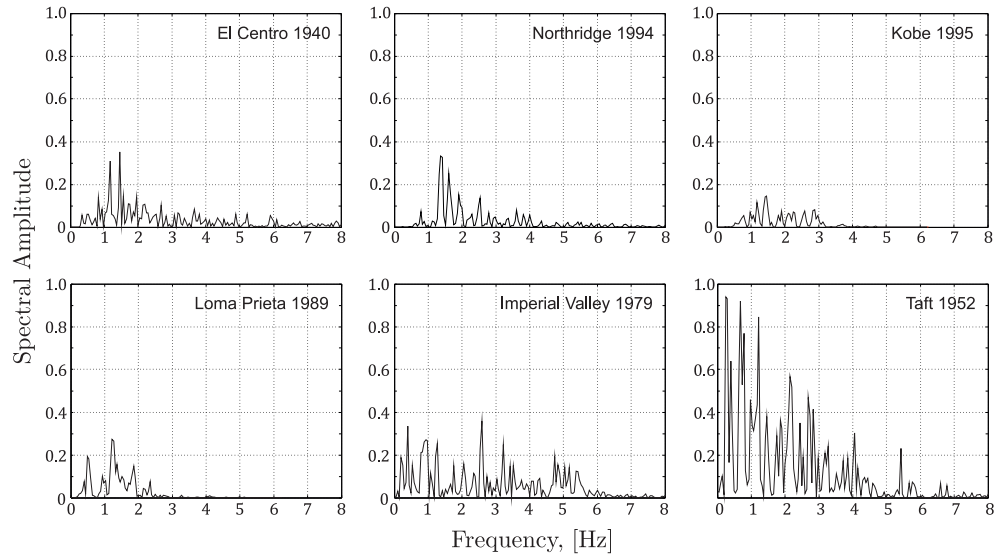
FIGURE 5.8: Fourier spectra of earthquake excitations.
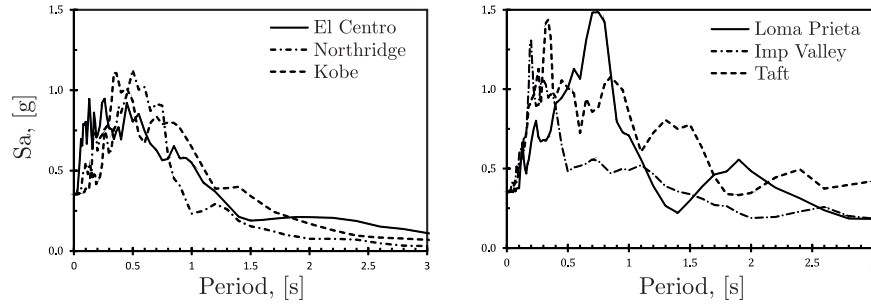
FIGURE 5.9: Response spectra of earthquake excitations, with 5% damping.

model used in this study was 0.50, 0.40 and 0.52% in the first, second and third mode of vibration, respectively. These values were in good agreement with the damping reported for Inaudi's model. Using the dimensions and cross sections for beams and columns, the first three natural frequencies of the frame resulted in 0.67, 1.88 and 3.16Hz.

The medium-rise steel structure was proposed by Ohtori et al. (2004) in a benchmark problem. The same frame was adapted for this investigation by including some minor modifications, e.g. rigid connections for all beams and columns and fully fixed supports at the base. These modifications did not have a significant influence on the dynamic properties of the frame. In the literature, the first five frequencies of vibration were indicated as 0.44, 1.18, 2.05, 3.09 and 4.27Hz, and the damping ratios corresponding to the first and fifth modes of vibration were 2%. In the model used in this investigation, the first five natural frequencies resulted in 0.49, 1.29, 2.23, 3.33 and 4.56Hz, whereas

the damping ratios of the first and second mode were 1.8 and 2.1%. These values are in good agreement with those of the benchmark model.

In the steel building, the lateral resistant system was comprised of only two strong moment frames. To contrast with that situation, a 6- and 10-storey, reinforced concrete frames were designed as part of this project. These two frames corresponded to interior slices of hypothetical office buildings. The first three frequencies of the low-rise structure were 0.65, 1.99 and 3.50Hz. The corresponding frequencies for the medium-rise frame were 0.50, 1.46 and 2.49Hz.

A concentric bracing-damper system was used to retrofit the four bare frame models. In this system, the friction dampers were installed between the braces and the beams. A concentric array was used because it allows higher control forces, by reducing the axial load and slenderness in the braces.

Finally, the description of six historical earthquakes used in the non-linear simulations was presented. The earthquakes included El Centro 1940, Northridge 1994, Kobe 1995, Loma Prieta 1989, Imperial Valley 1979 and Taft 1952. The set of records provided a wide range of excitation frequencies.

Chapter 6

Friction-based passive control

6.1 Introduction

In this Chapter, the efficiency of friction-based passive control is investigated for the set of 6- and 9-storey, steel frames and 6- and 10-storey, RC frames described in Chapter 5. A methodology for determining the dampers' capacity based on mechanical properties of the bare frame is described first. Non-linear simulations are then performed with the software *ConStruc*, developed as part of this research (Chapter 4). The performance of the control system is studied by comparing the global response of the bare and controlled structures, including top floor displacements, shear and axial loads at the base of the building, and energy dissipation. Also, to understand the mechanism of the optimum performance behind each system, the top floor displacement and acceleration is analysed in frequency domain by means of Fourier spectra.

6.2 Capacity of passive friction dampers

As described in Section 2.6 (Chapter 2), one type of simple friction damper consists of a series of steel plates bolted together, with a durable frictional interface between them, such as brass (Grigorian et al., 1993) or brake lining pads (Pall and Marsh, 1982).

The behaviour of a friction damper depends on two parameters: stiffness k_d and slip-load f_p, as shown in Fig. 2.6 on page 15. For friction dampers, there is a high initial stiffness which drops to zero after the slip-load is reached and the plates start moving relatively to each other. This allows for small elastic deformations, but large movement during the inelastic slippage of the plates to dissipate the energy.

The ith damper's slip-load can be modelled as the product of the friction coefficient and the clamping force, as established in Eq. 2.1 on page 14.

6.2.1 Determination of damper's capacity

Several studies on friction dampers indicate an optimum slip-load for which levels of response reduction and energy dissipation are maximum (e.g. Filiatrault and Cherry, 1987; Pall and Marsh, 1982; Pall and Pall, 2004). To determine such optimum value, different approaches for the distribution of the slip-loads in the structure have been used.

Among the first investigations, in the experimental tests performed by Aiken et al. (1988), the methodology used to determine the slip-load established that *"slippage in the dampers should not occur for wind and low to moderate earthquake loads (minimum bound); dampers should start slipping before the yield limit of any member of the structure is reached (upper bound); and slip-loads should be such that the energy dissipated within the structural system due to friction is maximised"*. Another method based on the inter-storey shear force was studied by Filiatrault and Cherry (1990), who also noted that small differences in the efficiency resulted between systems in which slip forces were scaled in proportion of shear force acting on each storey and those with uniform distribution of the total shear force. Furthermore, those authors proposed a design slip-load spectrum from which the optimum slip-load could be determined directly. The information required in such a formulation included the structural properties but also vibrational properties of the construction site, which suggests that the optimum load depends not only on the frame, but also on the excitation. In a later study, Dowdell and Cherry (1996) proposed a distribution based on the structural deformation and the mass of the building, such that $f_{p,i} = \lambda d_0^i \sum_{j=i}^{n} m_j$, where $f_{p,i}$ is the slip-load of damper at level i, λ is a factor of proportionality, d_0^i is the inter-storey displacement of the fundamental mode at level i, and the remaining term indicates the sum of masses above and including the storey i. In this expression, however, the slip-load depends on the excitation, which may limit the efficiency, as earthquakes are random in nature. Finally, the capacity of passive systems can also be determined proportionally to the stiffness and strength distribution in the main frame, as performed by Symans et al. (2008), who used a metallic yield device in a single storey, single bay frame, and Martinez-Rueda and Elnashai (1995), who used friction dampers in the soft storey of a multi-storey building.

In this research, the capacity of friction dampers, including slip-load and stiffness, was determined based on the structural properties of the bare frame, similarly to the approach proposed by Martinez-Rueda and Elnashai and Symans et al. This approach seemed convenient as the dampers' capacity would be independent of the characteristics

of the excitation, but their performance would be closely related to the motion intensity. The methodology is summarised in the following steps:

- For each inter-storey i, determine its stiffness $k_{s,i}$, yield load $f_{y,i}$ and yield deformation $\delta_{y,i}$, by means of pushover analysis (Chapter 5).

- Determine the passive slip-load $f_{p,i}$, as the ratio between the inter-storey's yield load and the damper's slip-load, i.e. $f_{p,i}/f_{y,i}$. In this project, such ratio varied from 0 to 2.5, where 0 indicates a bare frame and 2.5 a fully braced, or close to fully braced frame.

- Define the stiffness $k_{d,i}$ of the friction device higher than the corresponding inter-storey stiffness. For the medium-rise (9-storey) steel frame, a factor of 5 (i.e. $k_{d,i} = 5k_{s,i}$) was used. For all other frames, a factor of 10 was applied.

6.3 Performance of passive systems

6.3.1 Reduction of top floor displacement

The four bare frames were subjected to the action of the set of ground accelerations described in Chapter 5. The envelopes of maximum floor displacements of the frames are shown in Figs. 6.1 and 6.2, for the steel frames and RC frames, respectively. In those figures, it can be seen that the structural response of each frame was different when they were subjected to each earthquake, even if the ground excitations were scaled to the same PGA. These variations in the response are due to the frequency content of each earthquake, which would result in different excitation levels for different modes of vibration of the frame. As it can be observed in Figs. 6.1 and 6.2a and b, the largest displacements were caused by the Taft excitation for both PGA of 0.35g and 0.55g. The reason for this, as shown in Fig. 5.8 on page 62, is that Taft record is an extreme event with very broad range of excitation frequencies with high amplitude.

The response of the frames was modified by including the passive control described in Chapter 5. The top floor displacement of the controlled frames was lower than that of the bare frames in many cases. The levels of reduction varied between each earthquake and also depended on the slip-load of the dampers. In Figs. 6.3 and 6.4, the efficiency of the retrofit systems is presented as a plot between the ratio d_c/d_b (where d_c represents the top floor displacement of the controlled frame, and d_b is the top floor displacement of the bare frame), and the ratio $f_{p,i}/f_{y,i}$. As it can be seen, there is not a unique optimum slip-load level for all excitations. This makes evident the limited adaptability
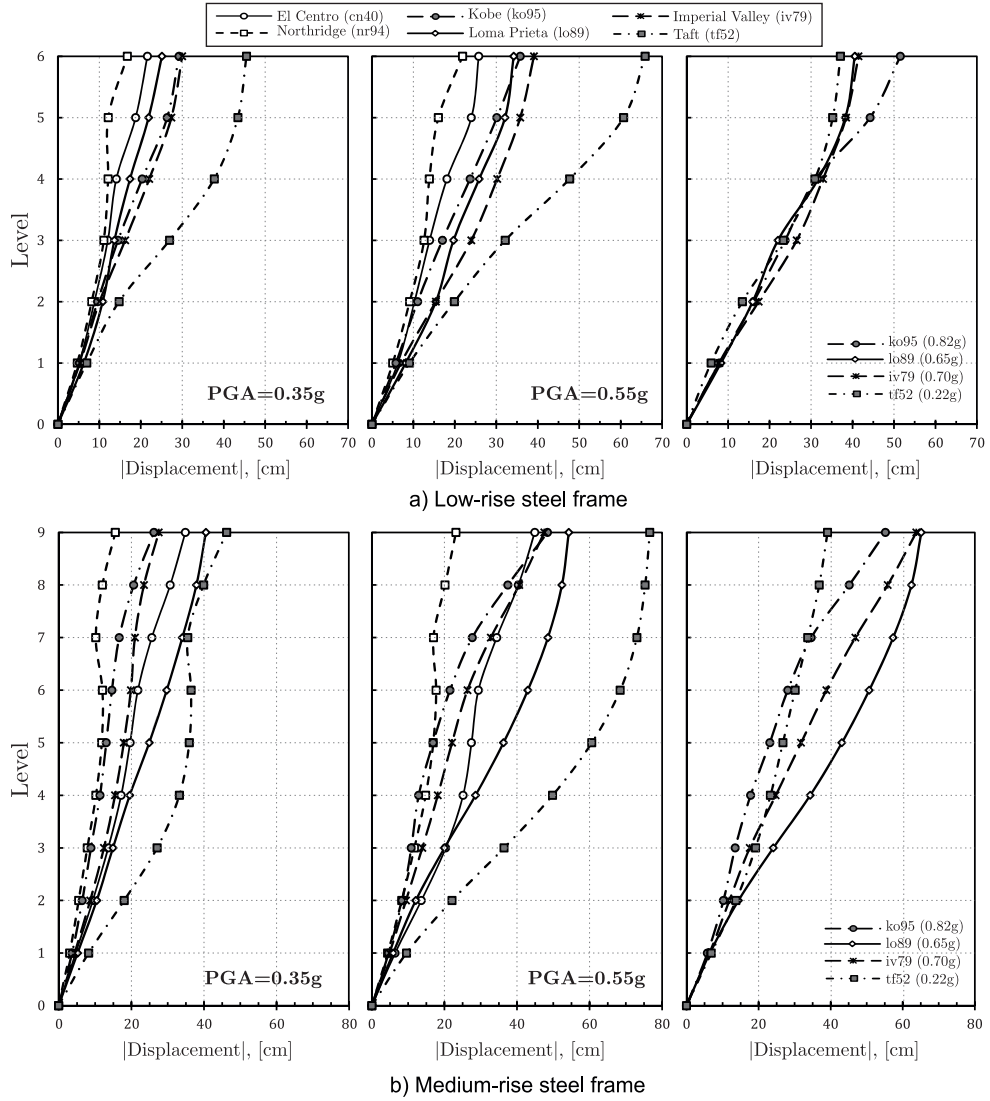
FIGURE 6.1: Envelope of maximum floor displacements of steel bare frames.

of the system. Furthermore, the limitation of the control system efficiency is evident for the medium-rise buildings under the Northridge excitation, which even leads to an increase of displacements for the RC frame (Fig. 6.4b).

Although one single value of optimum slip-load cannot be identified, there is a clear range of $f_{p,i}/f_{y,i}$ between 0.25 and 0.65 which produced good levels of reduction, in the majority of the earthquakes. Higher slip-loads, up to fully braced, or close to fully braced condition ($f_{p,i}/f_{y,i}$=2.50), were not as effective, showing no further significant reductions or, in many cases, allowing for an increase of the response.
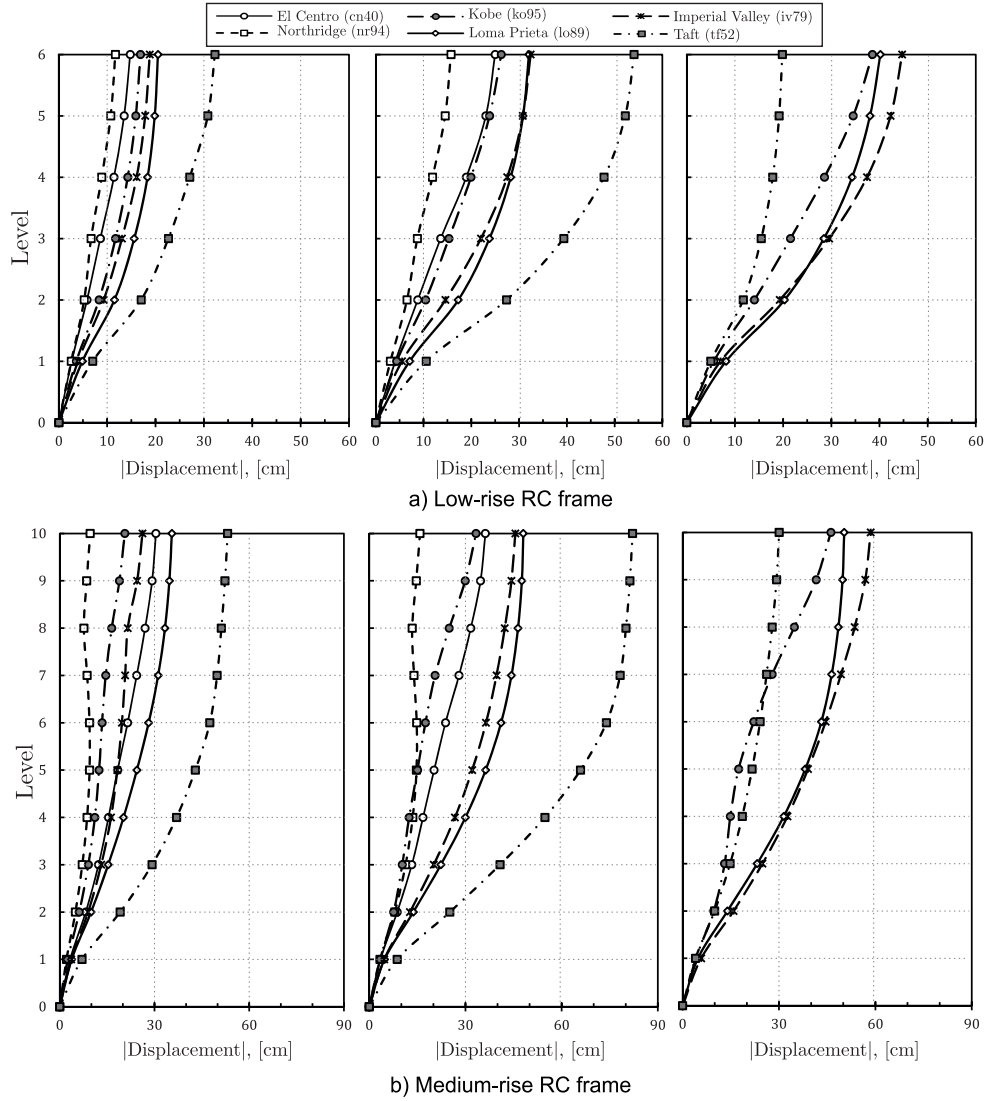
Figure 6.2: Envelope of maximum floor displacements of RC bare frames.

6.3.2   Increase of structural forces

The immediate effect of introducing a retrofit system in a bare frame is the increase of stiffness, which would normally lead to an increase of the inter-storey shear and axial loads in the columns. In general, for all controlled systems there was an increase of both base shear and axial load in the columns of the first floor, especially in those columns connecting with the braces, as seen in Fig. 6.5, where the ratios between the base shear or axial load of the controlled frames ($F_{b,c}$ or $F_{a,c}$, respectively) and the base shear or axial load of the bare frames ($F_{b,b}$ or $F_{a,b}$, respectively) are shown. It can be noted that there is a small interval of slip-loads up to $0.25f_{y,i}$ which produces a reduction of
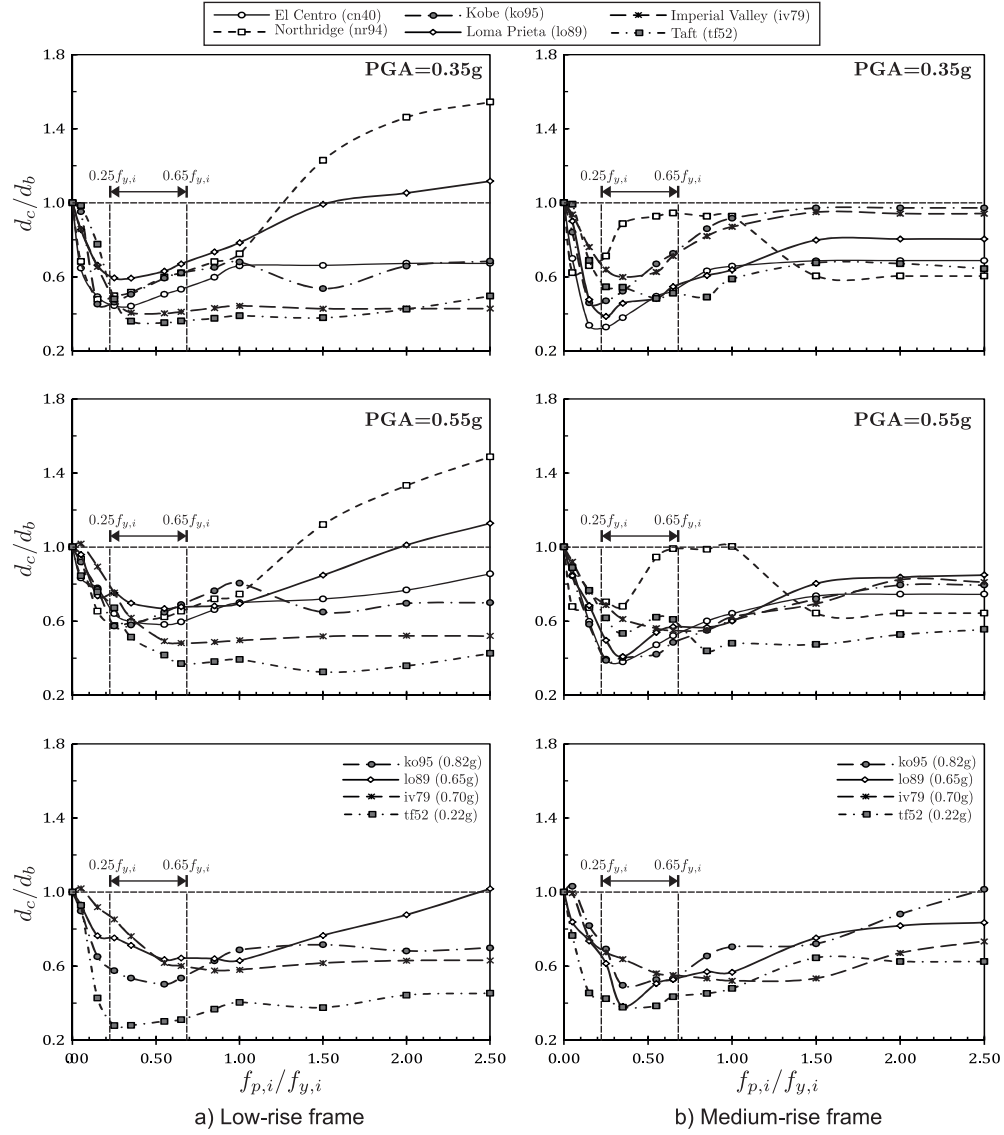
FIGURE 6.3: Top floor displacement ratios of steel frames with passive control: low-rise (left) and medium-rise (right).

forces, in many cases. However, this range of slip-loads was not identified as the one producing the largest reductions of deformations. The results show that, in the region with maximum reductions (i.e. $f_{p,i}/f_{y,i} = 0.25$ to 0.65), there is a reasonable increase in shear forces, and relatively steep increase in axial loads in the columns. Increase of ratios $f_{p,i}/f_{y,i}$ beyond 0.65 results in dramatic increase on both shear and axial loads.

This behaviour is a result of the energy dissipation in the friction devices. The fact that the forces (shear and axial) in the frame do not increase proportionally to the increase of
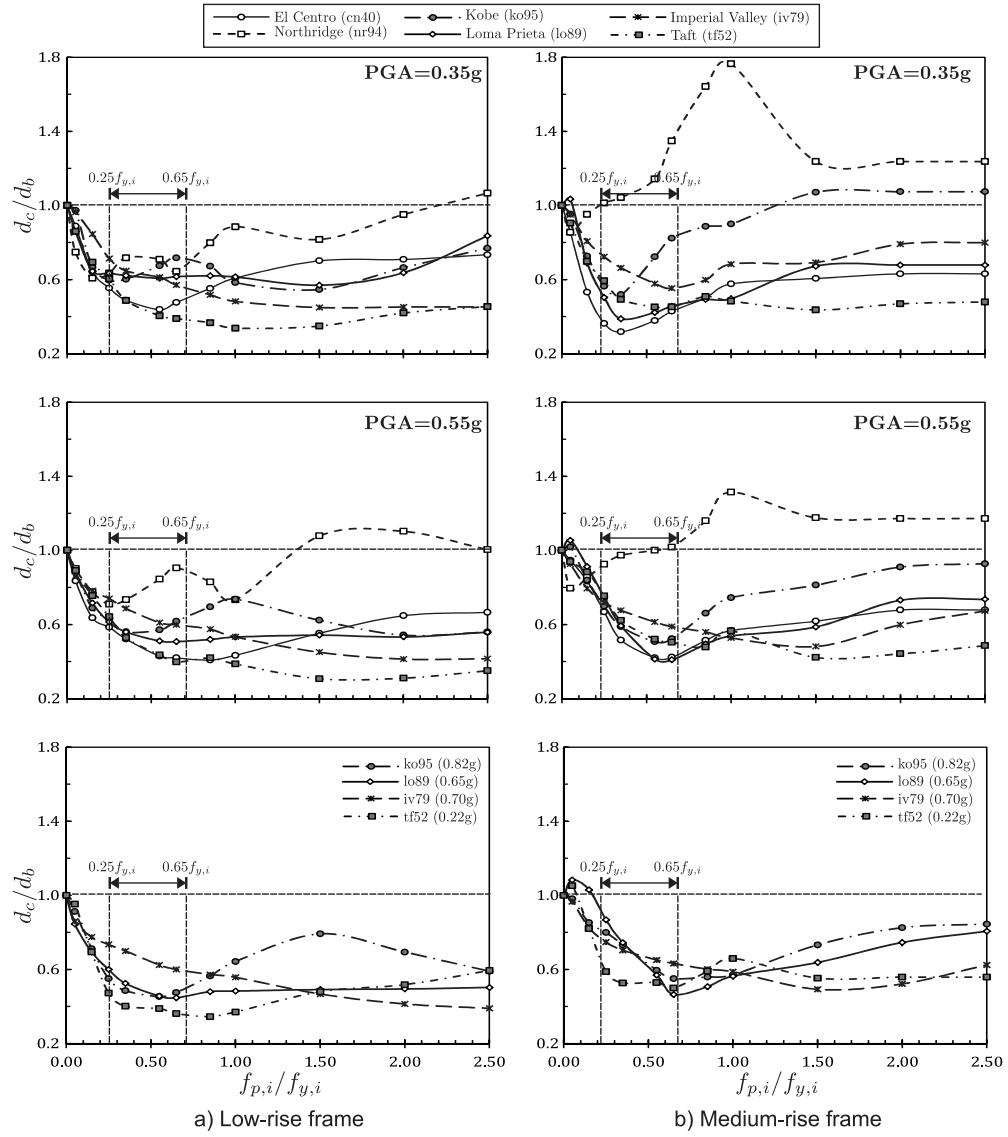
FIGURE 6.4: Top floor displacement ratios of RC frames with passive control: low-rise (left) and medium-rise (right).

the slip-load ratio $f_{p,i}/f_{y,i}$ in the region below 0.65, suggests that the increase of forces is offset by the reduction in deformations (as it was shown in Fig. 2.7 on page 15).
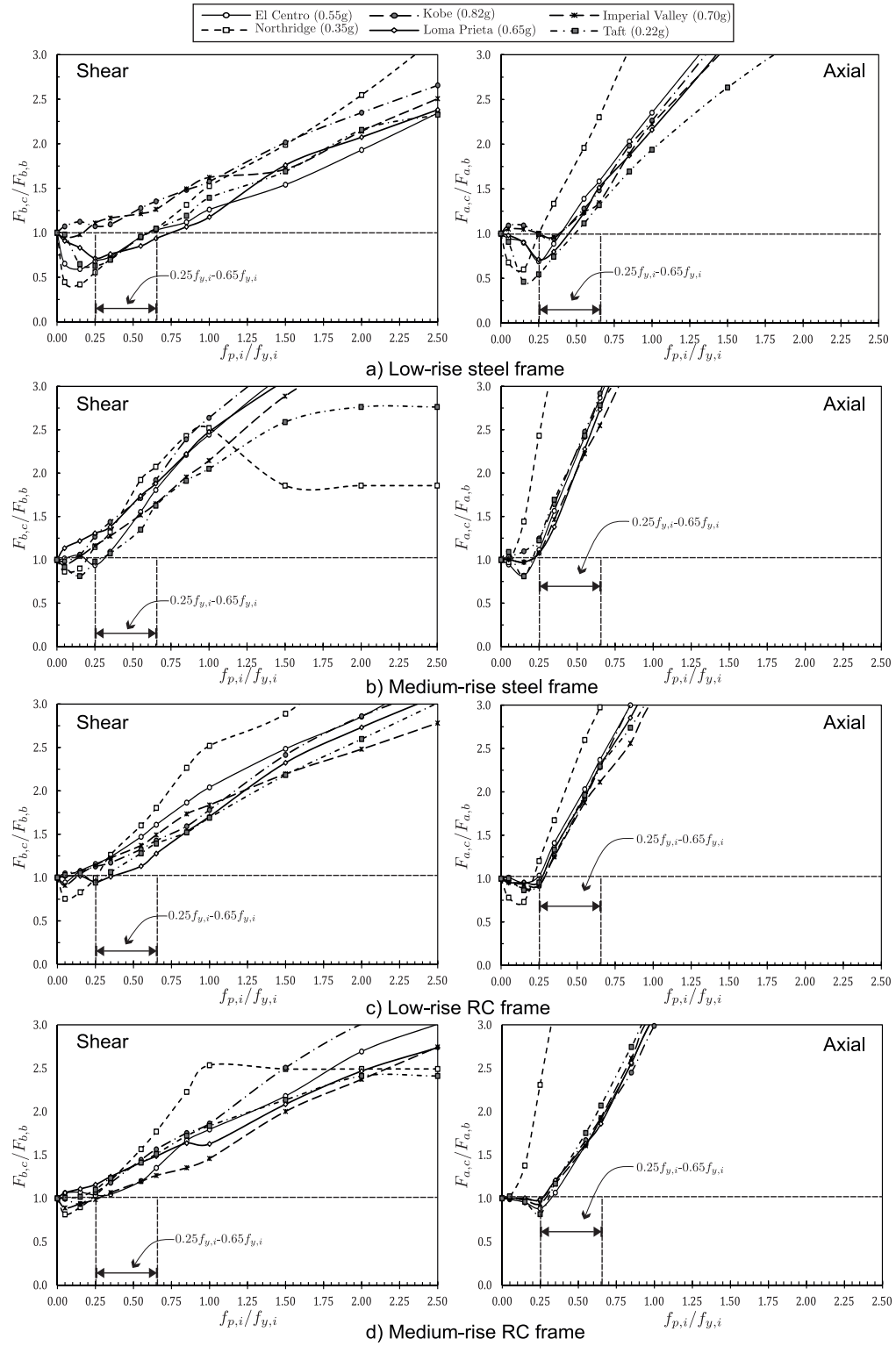
FIGURE 6.5: Ratios of shear and axial load in frames with passive control system.

6.3.3 Energy dissipation

Reduction of the frame response is related to the additional dissipative mechanism provided by the control system. Since the behaviour of the colums is assumed as elastic, the only dissipative elements in the bare frame are plastic hinges in the beams. The bracing system adds a limited amount of dissipation, especially in this investigation where the braces were designed to remain linear-elastic. The passive control, on the other hand, increases significantly the dissipative capacity of the structure. The optimum response reduction is closely related to the amount of energy dissipated through the hysteretic frictional mechanism, rather than that created by plasticity in the structural elements.

The proportions of external energy dissipated by beams and friction connections (ratios E_s/E_i and E_c/E_i, respectively) are shown in Fig. 6.6. The results show that for the bare frame ($f_{p,i}/f_{y,i} = 0$), large amounts of energy are dissipated in the beams, whereas with the introduction of friction dampers ($f_{p,i}/f_{y,i} > 0$), most of the energy is dissipated through slippage in the dampers, with very small proportion dissipated in the beams. This means that the damage in the frame is greatly reduced using the control system. It is also shown that the dissipative capacity added by the control system is reduced for slip-loads outside the range $f_{p,i}/f_{y,i} = 0.25$ to 0.65, indicating a lack of activation of the friction connections.

6.3.4 Frequency content of the seismic response

Fourier spectra of the top floor displacement and acceleration gives an indication of the mechanism behind each structural system. In general, the variation of the structural response results from the modification of the vibrational frequencies of the frames due to the activation of the dampers. This effect can result in avoiding resonant conditions, in which the frequency of the frame is equal to the frequency of the excitation.

The time history of the top floor displacement and the spectral amplitude of the top floor displacement and acceleration of the reference frames under different excitations are shown in Figs. 6.7 to 6.10. As shown in Fig. 6.7a, the displacement at the top floor of the low-rise steel frame was greatly reduced using the passive control with $f_{p,i}/f_{y,i} = 0.35$, but not as efficiently with the largest control force ($f_{p,i}/f_{y,i} = 2.50$), which is closer to a fully braced condition. This is related to the spectra shown in Figs. 6.7b and c, where the control with higher slip-load created large peaks at 1.40 and 3.90Hz. These two peaks are shifted from the peaks of the bare frame at 0.67, 1.88 and 3.16Hz, corresponding with its first, second and third mode, respectively. As it can be seen, the first and second modes had a predominance on the displacement and acceleration response, respectively.
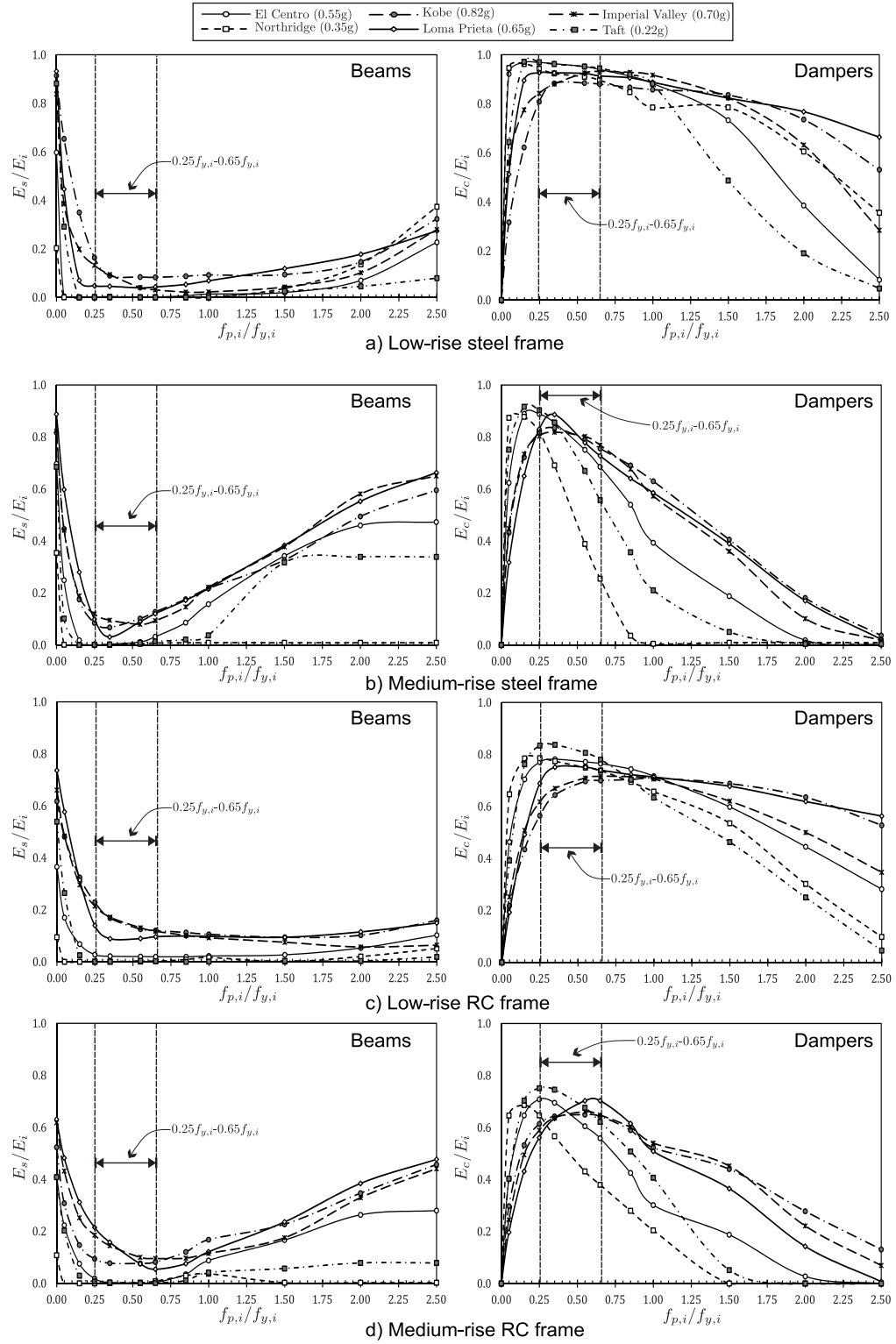
FIGURE 6.6: Ratios of hysteretic energy dissipated by beams and friction dampers.

The control with $f_{p,i}/f_{y,i} = 0.35$ had smaller amplitudes, with peaks at 1.2 and 1.5Hz, and not large amplification at any frequency.

Considering the medium-rise steel frame (Fig. 6.8), the control with ratios $f_{p,i}/f_{y,i}$ between 0.25 and 0.65 was not always effective for the Northridge excitation. In the case of Northridge with PGA of 0.55g, the displacements were significantly reduced for $f_{p,i}/f_{y,i} = 0.25$ and 0.35, and also for higher ratios, $f_{p,i}/f_{y,i} > 1.50$. The system with $f_{p,i}/f_{y,i} = 0.65$ was not very efficient, and produced practically the same response as the bare frame, but at different frequencies. The reason for this, as suggested by the spectra of Figs. 6.8b and c, is that there is a fully braced condition, which is suddenly changed by the pulse of the excitation. In the Fig. 6.8b, the control systems ($f_{p,i}/f_{y,i} = 0.35$, 0.65 and 2.50) produced peaks around the first frequency of fully braced condition (i.e. 1.09Hz). In fact, it can be seen that the higher slip-load resulted in amplitudes at 1.09Hz, indicating the braced condition, whereas the systems with $f_{p,i}/f_{y,i} = 0.35$ and 0.65 modified the frequencies due to activation/deactivation in the friction connections. However, in the case of the lower slip-load, the reduction of displacement was a result of the higher amount of energy dissipated by the dampers (Fig. 6.6b). In the Fig. 6.8c, the spectra of the control with $f_{p,i}/f_{y,i}$ of 0.65 and 2.50 are very similar up to 2.5Hz, when the dampers of the first controller are suddenly activated, hence dropping the amplitude at higher frequencies. The peaks for the bare frame correspond to the modes of vibration at 0.49, 1.29 and 2.23Hz, with a predominance of the second mode. The controller with $f_{p,i}/f_{y,i} = 0.35$ produced smaller amplitudes at different frequencies, mainly at 0.90, 1.40, 1.60 and 2.50Hz, which indicates a state of activation/deactivation of the dampers, and avoiding resonance with any of the frequency components of the earthquake.

A similar effect can be observed for the low-rise RC frame under the Northridge earthquake with PGA of 0.55g, although in this case the displacement was not reduced using a ratio $f_{p,i}/f_{y,i} = 2.50$. As shown in Fig. 6.9a, the control is less efficient for slip-loads greater than $0.35f_y$. Again, this effect is thought to be caused by the pulse-like type of the excitation. As shown in Fig. 6.9b, the spectra of the controlled systems show several peaks between 1.2 and 1.8Hz (with significantly larger amplitudes for the higher slip-load, $f_{p,i}/f_{y,i} = 2.50$), which indicates activation/deactivation of the dampers in the three systems. The reductions, then, are related to the amount of energy dissipated, which was higher for the system with $f_{p,i}/f_{y,i} = 0.35$. In Fig. 6.9c, the spectra of the systems also show peaks between 1.2 and 1.8Hz, with significantly larger amplitudes for the higher slip-load ($f_{p,i}/f_{y,i} = 2.50$), and one larger peak at 1.5Hz for the control with $f_{p,i}/f_{y,i} = 0.65$. The optimum control ($f_{p,i}/f_{y,i} = 0.35$) shows smaller amplitudes, which drop as the frequency increases, suggesting a continuous state of activation.

Finally, a comparison of the top floor displacements for the medium-rise RC frame under Loma Prieta with a PGA of 0.55g is shown in Fig. 6.10a. There was a reduction of the displacements using the control systems, but remarkably better for the slip-load of $0.35 f_{y,i}$. In the spectra of Figs. 6.10b and c, the predominant amplitude for the bare frame and control systems with slip-loads of $0.35 f_{y,i}$ and $0.65 f_{y,i}$ corresponds to the bare frame's fundamental mode at 0.50Hz, whereas the control with highest slip-load $(f_{p,i}/f_{y,i} = 2.50)$ shows the largest amplitude at 1.0Hz, which corresponds to the first frequency of a fully-braced system. In the case of acceleration, the systems with $f_{p,i}/f_{y,i} = 0.35$ and 0.65 show several peaks of small amplitude at different frequencies, including those of the bare and braced frame. This makes evident the mechanism of the passive control, which allows the frequencies of the structure to vary between those of a bare frame and those of fully and partially braced frames.
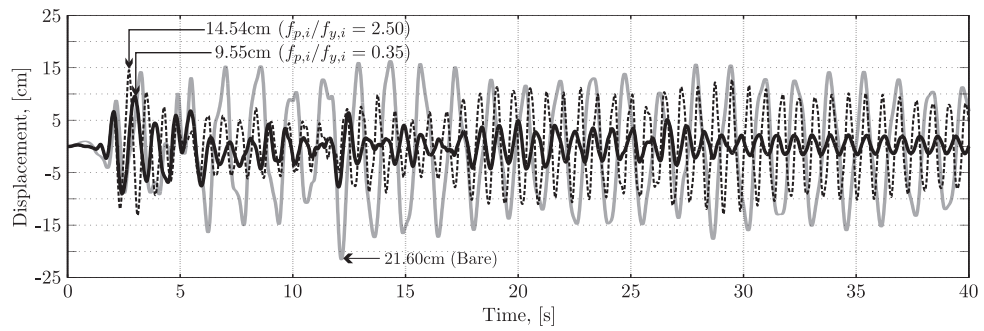
a) Time history of top floor displacement
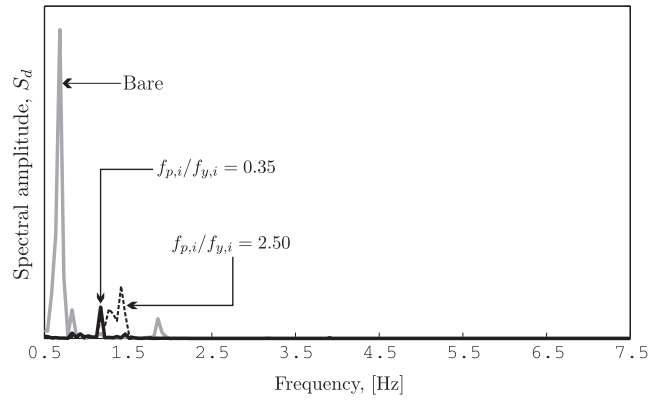
b) Spectral amplitude of top floor displacement
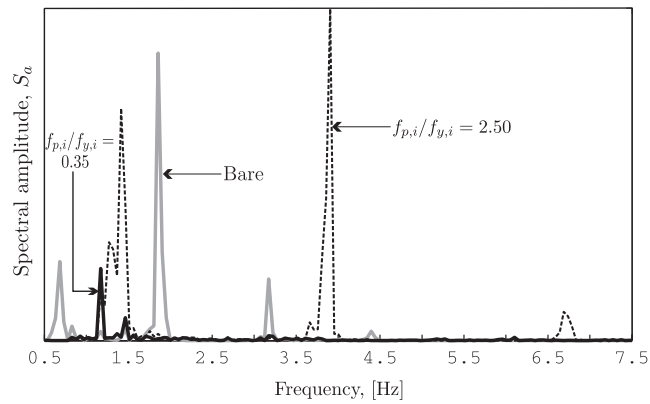
c) Spectral amplitude of top floor acceleration

FIGURE 6.7: Low-rise steel frame: Spectral amplitude of top floor displacement and acceleration, under El Centro (PGA=0.35g).
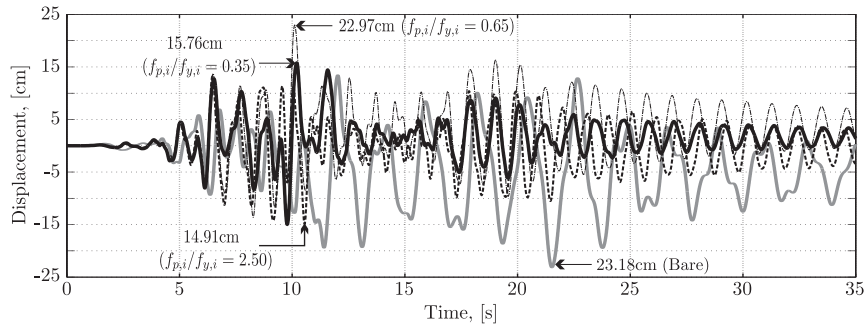
a) Time history of top floor displacement
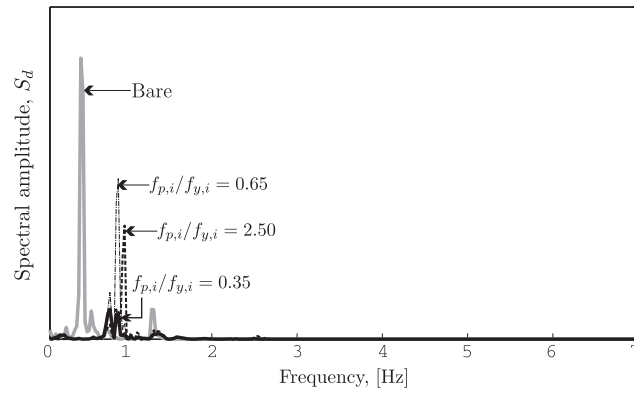
b) Spectral amplitude of top floor displacement
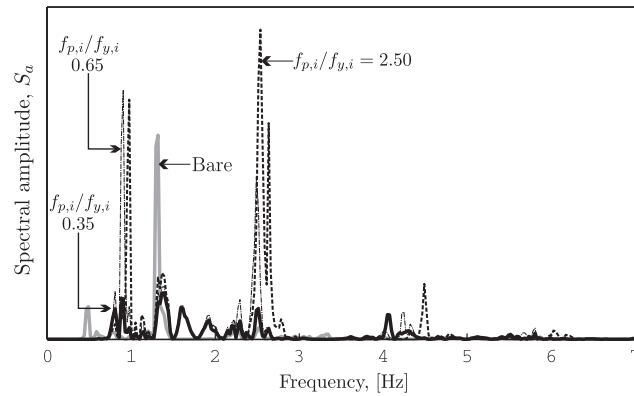
c) Spectral amplitude of top floor acceleration

FIGURE 6.8: Medium-rise steel frame: Spectral amplitude of top floor displacement and acceleration, under Northridge (PGA=0.55g).
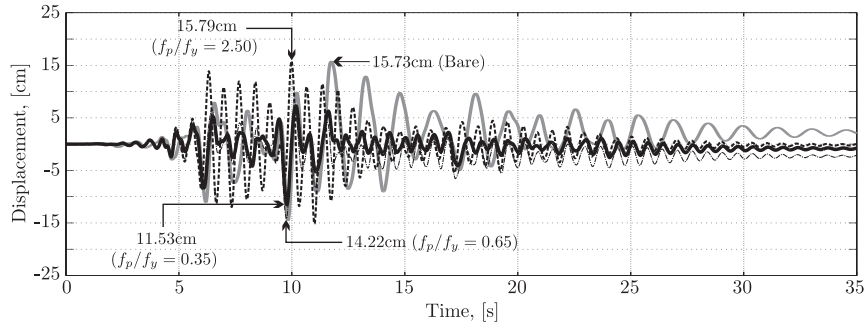
a) Time history of top floor displacement
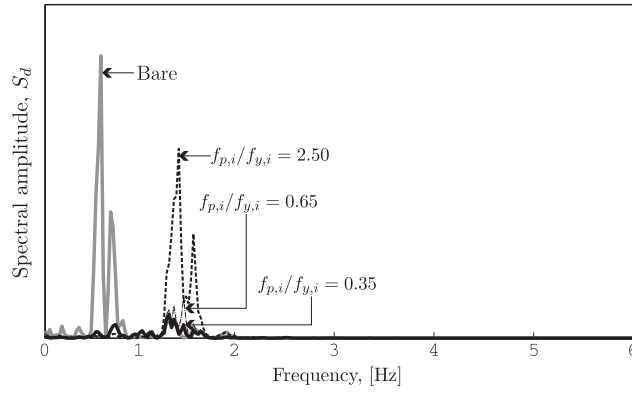
b) Spectral amplitude of top floor displacement
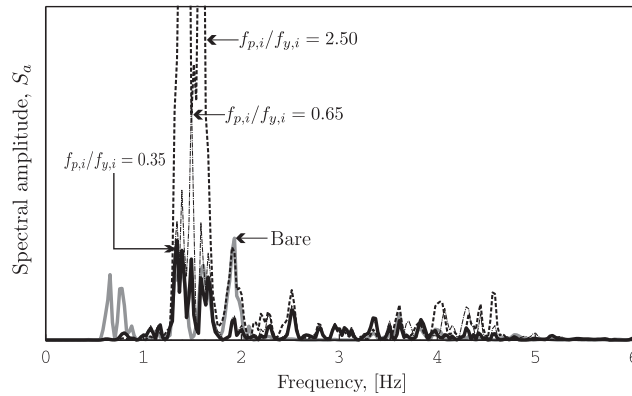
c) Spectral amplitude of top floor acceleration

FIGURE 6.9: Low-rise RC frame: Spectral amplitude of top floor displacement and acceleration, under Northridge (PGA=0.55g).
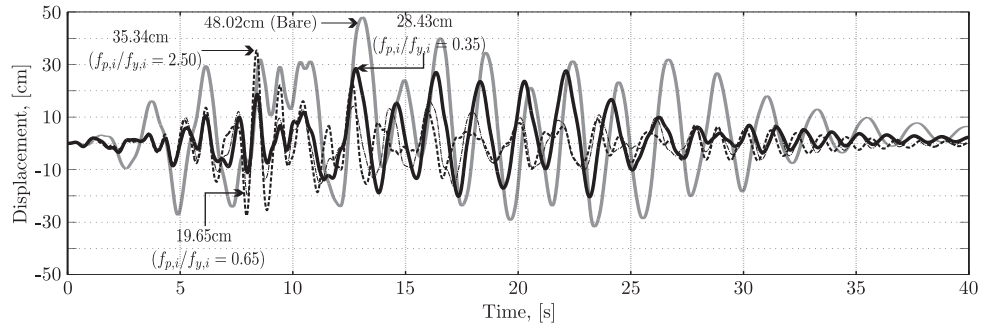
a) Time history of top floor displacement
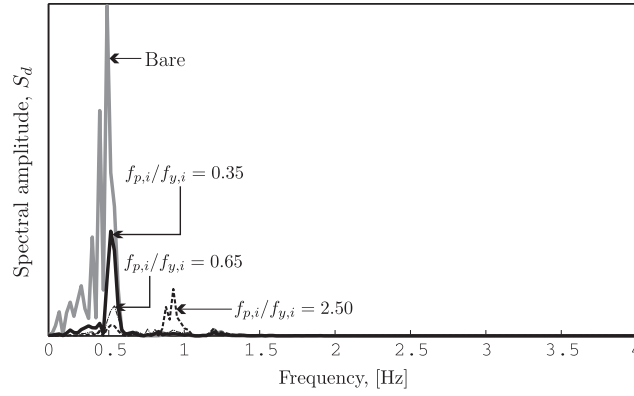
b) Spectral amplitude of top floor displacement
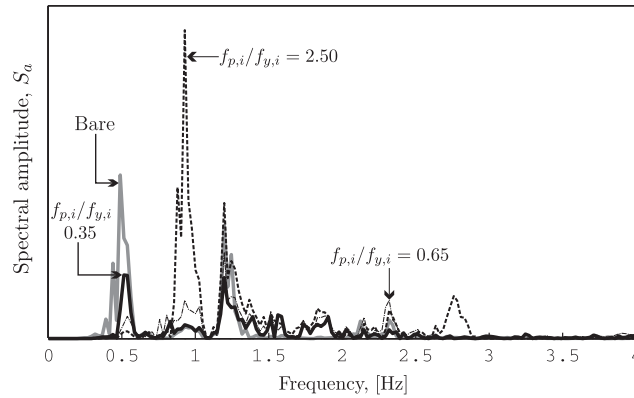
c) Spectral amplitude of top floor acceleration

FIGURE 6.10: Medium-rise RC frame: Spectral amplitude of top floor displacement and acceleration, under Loma Prieta (PGA=0.55g).

6.4 Concluding remarks

In this Chapter, a methodology for determining the capacity of passive dampers, including stiffness and slip-load, was presented. Such determination is based on structural properties of the bare frame, and thus it is independent of the predominant frequencies of the excitation source. The stiffness of the devices was proposed to be higher than the corresponding stiffness of the inter-storey where the damper is located. The slip-load $f_{p,i}$ was determined proportionally to the inter-storey yield load $f_{y,i}$, as the ratio $f_{p,i}/f_{y,i}$, which varied between 0 and 2.5. A value equal to 0 represented a bare frame condition, and 2.5 represented a fully-braced, or close to fully-braced frame condition.

In general, the response of the bare frames was reduced by including the passive control system. However, the results indicated that there is not a unique value of optimum slip-load, which would allow for the maximum response reductions, for all the earthquakes. Instead, there is a range of ratios $f_{p,i}/f_{y,i}$ between 0.25 and 0.65 that produced good response reductions for all the frames, under all excitations.

The immediate effect of introducing a control system was to increase the stiffness of the bare frame. This also produced an increase in the level of shear forces and axial loads at the base of the building. However, for a certain combination of reduction of the frame's deformation and low slip-loads, it is possible to reduce the force demand in the structure.

The proportions of energy dissipated during the earthquakes were also affected by using the control system. For the same range of ratios $f_{p,i}/f_{y,i}$ between 0.25 and 0.65, most of the energy was dissipated through the dampers, rather than by plastic hinges at the beams.

Finally, the mechanism of the control systems was analysed in frequency domain, by means of Fourier spectra of the frames' top floor displacement and acceleration. It was noticed that by introducing the control systems into the structure, there is a variation in the vibrational frequencies of the bare frame, which can avoid resonance conditions by shifting away from the predominant frequencies of the excitation. In the spectra shown in Figs. 6.7 to 6.10, it can be seen that the control system may vibrate in frequencies similar to a bare frame, a fully-braced frame and intermediate, partially braced frames.

Increased energy dissipation capacity is always beneficial, but the frequency response suggests that large differences in performance can be achieved by altering the dynamic characteristics of the frame during the earthquake.

Chapter 7

Semiactive control using existing algorithms

7.1 Introduction

Several algorithms existing in the literature were described in Section 2.7 (Chapter 2). A selection of those algorithms, including the modulated homogeneous friction control (Inaudi, 1997), the linear and smooth boundary layer controllers (He et al., 2003) and the Tri-D control (Chen and Chen, 2004c), were implemented in the program *ConStruc*. The performance of these control algorithms was evaluated by simulating the response of multi-storey buildings under a range of different earthquakes.

Those semiactive controllers were expected to show better performance than the passive systems, as a result of increased slippage of the connections, which is caused by modifying the slip-loads during the earthquake excitation. This enhanced slippage was expected to produce an increase of the damping in the structural system, which generally leads to smaller seismic responses.

The efficiency of those controllers was shown analytically and/or experimentally in the literature (Section 2.8). In those studies, the controllers were implemented in different structures, including 6-storey frame (Inaudi, 1997) for the MHF control, 3-storey frames (He et al., 2003; Ng and Xu, 2007) for the LBL and SBL, and a 20-storey frame (Chen and Chen, 2004c; Ng and Xu, 2007) and an experimental 12-storey scaled frame (Xu and Ng, 2008) for the SBL and Tri-D algorithms.

The efficiency of the four controllers was also investigated in this research project. Initially, a study to identify the effect of the parameters involved in each control law was

performed. In the study, non-linear simulations of the seismic response of the low-rise (6-storey) steel and medium-rise (10-storey) RC frames were performed. From the results, a feasible set of control parameters for each one of the four bare frames was identified. The set of six earthquakes described in Chapter 5 were exerted in those simulations. The results, as they are shown in this Chapter, confirm the efficiency of the control systems in reducing the seismic response of the frames.

7.2 Implementation of algorithms in *ConStruc*

The four control algorithms were implemented in the program *ConStruc* by means of the module **Control Strategy** (Fig. 4.5 on page 46). As described in Section 4.3, the control systems were implemented using a *feedback* strategy in which the information required by each algorithm (i.e. the local deformation δ_i, in this investigation), was *fed* by the main module of the program (i.e. the Newmark-β procedure). The rate of local deformation $\dot{\delta}_i$ across each damper i was calculated within the corresponding control sub-routine, where the appropriate control law was also applied to determine the variable control force $f_{s,i}(t)$, whose value was then returned to the main program.

The flow charts of the control sub-routines (as programmed in *ConStruc*), corresponding to the MHF, LBL, SBL and Tri-D algorithms are shown in Figs. 7.1 to 7.3, whereas the programming algorithms are presented in Tables 7.1 to 7.4. It should be noted that the block *Input data* shown in Figs. 7.1 to 7.3, indicates the input of pre-set parameters required by each controller (e.g. sampling time, friction coefficients, gain factors and/or initial slip-loads).
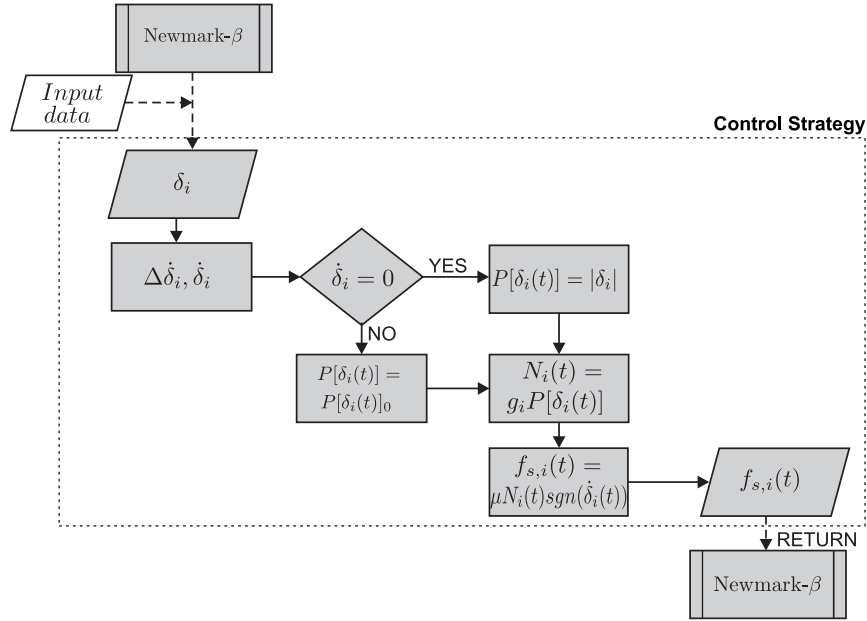
FIGURE 7.1: Flow chart of modulated homogeneous control (MHF).

TABLE 7.1: Modulated homogeneous friction control (MHF), programmed in *ConStruc*.

1. Initial time of analysis, t_0

   (a) Input data:
       Gain factor, g_i
       Sampling time: t_s

   (b) Initial deformation and velocity: $\delta_{0,i} = 0, P[\delta_i(t)]_0 = 0, \dot{\delta}_{0,i} = 0$

2. At every sampling time

   (a) Calculate the current velocity across the damper i:
       $\rightarrow \quad \Delta\dot{\delta}_i = \dfrac{\delta_i - \delta_{0,i}}{t_s}, \text{and } \dot{\delta}_i = \dot{\delta}_{0,i} + \Delta\dot{\delta}_i$

   (b) Check the velocity to determine if there is a local peak of deformation:
       $\rightarrow \quad$ if $\dot{\delta}_{0,i} > 0 \quad$ and $\quad \dot{\delta}_i < 0$
       $\rightarrow \quad$ or $\dot{\delta}_{0,i} < 0 \quad$ and $\quad \dot{\delta}_i > 0$
       $\rightarrow \quad$ then $P[\delta_i(t)] = |\delta_i|$
       $\rightarrow \qquad\quad P[\delta_i(t)]_0 = P[\delta_i(t)]$
       $\rightarrow \quad$ else $P[\delta_i(t)] = P[\delta_i(t)]_0$
       $\rightarrow \quad$ end

   (c) Calculate the normal force: $\quad \rightarrow \quad N_i(t) = g_i P[\delta_i(t)]$

   (d) Calculate the new slip-load: $\quad \rightarrow \quad f_{s,i}(t) = \mu N_i(t) sgn(\dot{\delta}_i(t))$

   (e) Set $\delta_{0,i} = \delta_i, \dot{\delta}_{0,i} = \dot{\delta}_i$
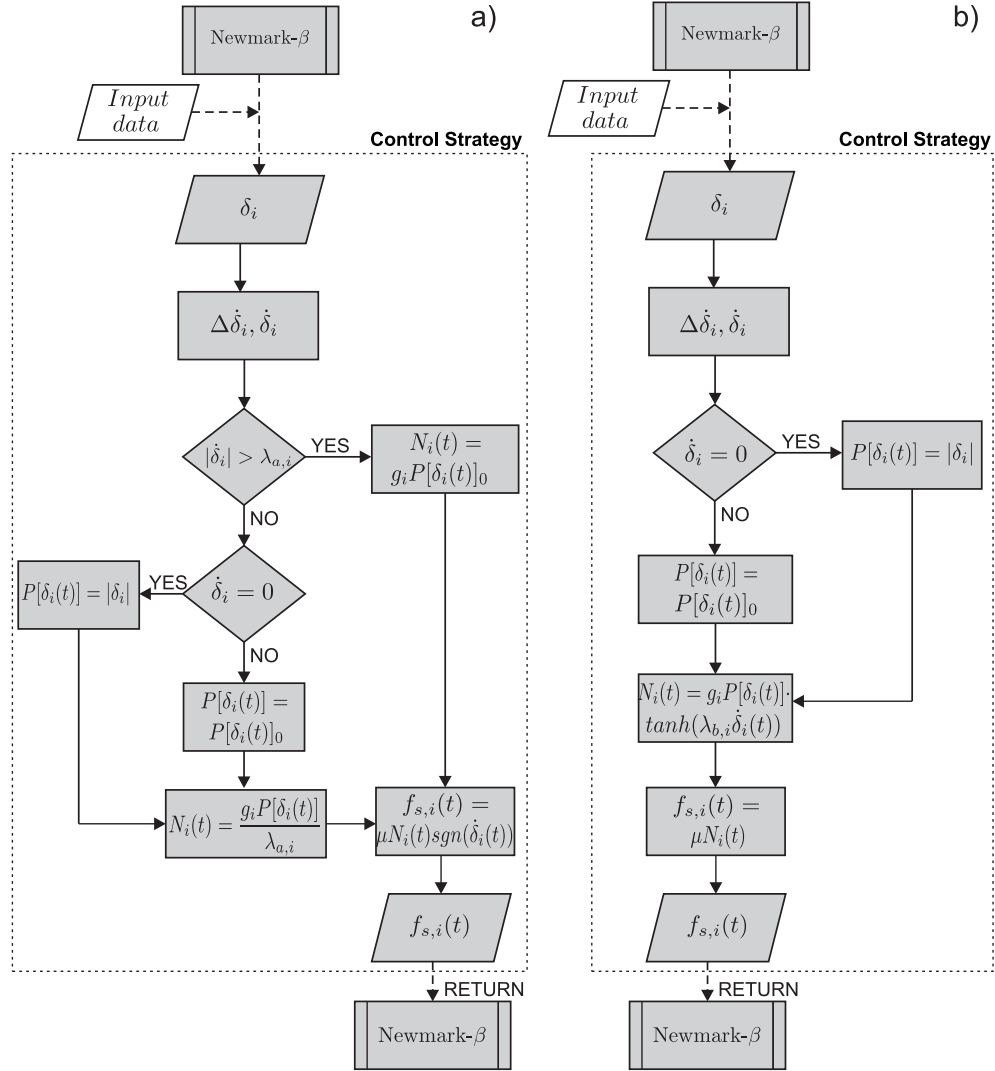
FIGURE 7.2: Flow chart of control with boundary layers: a) Linear boundary layer (LBL); b) Smooth boundary layer (SBL).

TABLE 7.2: Linear boundary layer (LBL) control, programmed in *ConStruc*.

1. Initial time of analysis, t_0

   (a) Input data:
       Gain factor, g_i
       Linear boundary layer, $\lambda_{a,i}$
       Sampling time: t_s

   (b) Initial deformation and velocity: $\delta_{0,i} = 0, \dot{\delta}_{0,i} = 0, P[\delta_i(t)]_0 = 0$

2. At every sampling time

   (a) Calculate the current velocity across the damper i:
       $\rightarrow \quad \Delta\dot{\delta}_i = \dfrac{\delta_i - \delta_{0,i}}{t_s}, \text{and } \dot{\delta}_i = \dot{\delta}_{0,i} + \Delta\dot{\delta}_i$

   (b) Determine the normal force, based on the value of current velocity:
       $\rightarrow \quad$ if $|\dot{\delta}_i| > \lambda_{a,i}$
       $\rightarrow \quad$ then $N_i(t) = g_i P[\delta_i(t)]_0$
       $\rightarrow \quad$ else
       $\rightarrow \qquad$ if $\dot{\delta}_{0,i} > 0 \quad$ and $\quad \dot{\delta}_i < 0$
       $\rightarrow \qquad$ or $\dot{\delta}_{0,i} < 0 \quad$ and $\quad \dot{\delta}_i > 0$
       $\rightarrow \qquad$ then $P[\delta_i(t)] = |\delta_i|$
       $\rightarrow \qquad\qquad P[\delta_i(t)]_0 = P[\delta_i(t)]$
       $\rightarrow \qquad$ end
       $\rightarrow \qquad N_i(t) = \dfrac{g_i P[\delta_i(t)]}{\lambda_{a,i}}$
       $\rightarrow \quad$ end

   (c) Calculate the new slip-load:
       $\rightarrow \quad f_{s,i}(t) = \mu N_i(t) sgn(\dot{\delta}_i(t))$

   (d) Set $\delta_{0,i} = \delta_i$, $\dot{\delta}_{0,i} = \dot{\delta}_i$

TABLE 7.3: Smooth boundary layer (SBL) control, programmed in *ConStruc*.

1. Initial time of analysis, t_0

    (a) Input data:
    Gain factor, g_i
    Smooth boundary layer, $\lambda_{b,i}$
    Sampling time: t_s

    (b) Initial deformation and velocity, $\delta_{0,i} = 0, \dot{\delta}_{0,i} = 0, P[\delta_i(t)]_0 = 0$

2. At every sampling time:

    (a) Calculate the current velocity across the damper i:
    $\rightarrow \quad \Delta\dot{\delta}_i = \dfrac{\delta_i - \delta_{0,i}}{t_s}, \text{and } \dot{\delta}_i = \dot{\delta}_{0,i} + \Delta\dot{\delta}_i$

    (b) Check the velocity to determine if there is a local peak of deformation:
    $\rightarrow \quad$ if $\dot{\delta}_{0,i} > 0 \quad$ and $\quad \dot{\delta}_i < 0$
    $\rightarrow \quad$ or $\dot{\delta}_{0,i} < 0 \quad$ and $\quad \dot{\delta}_i > 0$
    $\rightarrow \quad$ then $P[\delta_i(t)] = |\delta_i|$
    $\rightarrow \qquad P[\delta_i(t)]_0 = P[\delta_i(t)]$
    $\rightarrow \quad$ end

    (c) Calculate the normal force:
    $\rightarrow \quad N_i(t) = g_i P[\delta_i(t)] tanh(\lambda_{b,i}\dot{\delta}_i(t))$

    (d) Calculate the new slip-load:
    $\rightarrow \quad f_{s,i}(t) = \mu N_i(t)$

    (e) Set $\delta_{0,i} = \delta_i, \dot{\delta}_{0,i} = \dot{\delta}_i$
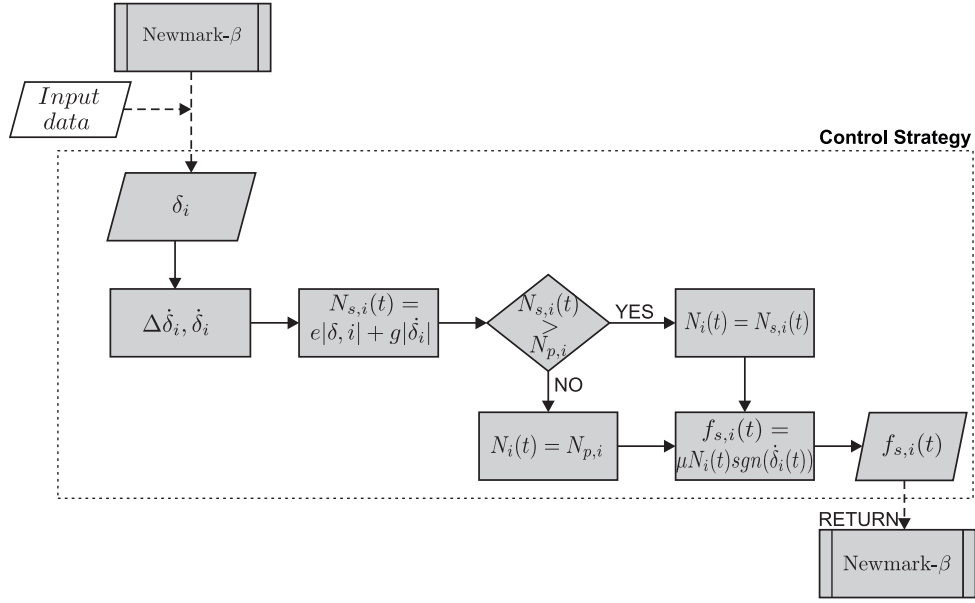
FIGURE 7.3: Flow chart of Tri-D control.

TABLE 7.4: Tri-D control, programmed in *ConStruc*.

1. Initial time of analysis, t_0

    (a) Input data:
        Gain factor, e
        Initial passive load, $N_{p,i}$
        Sampling time: t_s

    (b) Initial deformation and velocity: $\delta_{0,i} = 0, \dot{\delta}_{0,i} = 0$

    (c) Gain factor ratio $e/g = 2\pi f_f$

2. At every sampling time:

    (a) Calculate the current velocity across the damper i:
        $\rightarrow \quad \Delta\dot{\delta}_i = \dfrac{\delta_i - \delta_{0,i}}{t_s}, \text{and } \dot{\delta}_i = \dot{\delta}_{0,i} + \Delta\dot{\delta}_i$

    (b) Calculate the displacement-velocity dependant normal force:
        $\rightarrow \quad N_{s,i}(t) = e|\delta_i| + g|\dot{\delta}_i|$

    (c) Determine the new normal force:
        $\rightarrow \quad$ if $N_{s,i}(t) > N_{p,i}$
        $\rightarrow \quad$ then $N_i(t) = N_{s,i}(t)$
        $\rightarrow \quad$ else $N_i(t) = N_{p,i}$
        $\rightarrow \quad$ end

    (d) Calculate the new slip-load:
        $\rightarrow \quad f_{s,i}(t) = \mu N_i(t) sgn(\dot{\delta}_i(t))$

    (e) Set $\delta_{0,i} = \delta_i, \dot{\delta}_{0,i} = \dot{\delta}_i$

7.2.1 Verification of functionality of the controllers

The functionality of the controllers was verified by analysing a one storey, one bay frame with one friction damper, subject to a sinusoidal excitation with amplification and decay, as shown in Fig. 7.4. For simplicity, the sub-index i was removed from the control parameters, since $i = 1$. The MHF control was used with two gain factors g of 20kN/cm and 40kN/cm, and a unitary friction coefficient μ. As established by Eq. 2.3, the damper's slip-load was adjusted at every peak of the local deformation. The hysteretic curves shown in Fig. 7.5a, indicate the direct relation between the gain factor and the control force. It was possible to develop larger control forces by using the gain $g = 40$kN/cm, which led to smaller deformations, in comparison with the system using $g = 20$kN/cm. It should be noted, however, that larger control forces may also lock up the friction dampers.

The inclusion of the linear and smooth boundary layers into the homogeneous control produced a gradual variation of the slip-load, which eliminated the sharp corners of the hysteretic curves. Two linear layers $\lambda_a =$5cm/s and 15cm/s and two smooth layers $\lambda_b =$0.1 and 0.05 were used in combination with a gain factor $g = 20$kN/cm. As expected from the definition of the controllers in Eqs. 2.7 and 2.8, there was a gradual variation of the damper's slip-load, which was smoother for the SBL control with $\lambda_b = 0.05$ (Figs. 7.5b and c). A comparison of the time histories of slip-loads produced by the MHF, LBL and SBL controllers is shown in Fig. 7.6, where the sharp or gradual variation of the control force is evident for each system.

Reasonable results were also obtained when the Tri-D control was included in the frame model. In this case, the gain factors e and g (Eq. 2.11) were related by the ratio $e/g = 2\pi f_f$ (Chen and Chen, 2004c), where f_f represents the fundamental frequency of the frame. As this was only an exercise for verification of the controller, an arbitrary value of 10kN/cm was assigned to the gain factor e. Thus, the gain g was calculated as $10/2\pi f_f$. The passive slip-load $f_p = \mu N_p$ was assigned a value of 20kN. The resulting

a) Frame with control system   b) Input sinusoidal excitation
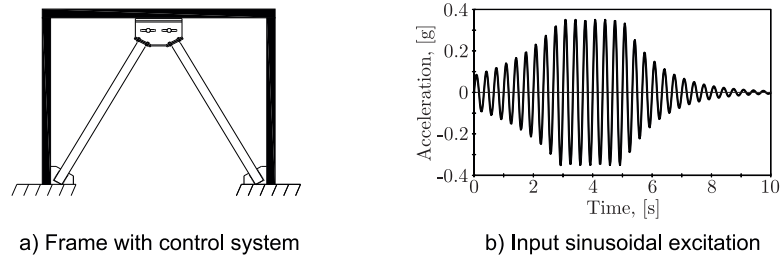
FIGURE 7.4: Frame and input excitation for verification of control systems.
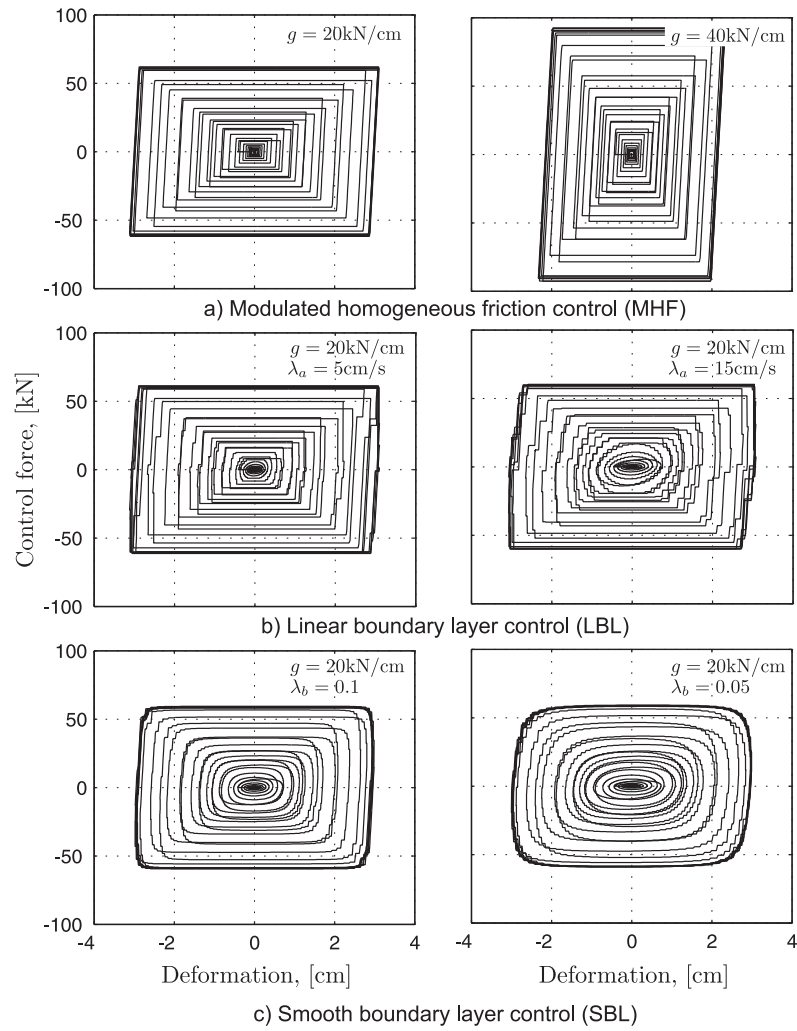
FIGURE 7.5: Hysteresis of damper using MHF, LBL and SBL controls.
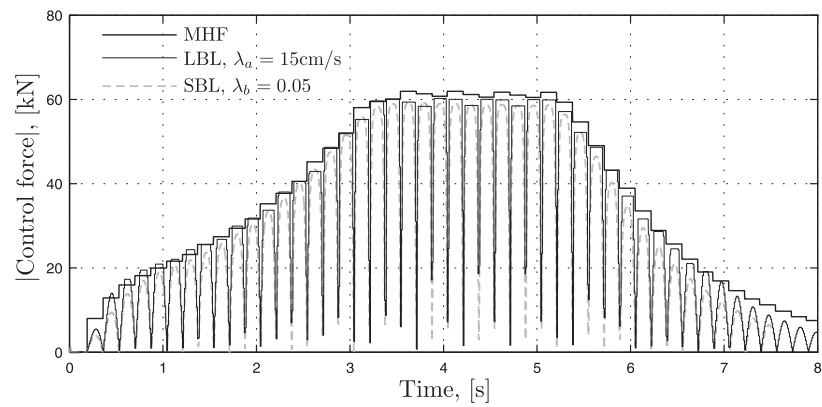
FIGURE 7.6: History of control forces using MHF, LBL and SBL controls.
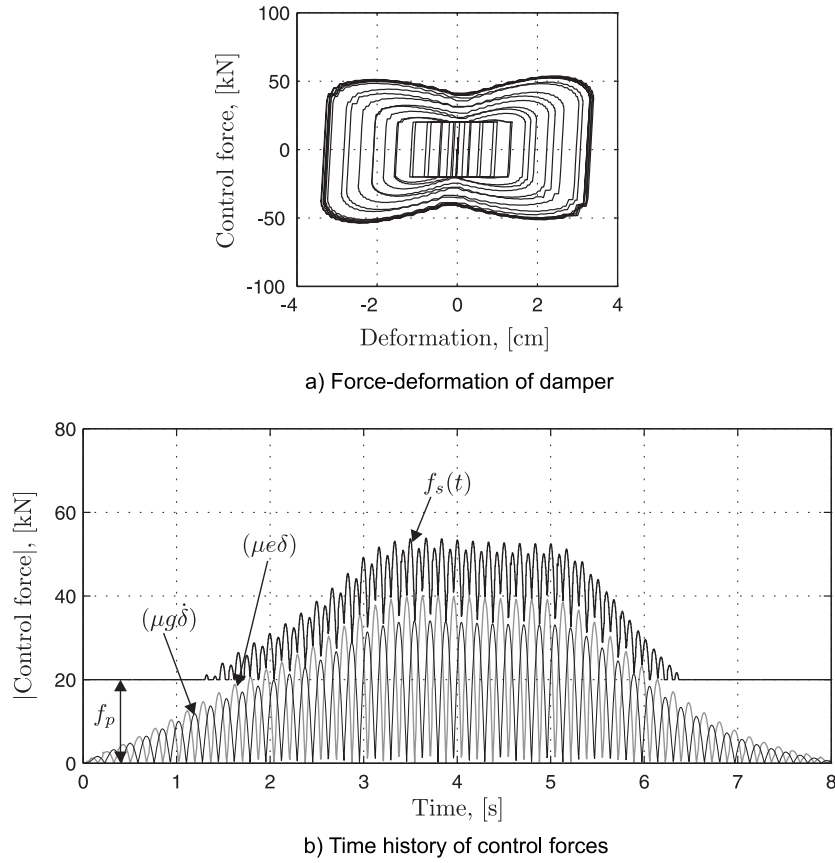
FIGURE 7.7: Control forces produced by Tri-D control.

hysteretic curves (Fig. 7.7a) showed an initial passive phase, corresponding to the slip-load f_p. Beyond this phase, the gradual variation of the slip-load due to the inclusion of forces related to the deformation and velocity (as indicated by Chen and Chen), can be noticed. The influence of each term of Eq. 2.11 in the control force can be observed in the time histories shown in Fig. 7.7b, where the control force $f_s(t)$ indicates the accumulation of the force produced by each term.

7.3 Parametric study of existing decentralised controllers

7.3.1 Definition of parameters

The influence of the control parameters (i.e. gain factors, boundary layers and/or initial passive load) in the performance of each control system was investigated by means of non-linear simulations. In the simulations, the four controllers were applied to the low-rise (6-storey) steel frame and the medium-rise (10-storey) RC frame, subjected to six

TABLE 7.5: Control parameters for study of existing *decentralised* controllers.

Controller	Frame	Gain g or e [1] [kN/cm]	λ_a [cm/s]	λ_b	f_p [f_p/f_y]
MHF	All	98.1, 490.5, 981	–	–	–
LBL	Low-rise steel Med-rise RC	98.1, 490.5, 981	8, 16, 24 6, 12, 18	–	–
SBL	All	98.1, 490.5, 981	–	1, 5, 10	–
Tri-D	Low-rise steel Med-rise RC frame	375, 1125, 1500 70, 135, 270	–	–	0.05, 0.15

Note 1. Gain g for MHF, LBL and SBL controllers, and gain e for Tri-D control.

different earthquakes: El Centro (0.55g), Northridge (0.35g), Kobe (0.82g), Loma Prieta (0.65g), Imperial Valley (0.70g) and Taft (0.22g). Depending on the control algorithm, different values were assigned to the control parameters, as summarised in Table 7.5.

Two values of the gain factor g_i used in the MHF control were similar to those used by Inaudi (1997) in his study, i.e. 98.1kN/cm and 490.5kN/cm. Also, for the purposes of this investigation, a third gain factor was defined as 981kN/cm, equivalent to 10 times the original smallest factor.

For the LBL and SBL controllers, the gain factors were assumed to be the same as for the MHF control. According to He et al. (2003), the *thickness* of the linear layer $\lambda_{a,i}$ in the LBL control should be a small value in the vicinity of zero velocity. In their study, those authors used layers in the order of 20cm/s for a base isolated building and 10cm/s for a 3-storey frame with dampers in each floor. In the present investigation, the *thickness* of the layer was determined as the ratio $\lambda_{a,i}/|\bar{\dot{x}}_{top}|$, where the variable $\bar{\dot{x}}_{top}$ represents the average of the top floor's maximum velocity, when the bare frame was subjected to the earthquakes mentioned before. Then, the *thickness* of the layer was defined as 5, 10 and 15% of the velocity, i.e. $\lambda_{a,i}/|\bar{\dot{x}}_{top}| = 0.05$, 0.10 and 0.15, resulting in $\lambda_{a,i}$ values of 8, 16 and 24cm/s (low-rise steel frame) and 6, 12 and 18cm/s (medium-rise RC frame).

The influence of the parameter $\lambda_{b,i}$ was studied by Ng and Xu (2007), who used the SBL algorithm to control the response of a building complex comprising a 20-storey building and a 3-storey podium. In their study, the authors used values for $\lambda_{b,i}$ of 5, 10 and 15. They concluded that the layer had only a minor influence on the seismic response of those structures, especially for the high-rise building. In the present investigation, the influence of the parameter in the seismic response of the 6- and 10-storey frames was investigated using three different $\lambda_{b,i}$ values of 1, 5 and 10.

In the case of the Tri-D control, two values of the initial slip-load $f_{p,i}$ were defined as 5 and 15% of the yield load $f_{y,i}$ corresponding to the ith storey where the dampers were located. In the case of the low-rise steel frame, as two dampers were installed on

every floor, each device carried half of that initial slip-load (i.e. $0.025f_{y,i}$ and $0.075f_{y,i}$, respectively). The selection of these values was based on the low initial slip-loads (around 10% of the maximum damper's slip-load) recommended by Chen and Chen (2004a), who determined that large initial passive slip-loads may lead to higher acceleration in the structure, due to the stick/slip effect in the damper.

Similar to the study by Chen and Chen (2004a), the ratio of gain factors e/g was defined as the circular frequency of the structure (Chen and Chen, 2004a), from where $e/g = 2\pi f_f$, with f_f indicating the fundamental frequency of the frame. An initial gain factor e_0, which would generate the maximum capacity of the damper at the time of maximum inter-storey deformation, was proposed as follows:

$$e_0 = \frac{\mu \bar{N}_p}{\bar{\delta}} \tag{7.1}$$

where $\mu \bar{N}_p$ represents the average of the maximum slip-load capacity of the dampers, which was defined as $f_{max,i} = 1.0f_{y,i}$. Again, for the low-rise steel frame, each damper carried half of that maximum load ($0.5f_{y,i}$). In Eq. 7.1, $\bar{\delta}$ represents the average of the maximum inter-storey deformations of the bare frame recorded in each earthquake.
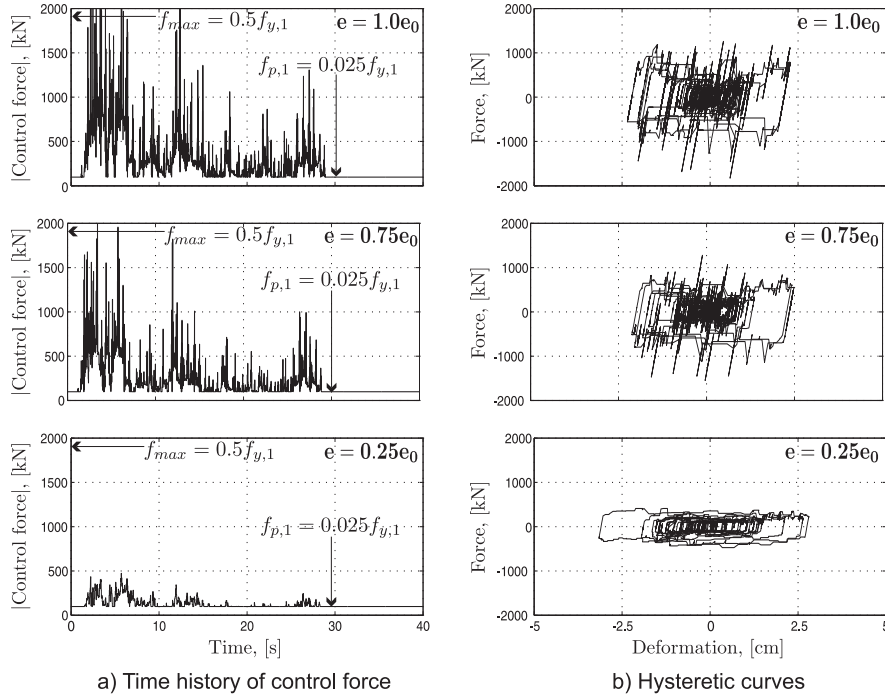
FIGURE 7.8: Control forces and hysteresis of damper 1 (ground floor) in the low-rise steel frame using Tri-D system with different gain factors; El Centro (0.55g) excitation.
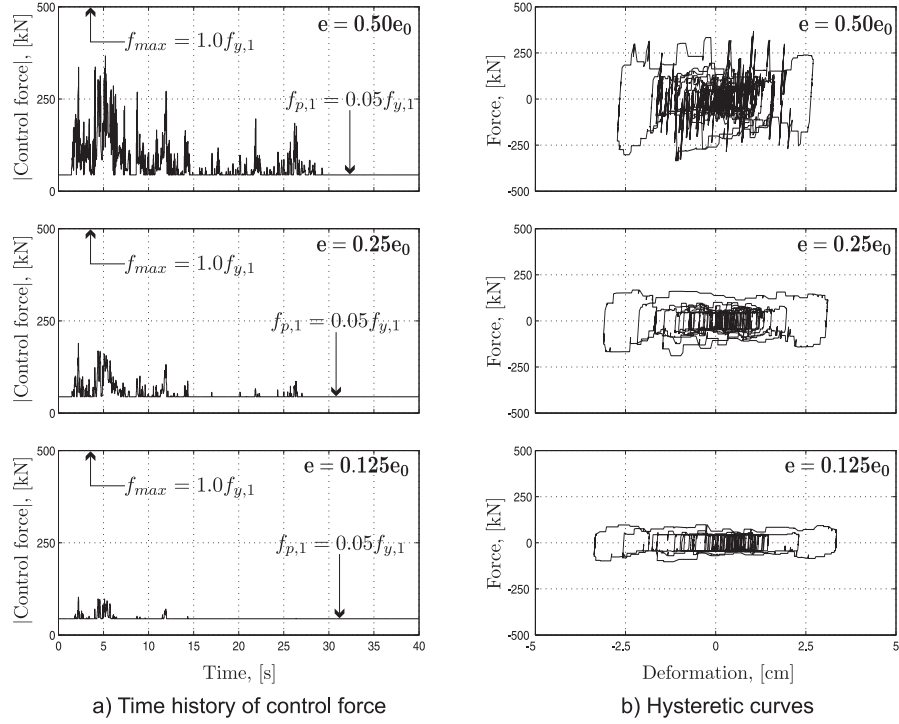
FIGURE 7.9: Control forces and hysteresis of damper 1 (ground floor) in the medium-rise RC frame using Tri-D control system with different gain factors; El Centro (0.55g) excitation.

After applying Eq. 7.1 for the low-rise steel frame, the value of e_0 was 1500kN/cm, considering a friction coefficient $\mu = 0.2$. To examine the effect of the gain factor in the control efficiency, two additional values for the gain e were defined as $0.75e_0$ and $0.25e_0$, resulting in 1125 and 375kN/cm, respectively. The gains $e = 1.0e_0$ and $e = 0.75e_0$ led to abrupt changes in the control force, which prevented a continuous activation of the damper. Furthermore, as shown in Fig. 7.8a, the control forces required by the system with $e = 1.0e_0$ and $e = 0.75e_0$ were often larger than the maximum capacity of each friction damper $(0.5f_{y,i})$, thus locking the devices and generating force spikes during the simulations, as shown in the force-deformation relation in Fig. 7.8b, for the frame under the El Centro earthquake (PGA=0.55g).

Following the same procedure for the medium-rise RC frame, the initial gain factor e_0 was calculated as 545kN/cm. In order to reduce the effect of the abrupt change during the seismic simulations observed in the steel frame, three smaller gains e were defined as $0.5e_0$, $0.25e_0$ and $0.125e_0$, which resulted in 270, 135 and 70kN/cm, respectively. As it can be observed in Fig. 7.9a, the control forces were smaller for each gain factor, but it also resulted in a more continuous, well defined hysteresis, as shown in Fig. 7.9b for the damper located in the ground floor, under the El Centro earthquake scaled to 0.55g.

7.3.2 Influence of control parameters on the performance of the systems

The influence of the control parameters on the performance of the control systems is shown in Figs. 7.10 and 7.11, as average ratios of controlled to uncontrolled response, in terms of displacements, accelerations and base shear.

For the low-rise steel frame, the ratios of controlled to uncontrolled (bare) top floor displacement (d_c/d_b) were reduced using higher gains in all the control systems, although such reduction was more significant for the MHF, LBL and SBL controllers (Fig. 7.10a). In the MHF algorithm, the displacement ratios were 0.95, 0.70 and 0.60 when gains g of 98.1, 490.50 and 981kN/cm were used, respectively. In the LBL and SBL algorithms, the increase of gain factors resulted in displacement ratios around 0.95, 0.70 and 0.60. In the case of the Tri-D controller, the ratio with the lowest gain was approximately 0.60, but it was further reduced to only 0.50 with the higher gains.

The *thickness* of the layers also influenced the displacements, although significantly only in the LBL control with medium and high gains (Fig. 7.10a). The layer $\lambda_{a,i}$ of 8cm/s produced smaller displacement ratios for both gains (0.70 and 0.65, respectively), whereas the layer of 16cm/s increased the ratios to 0.75 and 0.70, and the layer of 24cm/s increased them to 0.78 and 0.72. The influence of the parameter $\lambda_{b,i}$ was not significant, and similar reductions were obtained with any of the three layers ($\lambda_{b,i} = 1$, 5 and 10).

The initial passive load $f_{p,i}$ in the Tri-D control did not show a significant influence on the levels of reduction. Only a slight difference of about 5% could be observed for the lowest gain, with slightly smaller displacement when $f_{p,i} = 0.15f_{y,i}$ was used.

The efficiency of the controllers on top floor acceleration was also influenced by using different parameters, but such influence was only significant in the Tri-D control (Fig. 7.10b). The ratios a_c/a_b were approximately 0.85 for all gains, when the MHF control was used. In the case of the LBL algorithm, there was a small variability of less than 5% in the ratios produced by any of the gain factors. A small variability was also produced by the SBL control, although in this system there was a slightly higher influence of the layer *thickness* $\lambda_{b,i}$ when the high gain was included, which resulted in ratios of 0.82, 0.85 and 0.87 for $\lambda_{b,i} = 10$, 5 and 1, respectively. In the case of the Tri-D control, there was a significant influence of both the gain factor and the initial passive slip-load, which led to an increase of acceleration. In this controller, smaller accelerations were obtained when the higher initial slip-load was used, in comparison with the accelerations produced using the lower slip-load. In both cases, however, the ratios a_c/a_b increased with the gain factor. In the first case ($f_{p,i} = 0.15f_{y,i}$), the ratio increased from 0.82 to 1.0, whereas in the second case ($f_{p,i} = 0.05f_{y,i}$), this ratio increased from 0.84 to 1.2.
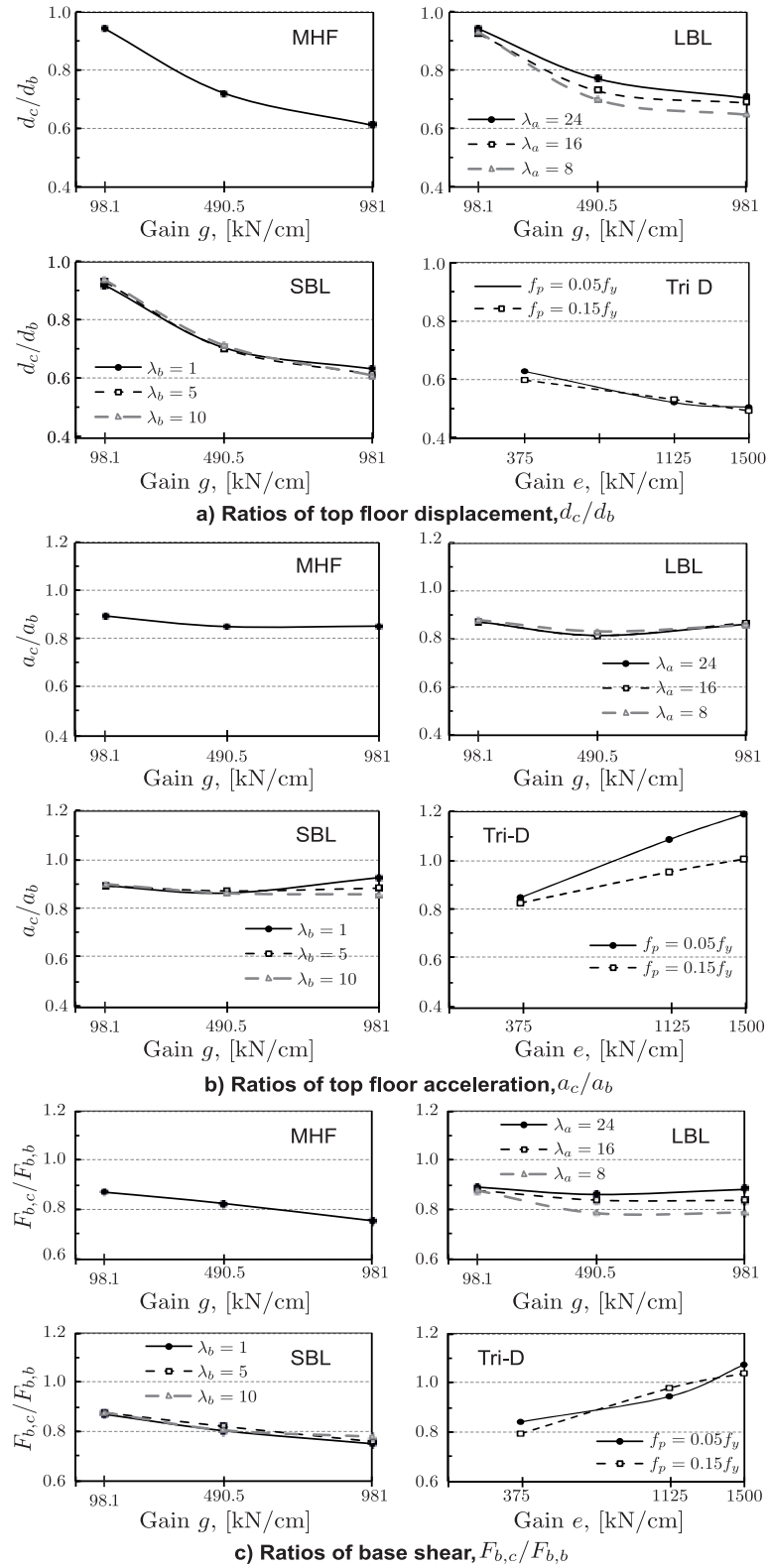
FIGURE 7.10: Low-rise steel frame: average ratios of response including control systems with different parameters.

The levels of base shear reduction in the low-rise steel frame were also influenced by the gain factor and other parameters already described. As it can be observed in Fig. 7.10c, the MHF, LBL and SBL controllers reduced the base shear using any of the gain factors. As indicated by the ratio $F_{b,c}/F_{b,b}$, similar levels of reduction were obtained for those three controllers, with ratios around 0.90 and 0.78 for the low and high gains, respectively. In the case of the LBL control, the parameter $\lambda_{a,i}$ also had an influence in the level of reduction, especially for the medium and high gains. For both factors, there was an increase of about 10% between the ratio produced by $\lambda_{a,i} = 8$ (i.e. 0.80) and that of $\lambda_{a,i} = 24$ (i.e. 0.90). In the case of the Tri-D control, when it was used in combination with the low, medium or high gain, the resulting ratios were around 0.80, 0.95 and 1.05, respectively, with very small variations between both levels of $f_{p,i}$.

For the medium-rise RC frame, as it can be seen in Fig. 7.11a, the top floor displacement was further reduced with higher gain factors, in all the controllers. In the case of the MHF algorithm, the ratios d_c/d_b varied from 0.95 to 0.72 for the low and high gains, respectively. In case of the LBL and SBL algorithms, it can be seen that both layers $\lambda_{a,i}$ and $\lambda_{b,i}$ did have an influence in the response. The ratios d_c/d_b varied from 0.95 to 0.80, for the LBL system, and from 0.95 to 0.68, for the SBL control, using the low and high gains. For both controllers, the maximum reductions were obtained using the high gain factor and $\lambda_{a,i} = 6$ or 12, and $\lambda_{b,i} = 5$ or 10, respectively. In the case of the Tri-D control, d_c/d_b varied between 0.90 and 0.80, for the low and high gains, respectively, with very small differences between the initial slip-loads.

The controllers were also slightly more efficient in reducing the accelerations when higher gains were used (Fig. 7.11b). In the case of the MHF, the ratios varied between 0.98 and 0.90 for the low and high gains. The ratios produced by the LBL and SBL were lower when the medium gain was used (around 0.90), but slightly increased when the higher gains were used. There was also an influence of the boundary layer, which led to some variations, more remarkable for the LBL algorithm with medium and high gains. In the case of the Tri-D control, neither the initial slip-load nor the gain factor influenced the acceleration, and the ratios were around 0.92.

Unlike the steel frame, the base shear of the controlled RC structure was either comparable to that of the bare frame, or increased for all the systems. As shown in Fig. 7.11c, the ratios $F_{b,c}/F_{b,b}$ varied between 0.98 (MHF system) and 1.25 (Tri-D system) for the low and high gains, respectively. This increment suggests that the inter-storey deformations in the frame were still significant, leading to high structural forces combined with the control forces. This agrees with the low levels of displacement reduction described before (Fig. 7.11a), which were around 33% for the MHF and SBL systems, and around 20% for the LBL and Tri-D controllers, respectively.

a) **Ratios of top floor displacement,** d_c/d_b

b) **Ratios of top floor acceleration,** a_c/a_b

c) **Ratios of base shear,** $F_{b,c}/F_{b,b}$
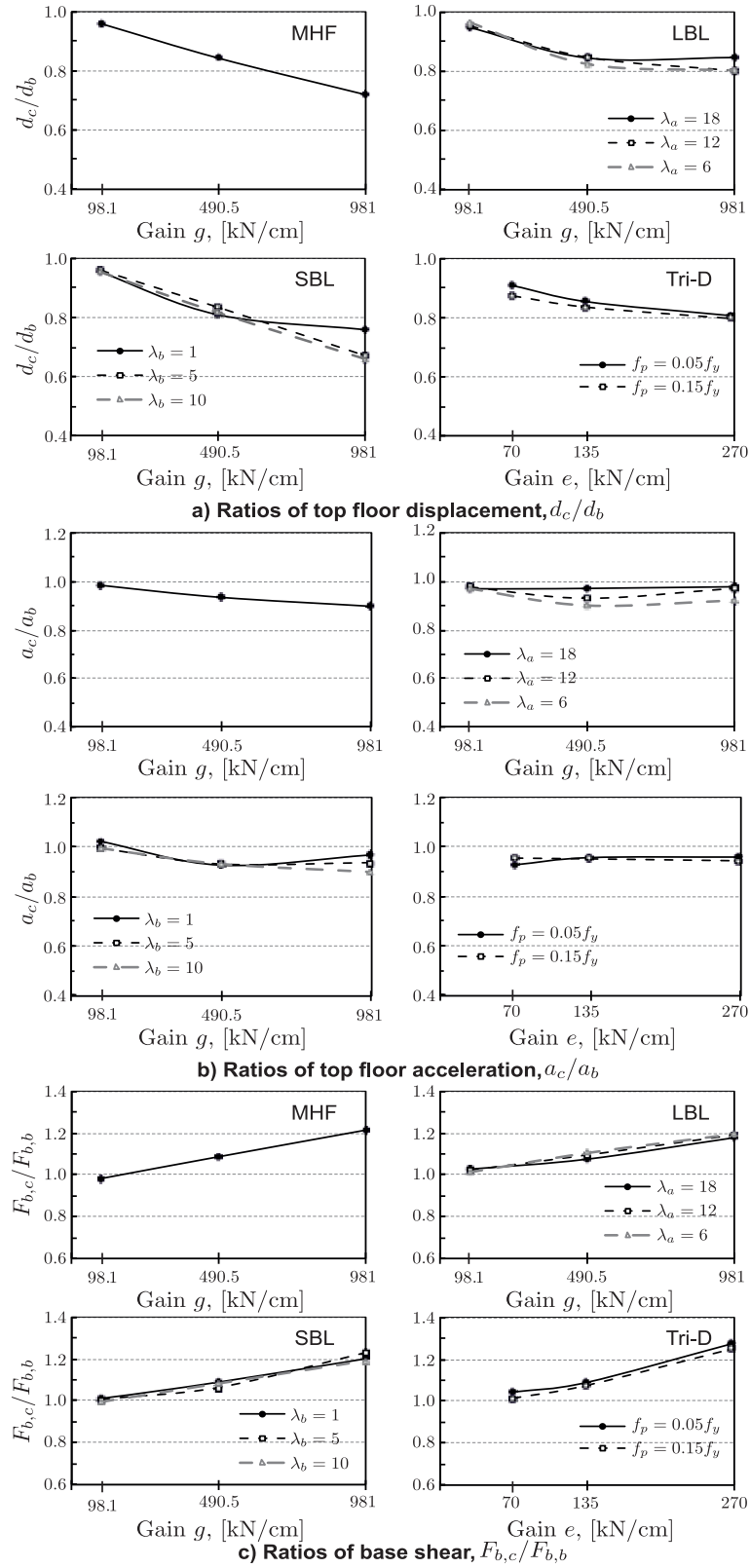
FIGURE 7.11: Medium-rise RC frame: Average ratios of response including control systems with different parameters.

7.4 Efficiency of decentralised controllers

After the investigation of the influence of control parameters, three controllers (MHF, SBL and Tri-D) were applied to the four multi-storey frames subjected to the El Centro, Northridge, Kobe, Loma Prieta, Imperial Valley and Taft earthquakes scaled to 0.35 and 0.55g. The LBL control was not applied to the structures because, as it was observed in the parametric study (Section 7.3), the performance was very similar to that of the SBL control, but it also showed more sensitivity to the *thickness* of the boundary layer $\lambda_{a,i}$.

The parameters selected for each controller were based on the study presented in the previous section. Three gain factors $g_i = 98.1$, 490.5 and 981kN/cm were included in the MHF and SBL systems. For the latter, a boundary layer $\lambda_{b,i} = 5$ was selected. In the case of the Tri-D system, the gain factor e was determined using the same methodology described in Section 7.3.1, applying the Eq. 7.1 to calculate an initial value e_0, which was then used to determine three different gains as $0.5e_0$, $0.25e_0$ and $0.125e_0$. Hence, the gains were 187.5, 375 and 750kN/cm for the low-rise steel frame; 655, 1310 and 2625kN/cm for the medium-rise steel frame; 50, 100 and 200kN/cm for the low-rise RC frame; and 65, 135 and 270kN/cm for the medium-rise RC frame. The initial slip-load $f_{p,i}$ was defined as $0.15f_{y,i}$, in all cases.

To measure the efficiency of control systems, a series of evaluation indices was proposed by Ohtori et al. (2004). Those indices evaluated different aspects of the structural response and of the performance of the controller. The evaluation was divided in four categories: building response (drift, acceleration and shear), building damage (ductility demand, energy dissipated and number of plastic hinges in the beams), demand in control devices (control force, stroke and power) and control strategy requirements (number of devices, number of sensors and computational requirements). Based on those indices, six indices were adopted for this study: three for building response, two for building damage and one for demand in control devices.

- **Building response indices**

The first three indices were used to evaluate the level of reduction of the structural response. Those indices are given by the following expressions:

$$J_1 = \max \left(\frac{\max \dfrac{|\delta_{c,i}|}{h_i}}{\max \dfrac{|\delta_{b,i}|}{h_i}} \right) \tag{7.2}$$

$$J_2 = \max\left(\frac{\max |\ddot{x}_{c,i}|}{\max |\ddot{x}_{b,i}|}\right) \tag{7.3}$$

$$J_3 = \max\left(\frac{\max |F_{b,c}|}{\max |F_{b,b}|}\right) \tag{7.4}$$

In the Eqs. 7.2 and 7.3, $|\delta_{c,i}|/h_i$ and $|\delta_{b,i}|/h_i$ represent the absolute values of the inter-storey drift of level i in the controlled and uncontrolled (bare) frames, respectively. The terms $|\ddot{x}_{c,i}|$ and $|\ddot{x}_{b,i}|$ are the absolute values of the maximum acceleration at level i (controlled and bare frames, respectively).

In the Eq. 7.4, the term $|F_{b,c}|$ represents the absolute value of the shear force at the base of the controlled frame, and $|F_{b,b}|$ is the absolute value of the maximum shear force at the base of the bare frame.

- **Building damage indices**

The distribution of the energy dissipated during the earthquake is a good indicator of the damage in the building. Thus, two indices for evaluation of the damage in the building are given by the following expressions:

$$J_4 = \left(\frac{E_h}{E_i}\right) \tag{7.5}$$

$$J_5 = \left(\frac{E_c}{E_i}\right) \tag{7.6}$$

The energy dissipated through damage in the beams is quantified by E_h, whereas the amount of energy dissipated through the frictional mechanism of the dampers is given by E_c. The term E_i represents the total energy exerted by the earthquake.

- **Control force indices**

Another factor evaluated in this investigation was the demand in the friction connections. The index for assessing the control force required by the algorithm is given by the following expression:

$$J_6 = \max\left(\frac{\max |f_{s,i}|}{f_{y,i}}\right) \tag{7.7}$$

where $f_{s,i}$ represents the control force required by the control algorithm, and $f_{y,i}$ is the storey shear force that creates the first plastic hinge in the upper beams of the corresponding storey.

7.4.1   Evaluation of building response

In general, lower values of the evaluation indices are desirable, as this would indicate a better performance of the control system and higher level of response reduction. The plots of the average indices $\bar{J}_1$ to $\bar{J}_3$ corresponding to the earthquakes scaled to 0.35g are shown in Fig. 7.12.

In average, all control systems were able to reduce the inter-storey deformation of the frames. The indices of reduction $\bar{J}_1$ (Fig. 7.12a), however, varied for each control system and were slightly better for the Tri-D control. The MHF and SBL systems were very efficient for the low-rise steel frame, with indices $\bar{J}_1$ of 0.87, 0.70 and 0.63 for the low, medium and high gains, respectively. Both systems also reduced the response in the medium-rise steel frame and low-rise RC frame, resulting in indices of 0.95 and 0.87, respectively, using the medium gain factor, and 0.92 and 0.80, using the high gain. In the medium-rise RC frame, the index $\bar{J}_1$ was 0.88 and 0.99, using the MHF with medium and high gain, respectively, and 0.90 and 0.83, using the SBL with medium and high gain. In the case of the Tri-D control, the indices did not vary significantly with the gain factors. The indices were around 0.58 for the low-rise steel frame, 0.64 for the medium-rise steel frame, and 0.74 for the medium-rise RC frame. In the case of the low-rise RC frame, the index $\bar{J}_1$ was around 0.80 for the low and medium gain, but the value dropped to 0.71 when the gain factor was used.

There was a variability in the average peak acceleration of the controlled frames (index $\bar{J}_2$), which was either increased of reduced, depending on the control system and the gain factor used (Fig. 7.12b). For the low-rise steel frame, the MHF control resulted in indices $\bar{J}_2$ of 0.87, 0.78 and 0.82, for the low, medium and high gain factors, respectively. Very similar values were obtained with the SBL control using low and medium gains. However, when the high gain factor was used, the index increased to 1.05. In the case of the medium-rise steel frame, the indices were almost the same for both controllers, resulting in 0.87 (low gain factor) and 0.76 (medium and high gain factors). In the case of the RC frames, both the MHF and SBL systems slightly reduced the acceleration when the low gain was used, resulting in $\bar{J}_2 = 0.98$, which was almost the same for the low and medium-rise frame. The two control systems, however, were inefficient when the higher gains were used. The MHF led to indices of 1.02 and 1.31 for the low-rise RC frame, and 1.20 and 1.42 for the medium-rise RC frame. The SBL led to indices of
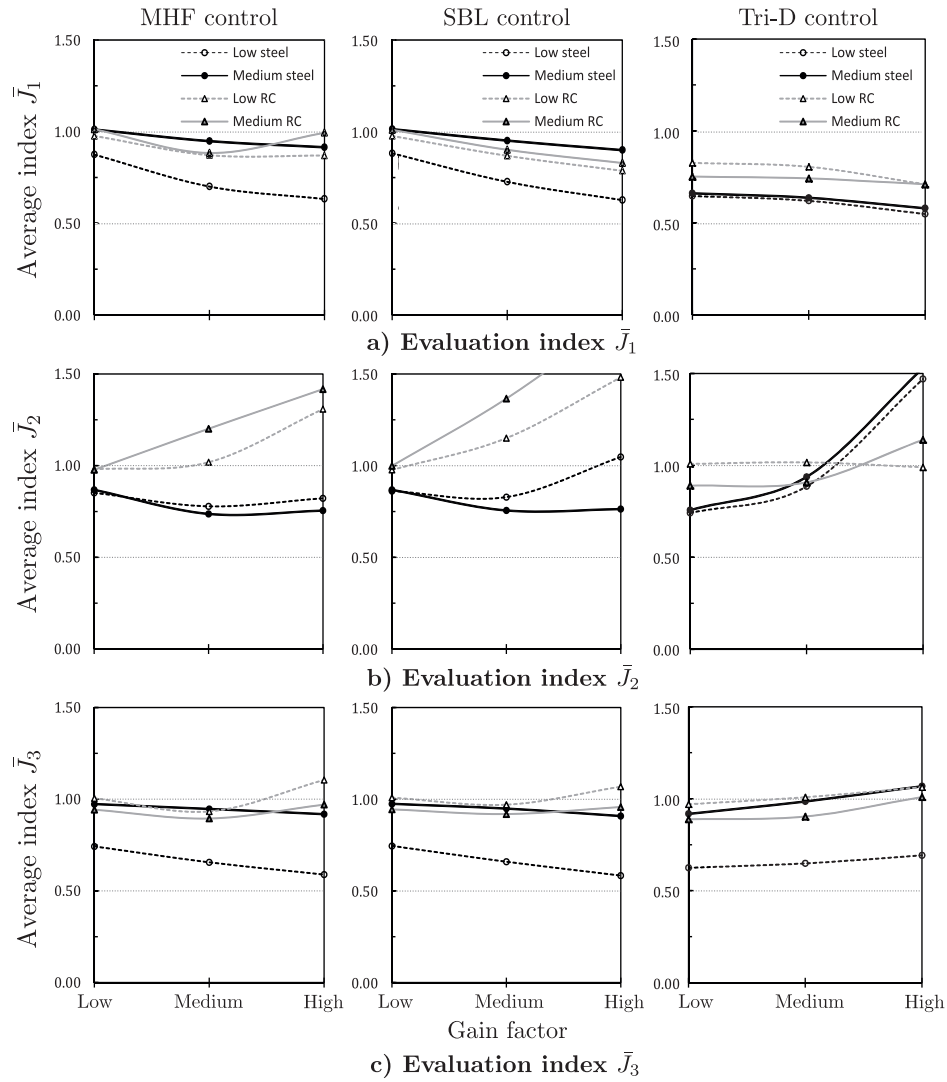
FIGURE 7.12: Indices $\bar{J}_1$ to $\bar{J}_3$ of the control systems included in the frame structures subjected to earthquakes scaled to 0.35g.

1.15 and 1.48 for the low-rise RC frame, and 1.37 and 1.8 for the medium-rise frame. In the case of the Tri-D control, the system with low and medium gain factors produced indices $\bar{J}_2$ of 0.74 and 0.89, respectively, for the low-rise steel frame; 0.76 and 0.91 for the medium-rise steel frame; 0.89 and 0.90 for the medium-rise RC frame; and around 1.0 for the low-rise RC frame. However, apart from the low-rise RC frame (whose index did not vary), the average indices of all other frames were increased to 1.47 (low-rise steel frame), 1.53 (medium-rise steel frame) and 1.14 (medium-rise RC frames), when the high gain factor was used.

The average index $\bar{J}_3$ (Fig. 7.12c) did not indicate significant increases of the shear force,

but important reductions in some cases. The smallest indices for any of the controllers were obtained for the low-rise steel frame. The indices were 0.74, 0.66 and 0.59 for the MHF system with low, medium and high gain, respectively, and were also very similar for the SBL control. In the case of the Tri-D system, the index was around 0.65, regardless of the gain factor. For all other frames, the three controllers produced similar indices. In the case of the MHF and SBL systems, the average index of the medium-rise frame was around 0.90, without significant variations between gain factors. Similarly, the indices of the medium-rise RC frame did not vary significantly with the gains, and were around 0.90. The indices of the low-rise RC frame, however, resulted in 1.01, 0.89 and 1.11, for the low, medium and high gains, respectively. In the case of the Tri-D control, the indices slightly increased with the gains, resulting for each gain in 0.89, 0.99 and 1.06 (medium-rise steel frame); 0.97, 1.01 and 1.06 (low-rise RC frame); and 0.87, 0.90 and 1.01 (medium-rise RC frame).

The performance indices J_1 to J_3 corresponding to the control systems with different gains are shown in Figs. 7.13 to 7.16, for each frame-earthquake system. In these figures, the indices corresponding to the excitations of the El Centro (cn40), Northridge (nr94), Kobe (ko95), Loma Prieta (lo89), Imperial Valley (iv79) and Taft (tf52) earthquakes scaled to 0.35g are shown in grey line, and the indices corresponding to the same earthquakes scaled to 0.55g are shown in black line. In most of the cases, all the control systems with medium and high gains were able to reduce the drift index J_1, when the frames were subjected to the earthquakes scaled to 0.35g. However, the efficiency of the systems was reduced for the earthquakes scaled to 0.55g, which may be attributed to the non-linear response of the main structure. The development of plastic hinges in the beams resulted in increase of energy dissipation in the main structure, but also reduced the lateral stiffness, leading to increased deformations.

In the case of the low-rise steel frame, the MHF and SBL systems with low gain ($g = 98.1$kN/cm) did not reduce the drift in the frame subjected to Northridge, Kobe and Taft excitations scaled to 0.55g (Fig. 7.13a). The system, however, was efficient for all other earthquakes, independently of the gain factor. The Tri-D control, on the other hand, produced indices J_1 smaller than 1.0, for any gain factor and for any earthquake scaled to either 0.35 or 0.55g.

The index J_2 (Fig. 7.13b) indicated an increase in the peak acceleration of the controlled frames, specially for Loma Prieta, Imperial Valley and Taft, using the MHF and SBL systems with the medium or higher gain factors. The Tri-D system was also not efficient when higher gain factors were applied, increasing the acceleration for the majority of the earthquakes.

FIGURE 7.13: Low-rise steel frame: Performance indices with existing control systems, for earthquakes scaled to 0.35g (grey line) and 0.55g (black line).

As it can be seen in Fig. 7.13c, the index J_3 indicated reductions of the base shear in most of the earthquakes, depending on the gain factor.

In the case of the medium-rise steel frame, the MHF and SBL systems were not efficient for the earthquakes scaled to 0.55g, but the Tri-D system produced reductions of the drift (index J_1) for both PGAs (Fig. 7.14a). The Tri-D system, on the other hand, led to significant increases of the indices J_2 (acceleration), specially when the system included higher gains, whereas the MHF and SBL systems, in general, produced indices J_2 around or below 1.0. Similarly, the indices J_3 (base shear), were slightly higher for the Tri-D system than those for the MHF and SBL algorithms, which moderately increased the
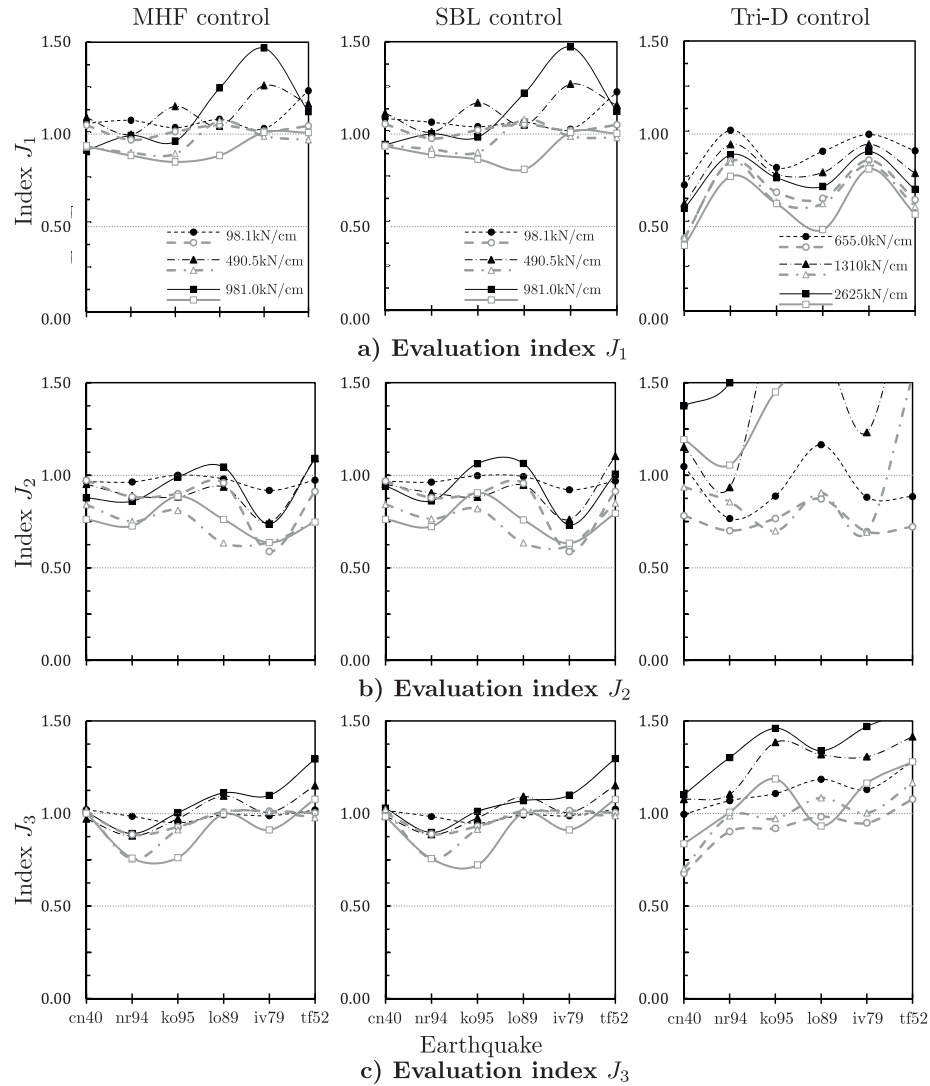
FIGURE 7.14: Medium-rise steel frame: Performance indices with existing control systems, for earthquakes scaled to 0.35g (grey line) and 0.55g (black line).

index when the system with higher gains was subjected to the Loma Prieta, Imperial Valley and Taft earthquakes.

In the case of the RC frames, the MHF and SBL systems were efficient or slightly increased the drift in the majority of the earthquakes (Figs. 7.15a and 7.16a). One exception was the medium-rise frame with higher gains under Taft (Fig. 7.16a), where the index J_1 resulted in high values, even in excess of 1.50. The Tri-D control was efficient in almost all the earthquakes, only slightly increasing the drift of the low-rise frame under Northridge (0.55g), when the low gain was used. In general, all three systems were inefficient for the acceleration, leading to significant increases in most of

the earthquakes, as it can be seen in Figs. 7.15b and 7.16b. Although in many cases the three systems reduced the base shear of the frames under the earthquakes scaled to 0.35g, there were increases in the shear force for the majority of stronger earthquakes with PGA of 0.55g (Figs. 7.15c and 7.16c). However, the increases in shear were moderate, as indicated by indices up to or below 1.5, in all earthquakes apart from Taft, whose index exceeded 1.50. For all systems, the highest values of the indices J_3 were produced in the frames subjected to the stronger earthquakes (PGA=0.55g), when the control systems included high gain factors. This is reasonable, as it indicates large structural forces due to large inter-storey deformations, combined with large control forces.

FIGURE 7.15: Low-rise RC frame: Performance indices with existing control systems, for earthquakes scaled to 0.35g (grey line) and 0.55g (black line).

MHF control SBL control Tri-D control

a) **Evaluation index J_1**

b) **Evaluation index J_2**

c) **Evaluation index J_3**

FIGURE 7.16: Medium-rise RC frame: Performance indices with existing control systems, for earthquakes scaled to 0.35g (grey line) and 0.55g (black line).

7.4.2 Evaluation of building damage

The indices J_4 and J_5 provided an indication of the energy dissipated by hysteretic mechanisms in the structure. In particular, the index J_4 was a good indicator of the damage in the frame, since it reflected the energy dissipated through inelastic deformations at the end of the beams. There was also a relation between those two indices, as it can be observed in Fig. 7.17 (corresponding to the low-rise steel frame), which shows the typical distribution of energy dissipated in the frames. Since, in general, the control systems with low gain factors resulted in large structural deformations and low control forces, the amount of seismic energy dissipated through the inelastic rotations at the

end of the beams was larger (as denoted by the high values of the index J_4), and the amount of energy dissipated through friction in the dampers was smaller (as denoted by the low values of J_5). As the gain factors increased, the predominant mechanism of dissipation changed from the plastic hinges in the beams, to the frictional work in the dampers.

As it can be seen in Fig. 7.17a and b, the Tri-D system was more efficient than the MHF and SBL in reducing the structural damage and increasing the dissipation in the dampers. In the case of the MHF and SBL controllers, there was more energy dissipated through damage when the low gain was used, in comparison with the same systems using medium and high gains. Contrasting to this, the Tri-D control allowed for low amounts of energy dissipated by the beams for all the frames, and larger amounts of energy dissipated in the friction connections, regardless of the gain factor used. This is reasonable, because the Tri-D control includes a relatively high initial slip-load ($f_{p,i} = 0.15 f_{y,i}$, in this case), unlike the MHF and SBL algorithms.
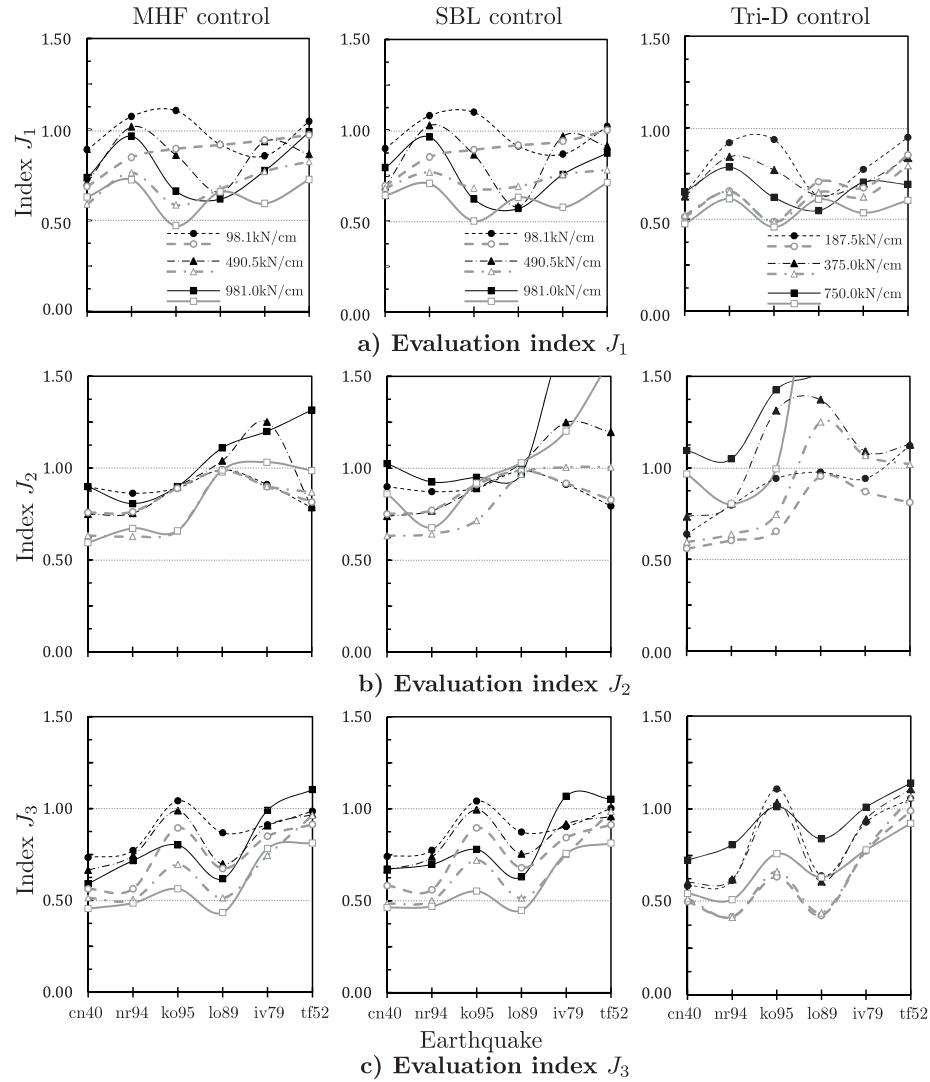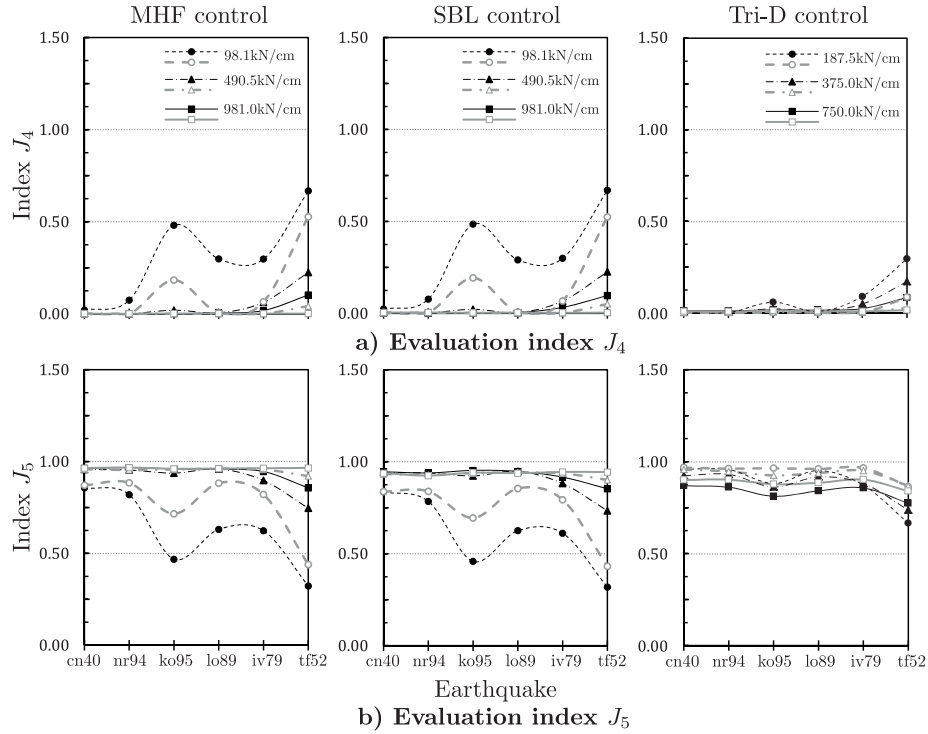

FIGURE 7.17: Typical performance indices J_4 and J_5 with existing control systems, for earthquakes scaled to 0.35g (grey line) and 0.55g (black line).

7.4.3 Evaluation of control forces

The control forces required by each algorithm were larger when the systems included higher gain factors. This was as expected, and resulted in largest reductions of deformation for those same gains. Two representative cases of required control force (index J_6) are shown in Fig. 7.18, corresponding to the low-rise steel frame and medium-rise RC frame.

In the case of the low-rise steel frame, the indices J_6 (Fig. 7.18a) indicated that the Tri-D system with the high gain factor required control forces in excess of $1.5f_{y,i}$, for most of the earthquakes with PGA=0.55g. The MHF and SBL controllers required control forces below $0.9f_{y,i}$, in the majority of the earthquakes, but the values exceeded $1.50f_{y,i}$ when the frame was subjected to the Taft excitation (PGA=0.55g) and the control system used the high gain.

A similar effect occurred for the medium-rise steel frame, where moderate control forces (indicated by indices J_6 below 0.60) were required by the MHF and SBL algorithms. Unlike the low-rise steel frame, the forces required under Taft earthquake did not increase. Again, the indices of the Tri-D system were higher than those of the MHF and LBL, resulting in values above 1.50 for the system with high gains, in most of the stronger earthquakes. These larger control forces, on the other hand, agree with the indices J_1, which were lower for the Tri-D system, in comparison with the other two controllers.

For the RC frames, the indices J_6 corresponding to the MHF and SBL systems were larger than those of the Tri-D algorithm. In the medium-rise frame (Fig. 7.18b), the Taft earthquake (0.55g) required control forces larger that $1.5f_{y,i}$, when the MHF and SBL systems included the medium or high gain factor. For these controllers, the forces were between 1.0 and $1.50f_{y,i}$ for the Loma Prieta and Imperial Valley earthquakes. For all other earthquakes, the control forces were below $0.90f_{y,i}$. The Tri-D system with any gain factor resulted in indices below 0.80 for most of the earthquakes. The only exceptions were Loma Prieta, Imperial Valley and Taft, where the indices resulted in 1.06, 0.94 and 1.40, respectively.

In the case of the low-rise frame, the indices produced by the MHF and SBL systems with high gain were higher than 1.0, and exceeded 1.5 when the frame was subjected to the Loma Prieta, Imperial Valley and Taft earthquakes, scaled to 0.55g. For this frame, the Tri-D system resulted in indices below 0.75, for all the earthquakes, regardless of the gain factor used.

An important aspect of the control algorithms is the actual forces acting in the connections, which depend on the seismic action and may not reach the required control force,

in which case the connections remain locked. If the actual force is equal to the control force, the connection is activated. This is an important factor for the performance of the controller, since activation or locking of the friction connections depends on that relation. An example of this effect is shown in Fig. 7.19, for the medium-rise RC frame including the MHF, SBL and Tri-D systems (with high gain factors). In the figure, the response shown corresponds to the frame's 7th storey, which had the highest relation of controlled to uncontrolled deformations (i.e. index J_1). The response shown corresponds to Taft excitation scaled to 0.35g. As it can be seen in the figure, the control forces produced by the MHF controller were very large, thus locking the friction connection and creating large residual deformations in the frame. This effect was alleviated by the SBL system, which produced control forces smaller than the MHF, and made the connection slide continuously. The Tri-D system produced control forces significantly smaller than the MHF and SBL systems, but also resulted in smaller deformations. This may be attributed to the relatively high initial slip-load (i.e. $0.15 f_{y,i}$) in this controller.
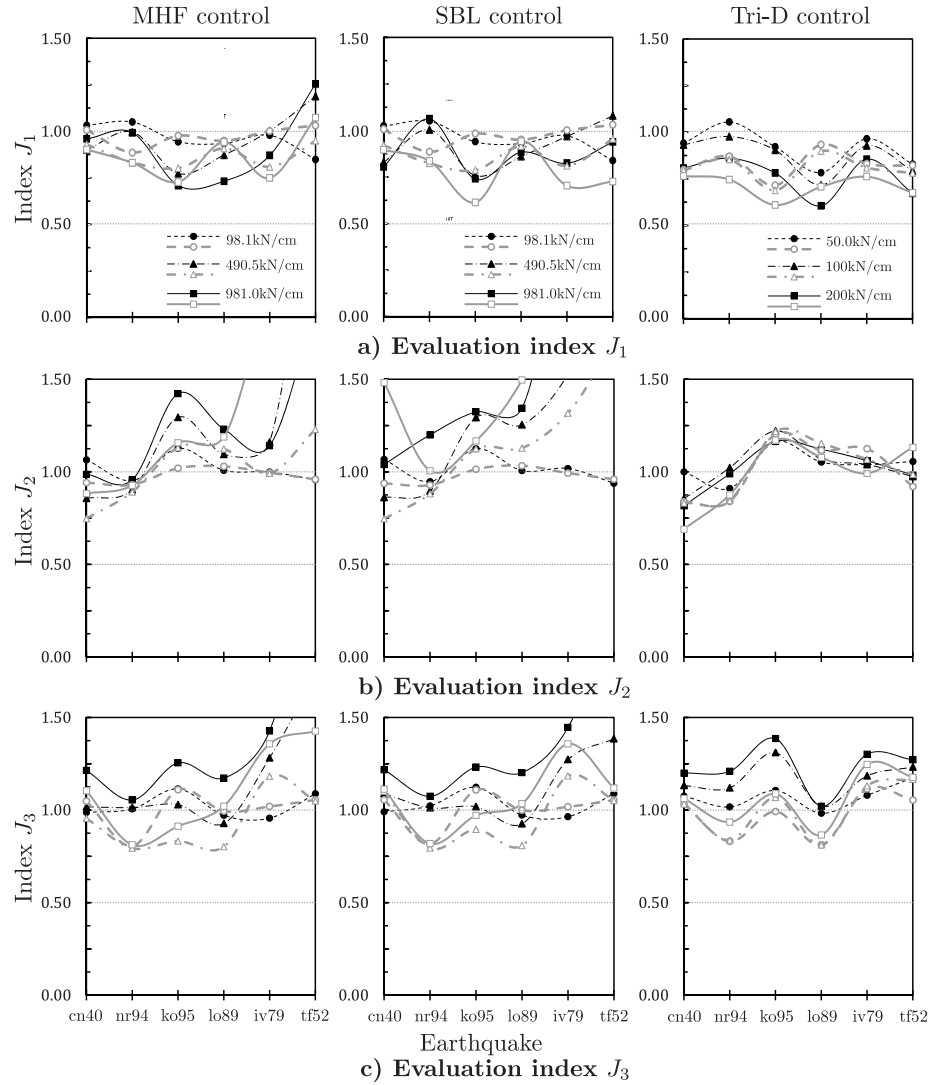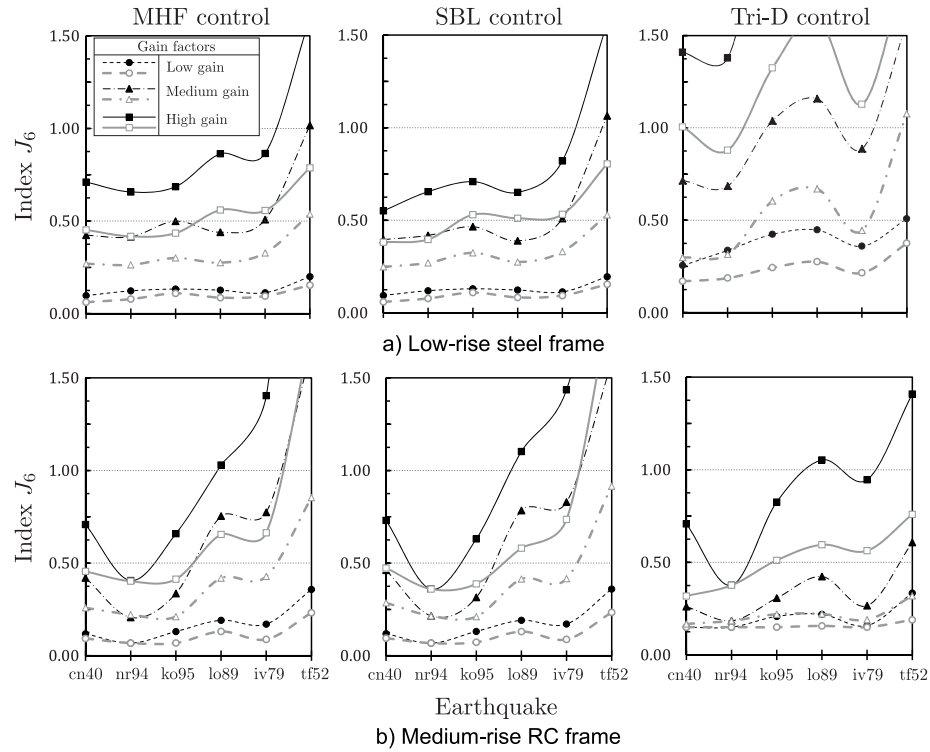

FIGURE 7.18: Control force indices with semiactive control systems, for earthquakes scaled to 0.35g (grey line) and 0.55g (black line).

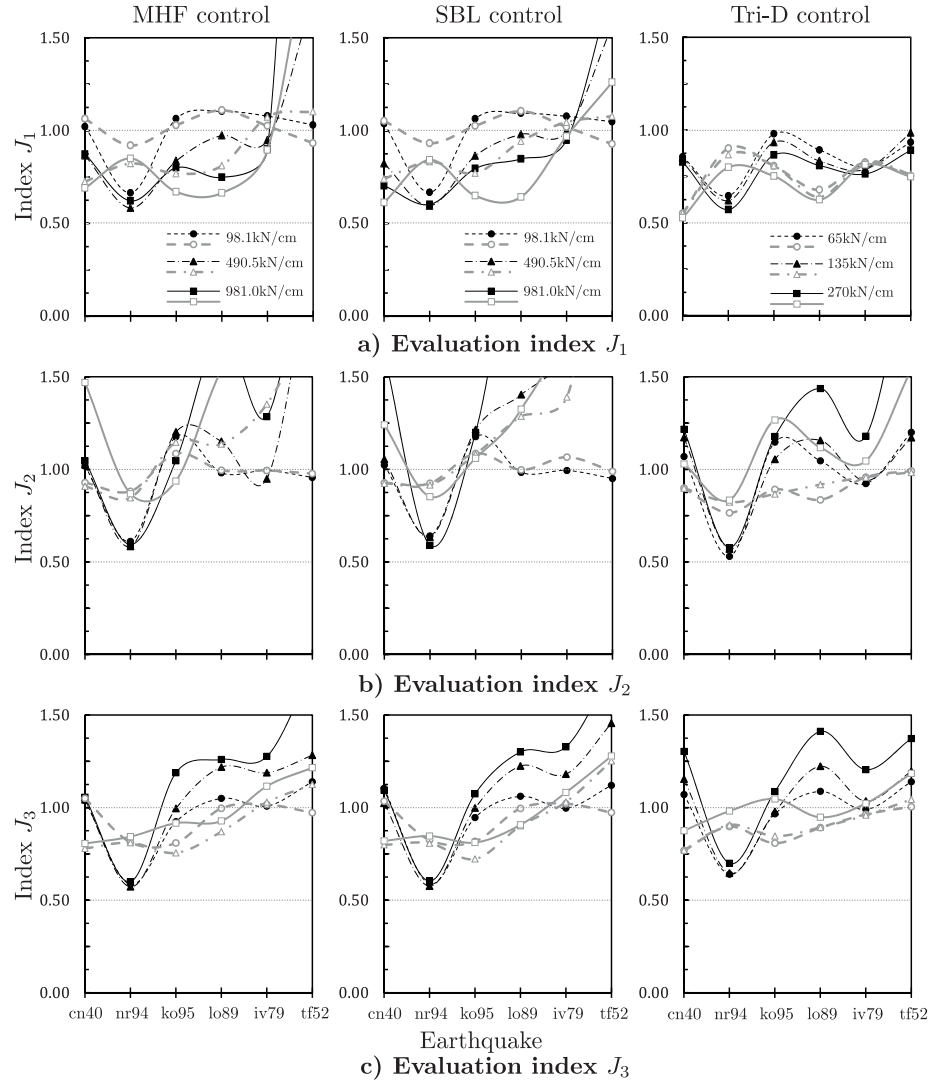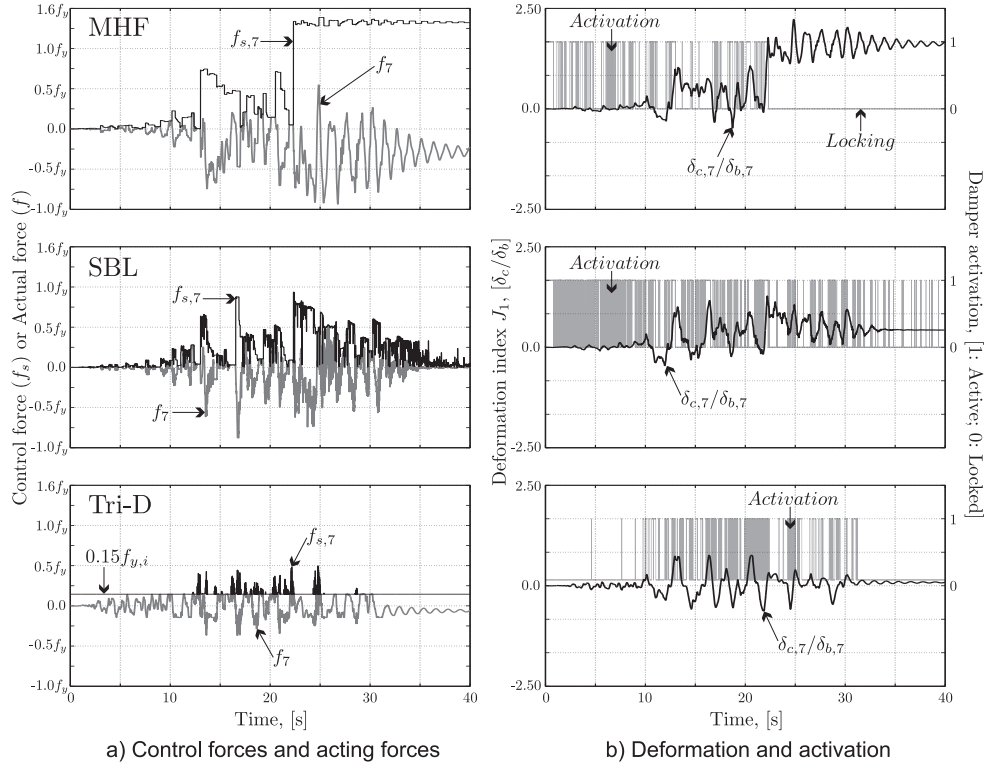FIGURE 7.19: Performance of friction connection in the medium-rise RC frame with different semiactive controllers, under Taft earthquake scaled to 0.35g.

7.5 Comparison of semiactive control and passive control

In general, the passive and semiactive systems reduced the level of deformations, in comparison with the bare frame, for certain levels of slip-loads (in the case of the passive control) or gain factors (in the case of the semiactive systems). However, in some cases, the inclusion of the control systems (either passive or semiactive) was not effective, and it led to increases in the deformation. This could be a result of changes in the stiffness of the structure and the resulting frequency content of the response.

As concluded in Chapter 6, there was an interval of passive slip-loads between $0.25f_{y,i}$ and $0.65f_{y,i}$ that resulted in reductions of the top floor displacement of the frames under any earthquake. That interval, as it can be observed in Figs. 7.20 to 7.23, generally reduced the maximum inter-storey deformations under each earthquake, as indicated by the index J_1.

The inclusion of the semiactive systems had different effects but, in general, it was beneficial and reduced the response of the frames. In Figs. 7.20 to 7.23, the indices J_1 corresponding to the highest gain factors are shown, along with the interval of control

forces (indices J_6) required by each algorithm. As it can be seen, the Tri-D control was more efficient than the MHF and SBL systems, allowing for the smallest indices J_1.

In comparison with the passive control, the combination of MHF and SBL systems improved the response of the buildings (either smaller of comparable to those of the passive system) in 30% of the analysed cases, whereas the Tri-D system improved the response in 62.5% of the cases. Considering the control forces, however, the semiactive systems, especially the Tri-D algorithm, often led to high control forces, even in excess of 2 times the highest optimum passive slip-load (i.e. $0.65f_{y,i}$).

The limited efficiency of the MHF and SBL algorithms was due to the low initial slip-load, which allowed for larger deformations in the early stages of response. Although the control forces increased along with the deformations, this increase was not sufficiently rapid to stop such deformations. An example of such an effect was shown in Fig. 7.19, where a sudden peak of ground acceleration created a large deformation and large control force in the frame with the MHF system, thus locking the connection. The SBL system alleviated the abrupt increase of slip-load, but it still resulted in deformations larger than the Tri-D system. This latter controller was more efficient due to the initial passive load $f_{p,i} = 0.15f_{y,i}$.
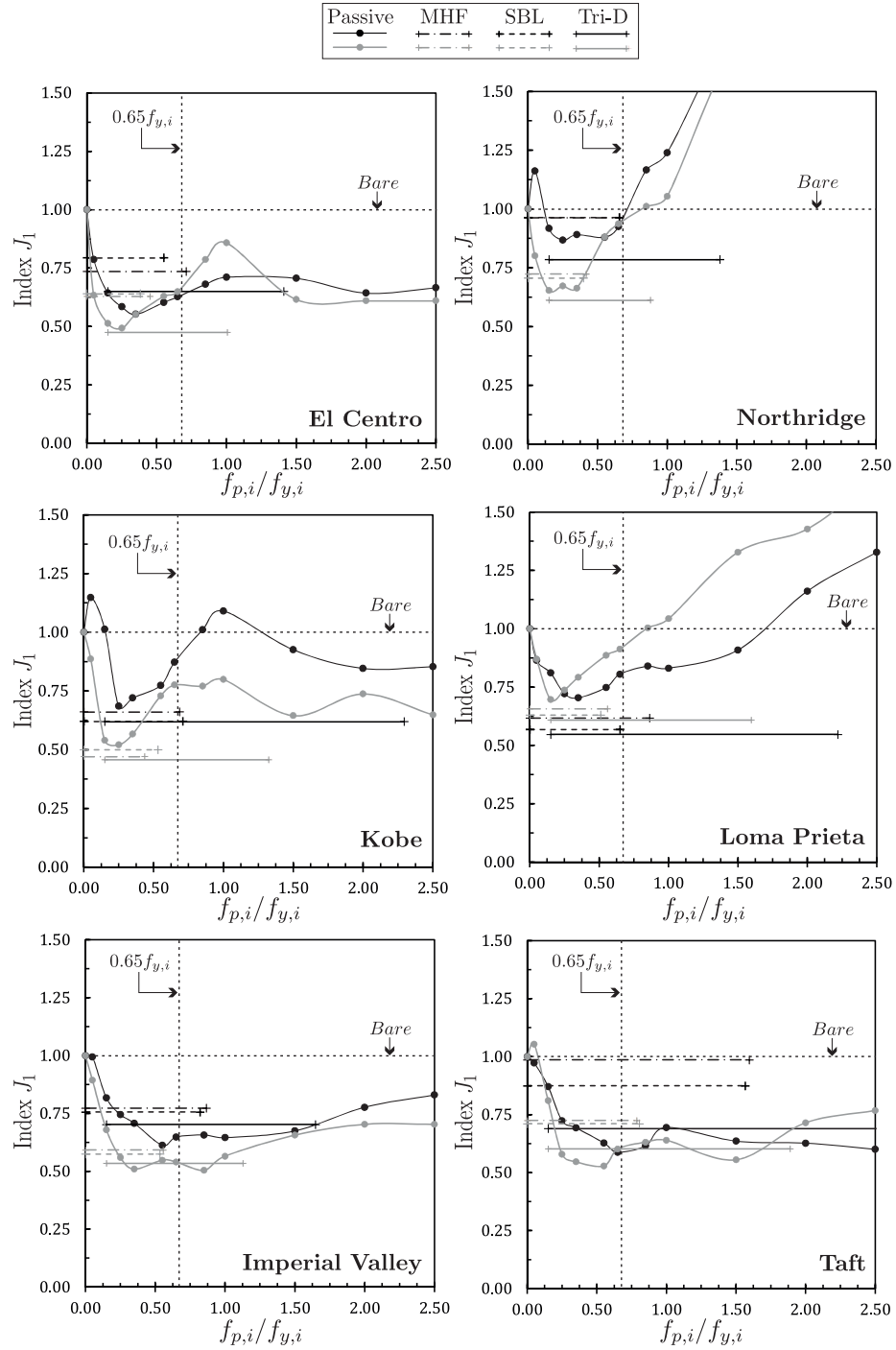
FIGURE 7.20: Low-rise steel frame: Comparison of indices J_1 between passive and semiactive systems, for earthquakes scaled to 0.35g (grey line) and 0.55g (black line).
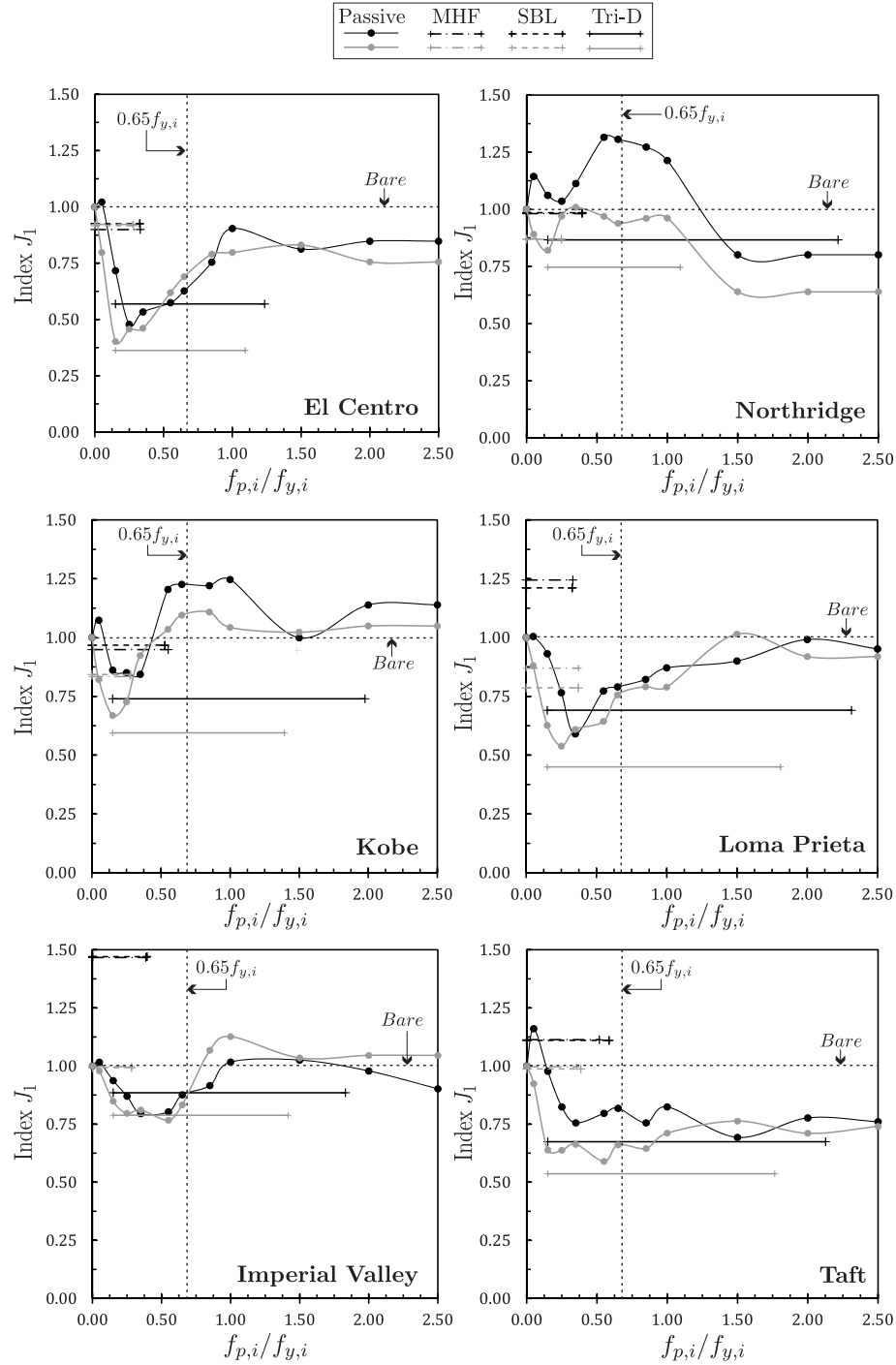
FIGURE 7.21: Medium-rise steel frame: Comparison of indices J_1 between passive and semiactive systems, for earthquakes scaled to 0.35g (grey line) and 0.55g (black line).
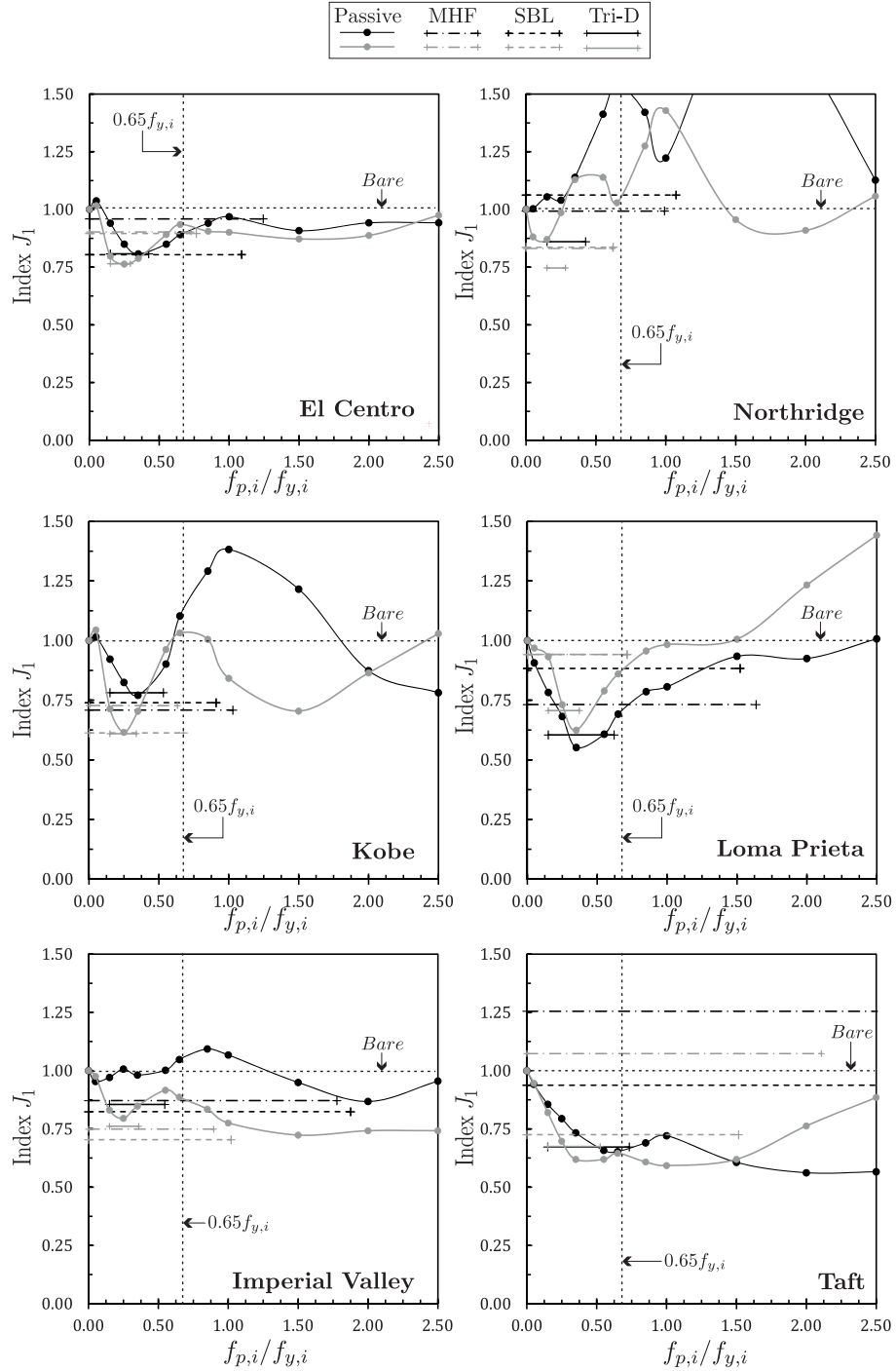
FIGURE 7.22: Low-rise RC frame: Comparison of indices J_1 between passive and semiactive systems, for earthquakes scaled to 0.35g (grey line) and 0.55g (black line).
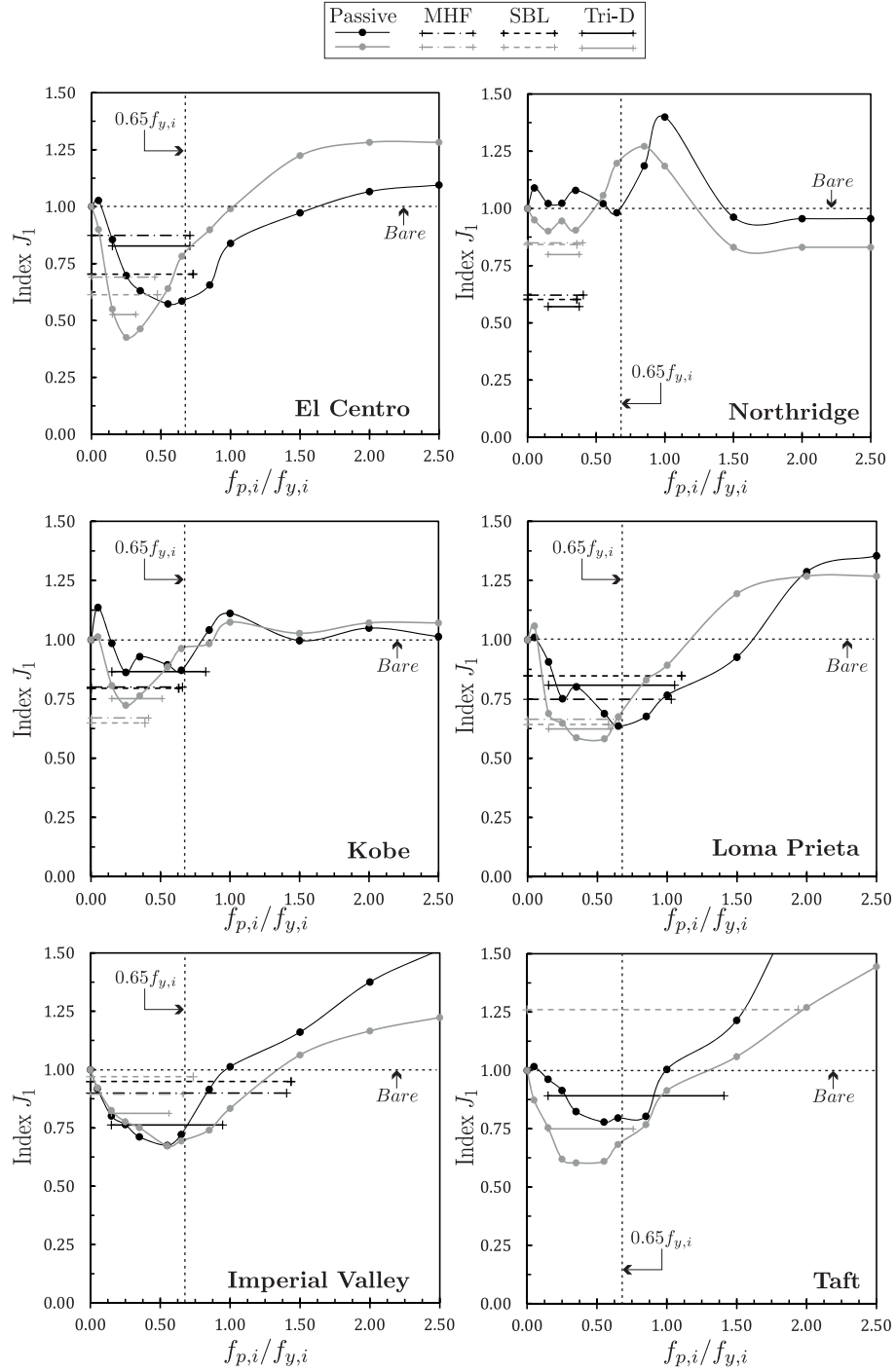
FIGURE 7.23: Medium-rise RC frame: Comparison of indices J_1 between passive and semiactive systems, for earthquakes scaled to 0.35g (grey line) and 0.55g (black line).

7.5.1 Frequency content of the seismic response

The modification of the seismic response in the buildings resulted from the increase of structural damping and the stiffness added (or removed) by the friction connections. To better understand the mechanism of the semiactive systems, the seismic response of the medium-rise steel frame under the El Centro earthquake (PGA=0.35g) was analysed in terms of its frequency content. The history of the top floor displacement (Fig. 7.24) of the frame with passive, SBL and Tri-D (both with medium gain factor) systems was divided in four segments of 10s, corresponding to different levels of seismic input intensity: high (0-10s), medium (10-20s), low (20-30s) and decay (30-40s).

As it can be observed in Fig. 7.24a to d, in all four segments the amplitude of the bare frame's response was higher than that of the controlled frames, with peaks corresponding to the first natural frequency of the bare frame (0.5Hz).

For the frame with passive control, there were peaks of amplitude at different frequencies, but within the range of 0.5Hz to 1.0Hz (i.e. the fundamental frequencies of the bare frame and the fully braced frame), which indicated the level of activation of the connections. As expected, the level of activation in the passive frames decreased as the slip-load increased. As a result, the response at the low frequencies was significantly reduced, but the response at higher frequencies (i.e. 1Hz, the frequency of fully braced frame) was increased. This is more evident for passive systems with higher slip-loads.

The semiactive systems showed more variability than the passive control. In the initial segment (0-10s), the SBL system did not react sufficiently rapid, hence not increasing the stiffness of the frame and showing large amplitudes at 0.5Hz. In the three following segments, the system had peaks at the same frequency (0.5Hz), but with much smaller amplitudes. This indicates that the stiffness of the frame remained low, but the energy dissipation (and consequently, the damping) was increased. The Tri-D system, on the other hand, produced peaks with amplitude significantly smaller than all other systems, at frequencies varying between 0.5Hz and 1.0Hz, without increasing the response of the higher frequencies. This shows that the Tri-D system increased both stiffness and damping in the structure.

The frequency content of the top floor acceleration (Fig. 7.24f) agrees with the mechanism previously described, with peaks corresponding to the frequencies of the frame with different conditions (bare, partially braced or fully braced). In this case, however, there was an influence of the higher modes in the response, which have small effect on the deformations of the structure.
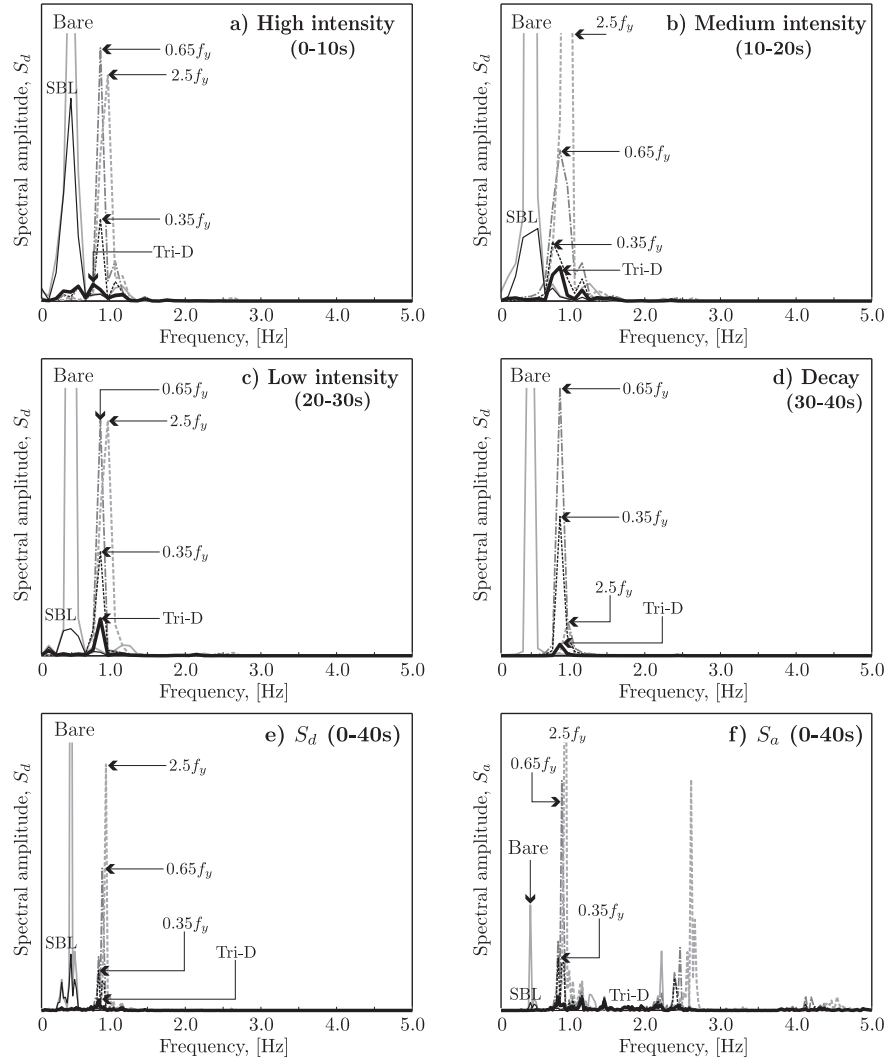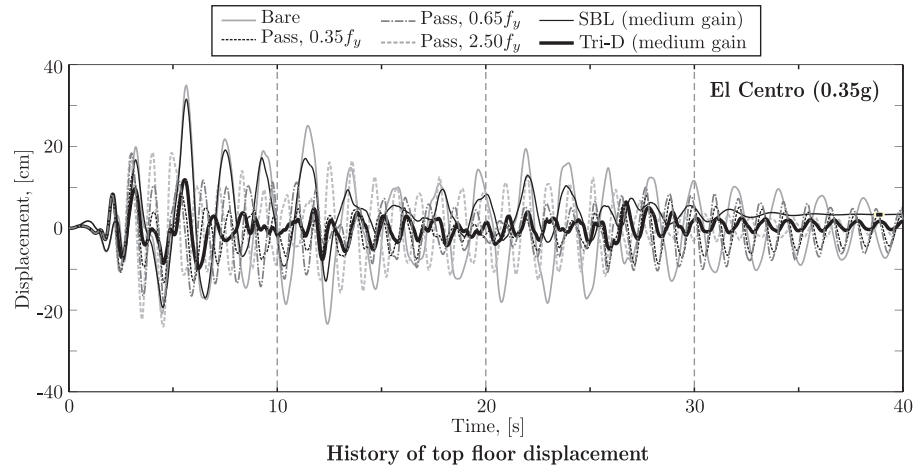
FIGURE 7.24: Medium-rise steel frame: Frequency content of the top floor displacement and acceleration, using different control systems.

7.6 Concluding remarks

The performance of the four decentralised control algorithms existing in the literature was evaluated by simulating the response of multi-storey buildings under a range of different earthquakes. The set of algorithms included the MHF control (Inaudi, 1997), the LBL and SBL control (He et al., 2003) and the Tri-D control (Chen and Chen, 2004c). The algorithms were implemented in the software *ConStruc*, developed as part of this research.

Initially, a parametric study was performed to investigate the influence of the control parameters in the performance of the systems. The study was performed by simulating the response of a low-rise (6-storey) steel frame and a medium-rise (10-storey) RC frame, subjected to the action of six historical earthquakes: El Centro (0.55g), Northridge (0.35g), Kobe (0.82g), Loma Prieta (0.65g), Imperial Valley (0.70g) and Taft (0.22g). In the simulations, three different gains were used for each control algorithm, as well as three different boundary layers in the LBL and SBL, and two different levels of initial slip-load $f_{p,i}$ in the Tri-D system. Generally, larger gain factors led to higher efficiency of the controllers: higher reduction of deformations and higher proportion of energy dissipated in the friction connections.

The efficiency of the semiactive control was examined for three algorithms (MHF, SBL and Tri-D) and three levels of gain factors. Since the SBL proved to be less sensitive than the LBL to the *thickness* of the boundary layer, the LBL was not used for further study.

In most of the analysed cases, all systems were efficient in reducing deformations with little or no increase in base shear (indices J_1 and J_3, respectively). One exception was for the frames under the Taft input, which in some cases resulted in increases of more than 50% in the shear force, in comparison with the bare frames.

The damage in the main structure (index J_4), characterised by energy dissipated in plastic hinges in the beams was also reduced by all control systems. This behaviour can be attributed to a combination of increased energy dissipation in the friction connections (resulting in increased structural damping) and changes in the stiffness of the structure (resulting in reduction of dynamic amplification).

The Tri-D control was the most efficient of the three controllers, resulting in very little damage in the main structure, for all frames, regardless of the gain factor and seismic input.

Higher PGA in the input excitation reduced the efficiency of the controllers, as the damage in the frame increased and the associated energy dissipation in the beams became proportionally larger than that in the friction connections.

The efficiency of the systems did vary from earthquake to earthquake and for some frames, for certain gain-input combinations, the deformations were larger than those of the uncontrolled systems. This condition, however, was rare for the systems with high gains, and occurred only in the MHF and SBL systems, accounting for 9.0% of the total analysed cases. This number further reduced to 6% of the analysed cases, when considering only moderate earthquakes (PGA=0.35g).

The comparison of the passive and the semiactive systems indicated a better performance of the Tri-D control (in terms of deformation reduction), which produced response levels comparable to or smaller than those of the passive system in 62.5% of the analysed cases. Also, the Tri-D algorithm did not result in large increases in response that were observed for the passive systems subjected to some seismic excitations (e.g. Northridge and Kobe, Fig. 7.21), even within the optimum range of slip-loads ($0.25f_{y,i}$ to $0.65f_{y,i}$).

The efficiency of the MHF and SBL algorithms was limited, and in some cases led to increases of the deformations, in comparison with the bare frame. The reason for this was that the initial stiffness of the frames was relatively low and the energy dissipation in the early stages of response was not sufficient to generate enough damping to reduce the deformations produced by the early large amplitudes of the seismic input. The MHF and SBL controllers were, in fact, less effective than the optimum passive systems, improving the response in only 30% of the cases. In comparison, the effectiveness of the Tri-D control was largely due to the relatively high initial slip-load ($f_{p,i} = 0.15f_{y,i}$) in the connections.

A drawback of the Tri-D control was that it required large control forces (more than $1.0f_{y,i}$, in many cases), which were outside of the interval of optimum slip-loads ($0.25f_{y,i}$ to $0.65f_{y,i}$).

This analysis shows that, in order to achieve good seismic control (i.e. reduction of deformations without using control forces higher than $0.65f_{y,i}$), there is a need for new, improved semiactive algorithms.

Chapter 8

New semiactive algorithms: TδVG, a decentralised system

8.1 Introduction

Previously, a friction-based passive control system and several existing semiactive controllers were applied to a set of four multi-storey frames (low- and medium-rise) and their efficiency was investigated by means of non-linear simulations of seismic response.

In general, the inclusion of the passive system in the multi-storey frames resulted in reduction of the structural response, for most of the earthquake excitations (Chapter 6). From the simulations, it was observed that the levels of response reduction varied for different values of the dampers' slip-loads. The efficiency of the system was optimum for a unique load (hence called optimum passive slip-load), which led to maximum reduction of the top floor displacement, associated with large amounts of energy dissipated in the friction connections and minimum damage in the frame. The optimum slip-load, however, varied for each frame under different earthquakes. It was concluded that, instead of a unique optimum slip-load for every frame, there was a narrow range of slip-loads with good levels of response reduction and energy dissipation for all the frames. In the study, such range of slip-loads varied between $0.25f_{y,i}$ and $0.65f_{y,i}$, where $f_{y,i}$ is the shear force that produces the first plastic hinge in the storey i. The lack of efficiency of the passive systems was evident in some cases, especially for near-fault type earthquakes, such as Northridge and Kobe, where the response of the frame was increased, even for some slip-loads within the optimum range.

In order to investigate possible solutions to the limited efficiency of the passive control, three semiactive controllers, taken from the literature, were applied to the set of frames

TABLE 8.1: Summary of *decentralised* controllers selected from the literature.

Modulated homogeneous friction control, MHF (Inaudi, 1997)

$$f_{s,i}(t) = g_i \mu |P[\delta_i(t)]| sgn(\dot{\delta}_i(t))$$
where:
$$P[\delta_i(t)] = \begin{cases} \delta_i(t) & \text{if } \dot{\delta}_i(t) = 0, \\ \delta_i(t-s) & \text{if } \dot{\delta}_i(t) \neq 0 \end{cases}$$

Linear boundary layer friction control, LBL (He et al., 2003)

$$f_{s,i}(t) = \begin{cases} g_i \mu |P[\delta_i(t)]| sgn(\dot{\delta}_i(t)) & \text{if } |\dot{\delta}_i(t)| > \lambda_{a,i}, \\ g_i \mu |P[\delta_i(t)]| \left(\dfrac{|\dot{\delta}_i(t)|}{\lambda_{a,i}} \right) sgn(\dot{\delta}_i(t)), & \text{if } |\dot{\delta}_i(t)| \leq \lambda_{a,i}, \end{cases}$$

Smooth boundary layer friction control, SBL (He et al., 2003)

$$f_{s,i}(t) = g_i \mu |P[\delta_i(t)]| tanh(\lambda_{b,i} \dot{\delta}_i(t))$$

Friction control w/passive, viscous and Reid damping, Tri-D (Chen and Chen, 2004c)

$$f_{s,i}(t) = \begin{cases} \mu N_{p,i} sgn(\dot{\delta}_i(t)), & \text{if } e|\delta_i(t)| + g|\dot{\delta}_i(t)| \leq N_{p,i}, \\ \mu \left(e|\delta_i(t)| + g|\dot{\delta}_i(t)| \right) sgn(\dot{\delta}_i(t)), & \text{if } e|\delta_i(t)| + g|\dot{\delta}_i(t)| > N_{p,i} \end{cases}$$

(Chapter 7). The three algorithms (MHF, SBL and Tri-D) were *decentralised* systems that adjusted the dampers' slip-loads during the ground motion, based on the *feedback* of local inter-storey deformation and/or velocity. One of the advantages of these systems was their simplicity, since adjustment of the slip-loads in each storey was proportional only to the local *feedback* information, using the pre-defined, constant gain factors g and e, as it is shown in Table 8.1. The LBL controller is also included in the table for purposes of comparison only, but it was not applied to the multi-storey frames as it was more sensitive to the *thickness* of the boundary layer than the SBL system, for similar levels of efficiency.

The results from the non-linear simulations indicated a variability in the efficiency of each control system. The MHF and the SBL controllers reduced the seismic response of the bare frame under most of the earthquakes, but in general, both algorithms were less effective than the optimum passive system, resulting in higher levels of response. The Tri-D algorithm, using a passive phase and two constant gain factors (each one to generate control forces associated with the deformation and the velocity, respectively), was the most efficient of all three semiactive controllers, producing levels of response either comparable or lower than those of the optimum passive control, depending on the seismic input. The reason for this, as it was concluded in the study, is that the efficiency of the Tri-D system is related to: i) the relatively high initial stiffness of the frame, due to relatively high initial slip-loads (in the order of $0.15 f_{y,i}$), which delayed the activation in the friction connections in the early stages of deformation; and ii) the increase of

structural damping, which resulted from the slippage in the friction connections, hence providing an additional mechanism for dissipation of seismic energy in the later stages of response.

One disadvantage that was observed for the semiactive controllers was the difficulty of tuning the constant gain factors, in order to generate control forces adequate to the intensity of the ground motion, without saturating the devices. This was also the main drawback of the Tri-D system, which required high levels of control forces, in many cases beyond the optimum range of passive loads ($0.25f_{y,i}$ to $0.65f_{y,i}$).

After investigating the efficiency of the passive and existing *decentralised* semiactive controllers, the need for an improved semiactive control system was evident. As a possible solution, the advantages of both the passive control and the *decentralised* control systems were combined in a new semiactive algorithm. The new system was designed to develop control forces within the optimum range of passive slip-loads, adjusting the gain factors as function of the ratio between inter-storey drifts and pre-defined maximum drift values. By combining such characteristics, it was expected that the controller would reduce significantly the inter-storey deformations, with low or moderate increase of shear forces in the frame.

8.2   Expected advantages of the new *decentralised* system

The passive system and the semiactive Tri-D algorithm reduced the seismic response of low- and medium-rise frames. Both systems, however, showed several drawbacks. The main disadvantage of the passive control was its lack of adaptability. In the case of the Tri-D system, it was difficult to tune the constant gain factors g and e, resulting in control forces significantly larger than the optimum passive system, for certain earthquake excitations.

The justification for development of a new *decentralised* semiactive control system was to reduce or eliminate those disadvantages, but also to combine desirable characteristics of both systems, which included adaptability, elasto-plastic behaviour, avoidance of sophisticated materials, adequate long term behaviour and simplicity to install, replace or recalibrate (Martinez-Rueda, 2002). Furthermore, an efficient semiactive system would be the one that kept levels of deformation comparable to the Tri-D control, but limiting the control forces within the optimum range of passive loads (i.e. between $0.25f_{y,i}$ and $0.65f_{y,i}$). An additional advantage of the new semiactive system would be to relate the control forces not only to the seismic response, but also to the structural properties of the frame, specifically to the limits of elastic deformation.

One solution for improving the performance of the semiactive control would be to adopt a centralised control strategy, which according to some researchers (Ng and Xu, 2007), eliminate the limitations on available information. However, *decentralised* architecture offers many advantages, such as faster control response, low cost and simplicity of implementation. A *decentralised* system also allows for simpler control algorithms, which can reduce the possibility of errors (Kobori et al., 1991). Besides, in a *decentralised* system, if one local controller fails, the whole system is not critically affected because there will be still other local controllers functioning.

8.3 Disadvantages of using constant gain factors

The semiactive controllers including constant gain factors may have limited efficiency in practical applications, due to the random nature of the ground motion and the actual slip-load capacity of the devices. By using constant gain factors without adequate tuning, two possible scenarios may occur:

- The gain factor is too high, in which case the damper may reach its maximum capacity even for low seismic loads, saturating and possibly locking the device. Whilst this may reduce the structural deformations, the level of shear and axial forces can be dramatically increased, as the structural behaviour would be similar to that of a fully braced system.

- The gain factor is too low, in which case the damper may not develop adequate control forces, hence slippage would occur during the entire ground motion, allowing for large deformations similar to those of a bare frame, especially in the early stages of response.

The possible disadvantage of using constant gain factors in a semiactive system was demonstrated by programming a simple control algorithm in *ConStruc*. This algorithm was *decentralised* and used the velocity across the dampers as only *feedback*.

In this algorithm, the velocity $\dot{\delta}_i(t)$ of each damper i was monitored continuously. Then, the maximum value of the velocity was determined at the end of a time interval of decision, Δt. The control force was determined as:

$$f_{s,i}(t) = \mu \left(g_i |\dot{\delta}_{max,i}|_{\Delta t} \right) sgn(\dot{\delta}_i(t)), \tag{8.1}$$

where g_i represents the constant gain factor, with units of force/velocity and $|\dot{\delta}_{max,i}|_{\Delta t}$ represents the absolute value of the maximum velocity within the interval Δt. The force

determined with Eq. 8.1 was applied throughout the following interval (i.e. $t + \Delta t$), when new values of $|\dot{\delta}_{max,i}|_{\Delta t}$ and $f_{s,i}(t)$ were determined.

The control algorithm of Eq. 8.1 was used to modify the response of the single storey frame shown in Fig. 7.4, in page 88. In the simulations, a coefficient $\mu = 0.2$ was used to characterise the interface of the friction connections. This value is reasonable, and has been used in other studies (Inaudi, 1997). The interval of decision Δt was defined as 0.4s, corresponding to the fundamental frequency of the frame. Also, three gain factors $g = 5$, 50 and 300kN(cm/s)^{-1} were applied as low, medium and high gains.

As shown in Fig. 8.1, the gain factor had an important influence on the performance of the control system. The level of activation of the damper was reduced for the control with higher gain $g = 300\text{kN-s/cm}$ (Fig. 8.1c), where the device was activated only at the beginning and towards the end of the excitation. Contrasting with that, in the control with low gain $g = 5\text{kN-s/cm}$ (Fig. 8.1a) the damper was activated practically during the whole excitation. An optimum level of control force was produced by the medium factor $g = 50\text{kN-s/cm}$ (Fig. 8.1b). The activation of the connection depends on the ratio between the required control force and the actual force in the connection.

The effect of the three constant gain factors on the deformation of the frame is shown in Fig. 8.2. The control with low gain resulted in a small reduction of deformation (only 25%), in comparison to the bare frame. The other two gain factors resulted in significant reductions of deformation (around 75%). However, the comparison between the medium and high gain factors shows larger control forces for $g = 300\text{kN-s/cm}$ (in the order of 2 times larger than those of $g = 50\text{kN-s/cm}$), for slightly higher reductions of deformation (only 30% smaller than those produced by the medium gain). Moreover, the increase of control forces is unjustified for levels of deformation well within the elastic limits of the frame.

8.4   Proposed target deformation with variable gain factors (TδVG) control

A new *decentralised* semiactive control strategy was introduced with the aim to improve some of the key drawbacks of the existing *decentralised* systems. The new *decentralised* system had the following characteristics:

- *Variable gain factors* (rather than pre-specified, constant values), that are adjusted as a function of the ratio between inter-storey drift values and pre-defined drift
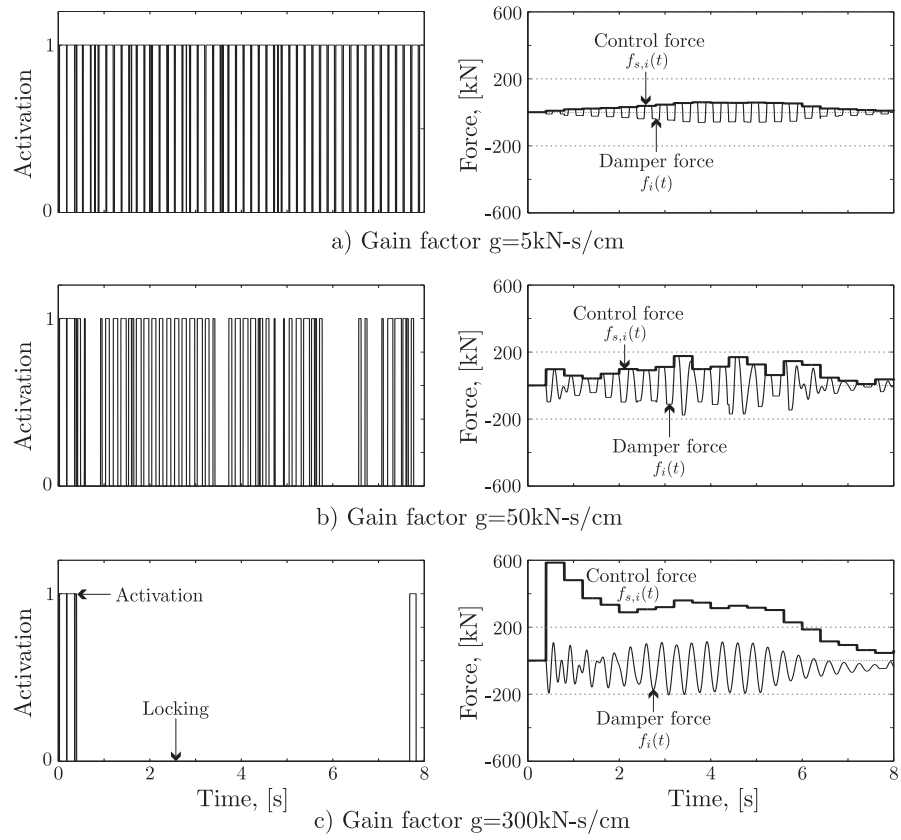
FIGURE 8.1: Performance of a velocity dependent semiactive control with constant gain factors.
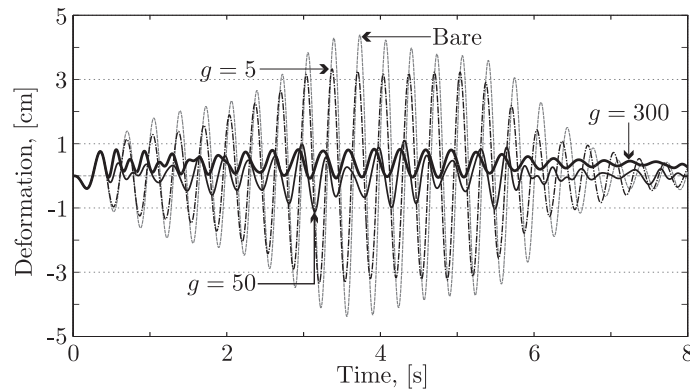
FIGURE 8.2: Time history of displacement of single storey frame with semiactive control.

limits (*target deformation*), which depend on the elastic deformation limits of the structure.

- *Control force limits*, within the optimum range of passive slip-loads (e.g. $0.25 f_{y,i}$ to $0.65 f_{y,i}$). The level of control forces is related directly to the actual resistance of the frame structure ($f_{y,i}$).

The minimum and maximum slip-loads ($f_{s1,i}$ and $f_{s2,i}$, respectively) and minimum and maximum inter-storey deformations ($\delta_{1,i}$ and $\delta_{2,i}$, respectively), are defined first. The limits of forces and deformations are then used to determine an initial control system (a simplified on-off strategy), as:

$$
f_{s,i}(t) = \begin{cases} f_{s1,i}\, sgn(\dot{\delta}_i(t)), & \text{if } |\delta_i| \leq \delta_{1,i} \\ f_{s2,i}\, sgn(\dot{\delta}_i(t)), & \text{if } |\delta_i| > \delta_{1,i} \end{cases}
\tag{8.2}
$$

where δ_i represents the current deformation of inter-storey i. The new system retains the advantages of the existing *decentralised* architecture.

In reality, the slip-load of a friction damper is modified by adjusting the clamping force in the connections. Hence, the Eq. 8.2 can be re-written as:

$$
f_{s,i}(t) = \begin{cases} \mu N_{1,i}\, sgn(\dot{\delta}_i), & \text{if } |\delta_i| \leq \delta_{1,i} \\ \mu N_{2,i}\, sgn(\dot{\delta}_i), & \text{if } |\delta_i| > \delta_{1,i} \end{cases}
\tag{8.3}
$$

where $N_{1,i}$ and $N_{2,i}$ represent the clamping force limits (minimum and maximum).

The controller of Eq. 8.3 seems adequate for small inter-storey deformations, where low slip-loads may allow slippage and dissipation of energy. However, increasing the clamping force to the maximum level ($N_{2,i}$) as soon as the deformation surpassed the threshold $\delta_{1,i}$ may result in locking of the friction connections. A better solution would be to gradually increase the clamping force as deformations increase (to prevent even larger deformations), and to reduce the slip-load gradually during the motion reversal. Combining this increase/reduce relation with the constraints of Eq. 8.3, a new expression for the controller can be established as:

$$
f_{s,i}(t) = \begin{cases} \mu N_{1,i}\, sgn(\dot{\delta}_i), & \text{if } |\delta_i| \leq \delta_{1,i} \\ \mu\,(N_{1,i} + g_i(\delta(t))\Delta N_i)\; sgn(\dot{\delta}_i), & \text{if } \delta_{1,i} < |\delta_i| \leq \delta_{2,i} \\ \mu N_{2,i}\, sgn(\dot{\delta}_i), & \text{if } |\delta_i| > \delta_{2,i} \end{cases}
\tag{8.4}
$$

In Eq. 8.4, ΔN_i represents the difference between the maximum and minimum clamping force, i.e. $\Delta N_i = N_{2,i} - N_{1,i}$, and $g_i(\delta(t))$ represents the variable gain factor, as function of the current deformation.

The factor $g_i(\delta(t))$ could be defined as a linear relation between the current deformation δ_i and the *target deformation* $\delta_{2,i}$. However, it would be more efficient to have a higher rate of adjustment of the slip-load at early stages of deformation. The gain factor can be expressed as:

$$g_i(\delta(t)) = \left(\frac{|\delta_i| - \delta_{1,i}}{\delta_{2,i} - \delta_{1,i}} \right)^{\alpha} \tag{8.5}$$

To determine an appropriate relation between δ_i, $\delta_{1,i}$ and $\delta_{2,i}$, three different values of α were examined:

i) a linear relation, $\alpha = 1$,

ii) a square root relation, $\alpha = 1/2$,

iii) a cubic root relation, $\alpha = 1/3$.

The three relations of $g_i(\delta(t))$ were used in the analysis of the low-rise (6-storey) steel frame and the medium-rise (10-storey) RC frame subjected to the El Centro, Northridge and Kobe earthquakes, with PGA of 0.35g. As shown in Fig. 8.3a and b, the $\alpha = 1/3$ relation resulted in smaller inter-storey deformations in both frames, for all earthquakes. The $\alpha = 1/3$ relation also resulted in smaller top floor displacements, especially for the El Centro and Kobe excitations. The top floor displacements of the steel frame with the $\alpha = 1/3$ relation were 16% and 6% smaller than those produced by the $\alpha = 1$ and $\alpha = 1/2$ relations, respectively, when the frame was subjected to the El Centro excitation (Fig. 8.4a), and 24% and 8% smaller when the frame was subjected to the Kobe earthquake (Fig. 8.4c). There were no significant differences in the top floor displacement when the frame was subjected to the Northridge earthquake (Fig. 8.4b). In case of the RC frame, the $\alpha = 1/3$ relation resulted in top floor displacements 18% and 8% smaller than the $\alpha = 1$ and $\alpha = 1/2$ relations, respectively, for the El Centro excitation, and 12% and 3% smaller for the Kobe earthquake. Similar to the steel frame, the difference in displacements under Northridge were not significant.

The reason for the difference in results, as shown in Fig. 8.5, was the faster increase of the control forces for smaller deformations, produced by the cubic root relation of the gain factor:

a) Low-rise steel frame

b) Medium-rise RC frame
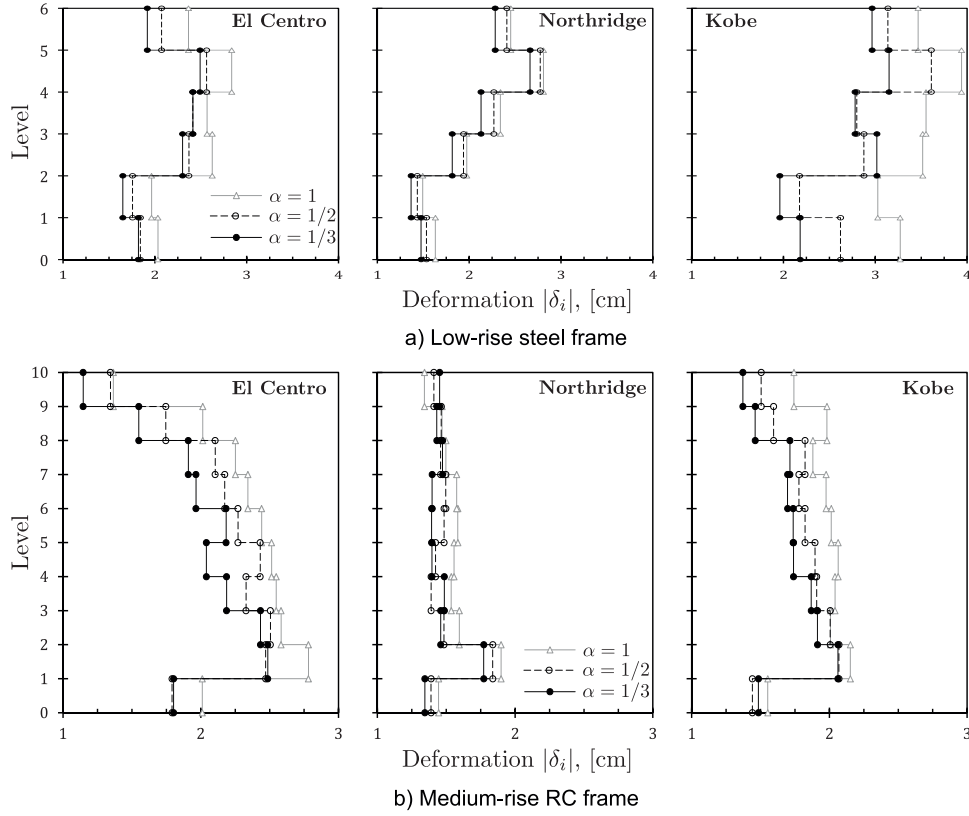
FIGURE 8.3: Storey deformation and top floor displacement of controlled frames with different relations of $g_i(\delta(t))$.

$$g_i(\delta(t)) = \left(\frac{|\delta_i| - \delta_{1,i}}{\delta_{2,i} - \delta_{1,i}} \right)^{1/3} .$$

By adjusting the control force only proportionally to the structural deformation, the algorithm of Eq. 8.4 may not guarantee the damper to slip back during the motion reversal, similarly to the passive systems and the MHF control. As a possible solution, an additional parameter depending on the velocity was used in the SBL control (He et al., 2003) as $tanh(\lambda_{b,i}\dot{\delta}_i)$, in which $\lambda_{b,i}$ was introduced to influence the smoothness of the clamping force variation (Chapter 7). In the control proposed in this study, a similar parameter depending only on the velocity was adopted as $tanh(\dot{\delta}_i)$. The elimination of the boundary layer $\lambda_{b,i}$ may limit the smoothness of the slip-load variation, but, according to the SBL results (presented in Section 7.3), such parameter did not have a significant influence on the seismic response of the frames when they were subjected to different earthquakes.
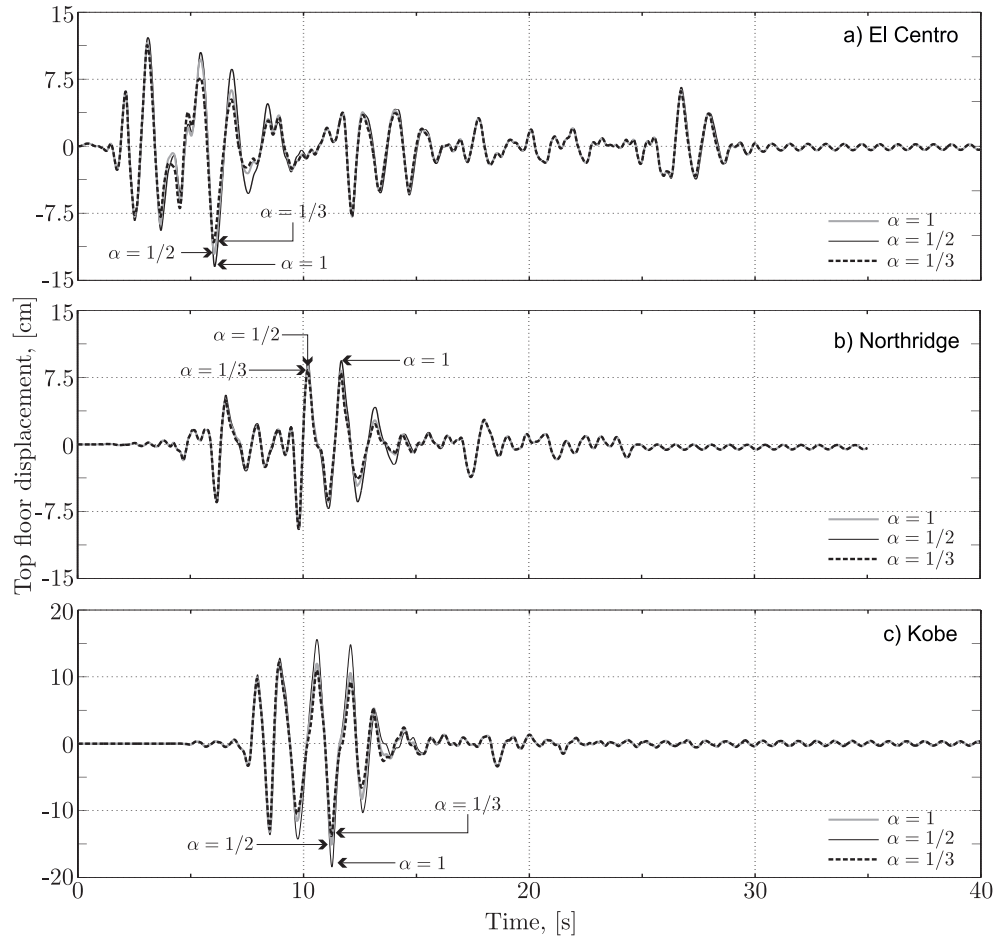
FIGURE 8.4: Low-rise steel frame: Time history of top floor displacements for *decentralised* control using different relations of $g_i(\delta(t))$.
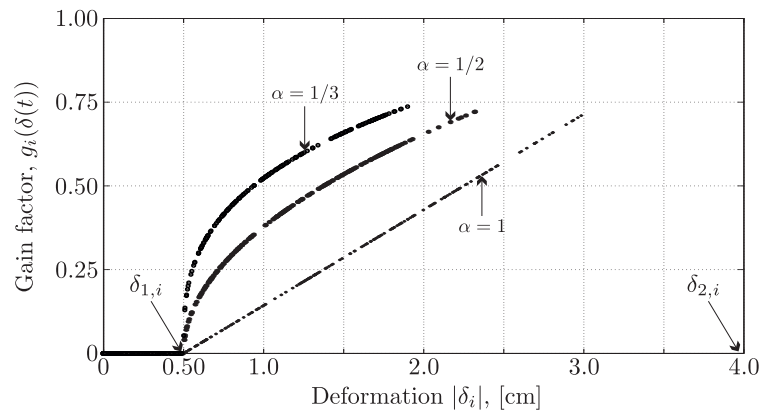
FIGURE 8.5: Gain factors using different relations of $g_i(\delta(t))$.

TABLE 8.2: *Decentralised* TδVG control system, programmed in *ConStruc*.

1. Initial time of analysis, $t_0 = t$

   (a) Input data:
       Force limits, $N_{1,i}, N_{2,i}$
       Deformation limits: $\delta_{1,i}, \delta_{2,i}$
       Sampling time: t_s

   (b) Initial deformation and velocity, $\delta_{0,i} = 0, \dot{\delta}_{0,i} = 0$

2. At every sampling time:

   (a) Calculate the current velocity across the damper i:
       $\rightarrow \quad \Delta\dot{\delta}_i = \dfrac{\delta_i - \delta_{0,i}}{t_s}, \text{and } \dot{\delta}_i = \dot{\delta}_{0,i} + \Delta\dot{\delta}_i$

   (b) Check the limits of deformation to determine $g_i(\delta(t))$:
       $\rightarrow \quad$ if $\delta_{1,i} < |\delta_i| \leq \delta_{2,i}$
       $\rightarrow \quad$ then $g_i(\delta(t)) = \left(\dfrac{|\delta_i| - \delta_{1,i}}{\delta_{2,i} - \delta_{1,i}} \right)^{1/3}$
       $\rightarrow \quad$ elseif $|\delta_i| \leq \delta_{1,i}$
       $\rightarrow \quad$ then $g_i(\delta(t)) = 0$
       $\rightarrow \quad$ else $g_i(\delta(t)) = 1$
       $\rightarrow \quad$ end

   (c) Calculate the normal force:
       $\rightarrow \quad N_i(t) = N_{1,i} + g_i(\delta(t))\Delta N_i$

   (d) Calculate the new slip-load:
       $\rightarrow \quad f_{s,i}(t) = \mu N_i(t)\, tanh(\dot{\delta}_i)$

   (e) Set $\delta_{0,i} = \delta_i, \dot{\delta}_{0,i} = \dot{\delta}_i$

The final controller including the velocity term was thus defined by the following expression:

$$f_{s,i}(t) = \begin{cases} \mu N_{1,i} tanh(\dot{\delta}_i), & \text{if } |\delta_i| \leq \delta_{1,i} \\ \mu \left(N_{1,i} + g_i(\delta(t))\Delta N_i\right) tanh(\dot{\delta}_i), & \text{if } \delta_{1,i} < |\delta_i| \leq \delta_{2,i} \\ \mu N_{2,i} tanh(\dot{\delta}_i), & \text{if } |\delta_i| > \delta_{2,i} \end{cases} \qquad (8.6)$$

or, in terms of control forces:

$$f_{s,i}(t) = \begin{cases} f_{s1,i} tanh(\dot{\delta}_i), & \text{if } |\delta_i| \leq \delta_{1,i} \\ (f_{s1,i} + g_i(\delta(t))\Delta f_{s,i})\, tanh(\dot{\delta}_i), & \text{if } \delta_{1,i} < |\delta_i| \leq \delta_{2,i} \\ f_{s2,i} tanh(\dot{\delta}_i), & \text{if } |\delta_i| > \delta_{2,i} \end{cases} \qquad (8.7)$$

where the factor $g_i(\delta(t))$ includes the cubic root relationship ($\alpha = 1/3$) previously examined, and $\Delta f_{s,i} = f_{s2,i} - f_{s1,i}$. The programming algorithm of the *decentralised* controller is presented in Table 8.2, and a flow chart is shown in Fig. 8.6.
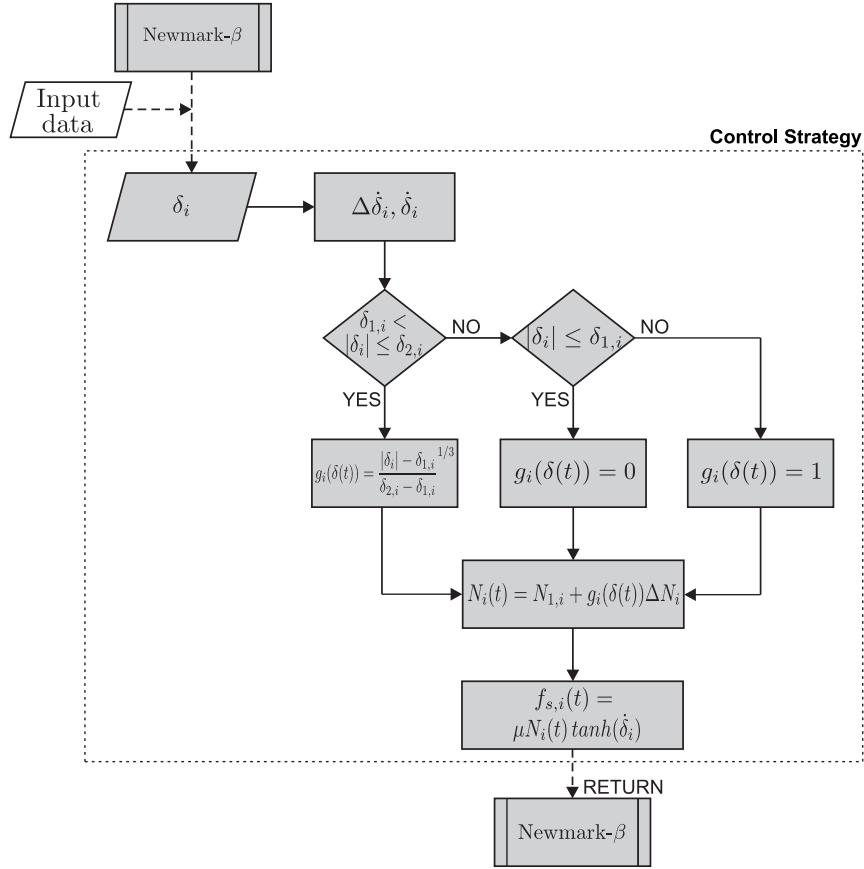
FIGURE 8.6: Flow chart of *decentralised* TδVG control system.

8.5 Efficiency of the new TδVG control system

8.5.1 Definition of control parameters

The efficiency of the *decentralised* control algorithm of Eq. 8.6 was investigated by means of simulations of non-linear response of four multi-storey frames (described in Chapter 4), subjected to six earthquakes: El Centro, Northridge, Kobe, Loma Prieta, Imperial Valley and Taft, all with PGA of 0.35g and 0.55g.

One of the objectives of the new algorithm was to increase the adaptability of the system through the variation of the dampers' slip-loads. Such variation, however, was related to the narrow range of passive slip-loads between $0.25f_{y,i}$ and $0.65f_{y,i}$, that showed good levels of response reduction (Chapter 6). Hence, the upper limit of control force $f_{s2,i}$ was defined as $0.65f_{y,i}$. In order to investigate the effect of allowing a larger variability of the slip-load, two values of the lower limit $f_{s1,i}$ were used as $0.05f_{y,i}$ and $0.25f_{y,i}$.

In the case of the steel frames, since two dampers were installed in every storey, each damper carried half of the force limits.

Another objective of the new algorithm was that it aimed at a *target deformation* $\delta_{2,i}$. In the simulations, this parameter was related to the yield deformation $\delta_{y,i}$ of the inter-storey i, determined in pushover analysis (Chapter 5). Hence, the limits of deformation $\delta_{1,i}$ and $\delta_{2,i}$ were defined as the ratios $\delta_{1,i}/\delta_{y,i}$ and $\delta_{2,i}/\delta_{y,i}$, respectively. The lower limit was defined as $\delta_{1,i}/\delta_{y,i} = 0.10$, i.e. the controller behaved passively for small deformations below 10% of the yield deformation. For the upper limit, three different values were defined as $\delta_{2,i}/\delta_{y,i} = 0.50, 0.75$ and 1.0, in order to reach the maximum capacity of the dampers only for significant levels of elastic inter-storey deformation.

8.5.2 Evaluation of building response

The average indices $\bar{J}_1$, $\bar{J}_2$ and $\bar{J}_3$ for evaluation of inter-storey drift, acceleration and base shear, corresponding to the control system with two levels of minimum slip-load ($f_{s1,i} = 0.05 f_{y,i}$ and $0.25 f_{y,i}$) and three levels of upper limit of deformation ($\delta_{2,i} = 0.50\delta_{y,i}$, $0.75\delta_{y,i}$ and $1.0\delta_{y,i}$) are shown in Fig. 8.7.

From the average of results corresponding to the earthquakes scaled to 0.35g, it can be seen in Fig. 8.7a that the new control system, using both $f_{s1,i} = 0.05 f_{y,i}$ and $0.25 f_{y,i}$, was efficient in reducing the inter-storey deformation, in comparison to the bare frame. As indicated by the index $\bar{J}_1$, the system with initial slip-load $f_{s1,i} = 0.25 f_{y,i}$ produced lower levels of deformation, with the index varying between 0.40 (for the low-rise steel frame) and 0.77 (for the low-rise RC frame). The levels of reduction did not vary significantly for different values of the limit of maximum deformation $\delta_{2,i}$.

In the case of the average peak acceleration, it can be seen in Fig. 8.7b that the control system with $f_{s1,i} = 0.25 f_{y,i}$ produced increases in the order of 50 to 70%, in all four frames, as indicated by the index $\bar{J}_2$. These values were lower than those of the system using $f_{s1,i} = 0.05 f_{y,i}$, which resulted in indices higher than 2 for all frames, apart from the low-rise steel frame, where the value varied between 1.62 and 1.84. The increase of peak acceleration was caused by rapid changes of stick/slip phases, which generated rattling in some floors. As an example, the time histories of acceleration in the top, third and first floors of the low-rise steel frame under the El Centro earthquake scaled to 0.35g (Fig. 8.8a), show that the maximum acceleration occurred when the controller introduced the maximum levels of slip-load (Fig. 8.8b) with a rapid change of activation/ deactivation of the friction dampers (Fig. 8.8c). In the Fig. 8.8a, it can also be seen that, once the rattling effect finished, the controlled frame had smaller acceleration than the
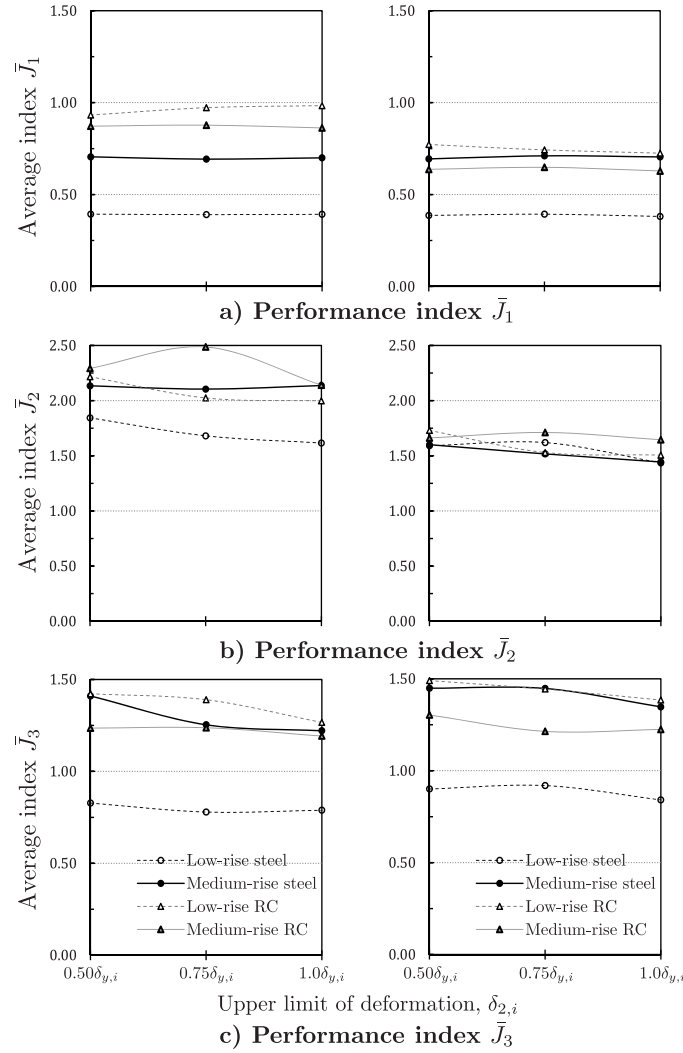
FIGURE 8.7: Average performance indices $\bar{J}_1$, $\bar{J}_2$ and $\bar{J}_3$ of *decentralised* TδVG control with $f_{s1,i} = 0.05 f_{y,i}$ (left) and $f_{s1,i} = 0.25 f_{y,i}$ (right), for earthquakes scaled to 0.35g.

uncontrolled structure. Therefore, the increase of peak acceleration was not considered as a critical, negative effect in the performance of the control system.

The new algorithm increased moderately the shear force at the base of the frames. As indicated by the index $\bar{J}_3$ (Fig. 8.7c), the average of shear force for the system with $f_{s1,i} = 0.25 f_{y,i}$ was reduced only for the low-rise steel frame, with an index around 0.90. For all other frames, the index varied between 1.21 (for the medium-rise RC frame) and 1.48 (for the medium-rise steel and low-rise RC frames). The system with $f_{s1,i} = 0.05 f_{y,i}$ also reduced the shear force in the low-rise steel frame, with an index around 0.80. Again, the shear force increased in all other frames, with indices between
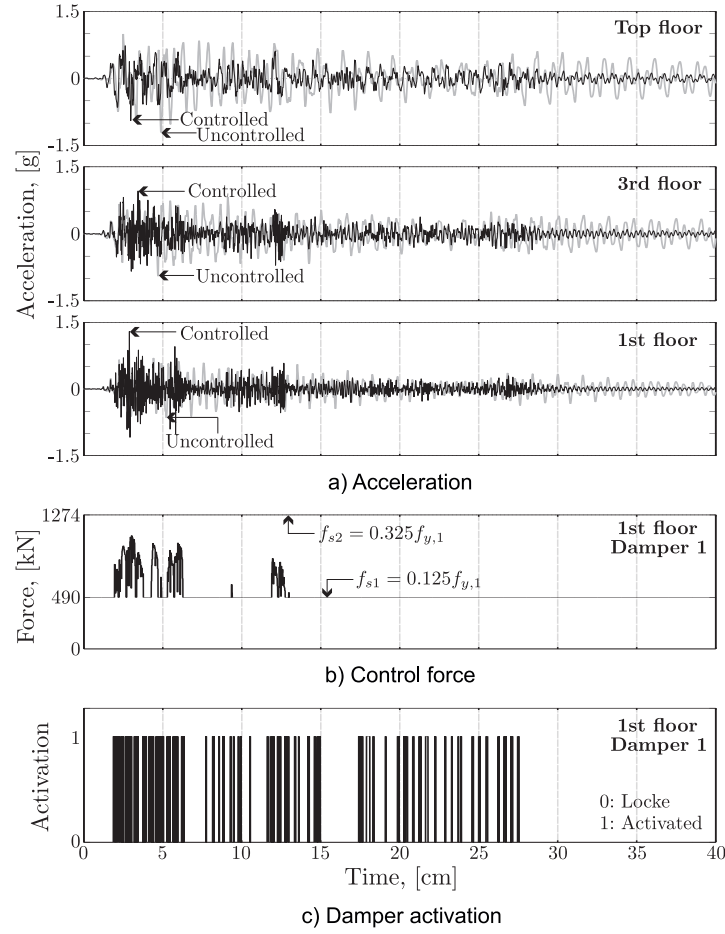
FIGURE 8.8: Low-rise steel frame: Time history of acceleration, control force and damper activation under the El Centro earthquake (PGA=0.35g).

1.24 and 1.40. For both control systems, the upper limit of deformation $\delta_{2,i}$ did not have a significant influence in the levels of the response.

The new control system was also efficient for the frames under the set of stronger earthquakes (PGA=0.55g), with smaller response obtained when the initial slip-load $f_{s1,i} = 0.25f_{y,i}$ was used. In this case, the values of the average index $\bar{J}_1$ were around 0.40 for the low-rise steel frame, and around 0.70 for all other frames. The average accelerations were increased, with indices $\bar{J}_2$ between 1.47 and 1.90. Due to the high levels of drift reduction, there was also an increase of the base shear. The increase, however, was moderate, as indicated by indices $\bar{J}_3$ ranging from 1.10, for the low-rise steel frame, to 1.60, for the medium-rise steel frame, and 1.40 for the two RC frames.

The results of the frames under each earthquake indicated lower levels of deformation (i.e. lower indices J_1) for the systems with $\delta_{2,i} = 1.0\delta_{y,i}$ (Figs. 8.9a to 8.12a), in 47% of

a) Performance index J_1

b) Performance index J_2

c) Performance index J_3
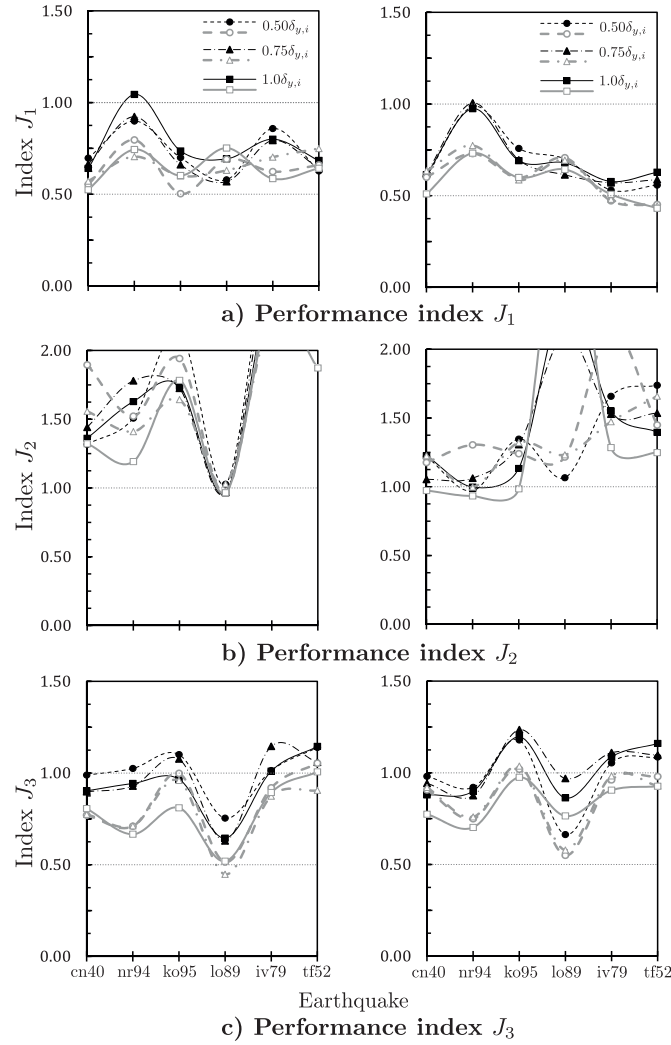
FIGURE 8.9: Low-rise steel frame: Performance indices J_1, J_2 and J_3 with TδVG control, for earthquakes scaled to 0.35g (grey line) and 0.55g (black line). Left: TδVG control with $f_{s1,i} = 0.05f_{y,i}$; Right: TδVG control with $f_{s1,i} = 0.25f_{y,i}$.

the analysed cases, followed by the systems with $\delta_{2,i} = 0.75\delta_{y,i}$ (34% of the cases) and $\delta_{2,i} = 0.50\delta_{y,i}$ (19% of the cases). Between the systems using either $f_{s1,i} = 0.05f_{y,i}$ or $f_{s1,i} = 0.25f_{y,i}$ in combination with $\delta_{2,i} = 1.0\delta_{y,i}$, the second system resulted in lower indices in the majority of the cases (73% of the cases). Due to the different characteristics of each earthquake (i.e. duration and frequency content), there was a large variability in the levels of response reduction, for each frame. In general, the system was less efficient for the stronger earthquakes (PGA=0.55g), especially for Northridge. Under this earthquake, the values of the index J_1 varied between 0.88 (for the low-rise RC frame) and 0.98 (for the low-rise steel frame and medium-rise RC frame). In the case of the medium-rise steel frame, the value of the index even increased to 1.1, which indicated

a) Performance index J_1

b) Performance index J_2

c) Performance index J_3
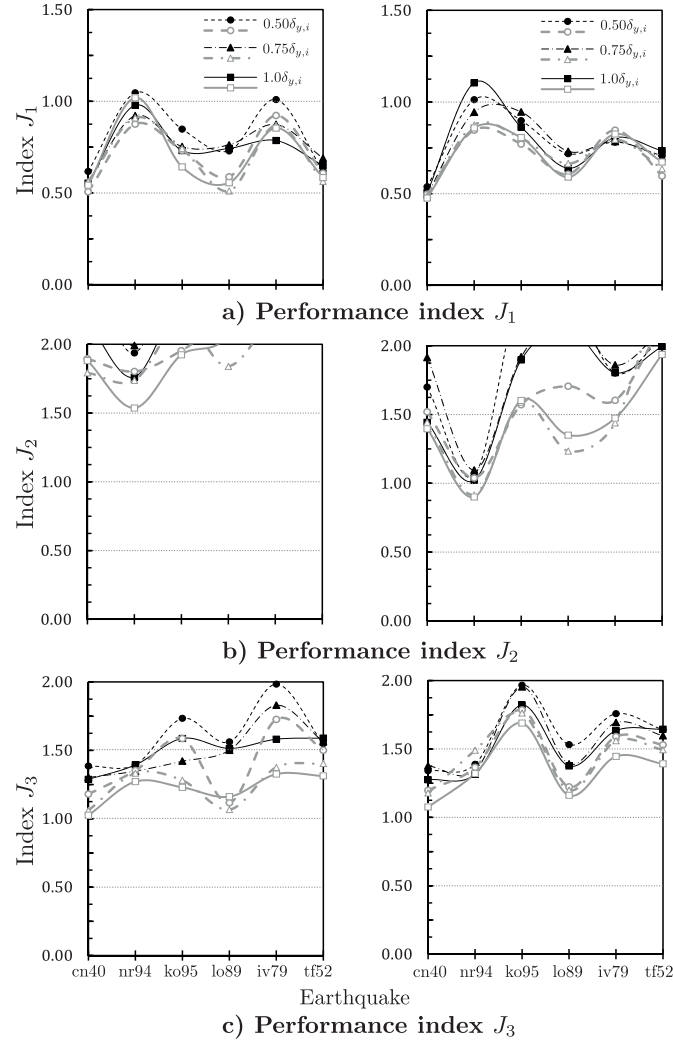
FIGURE 8.10: Medium-rise steel frame: Performance indices J_1, J_2 and J_3 with TδVG control, for earthquakes scaled to 0.35g (grey line) and 0.55g (black line). Left: TδVG control with $f_{s1,i} = 0.05f_{y,i}$; Right: TδVG control with $f_{s1,i} = 0.25f_{y,i}$.

a slight increase of the maximum deformation, in comparison to the bare frame.

As it can be seen in Figs. 8.9b to 8.12b, the new system produced high increases in the peak acceleration. In the great majority of the cases, the indices J_2 were higher than 1.0, and even exceeded 2.0 in many cases. However, as concluded before, this increase is due to the rapid changes in the stick/slip phases of the dampers. Outside of this transient effect, the accelerations in the controlled frames are lower than those of the bare frames.

The base shear (evaluated by the index J_3) was increased for all the controlled frames, apart from the low-rise steel frame (Figs. 8.9c to 8.12c). For the latter frame, the shear force was reduced for the majority of the earthquakes (scaled to either 0.35g or
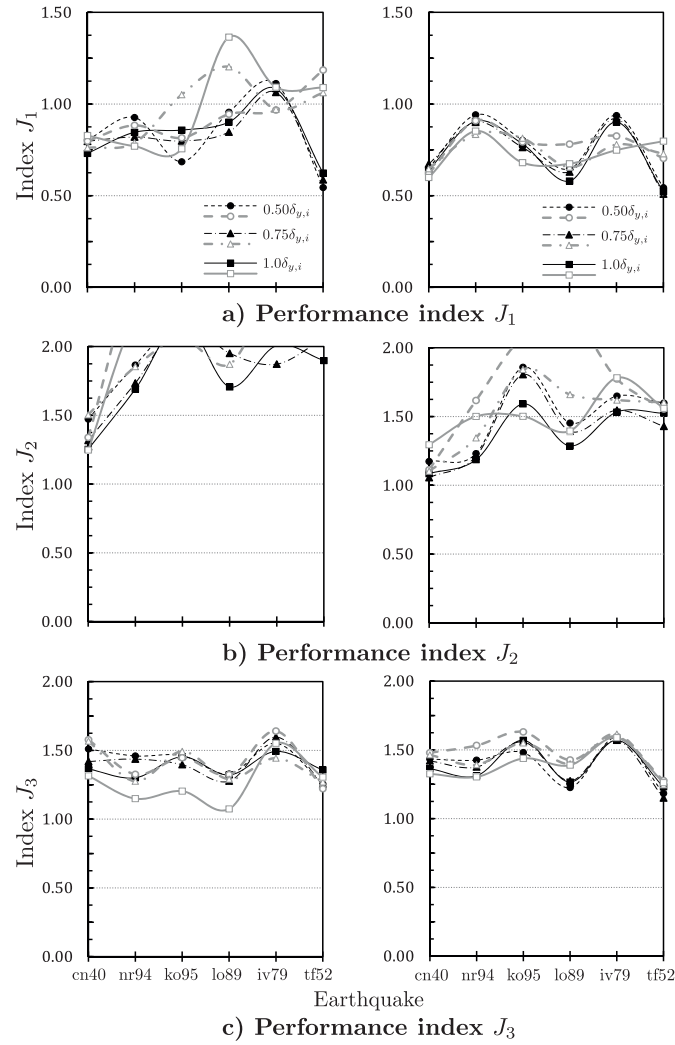
FIGURE 8.11: Low-rise RC frame: Performance indices J_1, J_2 and J_3 with TδVG control, for earthquakes scaled to 0.35g (grey line) and 0.55g (black line). Left: TδVG control with $f_{s1,i} = 0.05f_{y,i}$; Right: TδVG control with $f_{s1,i} = 0.25f_{y,i}$.

0.55g), and was slightly increased (in the order of 20%) only under Kobe, Imperial Valley and Taft earthquakes with PGA of 0.55g. The increase of shear in all other frames was moderate, in most of the cases, ranging from 10% to a maximum of 78%. The maximum increase of shear occurred for the medium-rise steel frame under Kobe earthquake scaled to 0.55g.

a) Performance index J_1

b) Performance index J_2

c) Performance index J_3
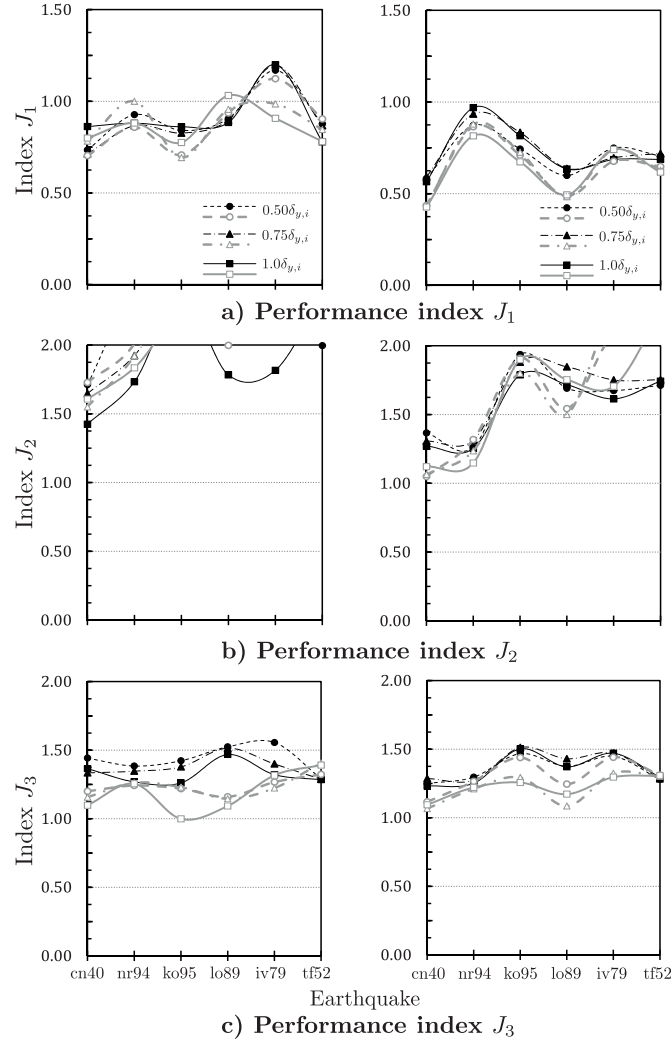
FIGURE 8.12: Medium-rise RC frame: Performance indices J_1, J_2 and J_3 with TδVG control, for earthquakes scaled to 0.35g (grey line) and 0.55g (black line). Left: TδVG control with $f_{s1,i} = 0.05f_{y,i}$; Right: TδVG control with $f_{s1,i} = 0.25f_{y,i}$.

8.5.3 Evaluation of building damage

The TδVG system reduced the inter-storey deformations sufficiently so as to avoid significant damage in the structure. As indicated by low values of the average index $\bar{J}_4$ (Fig. 8.13a), the structures practically remained elastic under the earthquakes scaled to 0.35g. For some strong earthquakes (0.55g), there was some little damage in the structure, but even in this case, it was not significant and the amount of energy dissipated through hysteresis in the beams was very small. The largest damage among all four buildings occurred in the medium-rise RC frame under the Taft excitation. In this situation, the index J_4 (Fig. 8.14a) was 0.21, which was, nevertheless, a very low value.

a) Performance index $\bar{J}_4$

b) Performance index $\bar{J}_5$
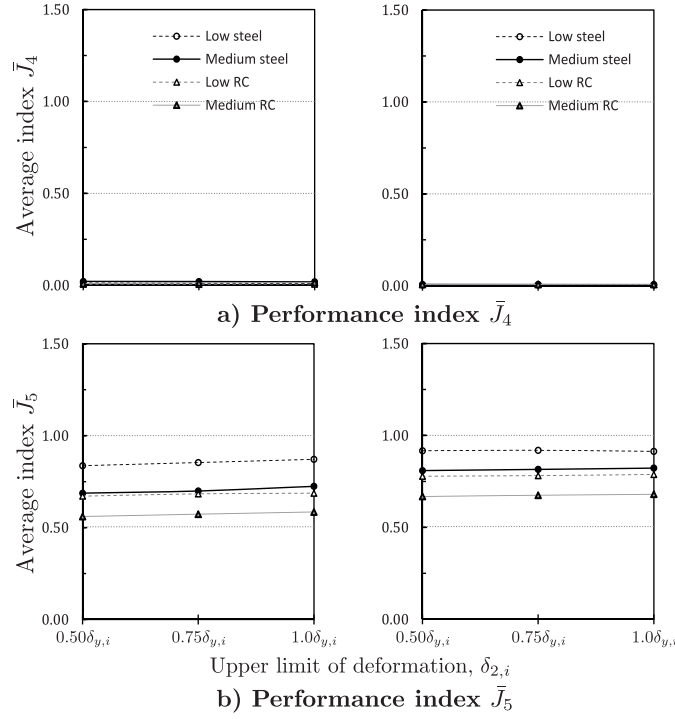
FIGURE 8.13: Average performance indices $\bar{J}_4$ and $\bar{J}_5$ of new TδVG control with $f_{s1,i} = 0.05 f_{y,i}$ (left) and $f_{s1,i} = 0.25 f_{y,i}$ (right), for earthquakes scaled to 0.35g.

As a result of the little damage in the beams, the slippage in the friction connections became the supplemental mechanism for energy dissipation in the frames. This situation is indicated by the high values of the average index $\bar{J}_5$ (Fig. 8.13b) and the index J_5 (Fig. 8.14b), corresponding to the medium-rise RC frame under each earthquake.

The distribution of the seismic energy in the frames with and without control is shown in Fig. 8.15. The inclusion of the control system had the immediate effect of increasing the stiffness of the bare frame, hence increasing the amount of energy exerted. This is reasonable because the energy is a reflection of the amount of work done by the structural elements, which was calculated as the product of the force and the displacement and/or deformation. Although an increase of the stiffness generally produced a reduction of the displacements in the frame, the level of structural forces was increased, resulting in a higher amount of energy exerted. Considering the distribution of energy in Fig. 8.15a, it can be seen that large amounts of energy were dissipated in the uncontrolled frame through two mechanisms: i) inherent structural (viscous) damping, and ii) damage in the beams. On the other hand, it can be seen that the mechanism of dissipation in the controlled frame (Fig. 8.15b) consisted mainly in the friction connections, with small amounts of energy being dissipated through the inherent structural damping, and none through damage in the beams, which means that the frame remained elastic.
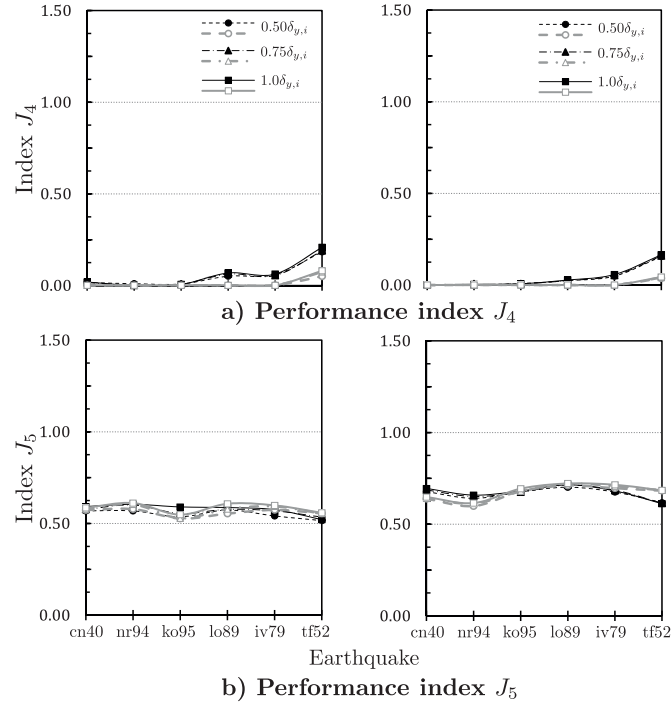
FIGURE 8.14: Medium-rise RC frame: Performance indices J_4 and J_5 with new TδVG control, for earthquakes scaled to 0.35g (grey line) and 0.55g (black line). Left: TδVG control with $f_{s1,i} = 0.05f_{y,i}$; Right: TδVG control with $f_{s1,i} = 0.25f_{y,i}$.
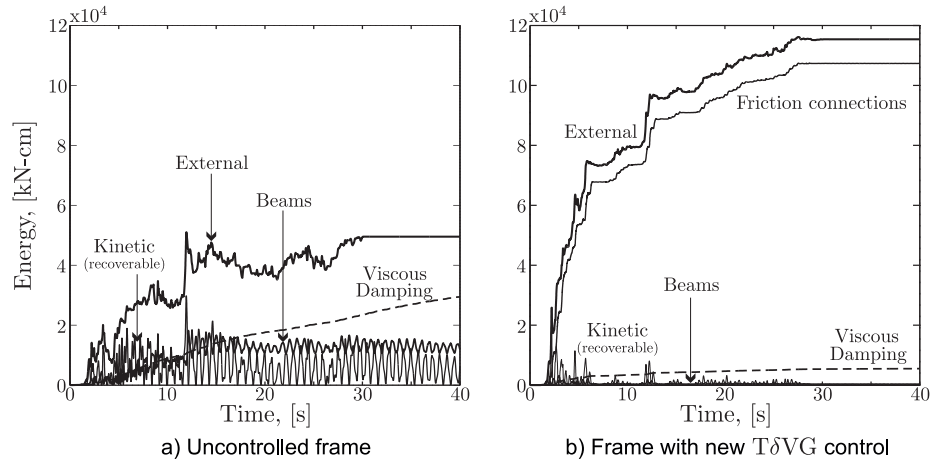
FIGURE 8.15: Low-rise steel frame: Distribution of energy in uncontrolled and controlled frames, under the El Centro earthquake (0.35g).

8.5.4 Evaluation of control forces

As it was designed, the level of control forces required by the algorithm (evaluated by the index J_6) varied within the optimum range of passive loads (i.e. $0.25f_{y,i}$ to $0.65f_{y,i}$). For most of the stronger earthquakes (PGA=0.55g), the controller required the maximum slip-load capacity of the dampers. However, for many of the moderate earthquakes (PGA=0.35g), the required control forces were below the maximum capacity, with values as high as $0.50f_{y,i}$.

In Figure 8.16, typical values of the index J_6 are shown for the low-rise steel and the medium-rise RC frames subjected to the earthquakes scaled to 0.35g (grey line) and 0.55g (black line).

a) Low-rise steel frame

b) Medium-rise RC frame
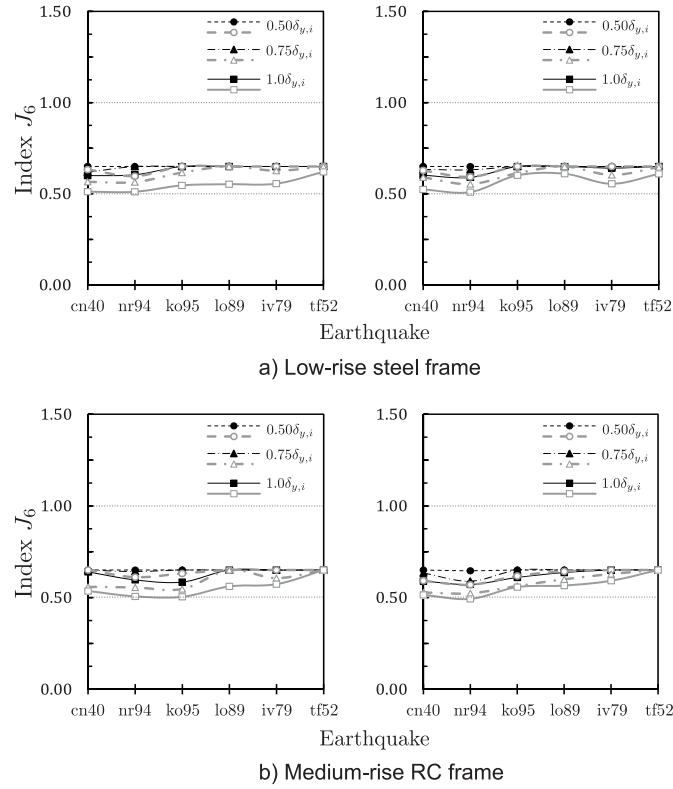
FIGURE 8.16: Performance index J_6 (control force) with new TδVG control, for earthquakes scaled to 0.35g (grey line) and 0.55g (black line). Left: TδVG control with $f_{s1,i} = 0.05f_{y,i}$; Right: TδVG control with $f_{s1,i} = 0.25f_{y,i}$.

8.6 Comparison of passive, Tri-D and TδVG control systems

8.6.1 Drift reduction and required control forces

The new TδVG control with $f_{s1,i} = 0.25f_{y,i}$ and $\delta_{2,i} = 1.0\delta_{y,i}$ was compared to the passive control and the semiactive Tri-D system (with $f_{p,i} = 0.15f_{y,i}$ and high gain factor), in terms of maximum drift reduction (index J_1) and range of required control forces, expressed as the ratio $f_{s,i}/f_{y,i}$. As it can be seen in Figs. 8.17 to 8.20, the two semiactive controllers reduced the maximum inter-storey drift of the bare frames under all earthquake excitations, although the level of reduction varied from frame to frame and earthquake to earthquake.

In comparison with the optimum passive control, the new TδVG improved the response of the frames in 62.5% of the analysed cases, showing the same level of efficiency than the Tri-D system. However, the disadvantage of the passive system was that the maximum reductions were obtained only for one slip-load, which was different for most of the earthquakes. In practical applications, this can limit the efficiency of the control strategy, since only one value of slip-load can be selected. On the other hand, the main disadvantage of the Tri-D algorithm, as it can be observed in Figs. 8.17 and 8.18, was the range of required control forces, which was significantly larger than $0.65f_{y,i}$, for most of the earthquakes, especially when this system was applied to the steel frames.

In comparison with the Tri-D algorithm, the TδVG control produced improvements in 54% of the cases. In the majority of the cases there were no significant differences between the levels of drift reduction produced by each control system. However, the new control algorithm produced those response levels by requiring much smaller control forces, capped by the upper limit of $0.65f_{y,i}$. This results in significant reduction in demand on the structural elements, the components of the friction connection and the control system.

The new system was not very efficient for the frames under the Northridge earthquake scaled to 0.55g. In the case of the low-rise steel frame and the medium-rise RC frame, the system only reduced the drift by 5%. In the case of the medium-rise steel frame, the drift was slightly increased around 10%. The reason for this can be attributed to the impulse of the excitation, which suddenly activates the friction connections, possibly creating some little damage and reducing the restoring forces in the structure.
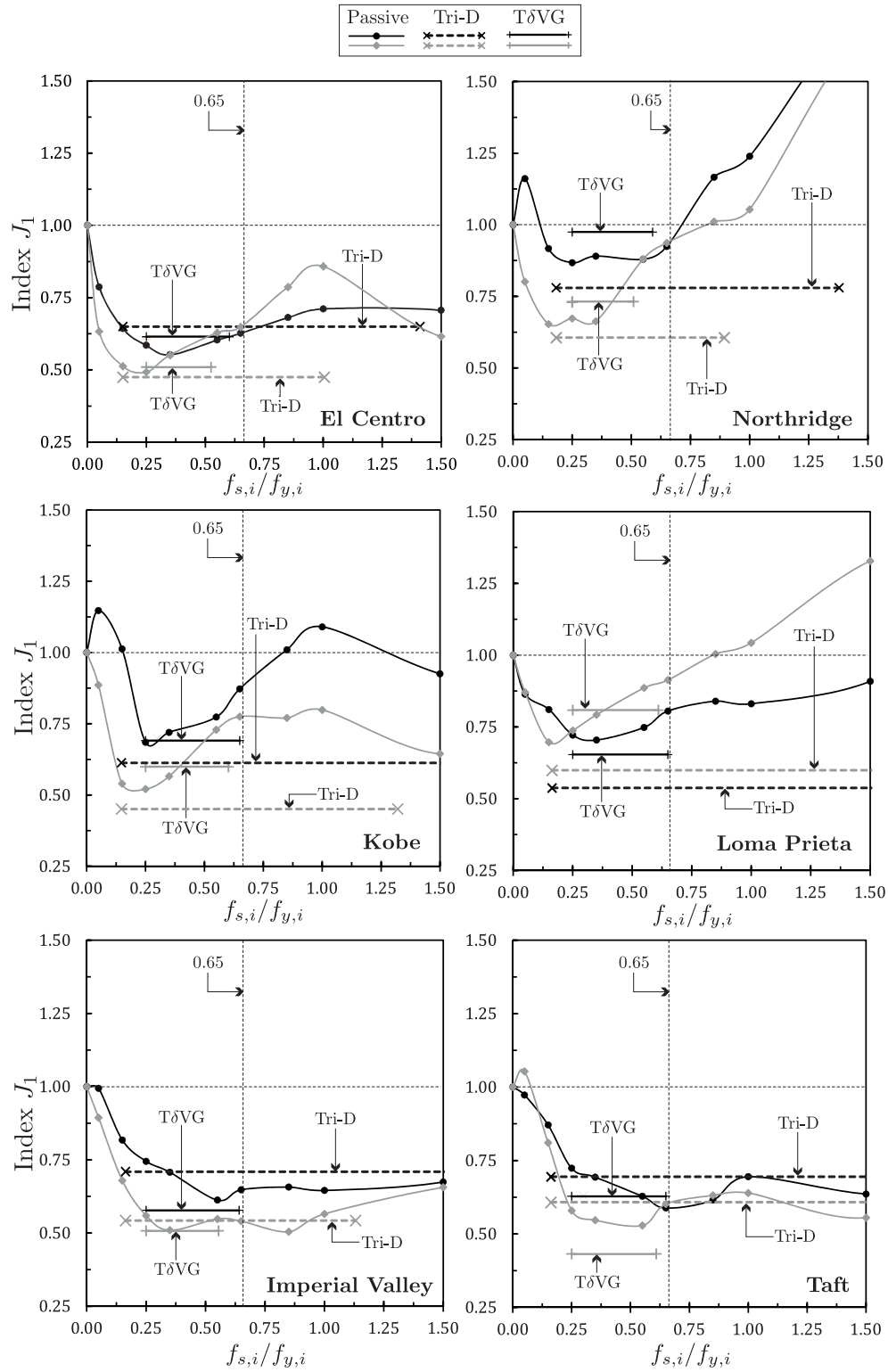
FIGURE 8.17: Low-rise steel frame: Comparison of drift reduction with passive control, existing semiactive Tri-D control and new semiactive TδVG control, for earthquakes scaled to 0.35g (grey line) and 0.55g (black line).
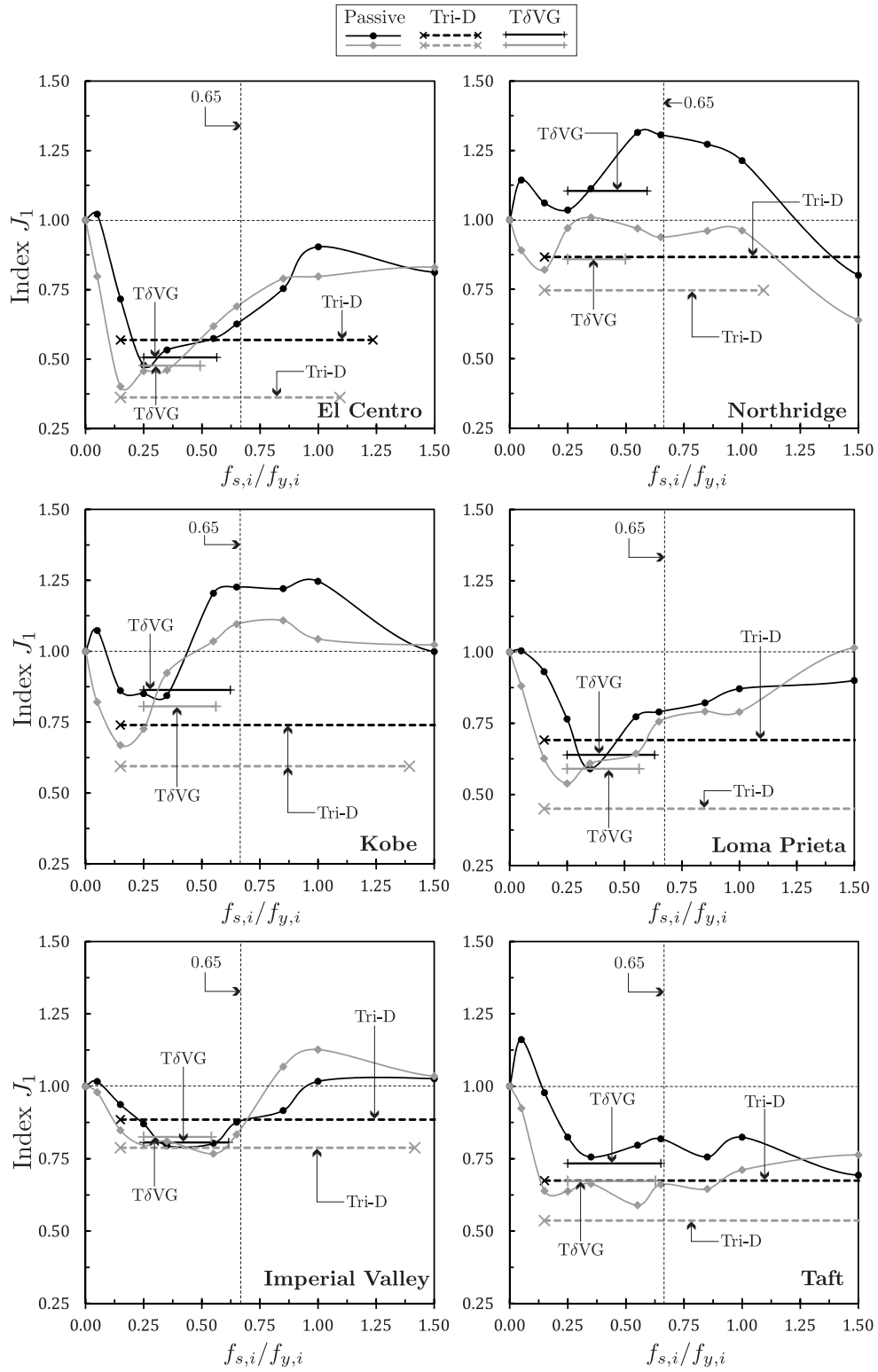
FIGURE 8.18: Medium-rise steel frame: Comparison of drift reduction with passive control, existing semiactive Tri-D control and new semiactive TδVG control, for earthquakes scaled to 0.35g (grey line) and 0.55g (black line).
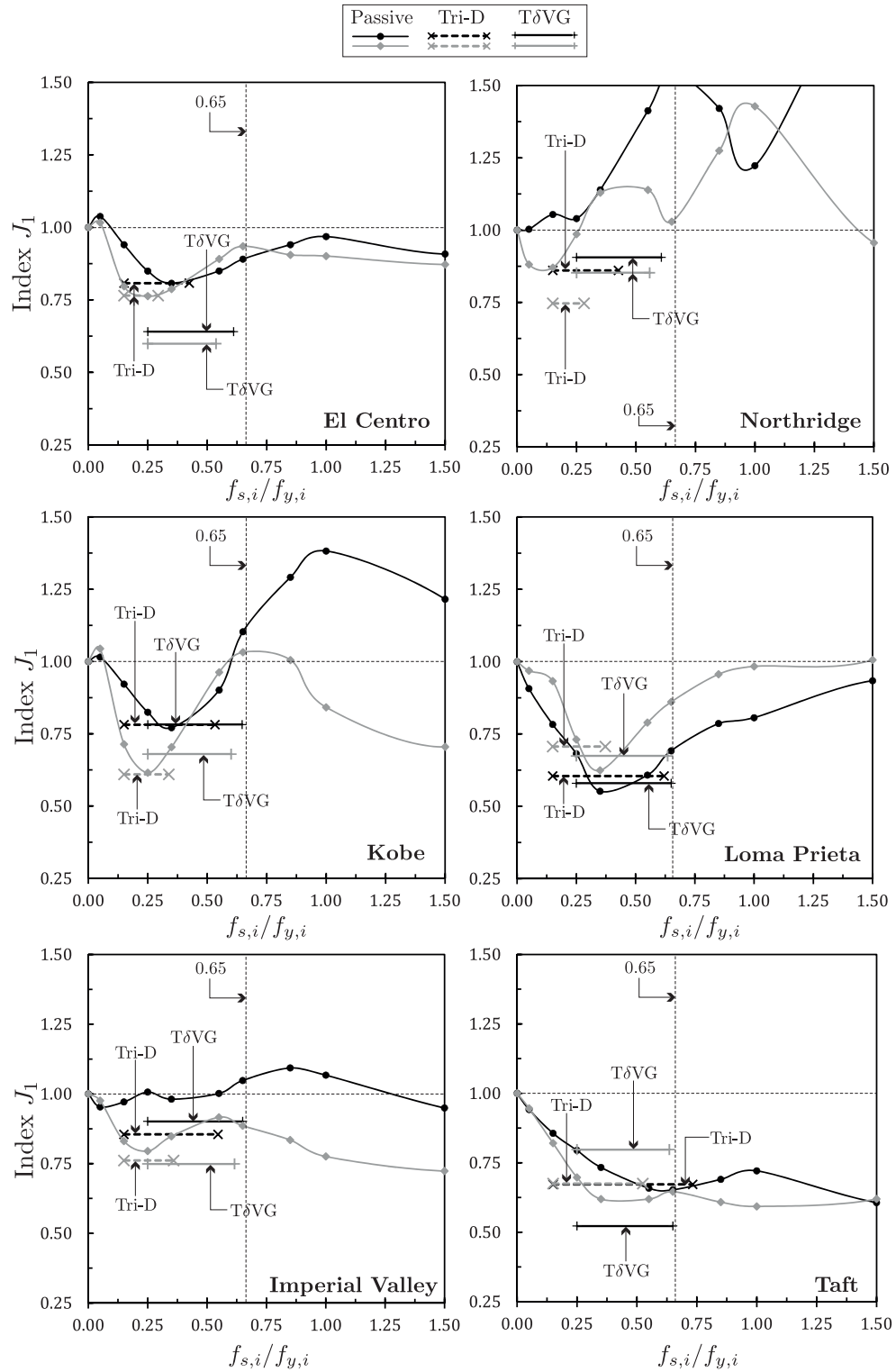
FIGURE 8.19: Low-rise RC frame: Comparison of drift reduction with passive control, existing semiactive Tri-D control and new semiactive TδVG control, for earthquakes scaled to 0.35g (grey line) and 0.55g (black line).
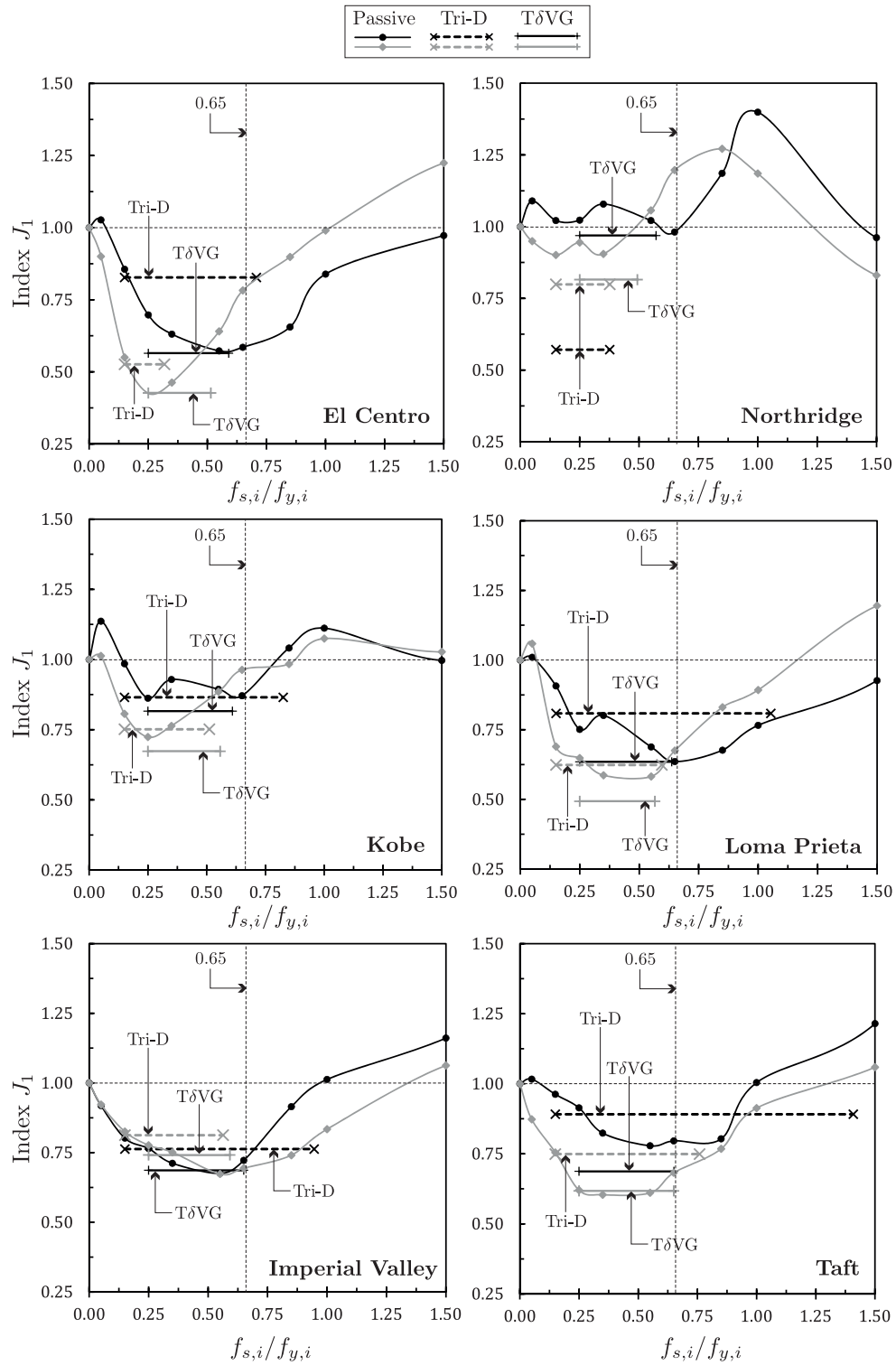
FIGURE 8.20: Medium-rise RC frame: Comparison of drift reduction with passive control, existing semiactive Tri-D control and new semiactive TδVG control, for earthquakes scaled to 0.35g (grey line) and 0.55g (black line).

8.6.2   Top floor displacement and drift distribution

The average top floor displacement produced by each control system was compared as the ratio of controlled to uncontrolled displacement (i.e. $\bar{d}_c/\bar{d}_b$). In the comparisons, the TδVG system with $f_{s1,i} = 0.25f_{y,i}$ and $\delta_{2,i} = 1.0\delta_{y,i}$ was included because this set of control parameters resulted in better levels of response reduction for the majority of the earthquakes.

As shown in Fig. 8.21, all three systems resulted in large reductions of the average top floor displacement, in some cases even more than 50%. In the case of the steel frames (Figs. 8.21a and b), the reductions produced by the Tri-D and TδVG systems were comparable to those of the optimum passive control (with small differences of about 5%). However, as it can be observed in the figures, the maximum reductions of the passive control were obtained for different values of slip-load. The Tri-D system resulted in better levels than the TδVG control, but considering that the deformations of the TδVG algorithm were within elastic limits of the frame, this improvement is not important. On the other hand, the control forces required by the Tri-D system were significantly larger (more than 2 times, in some cases), which leads to large axial forces in braces and columns.

In the case of the RC frames (Fig. 8.21b and c), large levels of displacement reduction were also produced by all three control systems, with small differences of up to 10% for the low-rise frame, and 20% for the medium-rise frame. The TδVG control resulted in responses comparable or slightly larger than the optimum passive control, but smaller than those of the Tri-D system.

As mentioned in Section 8.2, the efficiency of *decentralised* systems may be limited because there is no exchange of information between each local controller. This limitation, in the case of the Tri-D and the TδVG system was evident only as a non-uniform distribution of the inter-storey drift, even when the seismic response in each floor was largely reduced. As an example of the drift distribution, the history of top floor displacement and the envelopes of maximum drift and maximum control forces are shown in Figs. 8.22 and 8.23, for the frames under the El Centro earthquake scaled to 0.55g.
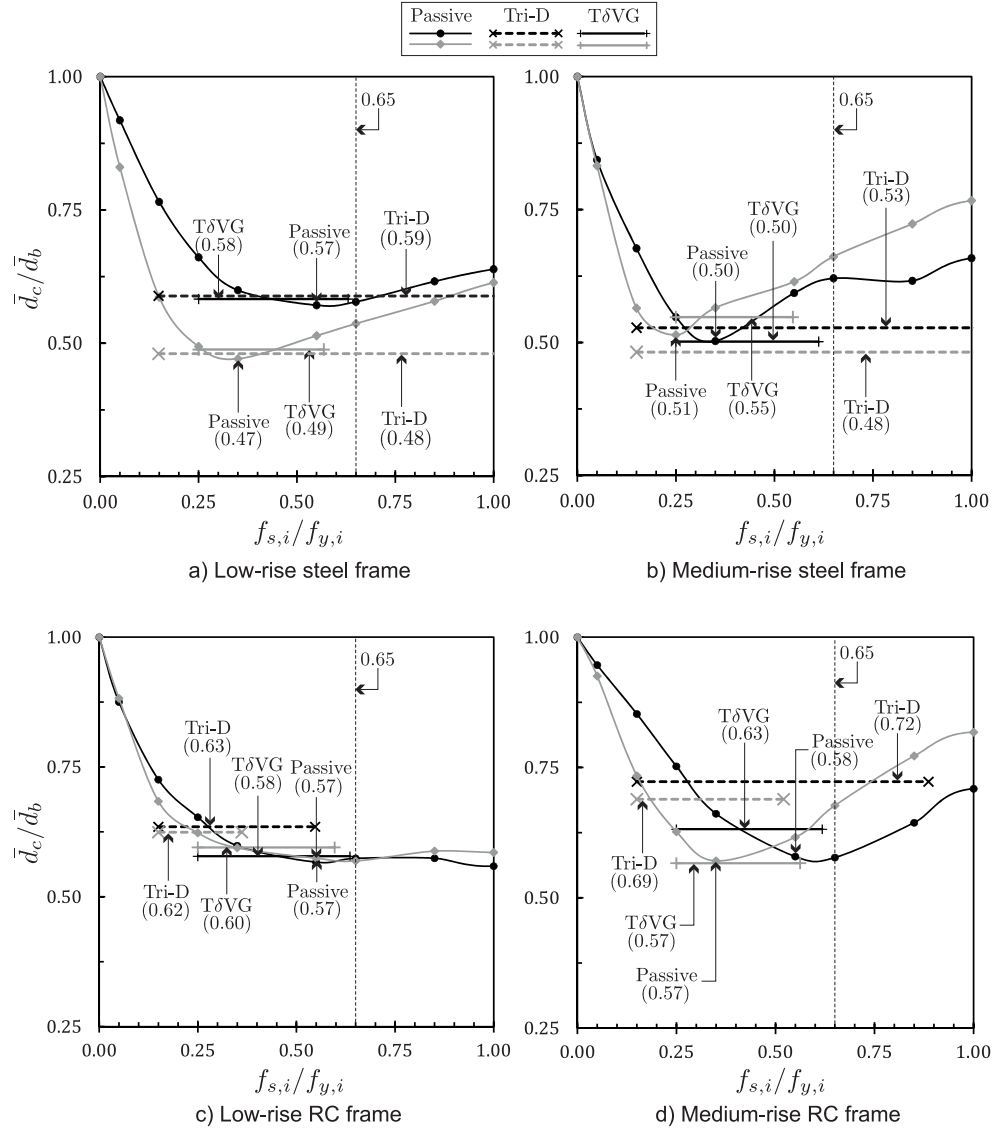
FIGURE 8.21: Comparison of top floor displacement (average) with passive, Tri-D and TδVG controllers, for earthquakes scaled to 0.35g (grey line) and 0.55g (black line).
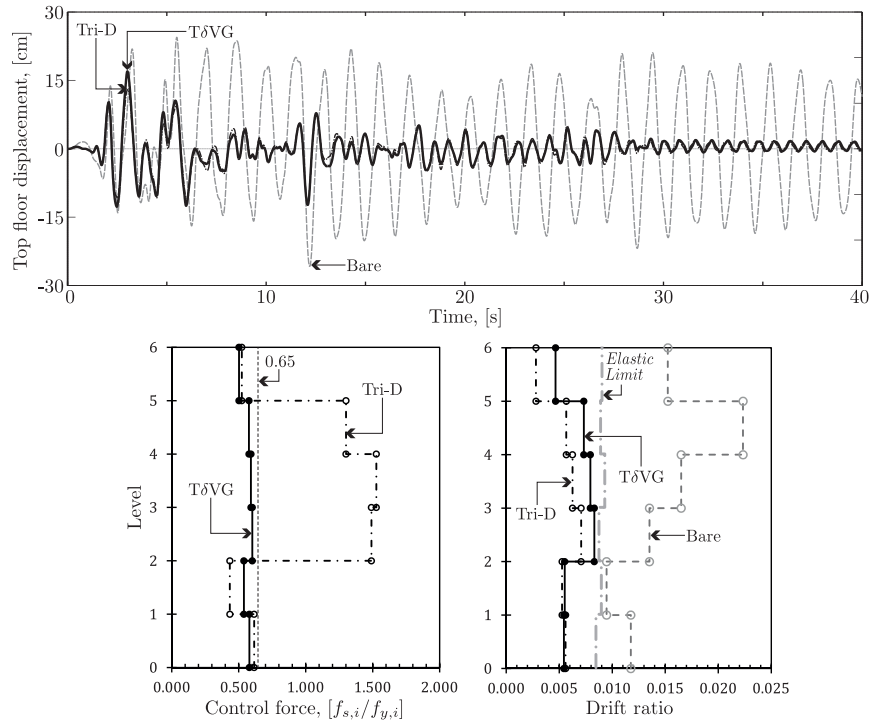
a) Low-rise steel frame
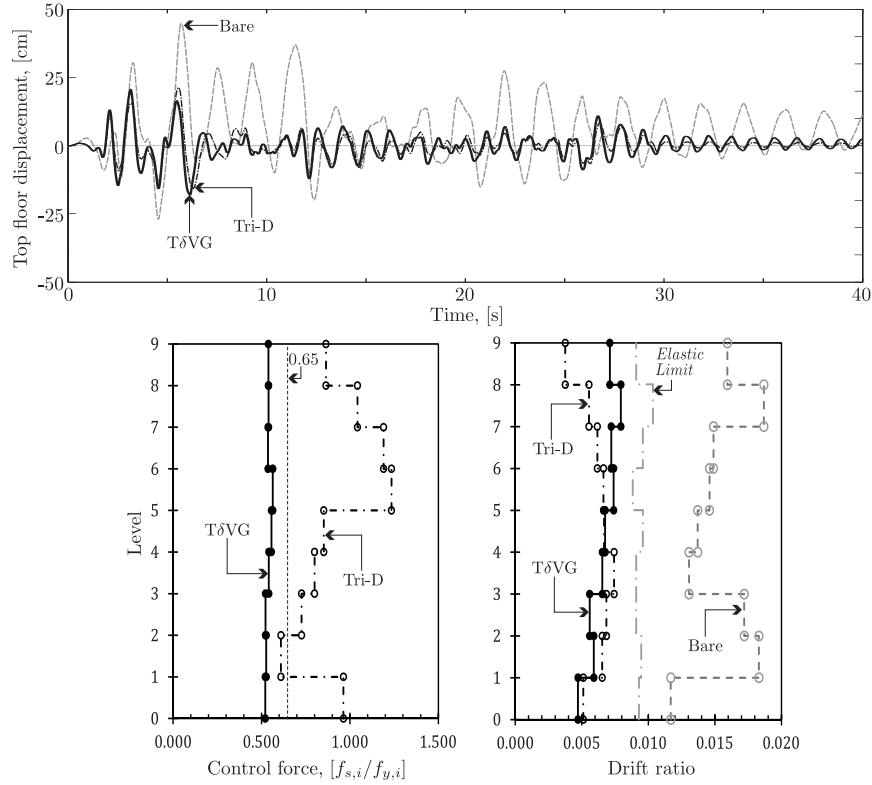
b) Medium-rise steel frame

FIGURE 8.22: Seismic response of steel frames with Tri-D and TδVG controllers, under the El Centro earthquake (0.55g).

a) Low-rise RC frame

b) Medium-rise RC frame
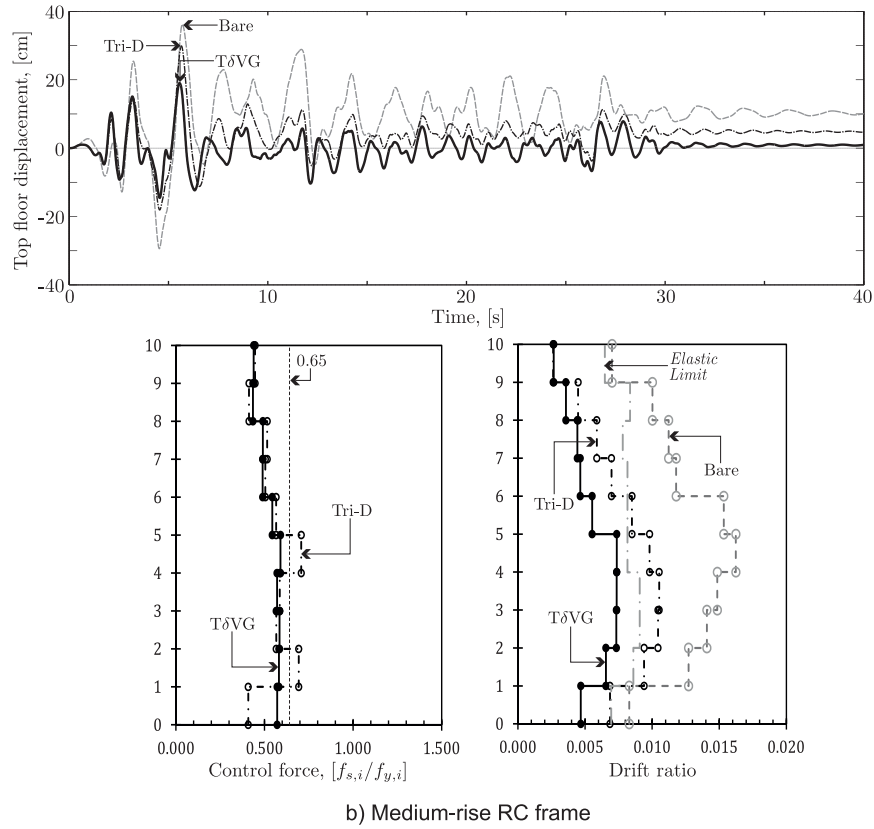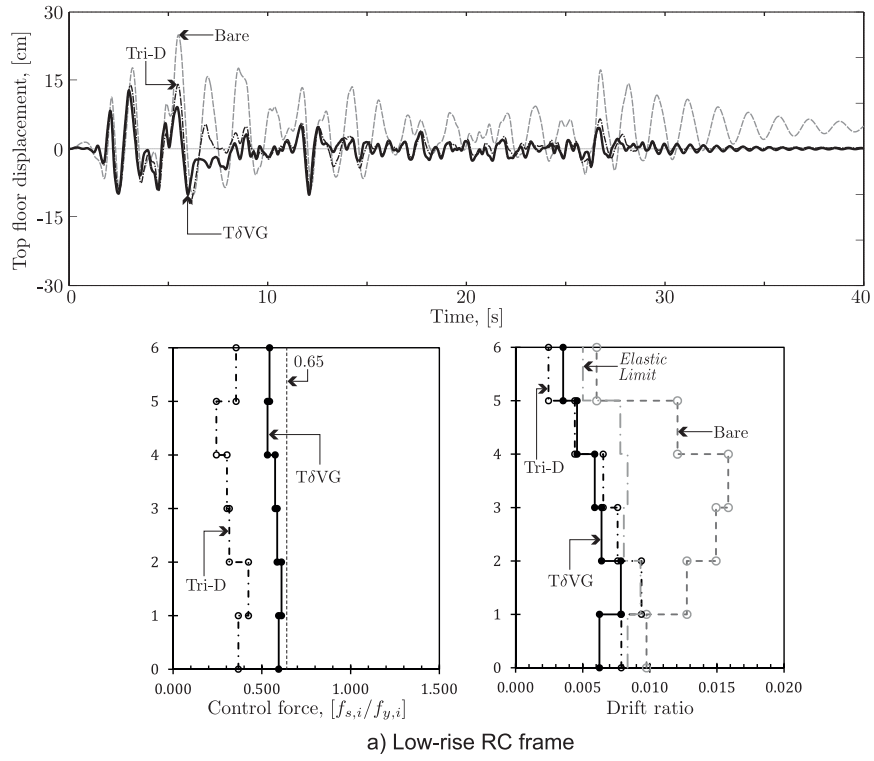
FIGURE 8.23: Seismic response of RC frames with Tri-D and TδVG controllers, under the El Centro earthquake (0.55g).

8.6.3 Frequency content of the seismic response

The modification of the seismic response in the controlled frames resulted from the increase of initial stiffness, the increase of structural damping and the variation of the dynamic properties of the frame due to the activation/deactivation of the dampers during the ground motion (Section 7.5.1).

In order to have an insight of the mechanism of the TδVG control, the top floor displacement of the medium-rise steel frame was analysed in terms of its frequency content and compared to the bare frame, the braced frame (represented by the passive system with $f_{s,i}/f_{y,i} = 2.5$) and the Tri-D system. The history of displacements of the frame under the El Centro earthquake (PGA=0.35g) was divided in four segments, according to the intensity of the excitation (high, medium, low and decay). As shown in Fig. 8.24, the spectral amplitude of the semiactive systems was much smaller than those of the bare frame and the braced frame. These two systems (bare and braced) showed peaks of amplitude corresponding to their fundamental frequencies (0.49Hz and 1.09Hz, respectively).

From 10s to 40s, both Tri-D and TδVG systems produced small peaks between 0.49Hz and 1.09Hz, with the largest amplitudes around 0.9Hz. Both systems, however, showed no significant amplification of any frequency component of the earthquake. This condition, in combination with no important peaks at 0.49Hz, indicated that the inclusion of the friction connections was effective in increasing the stiffness of the frame during the ground motion, but the smaller amplitudes in comparison with the braced system, indicated an increase of the structural damping, due to increased slippage in the connections.

8.7 Concluding remarks

A new semiactive control system was developed in order to overcome the limitations of existing passive control and four *decentralised* semiactive systems (MHF, LBL, SBL and Tri-D). The major limitation of those systems is their lack of adaptability. In the case of the passive control, the forces in the connections are pre-set and the best force distribution varies from earthquake to earthquake. In the case of the semiactive systems, the gain factors were constant, which again made it difficult to choose the right parameters for different structure-earthquake combinations, thus resulting in excessively large control forces.
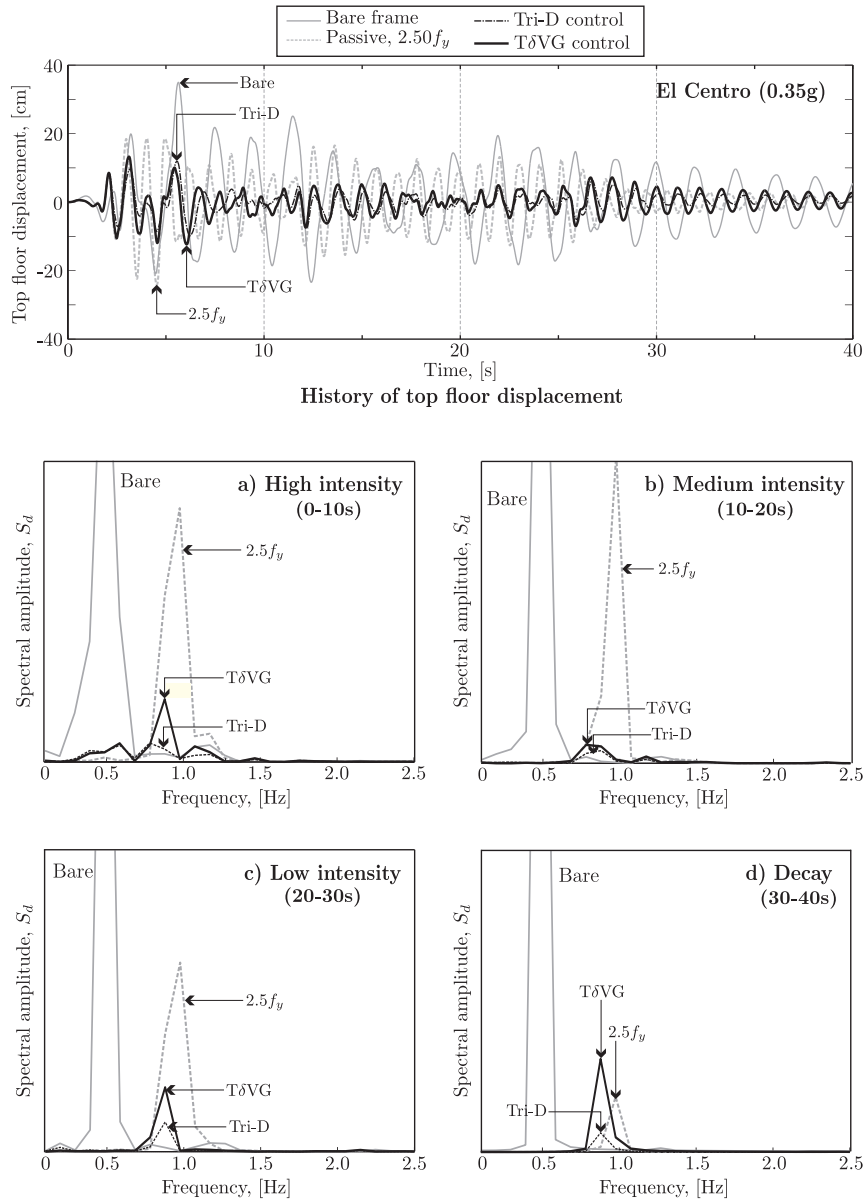
FIGURE 8.24: Medium-rise steel frame: Frequency content of top floor displacement with passive, Tri-D and TδVG controllers, under El Centro earthquake.

The new TδVG control system maintained the advantages of the passive and existing semiactive algorithms: simplicity of devices and *decentralised* control architecture. However, the novelties of the system are:

- *Variable gain factors* (rather than pre-specified, constant values), which are adjusted in accordance with the response and pre-defined characteristics of the structure. A cubic root relationship of the ratio between inter-storey drift values and

pre-defined drift limits (or *target deformation*, which depends on the elastic defor-
mation limits of the structure), was found to be the most effective of the relation-
ships examined in this study.

- *Control force limits*, within the optimum range of passive slip-loads (i.e. $0.25 f_{y,i}$ to
  $0.65 f_{y,i}$). The level of control forces is related directly to the actual resistance of the
  frame structure ($f_{y,i}$). The ratios used in this study (0.25 to 0.65) were determined
  on the basis of a parametric study with different buildings and earthquakes.

The TδVG system was applied to four multi-storey frames subjected to different earth-
quakes: El Centro, Northridge, Kobe, Loma Prieta, Imperial Valley and Taft, scaled to
0.35g and 0.55g. Different limits of *target deformation*, $\delta_{2,i}$, were also used in the control
algorithm. In general, the controller with largest limit of deformation (i.e. $\delta_{2,i} = 1.0\delta_{y,i}$)
and highest initial slip-load (i.e. $f_{s1,i} = 0.25 f_{y,i}$) was the most efficient in reducing de-
formations and top floor displacements, with moderate increases of the base shear in
average (in the order of 40%) or no increase at all (in the case of the low-rise steel
frame). The higher efficiency of the system with those control parameters was caused
by a mechanism similar to that of the existing semiactive algorithms (Chapter 7): i) an
increase of initial stiffness, in the early stages of deformation, due to delayed activation
of the friction connections, and ii) an increase of structural damping, which resulted
from the delay to reach the maximum slip-load, in the later stages of response.

The efficiency of the TδVG system was reduced for some seismic excitations with higher
PGA. This was the result of a smaller proportion of energy dissipated through the friction
connections and an increased proportion of energy dissipated through damage in the
beams, which, however, was very small in all cases. The level of control forces required
by the algorithm also increased for the frames under the set of stronger excitations,
reaching the upper-limit in most of the cases.

The responses produced by the new TδVG controller were compared with those of the
passive and the semiactive Tri-D systems. In general, the optimum passive system pro-
duced smaller inter-storey deformations than both semiactive controllers. However, due
to the lack of adaptability, the optimum slip-load varied from earthquake to earthquake.
On the other hand, it was observed that, for the semiactive systems, larger control forces
resulted in larger reductions of deformation. The main advantage of TδVG over Tri-
D algorithm was a significant reduction of maximum control forces ($0.65 f_{y,i}$ in TδVG
versus more than $1.5 f_{y,i}$, in some cases, in Tri-D). This resulted in a small increase of
deformations (compared to Tri-D), but since they were still within the elastic limits of
the structures, the performance of the structure was not affected.

Due to the *decentralised* architecture of the TδVG controller, there was no exchange of information between the local controllers. As a result, there was a non-uniform distribution of the inter-storey drift throughout the height of the frames. Whereas this situation did not affect the performance of the control, in terms of response reduction, one possible alternative would be to use a *partially decentralised* system in which the control forces were generated based on the relation of the local *feedback* to the global structural response.

Chapter 9

New semiactive algorithms: AδVG, a partially decentralised system

9.1   Introduction

In the previous Chapter, a new semiactive control algorithm (TδVG) was proposed as a solution to the limitations of existing passive and semiactive systems. This algorithm utilised variable gain factors which adjusted the slip-loads as a function of the relation between real-time inter-storey deformations and pre-defined deformation limits.

The TδVG control system was applied to a set of low-rise and medium-rise structures subjected to different seismic inputs. Similarly to the passive system and the semiactive Tri-D system (Chen and Chen, 2004c), this algorithm could achieve significant reductions of inter-storey deformation. In many cases, the new control produced deformations smaller than those of the passive and Tri-D systems. One clear advantage of the TδVG algorithm was the enhancement in adaptability of the control: significant response reductions were obtained using a range of relatively low slip-loads, which was within the range of optimum passive loads (i.e. $0.25f_{y,i}$ to $0.65f_{y,i}$, where $f_{y,i}$ is the shear force which produced the first plastic hinge in the storey i, determined from pushover analysis). The control forces produced by TδVG were significantly lower (even in the order of 50% lower, in some cases) than those in the Tri-D system, in most of the cases.

One possible limitation of the TδVG system was its (*totally*) *decentralised* architecture. However, from the results of the seismic simulations, the drawback of such an architecture was observed only in the non-uniform distribution of the inter-storey deformations

throughout the height of the buildings. This, however, was expected, because each controller reacted to local *feedback* only.

In order to investigate the potential for better levels of response reduction, along with more uniform distribution of inter-storey deformations, another control system was investigated in this study. The new algorithm uses a *partially decentralised* architecture, in which local, variable gain factors were determined as a function of the relations between local inter-storey deformations and their distribution along the height of the building. Similarly to the TδVG algorithm, the new system was designed to maintain the level of slip-loads within a range of relatively low values ($0.25f_{y,i}$ to $0.65f_{y,i}$).

9.2 Expected advantages of *partially decentralised* control systems

Similarly to passive systems, in (*totally*) *decentralised* semiactive systems, such as those examined in the previous chapters, the magnitude of the control forces depends only on local structural response. Although the efficiency of the control system can be high (in terms of large levels of response reduction), there can also be a non-uniform distribution of the deformations throughout the height of the buildings.

Partially decentralised systems, on the other hand, offer a possibility to control the distribution of deformations because the local controllers are inter-connected. In such a control architecture, the local controllers have a partial knowledge of the overall structural response. Thus, modifications in the local slip-loads would aim at adjusting the global response of the structure, in this case the distribution of inter-storey deformations.

Although requiring transference of information between local controllers, *partially decentralised* systems still allow for simple control algorithms, two of which were examined in this investigation. As illustrated in Fig. 2.8 on page 17 (Chapter 2), a *partially decentralised* system required a central computer in this research. However, the function of such computer was only to average the response, so that the local controllers would only process small amounts of information, similar to *decentralised* algorithms. This would avoid delays in generation of control signals.

In order to keep the simplicity of *decentralised* algorithms, in this study the *feedback* information used by the *partially decentralised* systems was limited to the inter-storey deformations. This could simplify monitoring tasks in practical applications by using a simple displacement sensor, such as a linear variable differential transducer (LVDT).

9.3 Proposed control algorithms

9.3.1 Algorithm for *partially decentralised* control with fixed force increment (FFI)

Based on the idea of *decentralised* modified bang-bang control proposed by Akbay and Aktan (1990) and Kannan et al. (1995), in which the control forces were adjusted at pre-defined time intervals by fixed force increments, a new, simple control algorithm was initially considered in this investigation.

The objectives of the new *partially decentralised* FFI controller were to reduce the seismic response of buildings and in the same time to produce a uniform distribution of the inter-storey deformations. In order to do so, the dampers' slip-loads were adjusted at pre-defined intervals of decision Δt, by either adding or subtracting pre-defined, fixed force increments $\Delta f_{s,i}$, which could be different for the damper on each storey i.

In the FFI controller, for a building with n-controllers (one per storey), their initial slip-loads were pre-set by following a design distribution (in this case proportional to the yield strength of each storey, $f_{y,i}$), as $f_{s1,i} = \alpha_i f_{y,i}$, where α_i is a factor of proportionality. The control force for the first floor $i = 1$ was kept constant throughout the earthquake (i.e. $|f_{s,1}(t)| = f_{s1,1} = \alpha_1 f_{y,1}$). The control forces on the other floors were varied during the ground excitation as:

$$
f_{s,i+1}(t) = \begin{cases}
\begin{aligned}
&\text{if } t < \Delta t: \quad \ldots \\
&\quad f_{s1,i+1} sgn(\dot{\delta}_{i+1}(t)) \\[1em]
&\text{if } t \geq \Delta t: \quad \ldots \\
&\quad (|f_{s,i+1}(t - \Delta t)| + \Delta f_{s,i+1})\, sgn(\dot{\delta}_{i+1}(t)), \quad \text{if } \left|\frac{\hat{\delta}_{i+1}(t)}{\hat{\delta}_i(t)}\right| > (1 + tol) \\[1em]
&\quad |f_{s,i+1}(t - \Delta t)| sgn(\dot{\delta}_{i+1}(t)), \quad \text{if } (1 - tol) \leq \left|\frac{\hat{\delta}_{i+1}(t)}{\hat{\delta}_i(t)}\right| \leq (1 + tol) \\[1em]
&\quad (|f_{s,i+1}(t - \Delta t)| - \Delta f_{s,i+1})\, sgn(\dot{\delta}_{i+1}(t)), \quad \text{if } \left|\frac{\hat{\delta}_{i+1}(t)}{\hat{\delta}_i(t)}\right| < (1 - tol)
\end{aligned}
\end{cases}
\tag{9.1}
$$

In Equation 9.1, the control force $f_{s,i+1}(t)$ represents an update of the slip-load determined in the previous interval $t - \Delta t$, by means of adding or subtracting the pre-defined, fixed force increment $\Delta f_{s,i+1}$. The system is *partially decentralised* because there is an

TABLE 9.1: Control parameters used for the *partially decentralised* FFI algorithm.

Case	Slip-load pre-sets	*tol*	$\Delta f_{s,i}$	Δt
1	$f_{s1,i} = 0.35 f_{y,i}$ $f_{s2,i} = 0.25 f_{y,i}$ $f_{s3,i} = 0.65 f_{y,i}$	0.10	$0.10 f_{s1,i}$	$T_f/2$
2	$f_{s1,i} = 0.35 f_{y,i}$ $f_{s2,i} = 0.25 f_{y,i}$ $f_{s3,i} = 0.65 f_{y,i}$	0.10	$0.10 f_{s1,i}$	T_f
3	$f_{s1,i} = 0.35 f_{y,i}$ $f_{s2,i} = 0.25 f_{y,i}$ $f_{s3,i} = 0.65 f_{y,i}$	0.10	$0.05 f_{s1,i}$	$T_f/2$
4	$f_{s1,i} = 0.65 f_{y,i}$ $f_{s2,i} = 0.25 f_{y,i}$ $f_{s3,i} = 0.65 f_{y,i}$	0.10	$0.05 f_{s1,i}$	T_f

exchange of information between consecutive controllers, i.e. the slip-load is determined based on the ratio between $\hat{\delta}_{i+1}(t)$ and $\hat{\delta}_i(t)$ (the maximum deformation of the storey $i+1$ and i, respectively, within the interval Δt). The parameter *tol* represents a pre-set tolerance of the ratio between consecutive inter-storey deformations.

In order to represent the physical constraints of the friction connections in practical applications, the magnitude of the slip-load was capped in the control algorithm. Thus, the control load varied within a pre-defined upper limit $f_{s2,i+1}$, and a lower limit $f_{s3,i+1}$.

The control system was applied to low- and medium-rise RC frames subjected to three earthquake inputs: El Centro, Northridge and Kobe, scaled to 0.55g. In the seismic simulations, different values for the control parameters of the FFI algorithm were used (Table 9.1). The initial, maximum and minimum slip-loads ($f_{s1,i}$, $f_{s2,i}$ and $f_{s3,i}$) were defined as $0.35 f_{y,i}$, $0.65 f_{y,i}$ and $0.25 f_{y,i}$, respectively. The tolerance for the ratio between consecutive deformations, *tol*, was defined as 0.10. The fixed force increment $\Delta f_{s,i}$ was defined as $0.10 f_{s1,i}$ and $0.05 f_{s1,i}$, and finally, the interval of decision Δt was defined as T_f and $T_f/2$, where T_f is the fundamental period of the frames.

The history of inter-storey deformation $\delta_i(t)$, maximum deformation in the previous interval of decision $\hat{\delta}_i(t)$, control force $f_{s,i}(t)$ and actual forces $f_i(t)$ in the dampers of storeys $i = 1$, 2 and 3 of the medium-rise RC frame, under El Centro input, are shown in Fig. 9.1. As required by the control the algorithm, the slip-load of the damper in storey 1 was not modified, but the dampers in floor 2 and 3 were adjusted by adding or subtracting the increment $\Delta f_{s,i}$. The ratios of deformation $|\hat{\delta}_{i+1}(t)/\hat{\delta}_i(t)|$ shown in Fig. 9.2 determined the action of the algorithm: for ratios beyond 1.1 or below 0.9 (since the tolerance *tol* was pre-specified as 0.10), the control force was increased or reduced, respectively; for ratios within that interval, the slip-load was not modified.
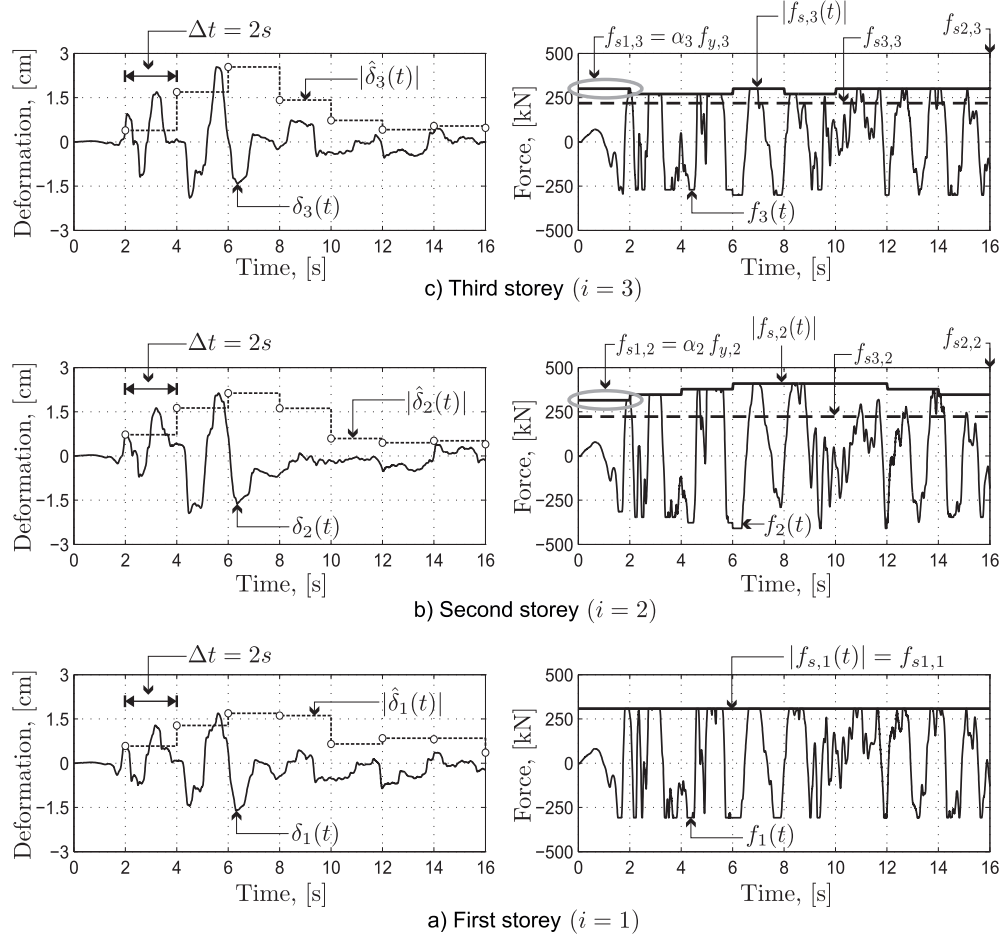
FIGURE 9.1: Time history of deformation and forces of medium-rise RC frame (first to third floor) with FFI control ($\Delta t = T_f = 2s$).
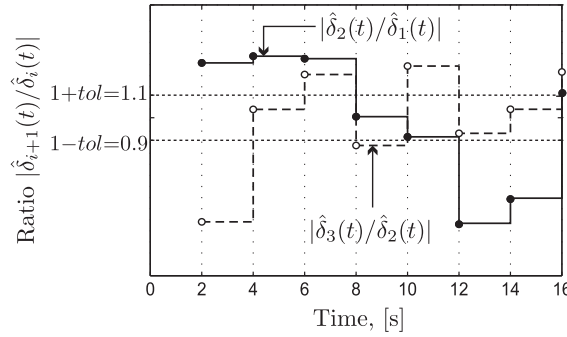
FIGURE 9.2: Ratios of deformation $|\hat{\delta}_{i+1}/\hat{\delta}_i|$ of medium-rise frame (first to third floor) with FFI control ($\Delta t = T_f = 2s$).
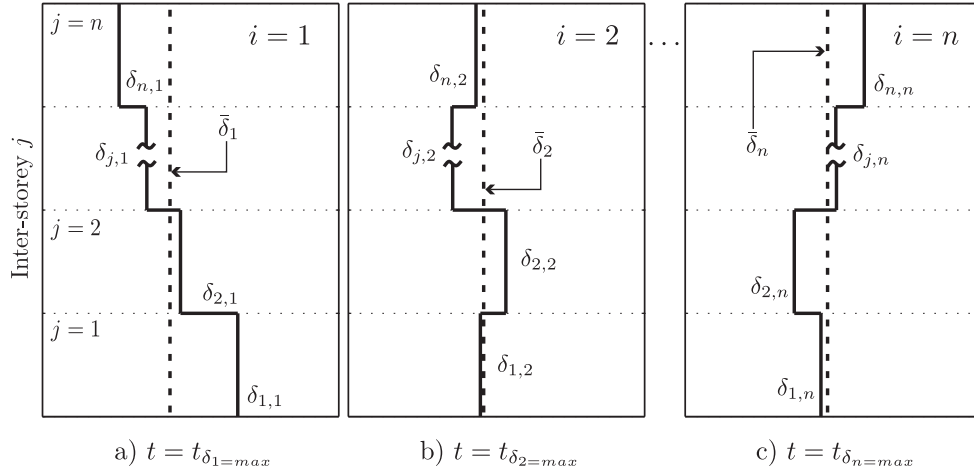
FIGURE 9.3: Parameters for calculation of the average $(\bar{\delta}_i)$ and the standard deviation (σ_i) of the absolute values of simultaneous deformations.

In order to evaluate the efficiency of the control system and to have an insight in the distribution of deformation in the structure (which was one objective of this *partially decentralised* system), two performance indices, J_7 and J_8, were defined. The index J_7 assess the ratio of inter-storey deformations of controlled to uncontrolled (bare) frames:

$$J_7 = \frac{\max(\bar{\delta}_{c,i})}{\max(\bar{\delta}_{b,i})} \qquad (9.2)$$

where $\bar{\delta}_c$ and $\bar{\delta}_b$ represent the average of absolute values of simultaneous inter-storey deformations in the building at the time of the ith maximum inter-storey deformation, for controlled and bare frames, respectively. The averages were calculated as:

$$\bar{\delta}_i = \frac{1}{n} \sum_{j=1}^{n} (\delta_{j,i}) \qquad (9.3)$$

where the sub-indices c and b were removed because the process is the same for either controlled or bare frame. In this equation, $\delta_{j,i}$ is the absolute value of deformation of inter-storey j at the time of maximum deformation of inter-storey i (Fig. 9.3).

The index J_8, on the other hand, evaluates the distribution of the inter-storey deformations, by means of ratios of standard deviation between controlled and bare frame. The index was calculated as:

$$J_8 = \frac{\max(\sigma_{c,i})}{\max(\sigma_{b,i})} \qquad (9.4)$$
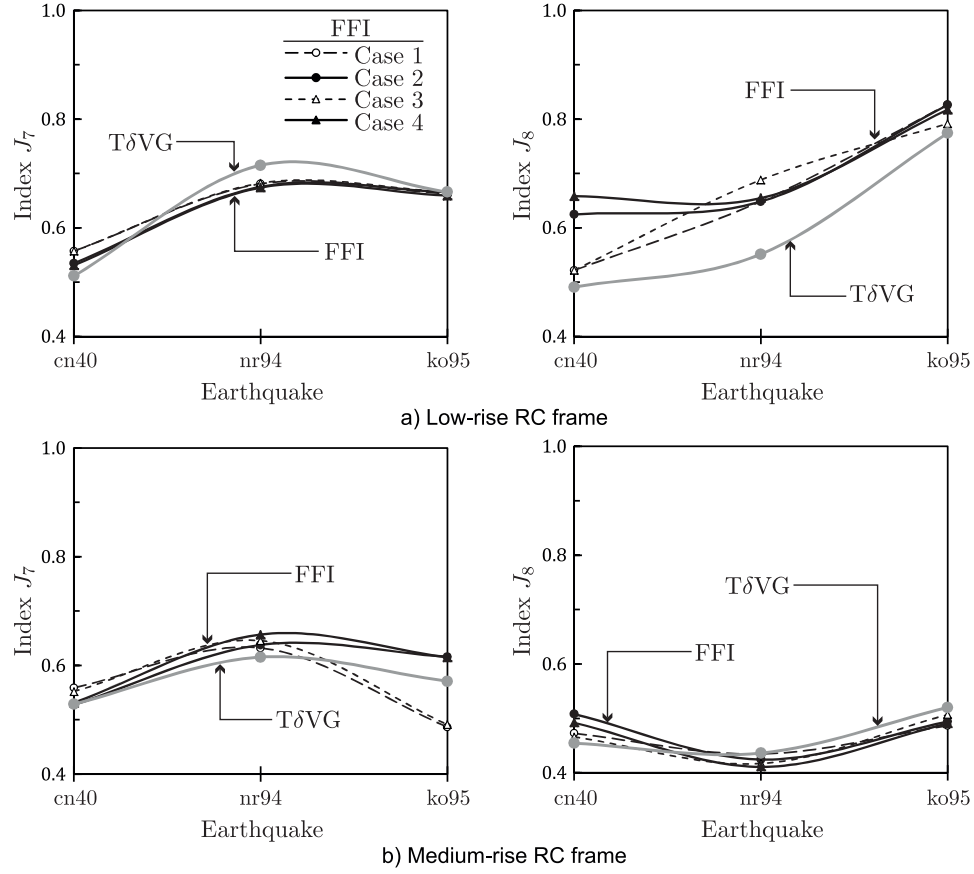
FIGURE 9.4: Indices of average deformation reduction (left) and deformation distribution (right) for frames with FFI control.

where $\sigma_{c,i}$ and $\sigma_{b,i}$ represent the standard deviation of the distribution of deformations in the building at the time of maximum deformation in the inter-storey i, for the controlled and bare frames, respectively. The standard deviation σ of either frame was given by:

$$\sigma = \left(\frac{1}{n} \sum_{j=1}^{n} \left(\delta_{j,i} - \bar{\delta}_i \right)^2 \right)^{1/2} \tag{9.5}$$

where n is the number of storeys in the building, $\delta_{j,i}$ is the absolute value of deformation of inter-storey j at the time of maximum deformation of inter-storey i, and $\bar{\delta}_i$ is the average inter-storey deformation of the building at the time of maximum deformation of inter-storey i (Fig. 9.3).

The results from the simulations showed that the FFI control reduced the deformation in the controlled frames, in comparison to the bare frame, for all three earthquakes. As shown in Fig. 9.4, the indices J_7 (average of simultaneous inter-storey deformation)

indicated reductions between 47% and 33%, for the low-rise frame, and between 50% and 35%, for the medium-rise frame, depending on the earthquake. The levels of reduction, as it can be seen in the same figure, were very similar to those of the TδVG system, which is reasonable, since the control forces in both systems were limited to the range $0.25f_{y,i}$ to $0.65f_{y,i}$. As it is shown in Fig. 9.4, the levels of reduction did not vary significantly in the four cases of analysis using different control parameters.

On the other hand, the FFI system was inefficient in producing more uniform distributions of the deformation than the *decentralised* algorithm. In Fig. 9.4, the index of deformation distribution (J_8) indicated a larger deviation for the new system, in the case of the low-rise frame, and no improvement, in the case of the medium-rise frame.

9.3.2 Control algorithm using average deformation with variable gain factors (AδVG)

The FFI control algorithm (Section 9.3.1) did not improve the distribution of the inter-storey deformations (in comparison with the *decentralised* TδVG system). A possible reason for the inefficiency was that the slip-load was adjusted by fixed force increments, rather than proportionally to the amount of deformation.

As a possible solution, another control algorithm using the average inter-storey deformation with variable gain factors (AδVG) was proposed as:

$$f_{s,i}(t) = \begin{cases} f_{s1,i}\, sgn(\dot{\delta}_i(t)) & \text{if } t < \Delta t \\ g_i(\delta(t))|f_{s,i}(t - \Delta t)|sgn(\dot{\delta}_i(t)) & \text{if } t \geq \Delta t \end{cases} \tag{9.6}$$

where $f_{s,i}(t)$ is the controlled slip-load of damper i, determined at the end of the current interval of decision (Δt), and $|f_{s,i}(t-\Delta t)|$ is the absolute value of the semiactive slip-load determined at the previous interval of decision ($t - \Delta t$). In the algorithm, the variable gain factor $g_i(\delta(t))$ was introduced to adjust the slip-loads as a function of the ratios between the local inter-storey deformations and their distribution along the height of the building. The variable gain factor was thus defined as:

$$g_i(\delta(t)) = \frac{|\hat{\delta}_i(t)|}{\bar{\hat{\delta}}(t)} \tag{9.7}$$

where $\hat{\delta}_i(t)$ represents the largest deformation of the inter-storey i, within the current interval of decision. The variable $\bar{\hat{\delta}}(t)$ represents the average of maximum deformations $|\hat{\delta}_i(t)|$ in all inter-storeys, determined at the end of the current interval Δt:
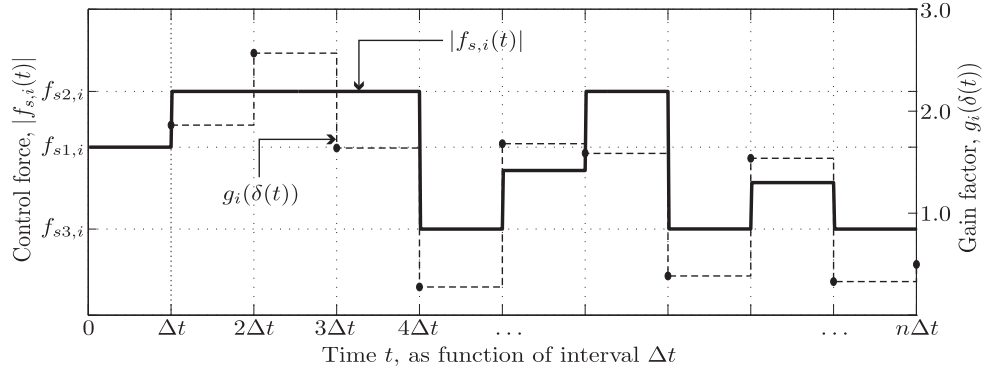
FIGURE 9.5: Schematic representation of new AδVG control algorithm.

$$\bar{\delta} = \frac{1}{n} \sum_{i=1}^{n} |\hat{\delta}_i(t)| \tag{9.8}$$

where n is the number of storeys in the structure. Similar to the FFI algorithm, in the AδVG system the slip-loads were capped by the upper and lower limits $f_{s2,i}$ and $f_{s3,i}$.

A schematic representation of the operation of the AδVG algorithm and its control parameters is shown in Fig. 9.5. The algorithm starts with a pre-defined initial slip-load $f_{s1,i}$, which is maintained during the first interval of decision (from $t = 0$ to $t = \Delta t$ seconds). At the end of the interval, the variable gain factor $g_i(\delta(t))$ is determined with Eq. 9.7 and used in Eq. 9.6 to determine the control force $f_{s,i}(t)$. This new force will be maintained until the end of the new interval ($t = 2\Delta t$). The process is repeated for the following intervals, i.e. $t = 3\Delta t$, $t = 4\Delta t$, and so on.

In terms of the clamping force in the friction connection, Eqs. 9.6 can be re-written as:

$$N_i(t) = \begin{cases} N_{1,i} & \text{if } t < \Delta t \\ g_i(\delta(t))N_i(t - \Delta t) & \text{if } t \geq \Delta t \end{cases} \tag{9.9}$$

$$f_{s,i}(t) = \mu N_i(t)\,sgn(\dot{\delta}_i(t)) \tag{9.10}$$

where $N_{1,i}$ and $N_i(t - \Delta t)$ are the initial clamping force and the clamping force determined in the previous interval of decision $t - \Delta t$, respectively. Similarly, the clamping force is constrained by upper and lower limits ($N_{2,i}$ and $N_{3,i}$, respectively):

$$N_i(t) = \begin{cases} N_{2,i} & \text{if } N_i(t) > N_{2,i} \\ N_{3,i} & \text{if } N_i(t) < N_{3,i} \end{cases} \tag{9.11}$$

9.3.3 Preliminary investigation of the efficiency of AδVG algorithm

The preliminary investigation of the efficiency of the new *partially decentralised* control algorithm was carried out by simulating the response of a medium-rise (10-storey, 3-bay) RC frame with an abrupt change of storey stiffness in the upper three levels (Caudana, 2009). The frame was modelled using a reduced modulus of elasticity to simulate a state of cracks. The first three natural frequencies of the frame were 0.49, 1.31 and 2.29Hz. In the simulations, the frame was subjected to the first 15 seconds of the El Centro, Northridge and Imperial Valley earthquakes, scaled to 0.35g (Caudana and Petkovski, 2013). The semiactive control system was applied to the frame as a possible solution to the limited efficiency and lack of adaptability of a passive control system in which optimum slip-loads varied for each earthquake, as shown in Fig. 9.6, and, in some cases, even resulted in increases of the response (i.e. under Northridge excitation).

In the simulations with the AδVG algorithm, two values of the maximum slip-load $f_{s2,i}$ were defined as $0.35f_{y,i}$ and $0.65f_{y,i}$, for El Centro and Imperial Valley, and $0.55f_{y,i}$ and $0.65f_{y,i}$ for Northridge. These values were selected in order to compare the response produced by the semiactive system with that of the passive system using the same values of slip-load. The initial and minimum slip-loads ($f_{s1,i}$ and $f_{s3,i}$, respectively), were defined as a ratio of the maximum slip-load: for all earthquakes, the ratios of initial load $f_{s1,i}/f_{s2,i}$ were 0.50, 0.75 and 1.0, whereas the ratios of minimum load $f_{s3,i}/f_{s2,i}$ varied at 0.10, 0.25, 0.50 and 0.75. The intervals Δt were defined as T_f, $T_f/2$ and $T_f/4$.

The results from the simulations indicated a good performance of the semiactive strategy, improving the seismic response of the frame. As indicated by the ratios of controlled to uncontrolled top floor displacement d_c/d_b (Fig. 9.7), the response of the system to all earthquakes was generally smaller, in comparison to the bare frame, and either slightly larger, similar or smaller than those of the passive system, depending on the combination
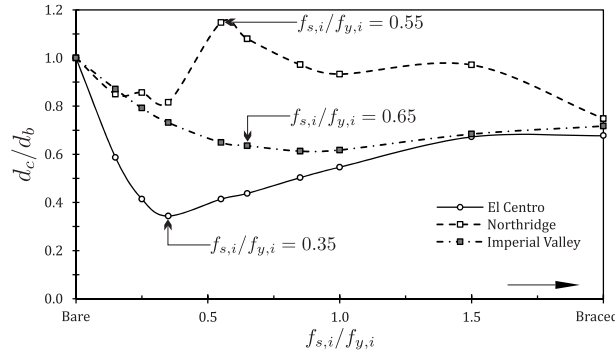
FIGURE 9.6: Ratios of top floor displacement of RC frame with passive control.

of control parameters used. The semiactive control was particularly beneficial for the Northridge excitation (Figs. 9.7e and f), avoiding the increase in response caused by the passive control with slip-loads of $0.55f_{y,i}$ and $0.65f_{y,i}$.
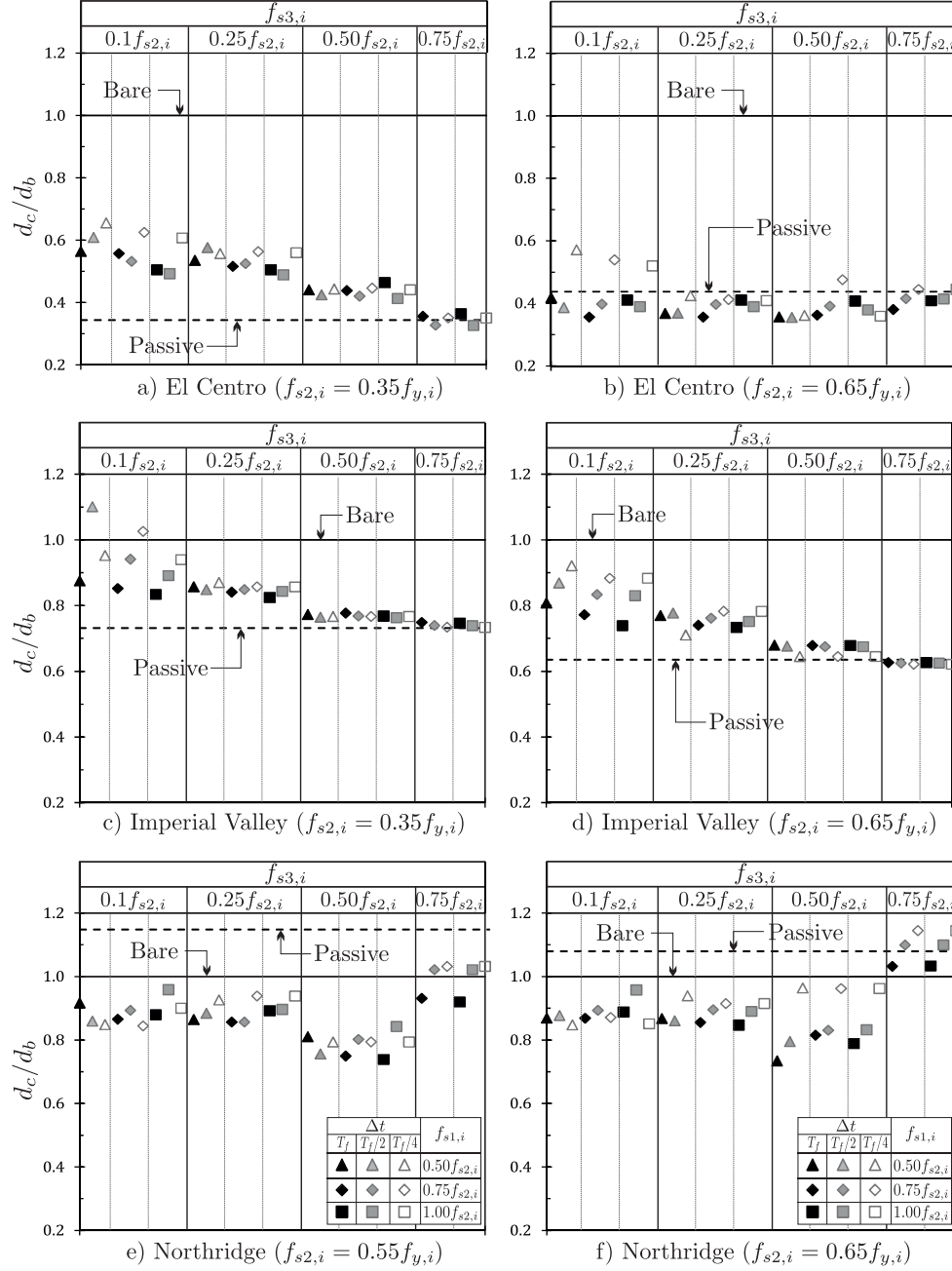
FIGURE 9.7: Top floor displacement ratios for passive and AδVG systems, with different control parameters.

For all three earthquakes, the control system tended to produce levels of response similar

to those of the passive strategy, for increased values of the minimum slip-load $f_{s3,i}$, i.e. when the range of slip-load variation was narrowed. Although there were no significant differences in the response using each interval of decision (in most of the cases), the system with longer interval of decision ($\Delta t = T_f$) resulted in smaller ratios d_c/d_b, for the majority of simulations (55% of analysed cases).

As indicated by the index J_8 (Fig. 9.8), there was a variability in the distribution of the deformation, but, in general, the semiactive system resulted in smaller indices than the passive control, especially for El Centro and Northridge inputs. In the case of the Imperial Valley earthquake, however, the values of the index J_8 were very similar to those of the passive system, with some exceptions when the system used the shorter interval of decision ($\Delta t = T_f/4$).

The deformed shapes of the frame at the time of maximum top floor displacements under each excitation are shown in Fig. 9.9. Apart from reducing the response of the bare frame for all earthquakes, the semiactive system prevented large deformations at the weaker upper levels, unlike the passive control. In the figure, the response of the frame with semiactive system using $f_{s1,i} = 0.50f_{s2,i}$, $f_{s3,i} = 0.50f_{s2,i}$ and $\Delta t = T_f$ under
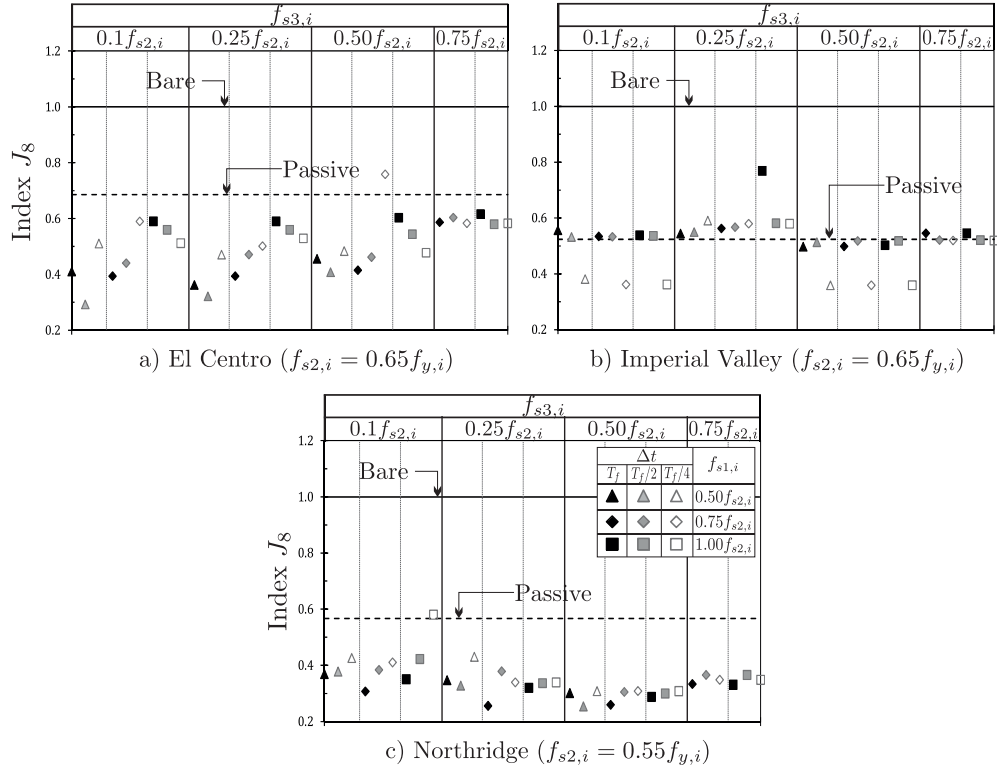
FIGURE 9.8: Index J_8 for medium-rise frame with passive and AδVG control.

the El Centro and Imperial Valley earthquakes is shown. In the case of Northridge, the response corresponds to the system using $f_{s1,i} = 0.75 f_{s2,i}$, $f_{s3,i} = 0.10 f_{s2,i}$ and $\Delta t = T_f$.

Although the new semiactive system was efficient in reducing the seismic response of the medium-rise frame and also produced more uniform distributions of inter-storey deformation in comparison with the passive system, one limitation was observed in the control forces: since the magnitude of the force $f_{s,i}(t)$ depended only on the relation of inter-storey deformation and global deformed configuration, there were cases where the control force was not reduced towards the end of the earthquake, similar to the *decentralised* MHF algorithm (Chapter 7). The reason for such an effect was that, towards the end of the excitation, the gain factor $g_i(\delta(t))$ still increased, even for small inter-storey deformations. As an example, the configuration of deformation of the frame acquired by the algorithm at each interval of decision (with $\Delta t = 2s$), from 15s to 25s (i.e. in the interval of response decay), are shown in Fig. 9.10, along with the gain factors and the corresponding control forces determined by the algorithm. As it can be seen, although the deformations at this stage were very small, the gain factor increased in
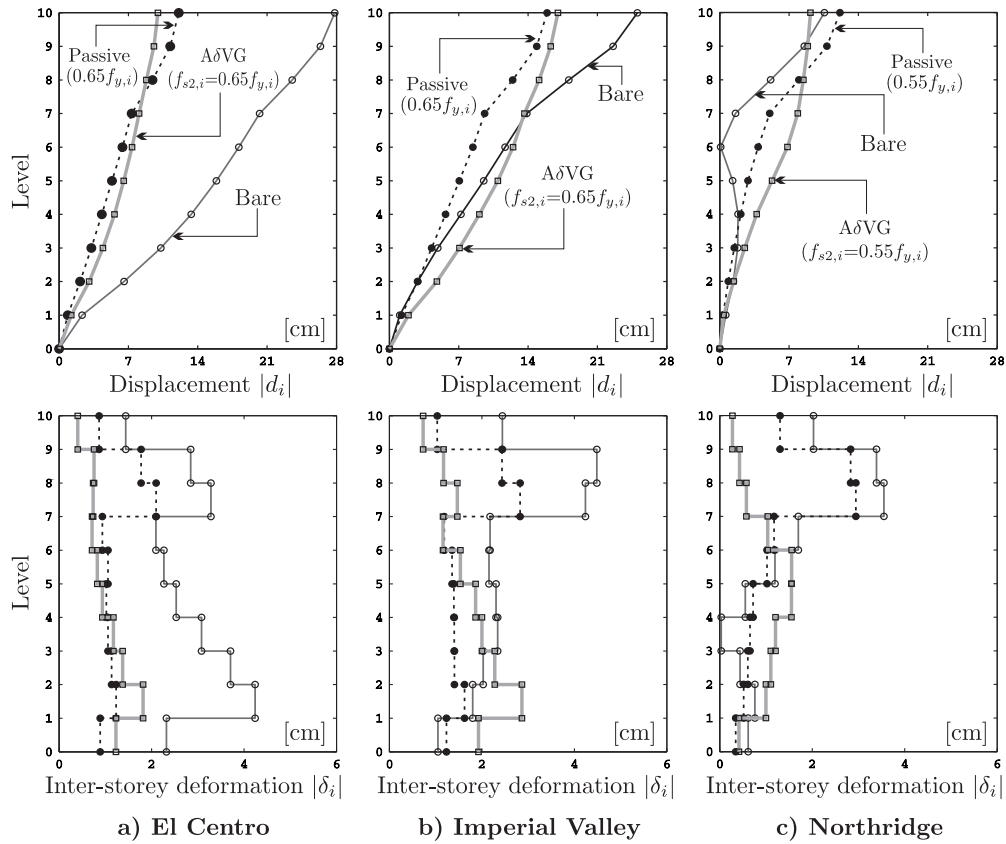
FIGURE 9.9: Absolute values of simultaneous displacements (top) and deformed configurations (bottom) at time of maximum top floor displacement.

some floors, resulting in large control forces at the end of the excitation. This situation leads to locking of the connections and permanent deformation of the frame after the earthquake.

a) **Deformed configuration** $|\hat{\delta}_i|$ **at control intervals** $\Delta t = 2s$, **[cm]**

b) **Gain factor** $g_i(\delta_i(t))$ **distribution at control intervals** $\Delta t = 2s$

c) **Slip-load** $f_{s,i}(t)$ **distribution at control intervals** $\Delta t = 2s$, **[kN]**
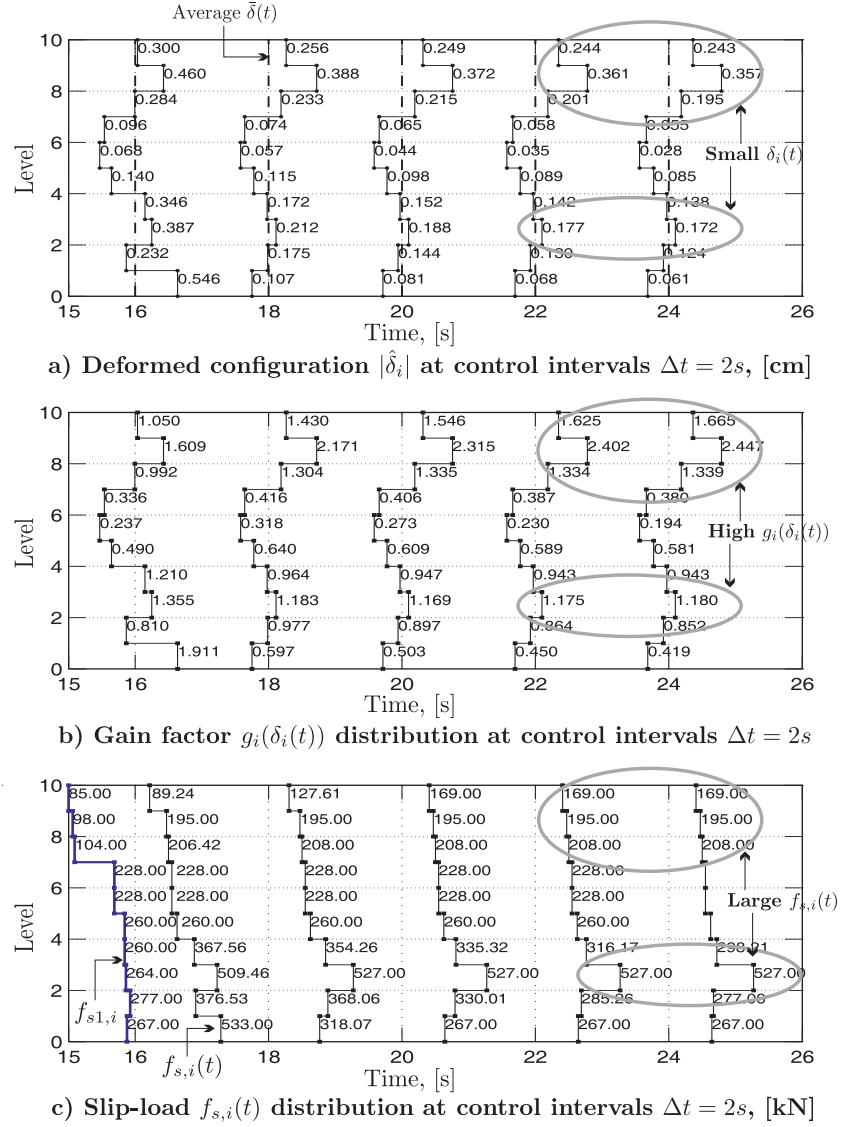
FIGURE 9.10: Response of the frame, control gains and forces during the decaying part of the earthquake (t>15s), with AδVG control.

9.3.4 Modified AδVG algorithm

As a possible solution to the large forces produced for very small deformations at the end of the ground excitation, one additional gain factor related to the velocity was introduced in the control algorithm. In order to investigate an appropriate factor, two different expressions were used to determine the second gain factor, as:

$$g_{2,i}(\dot{\delta}(t)) = \left(\frac{1}{n} \sum_{i=1}^{n} |\dot{\delta}_i| \right)^{\alpha} \tag{9.12}$$

and

$$g_{2,i}(\dot{\delta}(t)) = tanh(|\dot{\delta}_i|) \tag{9.13}$$

where $\dot{\delta}_i$ is the current velocity at the end of the interval of decision.

The gain factor calculated with Eq. 9.12 represents a global factor, which is dependent on the average of the velocity of all inter-storeys. Therefore, the same factor is applied to the controllers on each floor, during each interval of decision. In order to investigate the efficiency of this expression, two values of the factor α were used as 0.5 and 1.0.

On the other hand, the gain $g_{2,i}(\dot{\delta}(t))$ calculated with Eq. 9.13 represents a local factor, which depends only on the local inter-storey velocity.

The modified algorithm AδVG was thus re-written as:

$$f_{s,i}(t) = \begin{cases} f_{s1,i}\, sgn(\dot{\delta}_i(t)) & \text{if } t < \Delta t \\ g_i(\delta(t))g_{2,i}(\dot{\delta}(t))|f_{s,i}(t-\Delta t)|sgn(\dot{\delta}_i(t)) & \text{if } t \geq \Delta t \end{cases} \tag{9.14}$$

with the same restraining conditions as before.

The modified control was applied to a low-rise and medium-rise RC frames designed as part of this research (Chapter 5). These two frames were subjected to a stronger set of earthquakes: El Centro, Northridge and Kobe, scaled to 0.55g. In the simulations, the maximum and minimum control forces ($f_{s2,i}$ and $f_{s3,i}$) were defined as $0.65f_{y,i}$ and $0.25f_{y,i}$, respectively. The initial force $f_{s1,i}$ was defined as a function of the maximum slip-load, as $0.38f_{s2,i}$ (equivalent to $0.25f_{y,i}$), $0.75f_{s2,i}$ and $1.0f_{s2,i}$. The interval of decision Δt was defined as $T_f/4$, $T_f/2$ and T_f.

The results produced by the AδVG controller with three different settings for the $g_{2,i}(\dot{\delta}_i(t))$ gain factor:

(i) Eq. 9.12, with $\alpha = 0.5$: $g_{2,i}(\dot{\delta}(t)) = \left(\dfrac{1}{n}\sum\limits_{i=1}^{n}|\dot{\delta}_i|\right)^{0.5}$,

(ii) Eq. 9.12, with $\alpha = 1.0$: $g_{2,i}(\dot{\delta}(t)) = \left(\dfrac{1}{n}\sum\limits_{i=1}^{n}|\dot{\delta}_i|\right)^{1.0}$,

(iii) Eq. 9.13: $g_{2,i}(\dot{\delta}(t)) = tanh(|\dot{\delta}_i|)$,

are shown in Figs. 9.11, for the low-rise frame, and 9.12, for the medium-rise frame. As indicated by the indices J_7 and J_8, there was an influence of the length of the interval of decision, but in most of the cases, for both low-rise (Fig. 9.11) and medium-rise (Fig. 9.12) frames, the shorter interval ($\Delta t = T_f/4$) resulted in smaller deformations and smaller deviations. The system with gains determined with Eq. 9.12 (with $\alpha = 0.5$ and 1.0) showed large values of standard deviation (i.e. less uniform distribution of deformation) for the low-rise frame under Northridge and Kobe (Fig. 9.11b and c). Among the three gains, the factor $g_{2,i}(\dot{\delta}(t)) = tanh(|\dot{\delta}_i|)$ showed less sensitivity to Δt.

In order to investigate if any of the gain factors produced saturation-like effects, in which the friction connections stayed at its maximum or minimum capacity throughout the simulations, an additional evaluation index J_9 was calculated as:

$$J_9 = \max\left(\frac{\bar{f}_{s,i}}{f_{y,i}}\right) \tag{9.15}$$
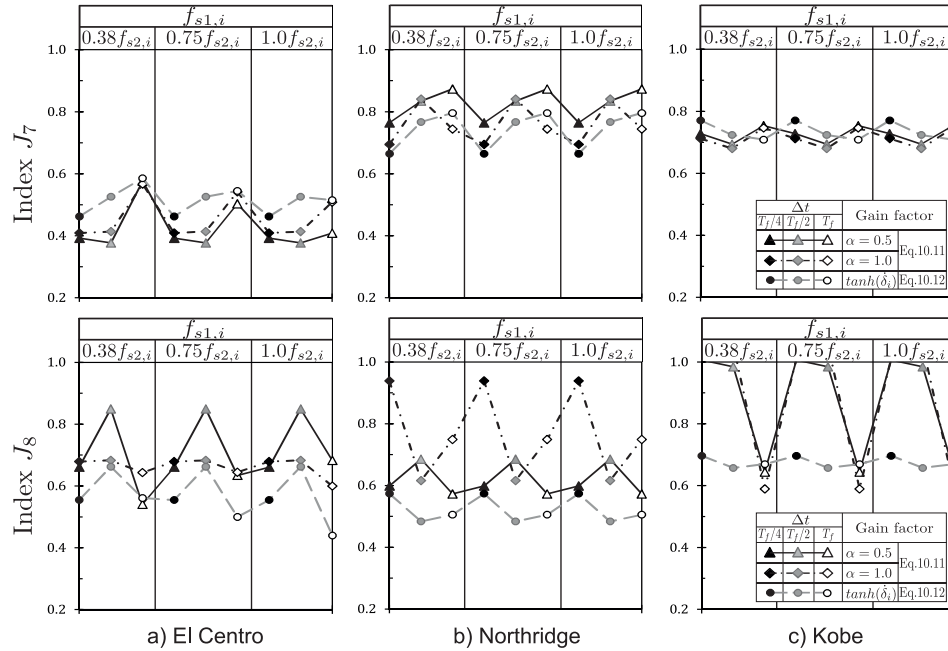
FIGURE 9.11: Low-rise RC frame: Indices J_7 (top) and J_8 (bottom) using different control parameters and gain factors.
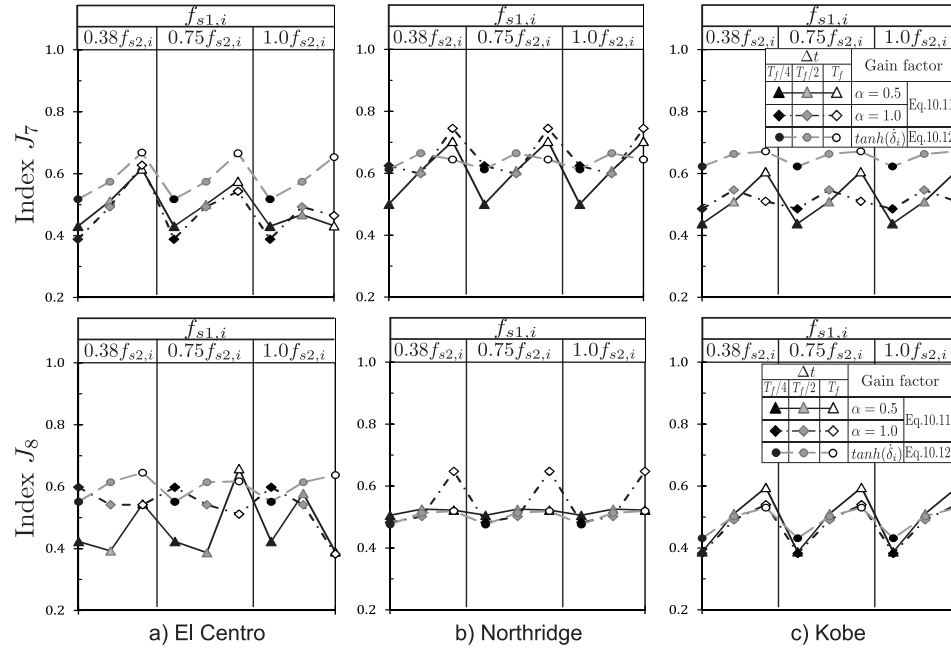
FIGURE 9.12: Medium-rise RC frame: Indices J_7 (top) and J_8 (bottom) using different control parameters and gain factors.
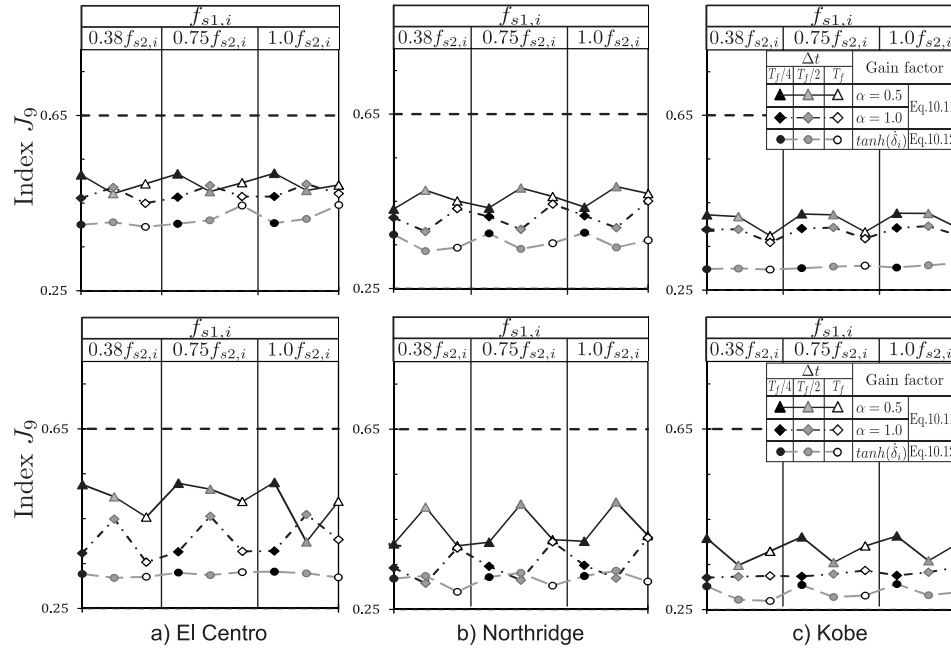
FIGURE 9.13: Index J_9 for low-rise frame (top) and medium-rise frame (bottom) using different control parameters and gain factors.

where $\bar{f}_{s,i}$ represents the average control force of damper i, throughout each simulation.

As it can be seen in Fig. 9.13, there was a variability in the control force, indicated by the index J_9, denoting that the saturation-like effects were avoided using any of Eqs. 9.12 or 9.13. However, as it can be seen in the same figure, the control forces generated in the algorithm by introducing the gain $g_{2,i}(\dot{\delta}(t)) = tanh(|\dot{\delta}_i|)$ were always smaller than those produced by the other two gains. This situation, in combination with lower sensitivity to the interval of decision, was the reason to adopt this factor for further investigation of this control algorithm.

A flow chart of the final algorithm is shown in Fig. 9.14, whereas the programming sequence is presented in Table 9.2.
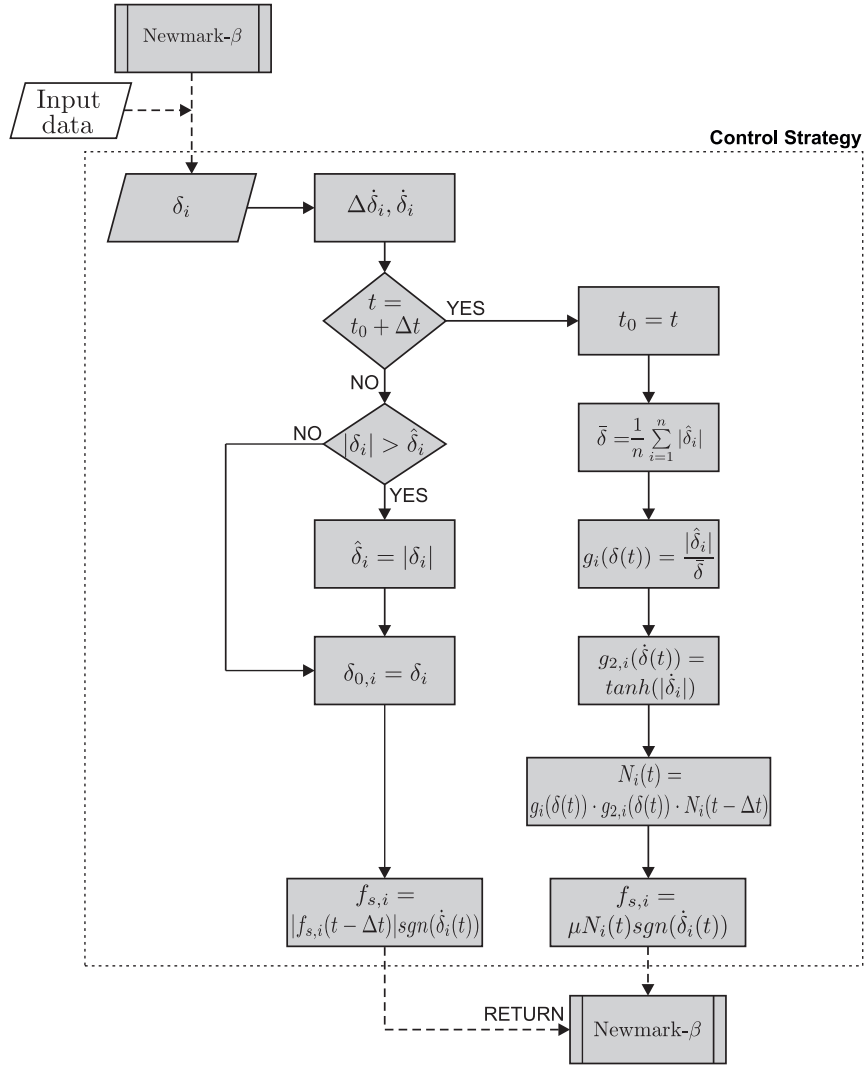
FIGURE 9.14: Flow chart of *partially decentralised* AδVG control system.

TABLE 9.2: Partially decentralised AδVG control, programmed in *ConStruc*.

1. Initial time of analysis, $t_0 = 0$

    (a) Input data:
        Force limits: $N_{1,i}, N_{2,i}, N_{3,i}$
        Interval of decision: Δt
        Sampling time: t_s

    (b) Set initial deformations and velocity: $\delta_{0,i} = 0, \hat{\delta}_i = 0, \dot{\delta}_{0,i} = 0$

2. At every sampling time, t_s

    (a) Calculate the current velocity across the damper i:
        $\rightarrow \quad \Delta\dot{\delta}_i = \dfrac{\delta_i - \delta_{0,i}}{t_s}, \text{and } \dot{\delta}_i = \dot{\delta}_{0,i} + \Delta\dot{\delta}_i$

    (b) Determine the maximum deformation $\hat{\delta}$ of each damper i:
        $\rightarrow \quad$ if $|\delta_i| > \hat{\delta}_i$
        $\rightarrow \quad$ then $\hat{\delta}_i = |\delta_i|$
        $\rightarrow \quad$ end

    (c) Set $\delta_{0,i} = \delta_i, \dot{\delta}_{0,i} = \dot{\delta}_i$

    (d) Determine the semiactive slip-load:
        $\rightarrow \quad f_{s,i}(t) = |f_{s,i}(t - \Delta t)|sgn(\dot{\delta}_i(t))$

3. When $t = t_0 + \Delta t$

    (a) Calculate average deformation and gain factors:
        $\rightarrow \quad \bar{\delta} = \dfrac{1}{n}\sum\limits_{i=1}^{n}|\hat{\delta}_i|$
        $\rightarrow \quad g_i(\delta(t)) = \dfrac{|\hat{\delta}_i|}{\bar{\delta}}$
        $\rightarrow \quad g_{2,i}(\dot{\delta}(t)) = tanh(|\dot{\delta}_i|)$

    (b) Determine the clamping force:
        $\rightarrow \quad N_i(t) = g_i(\delta(t)) \cdot g_{2,i}(\dot{\delta}(t)) \cdot N_i(t - \Delta t)$

    (c) Determine the new semiactive slip-load:
        $\rightarrow \quad f_{s,i}(t) = \mu N_i(t)sgn(\dot{\delta}_i(t))$

    (d) Set new time $t_0 = t$ and $\hat{\delta}_i = 0$

9.4 Efficiency of AδVG algorithm and comparison with decentralised TδVG control

In addition to the low- and medium-rise RC frames, the proposed control system was applied to the low- and medium-rise steel frames described in Chapter 5. Simulations of the seismic response of the frames were performed in the program *ConStruc*, using six different earthquakes as input: El Centro, Northridge, Kobe, Loma Prieta, Imperial Valley and Taft, all scaled to 0.55g.

In the control algorithm, the upper and lower limits of the slip-loads were defined as $0.65f_{y,i}$ and $0.25f_{y,i}$, respectively. Since the results of the previous simulations (Section 9.3.4) indicated that the initial slip-load did not affect significantly the efficiency of the system, in this new set of simulations the initial slip-load was defined as $0.25f_{y,i}$, in all the analysis cases.

On the other hand, the interval of decision Δt did affect the performance of the system. Even though the shortest interval ($\Delta t = T_f/4$) generally showed better results, the three intervals ($T_f/4$, $T_f/2$ and T_f) were used in the new set of simulations.

The results indicated a good performance of the control system, for all four frames, in terms of maximum inter-storey deformation and shear force (evaluated by the indices J_1 and J_3, respectively). As it can be seen in Fig. 9.15, the AδVG control with $\Delta t = T_f/2$ produced comparable or smaller indices J_1 than the system with other intervals, in all four frames under most of the earthquakes (in 75% of the cases), except for a few cases (e.g. El Centro, for the low-rise RC frame, and Taft, for the medium-rise RC frame), where the system using either the shortest interval ($\Delta t = T_f/4$) or the longest interval ($\Delta t = T_f$) resulted in significantly smaller responses. The levels of inter-storey deformation varied for each frame under each earthquake, but in general, the reductions (in comparison to the bare frame) could be as high as 50% (e.g. the medium-rise steel frame under El Centro earthquake). The control system, however, was not efficient in reducing the maximum inter-storey deformation of the frames under Northridge (apart from the low-rise steel frame). In the case of the medium-rise RC frame, the maximum inter-storey deformation was slightly increased, in the order of 15%.

Since the introduction of the control system increased the stiffness of the structures, there was also an increase of the shear forces. However, as shown in Fig. 9.16, the increases were not excessive, with a maximum value of 44% for the control system with $\Delta t = T_f/2$ (which occurred for the medium-rise RC frame under Loma Prieta earthquake). In the case of the low-rise steel frame, the system resulted in either reductions of the shear
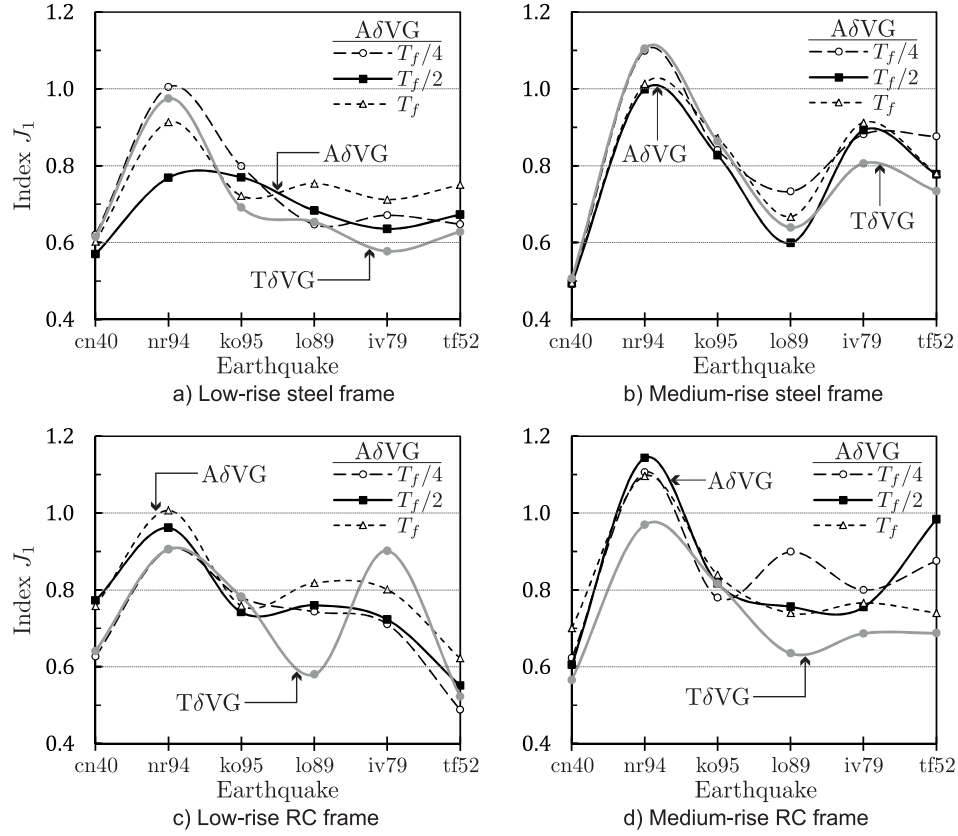
FIGURE 9.15: Performance index J_1 for multi-storey frames with new semiactive control systems AδVG and TδVG.

forces, in the order of 20% (for Loma Prieta input) or 30% (for El Centro and Northridge excitations), or very small increases (for all other earthquakes).

The comparison of indices J_1 and J_3 between the new *partially decentralised* AδVG system and the new *decentralised* system TδVG (Chapter 8) showed variable efficiency of each system, depending on the frame and the earthquake. For the majority of the earthquakes, the levels of maximum deformation produced by each control algorithm were not significantly different, with a maximum of 20% and 30% in the most notable cases: Northridge, for the low-rise steel frame, and Taft, for the medium-rise RC frame (Fig. 9.15a and d, respectively).

On the other hand, the comparison of the indices J_3 (base shear), indicated a better performance of the *partially decentralised* system. As it can be seen in Fig. 9.16, the levels of shear force produced by the AδVG were either comparable or smaller than those of the *decentralised* system TδVG, for all the frames under each earthquake.
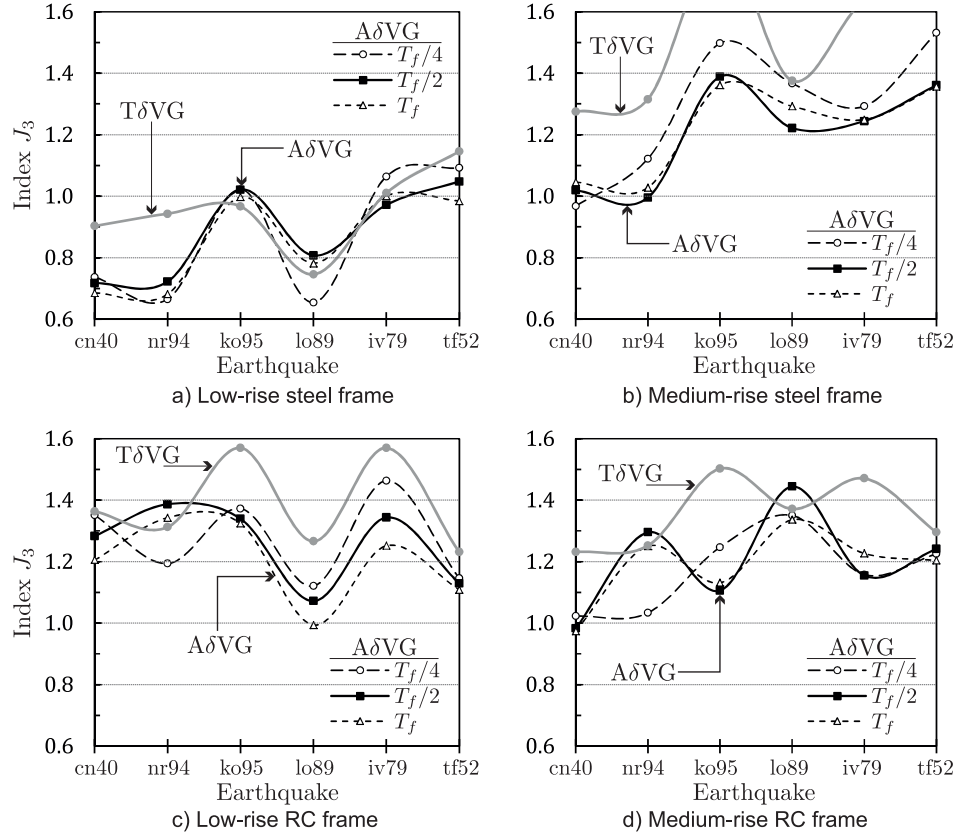
FIGURE 9.16: Performance index J_3 for multi-storey frames with new semiactive control systems AδVG and TδVG.

The average of maximum simultaneous deformations and their standard deviation (evaluated by indices J_7 and J_8, respectively) were also compared, as a means to verify if the *partially decentralised* system produced more uniform deformation distributions than the *decentralised* system. As it can be seen in Fig. 9.17, the values of the index J_7 were very similar between both controllers, with small differences of up to 20%. Similarly, both systems showed comparable levels of the index J_8, which indicated that the new system, despite being efficient in reducing the seismic response, was not able to introduce an effective control on the distribution of the inter-storey deformation. This situation, however, is not critical for the controller, because, as it can be seen in the same figure, the values of the index J_8 are relatively small, indicating small deviations of the deformation distribution, associated to relatively large reductions of the seismic response.
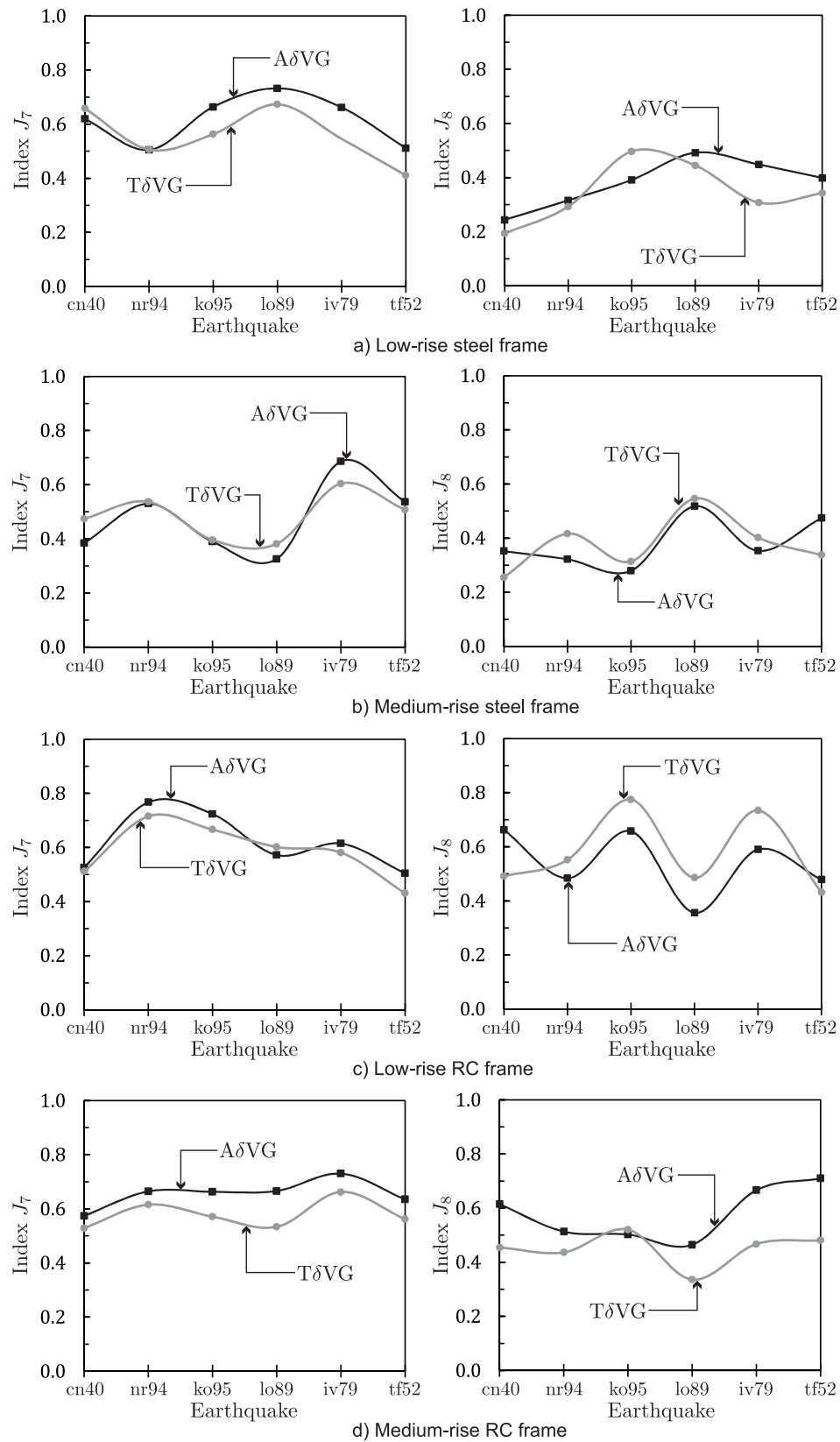
FIGURE 9.17: Performance index J_7 (left) and J_8 (right) for multi-storey frames with new semiactive control systems AδVG and TδVG.

9.5 Concluding remarks

New *partially decentralised* control algorithms were developed, in order to investigate whether or not it was possible to improve the performance of the *decentralised* TδVG control system (Chapter 8). An additional objective of the *partially decentralised* systems was to control the distribution of the inter-storey deformation throughout the height of the building.

The *partially decentralised* with fixed force increment (FFI) algorithm adjusted the dampers' slip-loads according to the relation between consecutive inter-storey deformations, by either adding or subtracting fixed increments of the slip-load. This algorithm showed good reductions of the average deformation of low- and medium-rise RC frames (in comparison to the bare frame), with levels similar to those of the *decentralised* TδVG system. However, comparison of the indices of standard deviation did not show any improvement by the new algorithm, in terms of deformation distribution.

A second system, the average deformation with variable gain factors (AδVG) algorithm, was developed as a possible solution. This new control system adjusted the dampers' slip-loads using variable gain factors. These factors determined the slip-loads proportionally to the ratios of local inter-storey deformation to global deformed configuration. A preliminary investigation of the efficiency of the system showed good levels of response reduction and improved distribution of the inter-storey deformation (in comparison to a passive system), when the semiactive control was applied to a medium-rise RC frame with significant differences of storey stiffness. However, the results also made evident the necessity to include a term related to the velocity, in order to prevent large residual control forces at the end of the ground excitations.

The final AδVG algorithm, including a velocity term (Eq. 9.14), was applied to a set of two low-rise and two medium-rise (steel and RC) frames, subjected to a series of six strong earthquakes. The results indicated a good performance of the new semiactive system in terms of maximum inter-storey deformation and maximum base shear, for the majority of the earthquakes. Similarly to the *decentralised* TδVG control, the *partially decentralised* system was less efficient when the frames were subjected to the Northridge excitation, resulting in slight increases of inter-storey deformation, in some cases.

In terms of average inter-storey deformation and its deviation, the AδVG algorithm did not show significant improvements, producing levels of average and deviation comparable to those of the *decentralised* TδVG system.

Chapter 10

Summary of results

10.1 Introduction

The methodology used in this research consisted of simulations of non-linear dynamic response of four different frame structures, analysed as bare frames, passively controlled frames (using bracing with friction dampers) and using four existing semiactive control algorithms (modulated homogeneous friction, MHF; linear and smooth boundary layer, LBL and SBL; friction control with passive, viscous and Reid damping, Tri-D) and two new algorithms developed as part of this research (target deformation with variable gain factors, TδVG; and average deformation with variable gain factors, AδVG).

All structure-control combinations were subjected to a set of six different earthquakes (historical records), scaled to two different peak ground acceleration levels, i.e. a total of 12 excitations. In addition, series of parametric studies of each control algorithm were performed using additional PGAs with four historical records.

A total of 1464 simulations (not including parametric studies) were performed using *ConStruc*, a new program developed here for non-linear dynamic analysis of frame structures equipped with semiactive control system. The full list of simulations, organised by control algorithm, is given in Table 10.1. In this table, the number of simulations includes only those used for comparison of performance between controllers, and do not include the simulations performed in the parametric studies of each algorithm.

The performance of all structures was assessed through indices (J_1 to J_8) that take into account the response of the buildings, in terms of deformations, accelerations and internal forces; damage of structural elements; and control forces required by the control algorithms.

TABLE 10.1: Number of simulations for comparison of controllers using *ConStruc*.

Control System	Parameters in simulations	Number of simulations
Passive	11 slip-load x 4 frames x 12 eq	528
MHF	3 gains x 4 frames x 12 eq	144
SBL	3 gains x 1 layer x 4 frames x 12 eq	144
Tri-D	2 $f_{p,i}$ x 3 gains x 4 frames x 12 eq	288
TδVG	2 $f_{s1,i}$ x 3 Δt x 4 frames x 12 eq	288
AδVG	1 $f_{s1,i}$ x 3 Δt x 4 frames x 6 eq	72
	Total	**1464**

The list of indices used for assessing the performance of the semiactive control systems in comparison with bare frames and passively controlled structures is summarised in Table 10.2, where the response parameter assessed is also indicated. The indices, in general, represent the ratios of maximum response between controlled and uncontrolled (bare) frames (e.g. δ_c vs δ_b). As it can be observed in the table, the indices J_1 to J_3 evaluate the building response (maximum drift, acceleration and shear force), the indices J_4 and J_5 evaluate the damage in the building (expressed as energy dissipated in the predominant dissipative mechanism), the index J_6 assess the maximum control force required by the algorithm, and finally, the indices J_7 and J_8 are a measurement of the deformation distribution along the height of the building (uniform or non-uniform). The last two indices were applied only to compare the performance of the new control algorithms.

TABLE 10.2: Indices for assessing of control performance.

Category	Index	Parameter assessed	Equation
Building response	J_1	Deformation	$J_1 = \max\left(\dfrac{\max(|\delta_{c,i}|/h_i)}{\max(|\delta_{b,i}/h_i)}\right)$
	J_2	Acceleration	$J_2 = \max\left(\dfrac{\max|\ddot{x}_{c,i}|}{\max|\ddot{x}_{b,i}|}\right)$
	J_3	Base shear	$J_3 = \max\left(\dfrac{\max|F_{b,c}|}{\max|F_{b,b}|}\right)$
Building damage	J_4	Energy dissipated through plastic hinges in beams	$J_4 = \left(\dfrac{E_h}{E_i}\right)$
	J_5	Energy dissipated through friction dampers	$J_5 = \left(\dfrac{E_c}{E_i}\right)$
Control force	J_6	Maximum control force required by the algorithm	$J_6 = \max\left(\dfrac{\max|f_{s,i}|}{f_{y,i}}\right)$
Deformation distribution	J_7	Average of simultaneous deformations	$J_7 = \dfrac{\max(\bar{\delta}_{c,i})}{\max(\bar{\delta}_{b,i})}$
	J_8	Standard deviation of simultaneous deformations	$J_8 = \dfrac{\max(\sigma_{c,i})}{\max(\sigma_{b,i})}$

10.2 Summary of results of passive control and semiactive algorithms, in terms of deformation, base shear and control force (indices J_1, J_3 and J_6)

The simulations of the frame with passive control showed the efficiency of the system in reducing the maximum inter-storey deformation of the bare frames (evaluated by the index J_1). For each earthquake, the response of the controlled frames varied with the dampers' slip-loads, but in general, for all earthquakes, there was a narrow range of slip-load values ($f_{p,i} = 0.25f_{y,i}$ to $0.65f_{y,i}$) that resulted in good levels of response reduction. Slip-loads beyond this range did not improve the performance of the control system, showing excessive increases of shear forces (assessed by the index J_3) acting on the structure, without significant reductions in deformation. The efficiency of the control system was limited for impulse-like excitations (i.e. Northridge), which in many cases led to increase of the frame response, even for slip-loads between $0.25f_{y,i}$ and $0.65f_{y,i}$ (i.e. medium-rise steel frame, low- and medium-rise RC frames).

For the passive control, the average index $\bar{J}_1$ indicated deformation reductions in the frame under moderate earthquakes (PGA=0.35g) between 40% (low-rise steel frame) and 25% (low-rise RC frame). For the stronger earthquakes (PGA=0.55g), as shown in Fig. 10.1, the reductions were smaller, varying between 30% (low-rise steel frame) and 17% (low-rise RC frame).

A parametric study of the semiactive algorithms MHF, LBL and SBL showed that their efficiency is related to the gain factor used. In general, larger gain factors led to smaller deformations in the frame. The *thickness* of the boundary layer did not significantly influence the performance of the LBL and SBL controllers. Only the SBL was selected for further study due to similar levels of frame response, in comparison with the LBL algorithm, but less sensitivity to the boundary *thickness*.

Since smaller deformations were produced by the MHF and SBL with high gain factor, these two systems were compared with the passive control. The comparison showed smaller levels of deformation for the passive control, for the majority of the earthquakes (only 14/48 and 15/48 analysis cases showed better or equal response with the MHF and SBL systems, respectively). In average, both the MHF and SBL controllers always resulted in indices $\bar{J}_1$ higher than those of the passive control (Fig. 10.1), with values higher than 1.0 in case of the medium-rise steel frame (using either MHF or SBL algorithm) and the medium-rise RC frame ($\bar{J}_1 = 1.54$, using MHF algorithm).

From the parametric study of the Tri-D algorithm, it was noticed that the initial slip-load $f_{p,i}$ and gain factors had a significant influence on the performance of the control.
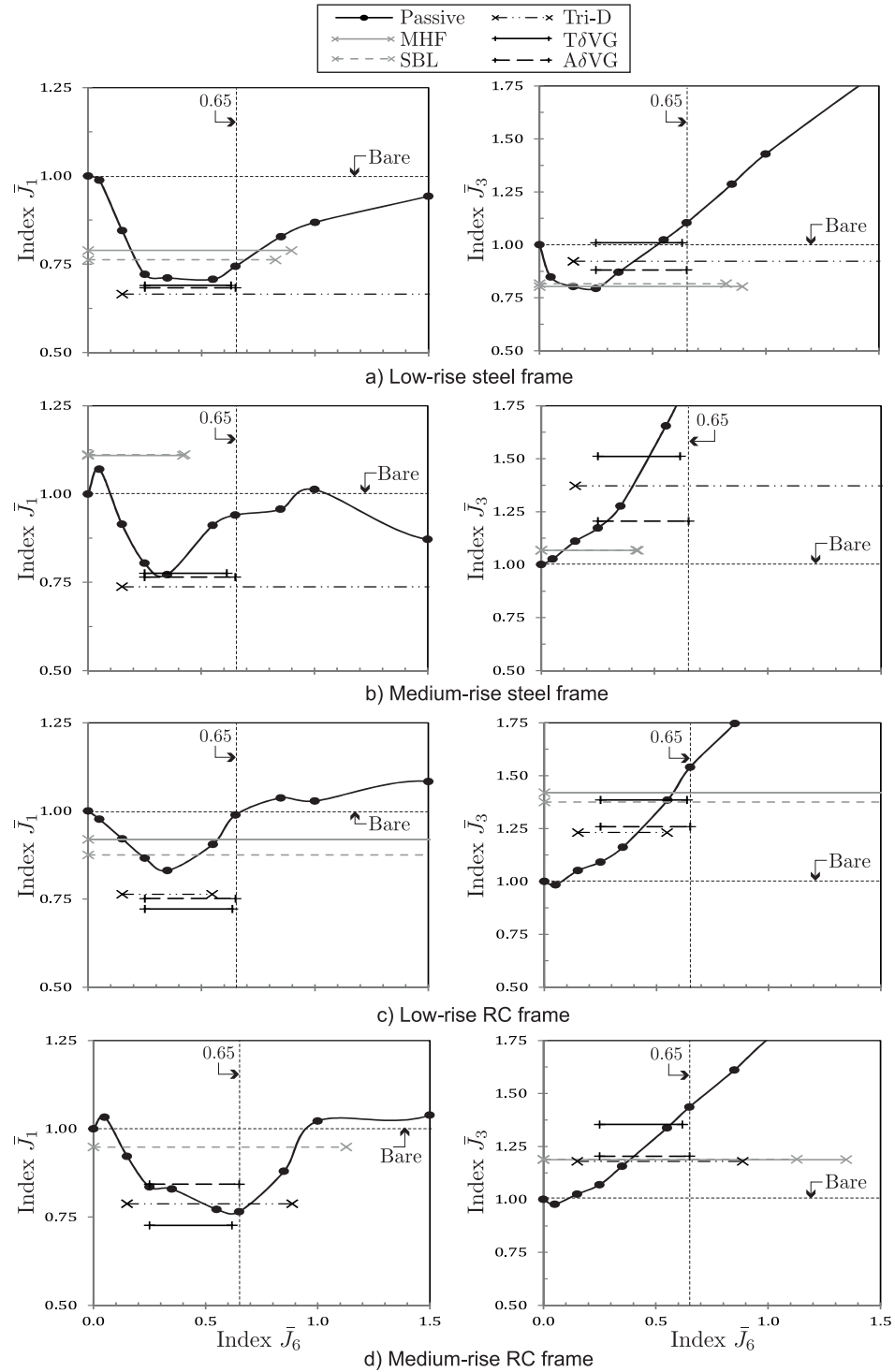
FIGURE 10.1: Average indices $\bar{J}_1$, $\bar{J}_3$ and $\bar{J}_6$ of frames with different control systems.

TABLE 10.3: Comparison of average performance indices for different control systems.

Control System	Average index $\bar{J}_1$	Average index $\bar{J}_3$	Average index $\bar{J}_6$	Cases[1]
Low-rise steel frame				
Optimum Passive	0.71	1.02	0.55	
MHF	0.79 (+11%)	0.80 (-22%)	0.90(+64%)	4/12
SBL	0.76 (+7%)	0.82 (-20%)	0.83 (+51%)	4/12
Tri-D	0.67 (-6%)	0.92 (-10%)	>1.5(>100%)	8/12
TδVG	0.69 (-3%)	1.01 (-1%)	0.63 (+15%)	6/12
AδVG	0.68 (-4%)	0.88 (-14%)	0.65 (+18%)	- -
Medium-rise steel frame				
Optimum Passive	0.77	1.28	0.35	
MHF	1.11 (+44%)	1.07 (-16%)	0.42 (+20%)	1/12
SBL	1.11 (+44%)	1.07 (-16%)	0.42 (+20%)	1/12
Tri-D	0.74 (-4%)	1.37 (+7%)	>1.5 (>100%)	9/12
TδVG	0.78 (+1%)	1.51 (+18%)	0.61 (+74%)	4/12
AδVG	0.76 (-2%)	1.21 (-5%)	0.65 (+86%)	- -
Low-rise RC frame				
Optimum Passive	0.83	1.16	0.35	
MHF	0.92 (+11%)	1.42 (+22%)	1.5 (>100%)	5/12
SBL	0.88 (+6%)	1.38 (+19%)	1.5 (>100%)	6/12
Tri-D	0.76 (-8%)	1.23 (+6%)	0.55 (+57%)	9/12
TδVG	0.72 (-13%)	1.39 (+20%)	0.64 (+83%)	9/12
AδVG	0.75 (-10%)	1.26 (+9%)	0.65 (+86%)	- -
Medium-rise RC frame				
Optimum Passive	0.77	1.44	0.65	
MHF	1.54 (+100%)	1.19 (-17%)	1.35 (+100%)	4/12
SBL	0.95 (+23%)	1.19 (-17%)	1.13 (+74%)	4/12
Tri-D	0.79 (+3%)	1.18 (-8%)	0.89 (+37%)	4/12
TδVG	0.73 (-5%)	1.35 (-6%)	0.62 (-5%)	11/12
AδVG	0.84 (+9%)	1.20 (-17%)	0.65 (0%)	- -

Note 1: Analysis cases where semiactive algorithm resulted in individual index J_1 equal or smaller than passive control, for 12 analysis cases (six earthquakes at 0.35 and 0.55g).

In general, higher values of these two parameters led to lower levels of response. In comparison to the optimum passive control, for every earthquake, the Tri-D algorithm using initial slip-load $f_{p,i} = 0.15 f_{y,i}$ and high gain factor, resulted in smaller or equal levels of peak deformation (indicated by the index J_1) in 30/48 cases. In average, the Tri-D algorithm resulted in larger reductions than the optimum passive control, as indicated by the index $\bar{J}_1$ (Fig. 10.1): for the low-rise steel frame, 33% vs 29% of reduction, respectively; medium-rise steel frame, 26% vs 23%; low-rise RC frame, 24% vs 17%; and slightly smaller for the medium-rise RC frame, 21% vs 23%. The main drawback of the Tri-D system, however, was the large range of control forces required by the algorithm (evaluated by the index $\bar{J}_6$), which, in the case of the steel frames, was more than 2 times the optimum range of passive slip-loads (i.e. $0.65 f_{y,i}$).

From these results, it was concluded that one limitation of the existing algorithms was the use of pre-defined, constant gain factors. This limitation was associated with slip-loads which were too low or too high, hence reducing the effectiveness of the systems.

As an alternative to the use of pre-defined, constant gain factors, the new TδVG control was developed in this project. The algorithm uses variable gain factors (rather than constant, pre-defined values), which adjust the control forces based on the relation of the local, real-time inter-storey deformation, and pre-defined upper and lower boundaries associated with the elastic limits of inter-storey deformations of the frame structures. The upper and lower limits of control forces were related to the range of optimum passive loads (i.e. $0.25f_{y,i}$ to $0.65f_{y,i}$). The dynamic simulations showed an increased efficiency when higher upper limits of deformation (i.e. $\delta_{2,i} = 1.0\delta_{y,i}$) were included in the algorithm, along with higher values of initial slip-load (i.e. $f_{s1,i} = 0.25f_{y,i}$).

In comparison with the optimum passive control, for every earthquake, the TδVG algorithm with $f_{s1,i} = 0.25f_{y,i}$ and $\delta_{2,i} = 1.0\delta_{y,i}$ resulted in lower or equal levels of deformation in 30/48 of the analysed cases, indicating the same level of efficiency as the Tri-D system, for much lower levels of required control forces. In average, deformation levels of the TδVG systems were 3%, 13% and 5% lower than those of the optimum passive system, for the low-rise steel frame, low-rise RC frame and medium-rise RC frame, respectively (Table 10.3). In the case of the medium-rise steel frame, its peak deformation with the TδVG system was 1% higher than that of the optimum passive control.

As it is shown in Fig. 10.1, the introduction of the control systems also resulted in the increase of shear forces (indicated by the index $\bar{J}_3$), in the majority of the frames, compared to those in the bare frames. Only in the case of the low-rise steel frame, there were reductions (with a maximum of 20%) of the base shear, for slip-loads below $0.55f_{y,i}$, in the case of the passive system. The MHF, SBL and Tri-D systems also resulted in reductions of the base shear, despite requiring a higher level of control forces. The reason for this is that the shear at the base results from the combination of the structural forces (due to simultaneous deformed configurations along the height of the building) and the control forces. The index J_3 is only a measure of the maximum control force at any storey, but does not reflect the configuration along the height of the building. The TδVG, requiring a maximum control force of $0.65f_{y,i}$, did not increase the shear force in this frame. For the rest of the structures, the semiactive systems produced reasonable increases of the shear, up to 50%. Similar increases were produced by the passive control, for slip-loads below $0.65f_{y,i}$.

The second control algorithm, AδVG, developed in this research, used a *partially decentralised* control architecture, in order to investigate the possibility of improving the performance of *decentralised* TδVG system, for the same range of control forces ($0.25f_{y,i}$ to $0.65f_{y,i}$). In this case, the control forces were adjusted based on the relation of local inter-storey deformations and the average deformation along the height of the building,

determined at pre-defined intervals of decision, Δt. Among three different intervals of decision, the system with interval $\Delta t = T_f/2$ (where T_f is the fundamental period of the frame), resulted in lower levels of response, for the majority of earthquakes (only six stronger earthquakes with PGA of 0.55g were used in these simulations). In comparison with the TδVG algorithm, the AδVG resulted in lower or equal levels of the index J_1 only in 11/24 cases. The indices J_7 and J_8, which assessed the average and standard deviation of maximum simultaneous deformations, did not show significant improvements when using this *partially decentralised* system. However, from the average indices $\bar{J}_1$ and $\bar{J}_3$ shown in Fig. 10.1, it can be seen that, although the AδVG resulted in comparable or slightly higher values of deformation, it also resulted in lower levels of base shear (indicated by the indices $\bar{J}_1$ and $\bar{J}_3$, respectively) in all the frames, showing about 25% lower forces, in comparison to the TδVG system. The lower level of shear forces is attributed to the smaller control forces acting simultaneously in the frame.

10.3   Concluding remarks

Passive and semiactive control systems applied to four multi-storey frames showed variable efficiency depending on different factors. In case of the passive control, the efficiency was closely related to the dampers' slip-load. Maximum response reductions were achieved for optimum slip-loads, which varied between the frames and the earthquakes. For all frames, however, the range of slip-loads $0.25f_{y,i}$ to $0.65f_{y,i}$ resulted in good levels of response reduction. In the case of the existing semiactive algorithms, the efficiency was strongly related to pre-defined, constant gain factors.

In comparison to the passive control, the MHF and SBL systems showed an improvement in only 30% of the analysis cases (determined as the number of cases with equal or lower levels of deformation, over a total of 48 cases).

The Tri-D algorithm, on the other hand, showed an improvement in 62.5% of cases, in comparison to the optimum passive control. Furthermore, in average, this semiactive system resulted in reductions of 6%, 4% and 8% over the deformations of the average passive system, for the low-rise steel frame, medium-rise steel frame and low-rise RC frame, respectively. Only in the case of the medium-rise RC frame, there was a slight increase of 3% over the optimum passive.

One drawback of the existing algorithms was the large range of required control forces. In the case of the Tri-D algorithm, the required forces were more than two times higher than the optimum passive loads (i.e. $0.65f_{y,i}$), in some cases.

As a possible solution, the TδVG algorithm, which used variable gain factors, was developed in this project. The efficiency of this control was similar to the Tri-D, with an improvement in 62.5% of all analysed cases, compared to the optimum passive. The difference between the Tri-D and the TδVG algorithm was the level of control forces required. The maximum force required by the TδVG system was close to $0.65f_{y,i}$, which was similar to the optimum passive range, and more than two times lower than the forces required by the Tri-D control.

Considering the base shear, all semiactive control systems resulted in moderate increases of up to 50%, in comparison to the bare frame. However, the base shear forces were similar to those obtained for the passive systems with high slip-load (i.e. $0.65f_{y,i}$).

The second control algorithm, AδVG, also used variable gain factors, but it was applied using a *partially decentralised* architecture. In comparison to the TδVG algorithm, the AδVG resulted in comparable or slightly higher deformations, for all four frames. However, this control resulted in smaller shear forces, below 25% of those in the TδVG. These smaller forces denoted a combination of smaller control forces acting simultaneously in the buildings.

Chapter 11

Conclusions and recommendations for future work

11.1 Conclusions on the performance of the new control systems

The introduction of the new control algorithms alleviated some of the limitations of the existing control algorithms, especially those related to the required control forces, without compromising the simplicity of implementation in frame structures.

A possible limitation of existing semiactive algorithms is associated with the use of pre-defined, constant gain factors. By using these constant factors, it is possible to produce inappropriate control forces (either too small or too large), leading to a limited reduction of deformations and/or excessive increases of shear forces.

The levels of response reduction achieved by the new *decentralised* TδVG and *partially decentralised* AδVG algorithms were, in general, comparable to those of the passive control system (within the optimum range of slip-loads) and those of the existing semiactive algorithms. One advantage of the new controllers is that the levels of response reduction were achieved for much smaller levels of control forces. This is important because, by capping the control forces to reasonable levels, the adaptability and reliability of the control was enhanced, as the new systems would prevent excessive additional forces acting on braces and other structural members, especially the axial loads on columns.

11.2 Conclusions on the mechanisms of control systems

From the results obtained in this research, the conclusions on the mechanism of friction-based control systems are:

- The passive control system applied to multi-storey frames reduced their seismic response, with varied efficiency depending on the slip-load capacity of the dampers. For different earthquakes, there were different optimum slip-loads producing largest levels of response reduction, associated with large levels of energy dissipated by the friction connections. The mechanism behind the performance of passive systems consists in the variation of the vibrational frequencies of the bare frame, which can avoid resonance conditions by shifting away from the predominant frequencies of the excitation. As such, the frequencies of a passively controlled frame may vary between those of a bare frame (when all dampers are activated), those of a fully braced frame (when all dampers are locked), or as intermediate, partially braced frames.

- The performance of semiactive algorithms greatly depends on their control parameters, especially the initial slip-load and gain factors. The first parameter has a direct influence in the delayed activation of the friction connections, whereas the gain factors make the control forces proportional to the structural response. In addition to shifting the frequencies of the bare frame due to activation/locking of the friction connections (similar to passive systems), the mechanism of semiactive systems is also governed by a combination of (i) initial increase of structural stiffness (due to delayed activation of the connections), which avoids deformations at early stages of the seismic response, and (ii) the increase of structural damping (due to slippage in the connections) in the later stages of response.

11.3 Recommendations for future work

The results obtained in this research demonstrated some of the limitations of existing passive and semiactive control systems, especially in terms of limited adaptability, the former systems, and inappropriate control forces, the latter. This research also demonstrated that the two new semiactive control systems, i.e. TδVG and AδVG, overcome some of the limitations of the existing control systems, and are, thus, a viable alternative for structural control. However, the performance of the control systems was investigated under a series of modelling assumptions. It would be interesting, in a future work, to investigate such performance using refined structural models, which included the following:

- Non-linearity in the columns, which would constitute another hysteretic mechanism for dissipation of seismic energy, but it would also reduce the stiffness (and the restoring forces) of the frame structure.

- A refined hysteretic model of both beams and columns, which included non-linearities due to shear deformation and also degradation of stiffness.

- A non-linear behaviour of the braces, including failures due to axial load and buckling.

Since refined hysteretic models of the structures could be used, it would also be interesting to check the actual available ductility and the ductility demand. In the present investigation, it was assumed that the beam elements supplied sufficient ductility, regardless of the magnitude of the inelastic rotations. The effectiveness of the control systems in high-rise buildings would be another aspect for further investigation.

Regarding the control system, possible future work may include investigation of optimal control configurations (e.g. locations and capacity of the friction dampers). Further work could also include simulation of cases with failure of one or more autonomous controllers (which would result in a hybrid passive-semiactive system), and its effect on the control performance.

Furthermore, as a recommendation for future work, experimental investigation would validate the results obtained from analytical models, either from this research or those obtained using the recommendations previously mentioned. Experimental testing would require development of a control device prototype and would allow to investigate different aspects of the control, such as effect of delays in the control signals and in the generation of required control forces.

Appendix A

ConStruc© v1.0: User Guide

The computer program *ConStruc* v1.0 developed as part of this research does not include a graphical user interface. In order to perform static or dynamic simulations, the data must be declared in three different input files, containing information for definition of the frame model and type of analysis, the parameters for seismic time-history analysis, and the seismic input, respectively.

The data in each of these three files ("inputdata1-FR.m","inputdata2-EQ.m" and "inputEQ.m") must be declared inside data matrices, following a pre-defined order. The declaration of data is based on the format used by Drain-2DX (Prakash et al., 1993), although not as rigorous, in terms of spacing and precise positioning of the parameters in the input files.

A.1   Input file: "inputdata1-FR.m"

Geometry of the frame and assignment of sections and supports

TABLE A.1: Data matrix: **matNod**, for definition of nodes and their coordinates.

Parameter	Column	Comments
n_i	1	Consecutive numbering of the nodes in the frame. It is recommended that numbering starts lower to upper floors, left to right. Also, nodes corresponding to dampers **must** be numbered after all elements. One node per line, starting with number 1.
x_i	2	x-coordinate and y-coordinate of the node i, in global coordinate system (see Fig. 4.1 on page 38).
y_i	3	

TABLE A.2: Data matrix: **matSupp**, for support conditions.

Parameter	Column	Comments
n_i	1	Corresponding node number. One node per line. *Note:* This version of *ConStruc* only accepts supports at the base of the building, with fully restrained conditions in x, y and z (rotation).
rx_i	2	For each direction:
ry_i	3	1: For restrained condition.
rz_i	4	0: For unrestrained condition.

TABLE A.3: Data matrix: **matCol**, for definition of column elements.

Parameter	Column	Comments
Col_i	1	Consecutive numbering of columns. It is recommended to start with columns of lower to upper levels, left to right. One column per line.
$n_{i,i}$	2	Number of the i-th column's nodes i and j (see Fig. 4.1 on
$n_{j,i}$	3	page 38)
$Group$	4	For columns: 1
$Type$	5	For columns: 1 -Beam-column element (see Section 4.2.1 on page 38)
$CroSec$	6	Number of the corresponding cross-section (see also Table A.7)
$Y_{i,i}$	7	Number of the corresponding yield surface of nodes i and j.
$Y_{j,i}$	8	**Note:** For columns= 0.
βeta	9	Rayleigh β coefficient for modelling of inherent viscous damping (see Section 4.2.4 on page 43)

TABLE A.4: Data matrix: **matBeam**, for definition of beam elements.

Parameter	Column	Comments
$Beam_i$	1	Consecutive numbering of the beams. It is recommended to start with beams of lower to upper levels, left to right. **Note:** The numbering must continue the sequence after columns numbering.
$n_{i,i}$	2	Number of the i-th beam's nodes i and j (see Fig. 4.1 on
$n_{j,i}$	3	page 38)
$Group$	4	For beams: 2
$Type$	5	For beams: 1 -Beam-column element (see Section 4.2.1 on page 38)
$CroSec$	6	Number of the corresponding cross-section (see also Table A.7)
$Y_{i,i}$	7	Number of the corresponding yield surface of nodes i and j
$Y_{j,i}$	8	(see also Table A.8)
βeta	9	Rayleigh β coefficient for modelling of inherent viscous damping (see Section 4.2.4 on page 43)

TABLE A.5: Data matrix:**matBar**, for definition of bar elements.

Parameter	Column	Comments
Bar_i	1	Consecutive numbering of the bars. It is recommended to start with bars of lower to upper levels, left to right. **Note:** The numbering must continue the sequence after beams numbering.
$n_{i,i}$	2	Number of the i-th bar's nodes i and j (see Fig. 4.1 on page
$n_{j,i}$	3	38)
$Group$	4	For bars: 3
$Type$	5	For bars: 2 -Bar element (see Section 4.2.1 on page 38)
$CroSec$	6	Number of the corresponding cross-section (see also Table A.7)
$Y_{i,i}$	7	Number of the corresponding yield surface of nodes i and j.
$Y_{j,i}$	8	**Note:** For bars=0.
βeta	9	Rayleigh β coefficient for modelling of inherent viscous damping (see Section 4.2.4 on page 43)

TABLE A.6: Data matrix: **matDamper**, for definition of friction damper elements.

Parameter	Column	Comments
$Damper_i$	1	Consecutive numbering of the dampers. It is recommended to start with dampers of lower to upper levels, left to right. One damper per line, starting with number 1.
$n_{i,i}$	2	Number of the i-th damper's nodes i and j (see Fig. 4.1 on
$n_{j,i}$	3	page 38)
$Type$	4	For dampers: 4 -Zero length element (see Section 4.2.1 on page 38)
Ys_i	5	Number of the corresponding damper's capacity (see also Table A.9)
βeta	6	Viscous damping coefficient. **Note:** For friction dampers=0.
Dir	7	Direction of the damper mechanism (1-for axial direction; 2-for transversal direction). **Note:** For the friction dampers=1.

Definition of mechanical properties and loading conditions

TABLE A.7: Data matrix: **matProp**, for description of mechanical properties.

Parameter	Column	Comments
$CroSec_i$	1	Consecutive numbering of the cross-sections.
$Asect$	2	Area
$Esect$	3	Modulus of elasticity
$\kappa appa$	4	Ratio of post-yield to initial stiffness of beams (see Section 4.2.1 on page 38)

TABLE A.8: Data matrix: **matYield2**, for description of beams' yield surfaces.

Parameter	Column	Comments
Y_i	1	Consecutive numbering of the yield surface.
$Type$	2	Type of yield surface. **Note:** For beams=2 (bending moment only)
M_{y+}	3	Positive moment of resistance of the section
M_{y-}	4	Negative moment of resistance of the section

TABLE A.9: Data matrix: **matYield4**, for description of dampers' capacity.

Parameter	Column	Comments
Ys_i	1	Consecutive number of the damper's capacity.
k_d	2	Stiffness
$\kappa appa$	3	Ratio of post-yield to initial stiffness. **Note:** For friction dampers=0.
F_{y+}	4	Passive slip-load, in positive and reversal direction of mo-
F_{y-}	5	tion. **Note:** For SA control, F_{y+} and $F_{y-} = 0$.

TABLE A.10: Data matrix: **matLoad**, for description of external, static, nodal loads.

Parameter	Column	Comments
n_i	1	Initial node to be loaded.
n_j	2	Final node to be loaded.
f_x	3	Nodal load in x-direction.
f_y	4	Nodal load in y-direction.
m_z	5	Bending moment.
Δ_n	6	Nodal increment to generate nodes with same loading condi- tions, i.e. $n_i : \Delta_n : n_j$.

TABLE A.11: Data matrix: **matMass**, for generation of mass matrix.

Parameter	Column	Comments
n_i	1	Initial node to be assigned with mass.
n_j	2	Final node to be assigned with mass.
M_x	3	x-translational, y-translational and rotational masses.
M_y	4	**Note:** This version of *ConStruc* uses only x-translational
M_z	5	masses in the analysis.
Δ_n	6	Nodal increment to generate nodes with same mass, i.e. $n_i : \Delta_n : n_j$.
$\alpha lpha$	7	Rayleigh $\alpha lpha$ coefficient for modelling of inherent damping (see Section 4.2.4 on page 43).

Type of analysis

TABLE A.12: Data matrix: **AnlType**, for specification of analysis type.

Parameter	Column	Comments
$Option1$	1	1: For static analysis;
		2: For dynamic analysis.
$Option2$	2	1: For linear-elastic analysis;
		2: For non-linear analysis.
$Option3$	3	Control algorithm (see also Tables A.13 to A.17)
		0: No control
		1: Passive control
		81: Modulated homogeneous friction (MHF) control
		51: Linear boundary layer (LBL) control
		121: Smooth boundary layer (SBL) control
		85: Tri-D control
		61: TδVG control
		57: AδVG control

Control parameters for semiactive algorithms

The following information, corresponding to the control parameters required by each algorithm, must be declared in the data matrix **CSinput**. The number of columns in this matrix varies depending on the algorithm used.

TABLE A.13: Control parameters for MHF algorithm.

Parameter	Column	Comments
Ys_i	1	Consecutive number of damper's capacity.
μ	2	Friction coefficient.
$f_{s1,i}$	3	Initial and maximum slip-load. **Note:** For MHF=0.
$f_{s2,i}$	4	
g_i	5	Gain factor.
t_s	6	Sampling time.
$Rate$	7	Loading rate. **Note:** Not activated in *ConStruc* v1.0.

TABLE A.14: Control parameters for LBL and SBL algorithms.

Parameter	Column	Comments
Ys_i	1	Consecutive number of damper's capacity.
μ	2	Friction coefficient.
$f_{s1,i}$	3	Initial and maximum slip-load. **Note:** For LBL and SBL =
$f_{s2,i}$	4	0.
g_i	5	Gain factor.
t_s	6	Sampling time.
$\lambda ambda$	7	*Thickness* of boundary layer.
$Rate$	8	Loading rate. **Note:** Not activated in *ConStruc* v1.0.

TABLE A.15: Control parameters for Tri-D algorithm.

Parameter	Column	Comments
Ys_i	1	Consecutive number of damper capacity.
μ	2	Friction coefficient.
e	3	Gain factor e.
f_f	4	First frequency of the frame [Hz].
$f_{p,i}$	5	Pre-defined passive slip-load.
$f_{s2,i}$	6	Maximum slip-load. **Note:** For Tri-D = 0.
t_s	7	Sampling time.

TABLE A.16: Control parameters for TδVG algorithm.

Parameter	Column	Comments
Ys_i	1	Consecutive number of damper capacity.
μ	2	Friction coefficient.
d_{min}	3	Lower limit of deformation.
d_{max}	4	Upper limit of deformation.
$f_{s1,i}$	5	Initial (minimum) slip-load.
$f_{s2,i}$	6	Maximum slip-load.
t_s	7	Sampling time.

TABLE A.17: Control parameters for AδVG algorithm.

Parameter	Column	Comments
Ys_i	1	Consecutive number of damper capacity.
μ	2	Friction coefficient.
$f_{s1,i}$	3	Initial slip-load.
$f_{s2,i}$	4	Maximum slip-load.
$f_{s3,i}$	5	Minimum slip-load.
Δt	6	Interval of decision [s].
Blank	7	0.
Blank	8	0.
t_s	9	Sampling time, [s].
$Rate$	10	Loading rate and trigger deformation. **Note:** Not activated
d_{min}	11	in *ConStruc* v1.0.

Output

The software automatically produces a plot of the frame's *wire view*, showing its general dimensions. In this *wire view*, the plastic hinges (if any) at the ends of the beams are also showed, with size allocated proportionally to the amount of energy dissipated.

In addition to this, the software also gives the option to plot other results, as described in the following tables:

TABLE A.18: Data matrix: **disPlot**, for nodal displacements.

Parameter	Column	Comments
n_i	1	Initial node to be plotted.
n_j	2	Final node to be plotted.
Δ_n	3	Nodal increment to generate nodes, i.e. $n_i : \Delta_n : n_j$.
key	4	100: to plot x-translations, y-translations and z-rotations.

TABLE A.19: Data matrix: **levdefoPlot**, for inter-storey deformations.

Parameter	Column	Comments
		Only 2 lines of data:
		Line 1: Upper floor nodes.
		Line 2: Lower floor nodes.
n_i	1	Initial node.
n_j	2	Final node.
Δ_n	3	Nodal increment to generate nodes, i.e. $n_i : \Delta_n : n_j$.

TABLE A.20: Data matrix: **forcePlot**, for beam-column element forces.

Parameter	Column	Comments
E_i	1	Initial element.
E_j	2	Final element.
Δ_E	3	Increment to generate elements, i.e. $E_i : \Delta_E : E_j$.

TABLE A.21: Data matrix: **barraPlot**, for bar element forces.

Parameter	Column	Comments
B_i	1	Initial bar element.
B_j	2	Final bar element.
Δ_B	3	Increment to generate elements, i.e. $B_i : \Delta_B : B_j$.

TABLE A.22: Data matrix: **damPlot**, for damper action ($f - \delta$ curve, history of control force, deformation, acting force and activation).

Parameter	Column	Comments
D_i	1	Initial damper element.
D_j	2	Final damper element.
Δ_D	3	Increment to generate damper elements, i.e. $D_i : \Delta_D : D_j$.

TABLE A.23: Data matrix: **bshPlot**, for shear forces.

Parameter	Column	Comments
		One line per storey. Order must be lower to top storey.
C_i	1	Initial column in the storey.
C_j	2	Final column in the storey.
Δ_C	3	Increment to generate columns, i.e. $C_i : \Delta_C : C_j$.
B_i	4	Initial and final brace in the storey. **Note:** 0, if there are
B_j	5	no braces.
Δ_B	6	Increment to generate bars, i.e. $B_i : \Delta_B : B_j$.

TABLE A.24: Data matrix: **axlPlot**, for axial force on columns.

Parameter	Column	Comments
		One line per storey. Order must be lower to top storey.
C_i	1	Initial column in the storey.
C_j	2	Final column in the storey.
Δ_C	3	Increment to generate columns, i.e. $C_i : \Delta_C : C_j$.

A.2   Input file: "inputdata2-EQ.m"

Parameters for time-history analysis

TABLE A.25: Data matrix: **parameters**.

Parameter	Column	Comments
$A_{g,0}$	1	Initial acceleration=0.
t_1	2	Initial time of simulation.
t_2	3	Final time of simulation.
dt	4	Time step for analysis. **Note:** inT/dt **must** be an integer (see also Table A.26).
Blank	5	0

TABLE A.26: Data matrix: **accelParam**, for definition of ground acceleration parameters.

Parameter	Column	Comments
$Form$	1	Format of the acceleration input: (see also Section A.3) 1: For data in rows. 2: For data in columns.
$tSca$	2	Time scale factor. **Note:** In this version of *ConStruc*= 1.0.
$aSca$	3	Acceleration scale factor.
inT	4	Sampling time of acceleration data (see also Table A.25).
stT	5	Initial time of acceleration data.

A.3   Input file: "inputEQ.m"

The third input file contains the ground acceleration data. Such data must be declared in the data matrix **EQinput** (acceleration only), arranged either in rows or in columns.

Appendix B

# Selected examples of verification of non-linear simulations

The computer program for non-linear simulations developed as part of this research was verified by comparing the results of several structures under different earthquakes. For the comparisons, the seismic response of the frames was also simulated using Drain-2DX, a popular academic software developed in the early 1990s (Allahabadi and Powell, 1988; Prakash et al., 1993).

The simulations were performed in the two computer programs using similar parameters, including a time step dt of 0.005s. Non-linearity was included in beams and/or dampers only. In order to simulate elastic response of columns and bars in Drain-2DX, high values of the resistance were specified in the models.

One feature of Drain-2DX is the ability to reduce the degrees of freedom at the inter-storey level by slaving secondary nodes to a master node. This option, however, was deactivated because there is not matrix condensation (i.e. reduction of degrees of freedom) in *ConStruc*. Another difference between the two programs is the use of overshoot factors for earlier yielding of elements in Drain-2DX, which aims at speeding up the analysis. Since *ConStruc* does not have that option, a small overshoot factor of 0.01 was used in Drain-2DX.
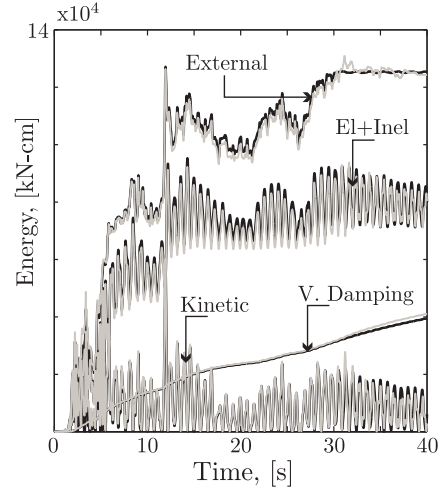
B.1   Low-rise steel frame

The response of the low-rise steel frame (Chapter 5) was simulated using El Centro 1940 with a PGA of 0.55g, Kobe 1995 with a PGA of 0.82g, and Taft 1952 with PGA of 0.55g.
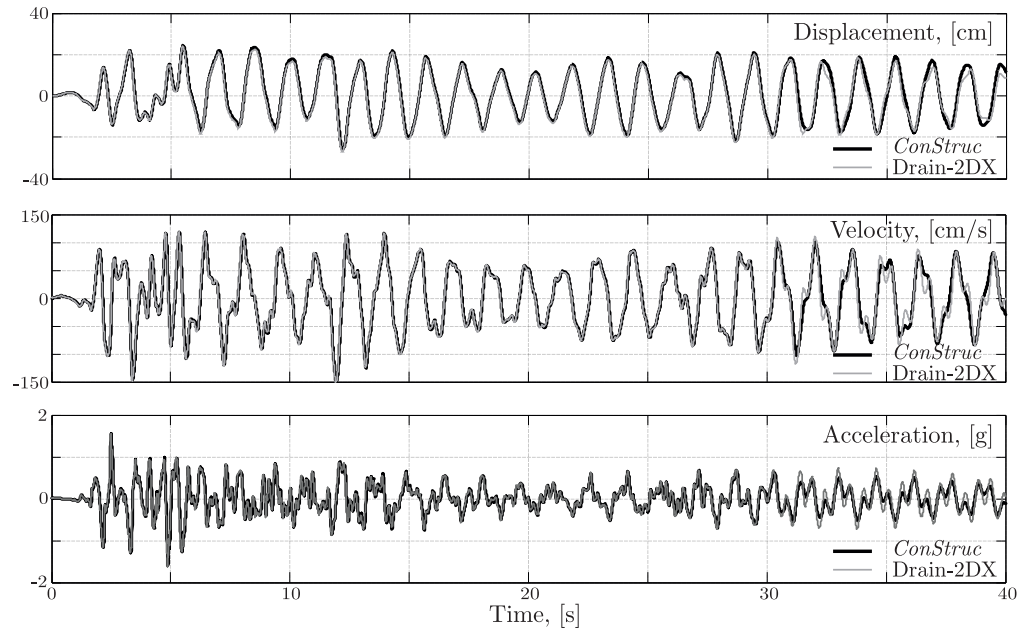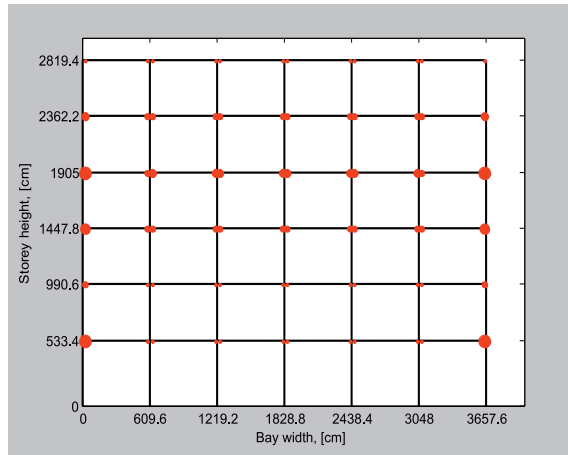
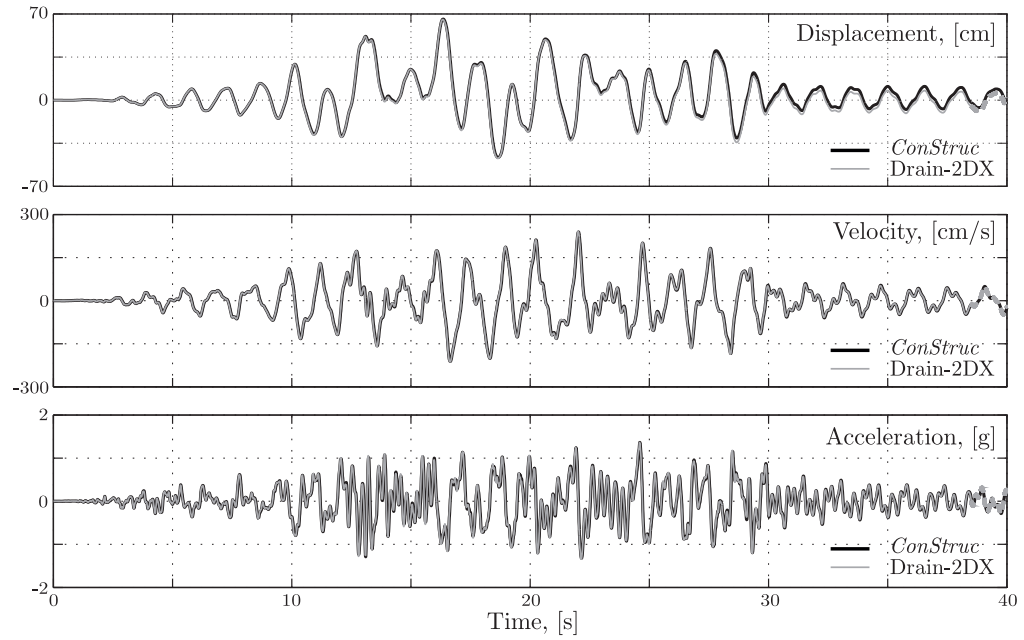a) Time history of bare frame's top floor's response (El Centro)
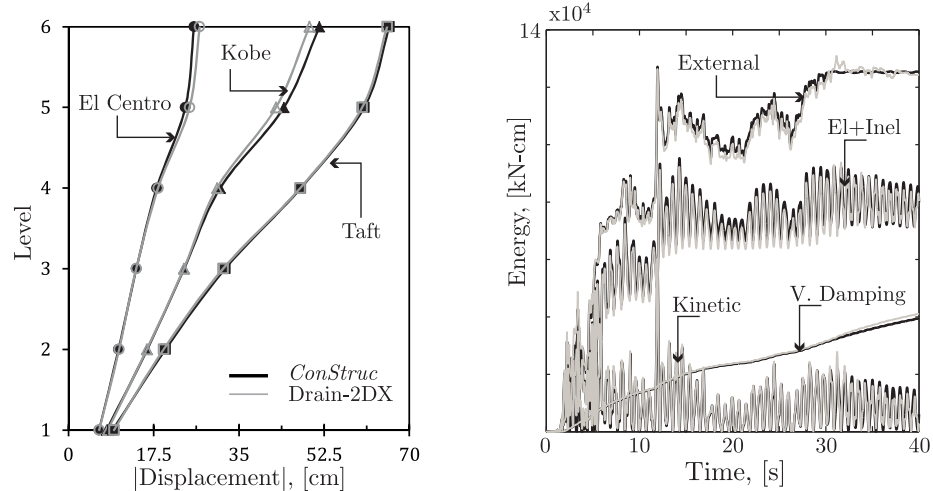
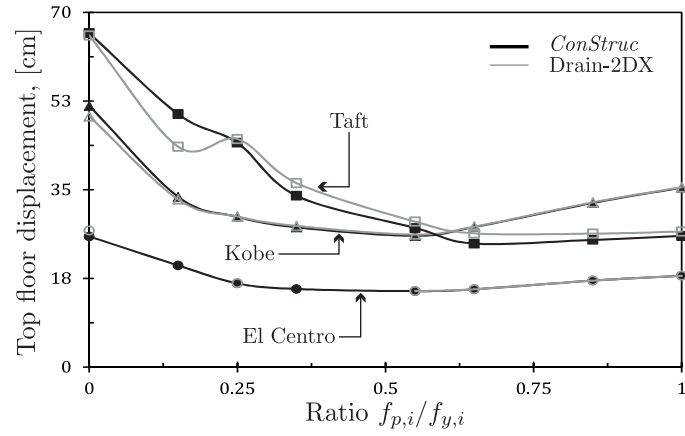b) Envelope of bare frames's displacement

c) Seismic Energy (El Centro)

d) Wire-view of bare frame under El Centro, using *ConStruc*

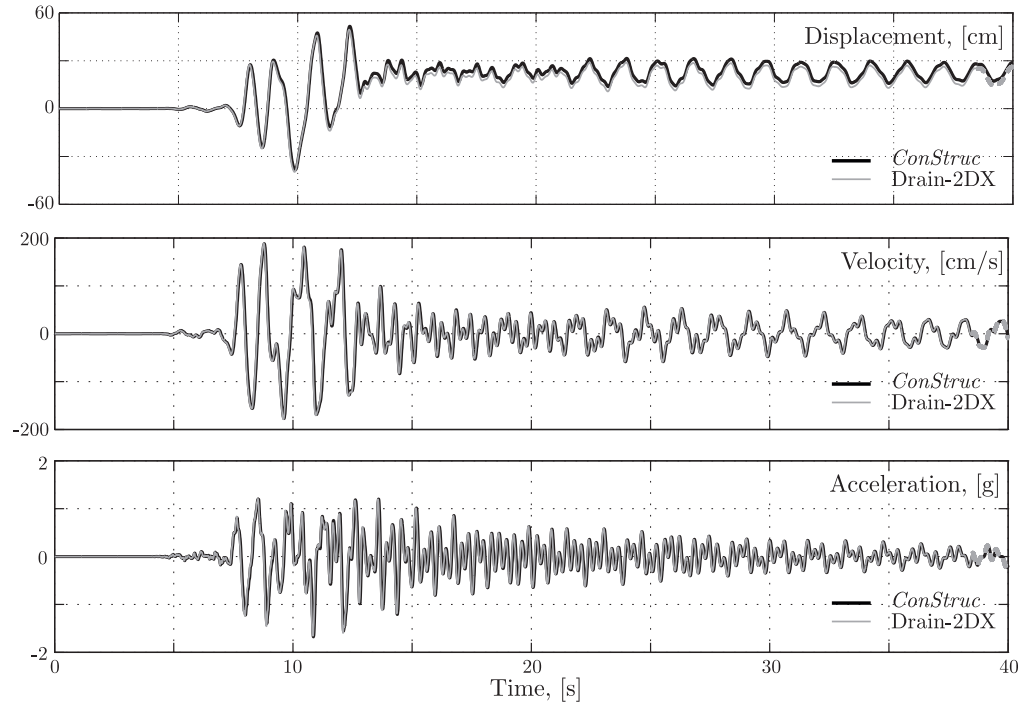FIGURE B.1: Seismic response of low-rise frame, using *ConStruc* and Drain-2DX.

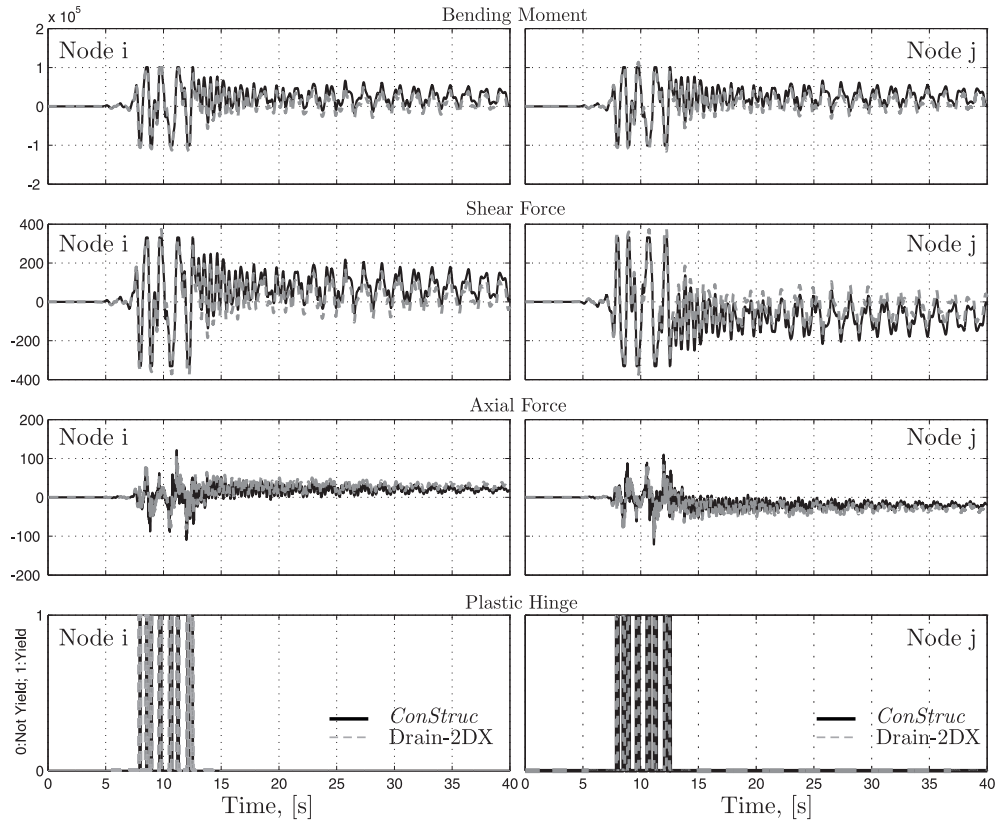a) Time history of bare frame's top floor's response (Taft)

b) Maximum top floor displacement of frame with passive control

c) Wire-view of frame with passive control, $(f_{p,i}/f_{y,i} = 0.35)$ under Taft, using *ConStruc*
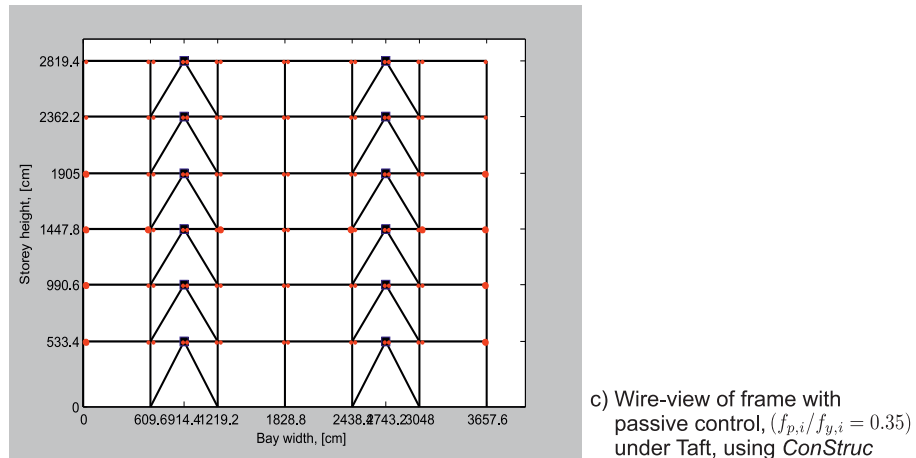
FIGURE B.2: Seismic response of low-rise steel frame with passive control, using *ConStruc* and Drain-2DX.

a) Time history of bare frame's top floor's response (Kobe)

b) Time history of forces and plastic hinges in bare frame's beam element (Kobe)

FIGURE B.3: Seismic response of low-rise frame, using *ConStruc* and Drain-2DX.

B.2 Medium-rise steel frame

a) Time history of bare frame's top floor's response (Northridge)

b) Envelope of bare frame's displacement

c) Seismic Energy (Northridge)

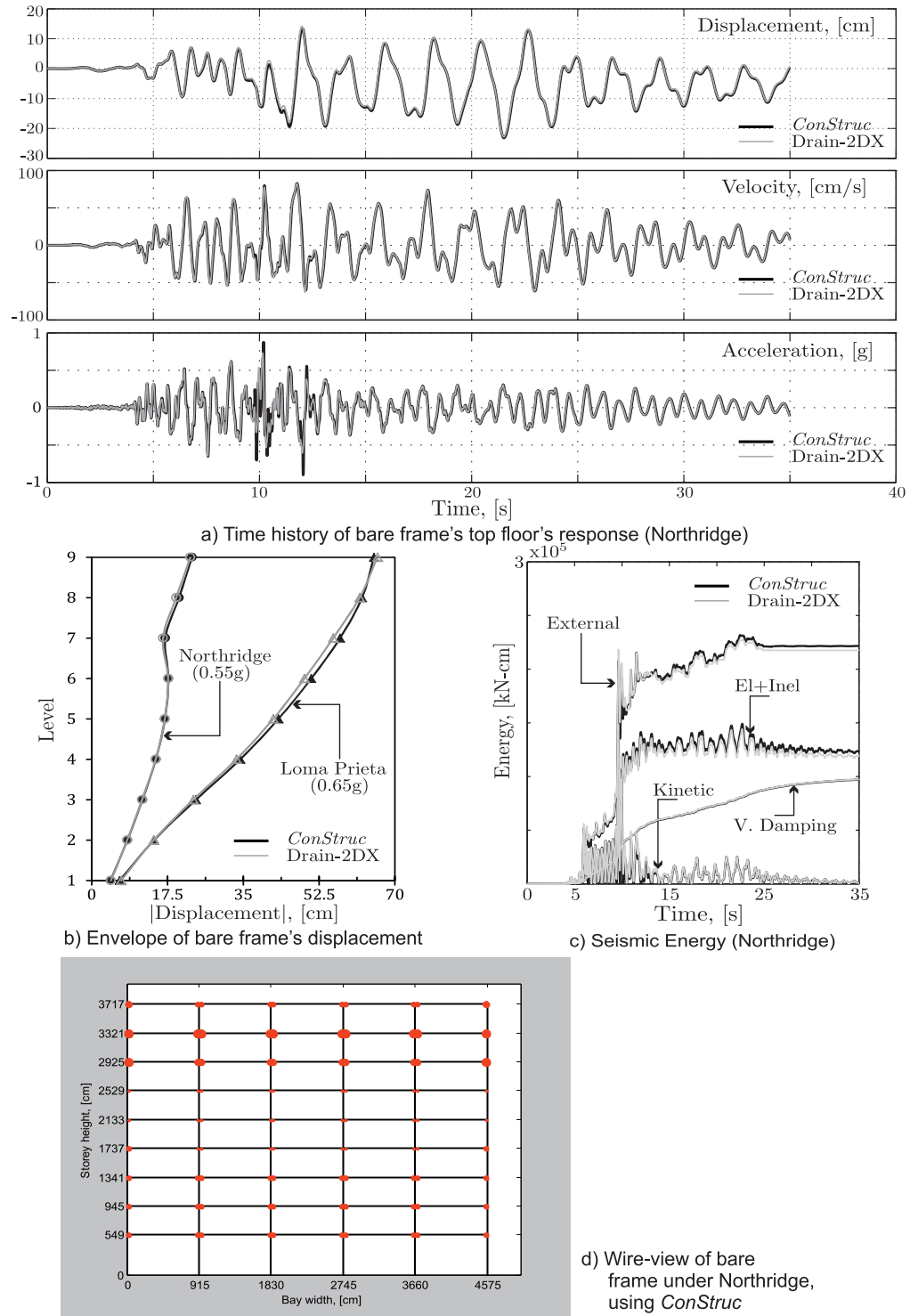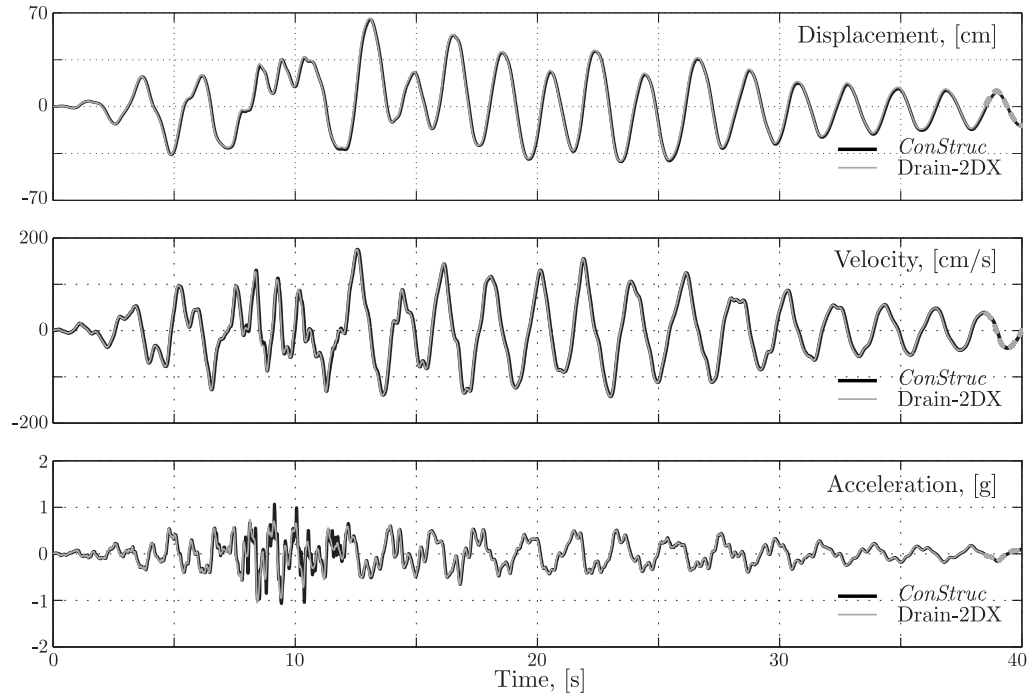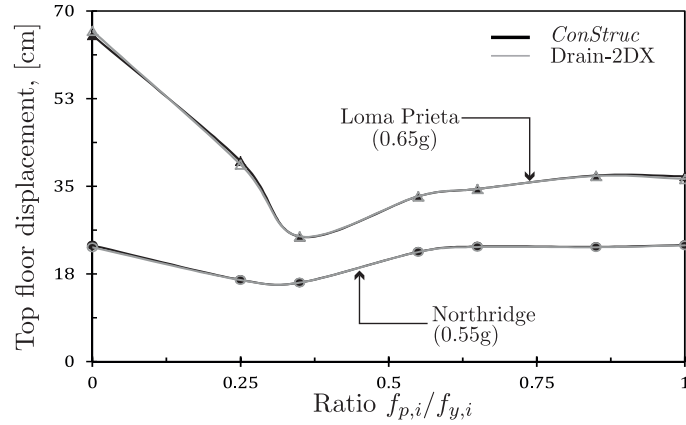d) Wire-view of bare frame under Northridge, using *ConStruc*

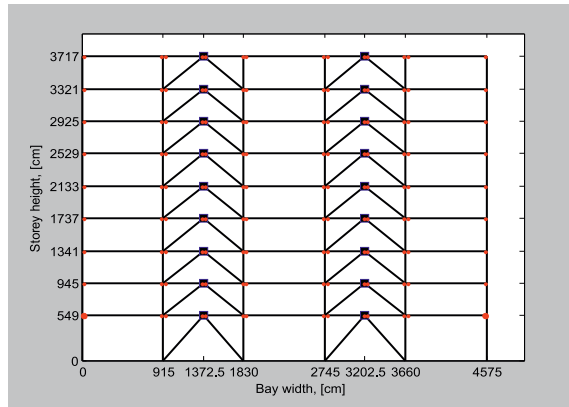FIGURE B.4: Seismic response of medium-rise frame, using *ConStruc* and Drain-2DX.

a) Time history of bare frame's top floor's response (Loma Prieta)

b) Maximum top floor displacement of frame with passive control

c) Wire-view of frame with passive control ($f_{p,i}/f_{y,i} = 0.35$) under Loma Prieta, using *ConStruc*

FIGURE B.5: Seismic response of medium-rise frame with passive control, using *ConStruc* and Drain-2DX.

B.3   Low-rise RC frame

a) Time history of bare frame's top floor's response (Loma Prieta)

b) Envelope of bare frames's displacement

c) Seismic Energy (Loma Prieta)

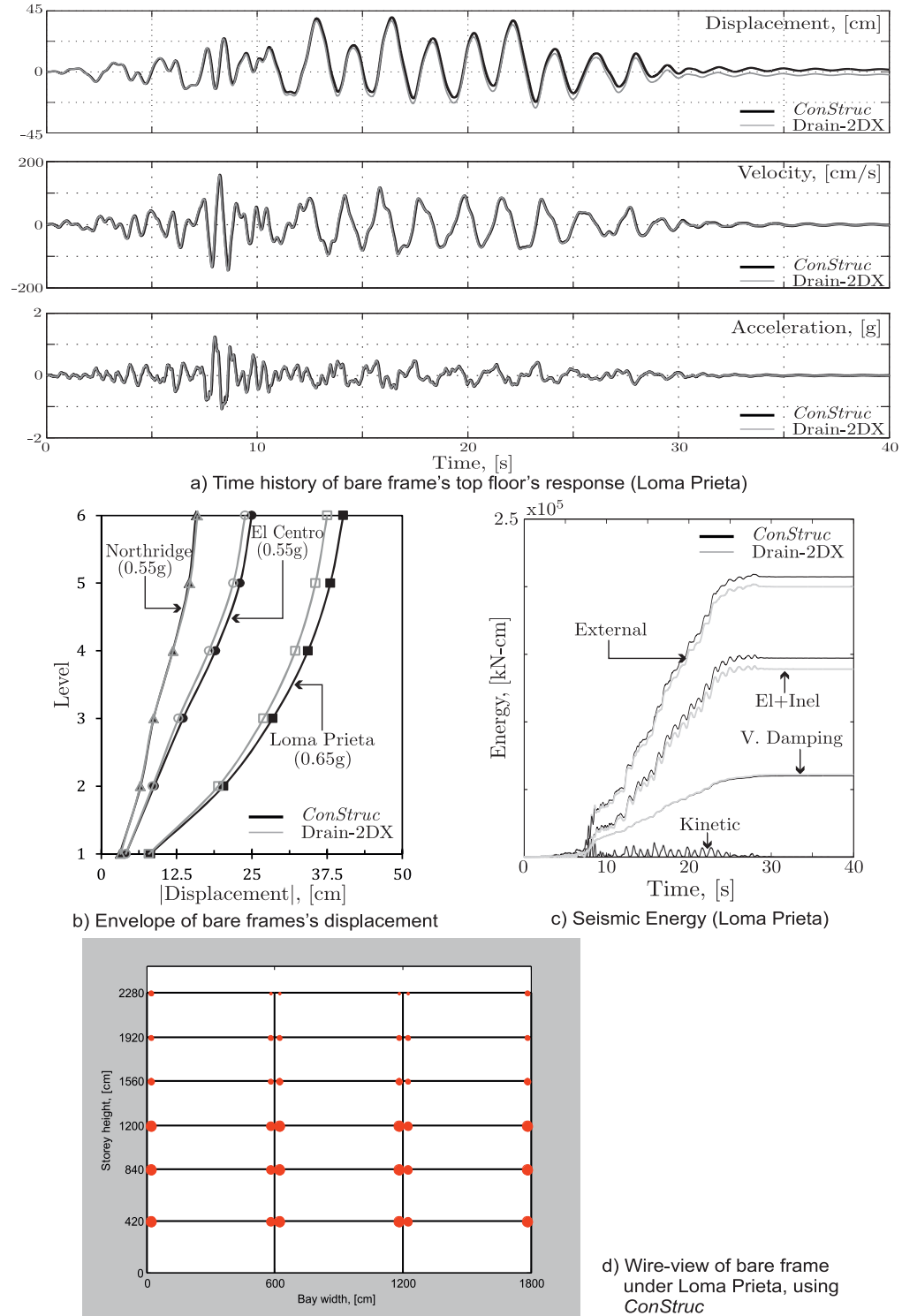d) Wire-view of bare frame under Loma Prieta, using *ConStruc*

FIGURE B.6: Seismic response of low-rise frame, using *ConStruc* and Drain-2DX.

a) Time history of controlled frame with $f_{p,i}/f_{y,i} = 0.35$ (Loma Prieta)

b) Maximum top floor displacement of frame with passive control

c) Distribution of energy in frame with passive control, $(f_{p,i}/f_{y,i} = 0.35)$ under Loma Prieta

FIGURE B.7: Seismic response of low-rise RC frame with passive control, using *ConStruc* and Drain-2DX.

B.4 Medium-rise RC frame

a) Time history of bare frame's top floor's response (El Centro)

b) Envelope of bare frames's displacement

c) Seismic Energy (Kobe)

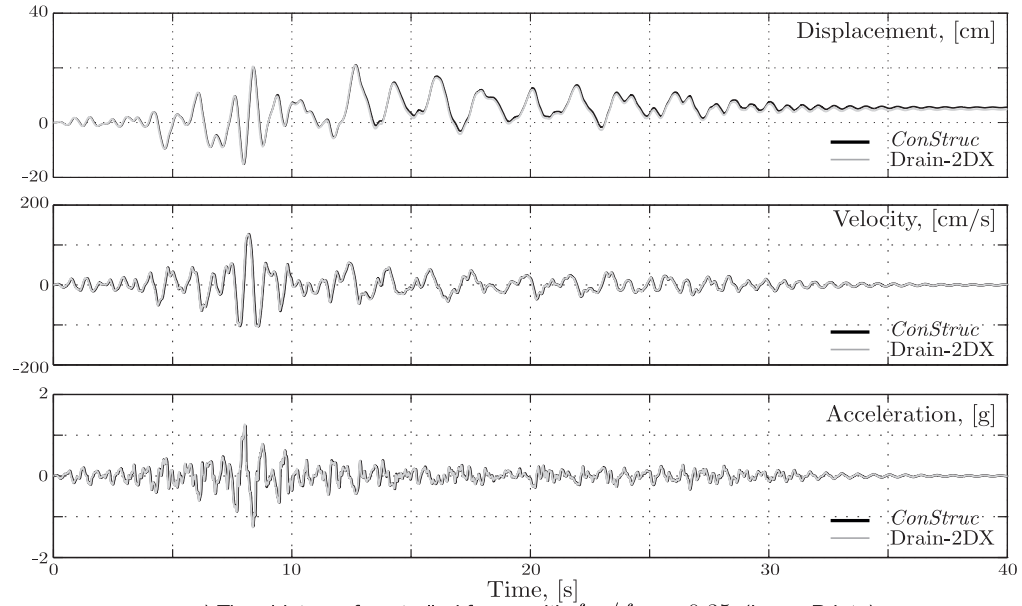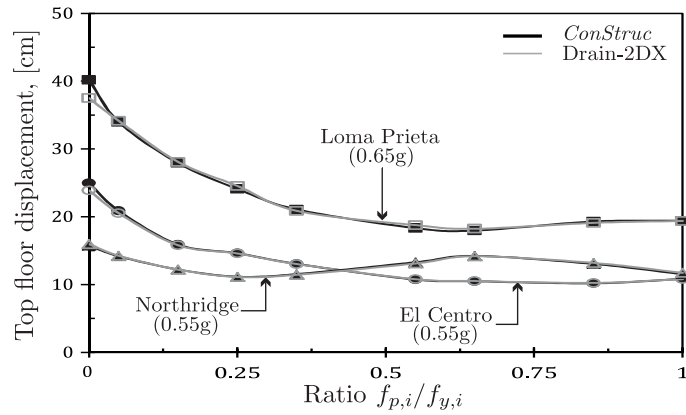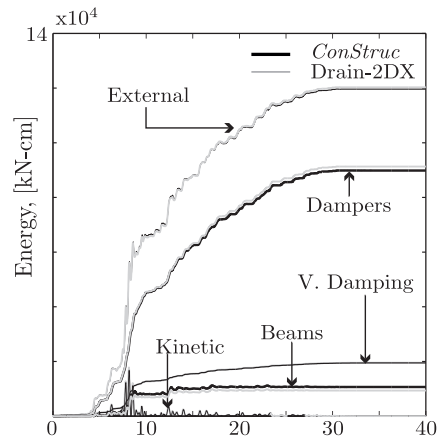d) Wire-view of bare frame under Kobe, using *ConStruc*
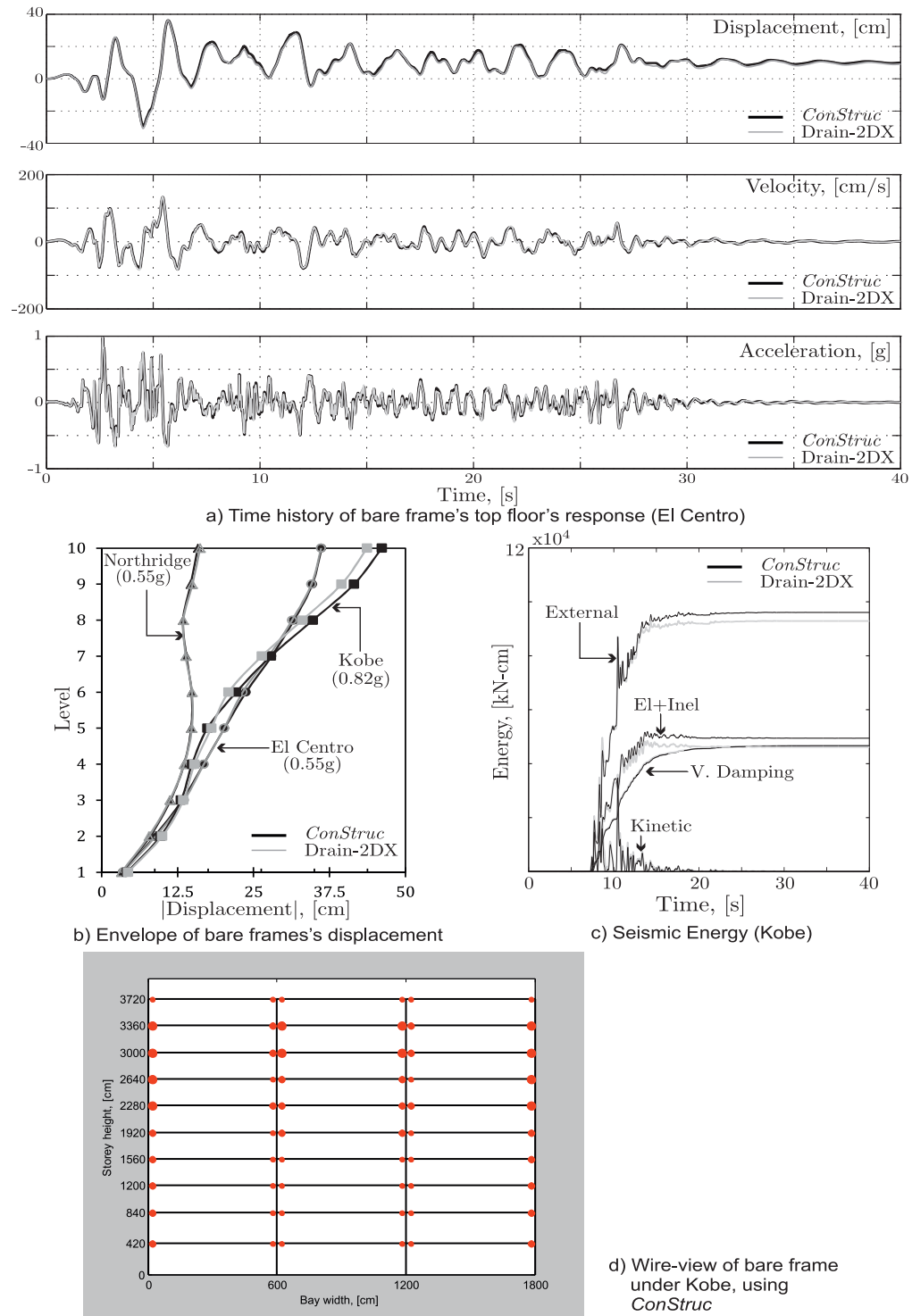
FIGURE B.8: Seismic response of medium-rise frame, using *ConStruc* and Drain-2DX.

a) Time history of controlled frame with $f_{p,i}/f_{y,i} = 0.05$ (Kobe)

b) Maximum top floor displacement of frame with passive control

c) Wire-view of frame with passive control, $(f_{p,i}/f_{y,i} = 0.05)$ under Kobe, using *ConStruc*

FIGURE B.9: Seismic response of medium-rise RC frame with passive control, using *ConStruc* and Drain-2DX.
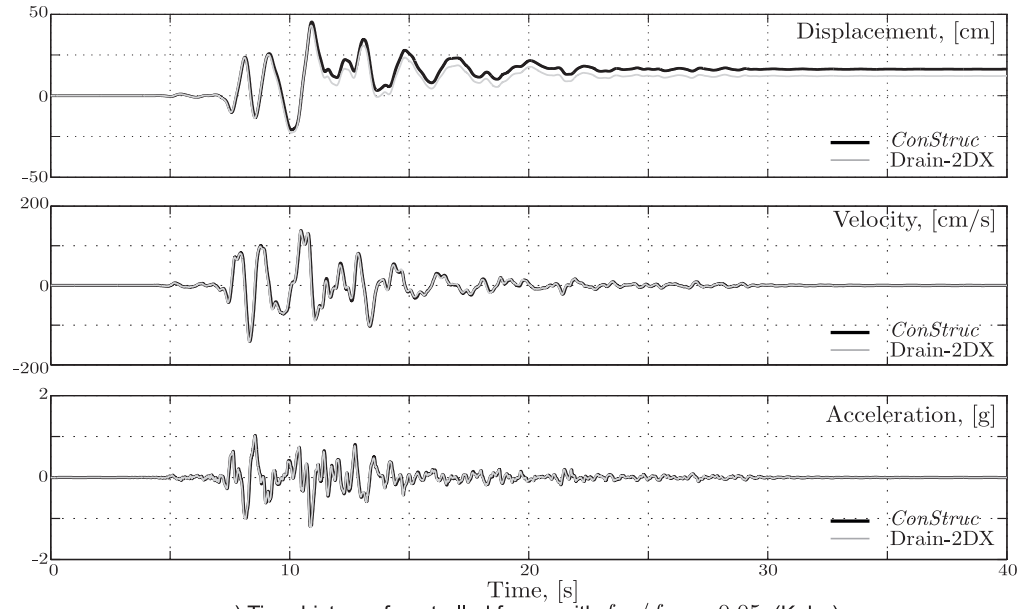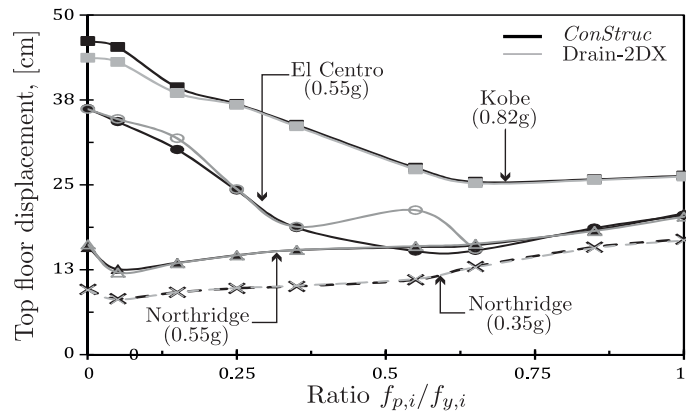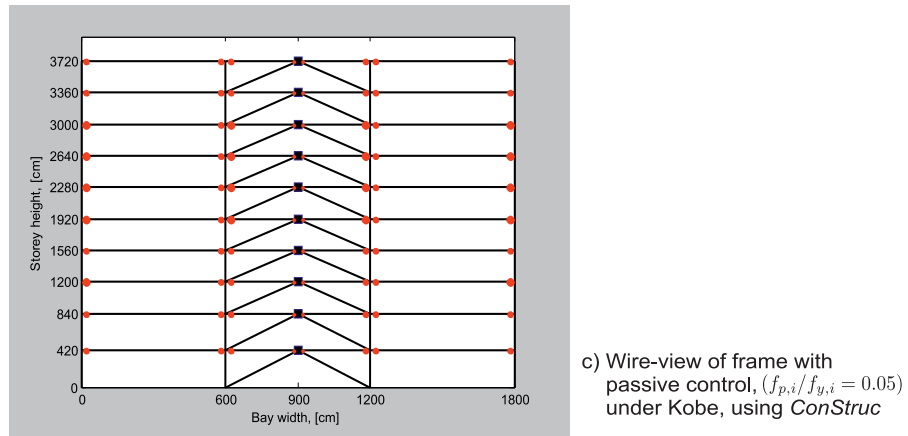
Bibliography

Agrawal, A. & J. Yang (1998). Design of passive dampers using active control theories. In S. C. Liu (Ed.), *Smart Systems for Bridges, Structures, and Highways*, Volume 3325 of *Proc. of SPIE - The International Society for Optical Engineering*, pp. 199–210.

Aiken, I. (1996). Passive energy dissipation -Hardware and applications. In *Los Angeles County and SEAOSC Symposium on Passive Energy Dissipation Systems for New and Existing Buildings*, Los Angeles, California.

Aiken, I., J. Kelly, & A. Pall (1988). Seismic response of a nine-story steel frame with friction damped cross-bracing. In *Ninth World Conference on Earthquake Engineering*, Tokyo and Kyoto, Japan.

Akbay, Z. & H. Aktan (1990). Intelligent energy dissipation devices. In *Proc. of the Fourth U.S. National Conference on Earthquake Engineering*, Volume 3, Palm Springs, California, pp. 427–435.

Allahabadi, R. & G. Powell (1988). *DRAIN-2DX user guide*, Volume 88. University of California, Earthquake Engineering Research Center, College of Engineering.

Apostolakis, G. & G. Dargush (2010). Optimal seismic design of moment-resisting steel frames with hysteretic passive devices. *Earthquake Engineering & Structural Dynamics 39*(4), 355–376.

Arfiadi, Y. & M. Hadi (2000). Passive and active control of three-dimensional buildings. *Earthquake Engineering & Structural Dynamics 29*(3), 377–396.

Aydin, E., M. Boduroglu, & D. Guney (2007). Optimal damper distribution for seismic rehabilitation of planar building structures. *Engineering Structures*.

Casciati, F., G. Magonette, & F. Marazzi (2006). *Technology of semiactive devices and applications in vibration mitigation*. Chichester, England: John Wiley and Sons.

Casciati, F., J. Rodellar, & U. Yildirim (2012). Active and semi-active control of structures -theory and applications: A review of recent advances. *Journal of Intelligent Material Systems and Structures 23*(11), 1181–1195.

Caudana, H. (2009). The mechanisms behind the optimum performance of systems for passive control of the seismic response of reinforced concrete frames. Masters dissertation, The University of Sheffield.

Caudana, H. & M. Petkovski (2013). Friction-based semiactive control of multi-storey frames. Paper presented at the 11th International Conference on Structural Safety and Reliability. Columbia University, New York.

Chandra, R., M. Masand, S. Nandi, C. Tripathi, R. Pall, & A. Pall (2000). Friction-dampers for seismic control of La Gardenia Towers South City, Gurgaon, India. In *12th World Conference on Earthquake Engineering*, Auckland, New Zealand.

Chen, C. & G. Chen (2001). A high efficiency control logic for semi-active friction dampers. In *Structures 2001: A structural engineering odyssey*, Washington, DC, pp. 1–11.

Chen, C. & G. Chen (2004a). Comparative study on semi-active control algorithms for piezoelectric friction dampers. In *Proc. of SPIE - The International Society for Optical Engineering*, Volume 5391, pp. 578–586.

Chen, C. & G. Chen (2004b). Shake table tests of a quarter-scale three-storey building model with piezoelectric friction dampers. *Structural Control and Health Monitoring 11*(4), 239–257.

Chen, G. & C. Chen (2000). Behavior of piezoelectric friction dampers under dynamic loading. In *Proc. of SPIE - The International Society for Optical Engineering*, Volume 3988, pp. 54–63.

Chen, G. & C. Chen (2004c). Semiactive control of the 20-story benchmark building with piezoelectric friction dampers. *Journal of Engineering Mechanics-Asce 130*(4), 393–400.

Cheng, F., H. Jiang, & K. Lou (2008). *Smart structures : innovative systems for seismic response control*. London: CRC Press.

Cherry, S. & A. Filiatrault (1993). Seismic response control of buildings using friction dampers. *Earthquake Spectra 9*(3), 447–466.

Cho, C. & M. Kwon (2004). Development and modeling of a frictional wall damper and its applications in reinforced concrete frame structures. *Earthquake Engineering & Structural Dynamics 33*(7), 821–838.

Chopra, A. (1995). *Dynamics of structures: theory and applications to earthquake engineering*. Upper Saddle River, NJ: Prentice-Hall.

Ciampi, V., M. De Angelis, & F. Paolacci (1995). Design of yielding or friction-based dissipative bracings for seismic protection of buildings. *Engineering Structures 17*(5), 381–391.

Clough, R. & J. Penzien (2003). *Dynamics of structures* (3rd edition ed.). Berkeley: Computers and Structures, Inc.

Constantinou, M., T. Soong, & G. Dargush (1998). *Passive energy dissipation systems for structural design and retrofit.* MCEER Monograph Series No. 1. Buffalo, N.Y.: MCEER.

Datta, T. (2003). A state-of-the-art review on active control of structures. *ISET Journal of Earthquake Technology 40*(1), 1–17.

Dowdell, D. & S. Cherry (1996). On passive and semi-active friction damping for seismic response control of structures, Paper No. 957. In *Proc. Eleventh World Conference on Earthquake Engineering*, UK. Elsevier Science Ltd.

Durmaz, O., W. Clark, D. Bennett, J. Paine, & M. Samuelson (2002). Experimental and analytical studies of a novel semi-active piezoelectric coulomb damper. In G. S. Agnes (Ed.), *Smart Structures and Materials 2002: Damping and Isolation*, Volume 4697 of *Proc of SPIE - The International Society for Optical Engineering*, pp. 258–273.

Dyke, S., B. Spencer Jr, P. Quast, & M. Sain (1995). Role of control-structure interaction in protective system design. *Journal of Engineering Mechanics 121*(2), 322–338.

European Committee for Standardization (1992). *Eurocode 2: Design of concrete structures, Part 1-1: General rules and rules for buildings, BS EN1992-1-1:2004.*

European Committee for Standardization (1998). *Eurocode 8: Design of structures for earthquake resistance, Part 1: General rules, seismic actions and rules for buildings, BS EN1998-1:2004.*

Filiatrault, A. & S. Cherry (1987). Performance evaluation of friction damped braced steel frames under simulated earthquake loads. *Earthquake Spectra 3*(1), 57–78.

Filiatrault, A. & S. Cherry (1990). Seismic design spectra for friction damped structures. *Journal of Structural Engineering 116*(5), 1334–1355.

FitzGerald, T., T. Anagnos, M. Goodson, & T. Zsutty (1989). Slotted bolted connections in aseismic design for concentrically braced connections. *Earthquake Spectra 5*(2), 383–391.

Grigorian, C., T. Yang, & E. Popov (1993). Slotted bolted connection energy dissipators. *Earthquake Spectra 9*(3), 491–504.

He, W., A. Agrawal, & J. Yang (2003). Novel semiactive friction controller for linear structures against earthquakes. *Journal of Structural Engineering 129*(7), 941–950.

Housner, G., L. Bergman, T. Caughey, A. Chassiakos, R. Claus, S. Masri, R. Skelton, T. Soong, B. Spencer, & J. Yao (1997). Structural control: past, present, and future. *Journal of Engineering Mechanics-Asce 123*(9), 897–971.

Ikeda, Y. (2009). Active and semi-active vibration control of buildings in Japan -practical applications and verification. *Structural Control and Health Monitoring 16*(7-8), 703–723.

Inaudi, J. (1997). Modulated homogeneous friction: A semi-active damping strategy. *Earthquake Engineering & Structural Dynamics 26*(3), 361–376.

Jansen, L. & S. Dyke (2000). Semiactive control strategies for MR dampers: Comparative study. *Journal of Engineering Mechanics -ASCE 126*(8), 795–803.

Kannan, S., H. Uras, & H. Aktan (1995). Active control of building seismic response by energy dissipation. *Earthquake Engineering & Structural Dynamics 24*(5), 747–759.

Kobori, T. (1996). Future direction on research and development of seismic-response-controlled structures. *Microcomputers in Civil Engineering 11*(5), 297–304.

Kobori, T., N. Koshika, K. Yamada, & Y. Ikeda (1991). Seismic-response-controlled structure with active mass driver system. Part 1: Design. *Earthquake Engineering & Structural Dynamics 20*(2), 133–149.

Kobori, T., M. Takahashi, T. Nasu, N. Niwa, & K. Ogasawara (1993). Seismic response controlled structure with active variable stiffness system. *Earthquake Engineering & Structural Dynamics 22*(11), 925–941.

Laflamme, S., D. Taylor, A. M, & J. Connor (2012). Modified friction device for control of large-scale systems. *Structural Control and Health Monitoring 19*(4), 548–564.

Lin, C., G. Lin, & J. Wang (2010). Protection of seismic structures using semi-active friction TMD. *Earthquake Engineering & Structural Dynamics 39*(6), 635–659.

Lin, G., C. Lin, L. Lu, & Y. Ho (2012). Experimental verification of seismic vibration control using a semi-active friction tuned mass damper. *Earthquake Engineering & Structural Dynamics 41*(4), 813–830.

Lynch, J. & K. Law (2002). Decentralized control techniques for large-scale civil structural systems. In *Proc of the 20th International Modal Analysis Conference (IMAC XX)*, Los Angeles, California. Society of Photo-Optical Instrumentation Engineers.

Martelli, A. & M. Forni (2008). State of the art of the development and application of anti-seismic systems in Europe and other countries. *AIP Conference Proceedings 1020*(1), 1272–1293.

Martinez-Romero, E. (1993). Experiences on the use of supplementary energy dissipators on building structures. *Earthquake Spectra 9*(3), 581–625.

Martinez-Rueda, J. E. (2002). On the evolution of energy dissipation devices for seismic design. *Earthquake Spectra 18*(2), 309–346.

Martinez-Rueda, J. E. & A. S. Elnashai (1995). A novel technique for the retrofitting of reinforced concrete structures. *Engineering Structures 17*(5), 359–371.

Mazzolani, F. (2001). Passive control technologies for seismic-resistant buildings in Europe. *Progress in Structural Engineering and Materials 3*(3), 277–287.

Nagarajaiah, S. (2000). Structural vibration damper with continuously variable stiffness. U.S. Patent 6,098,969, 2000.

Nagarajaiah, S., S. Dyke, J. Lynch, A. Smyth, A. Agrawal, M. Symans, & E. Johnson (2008). Current directions of structural health monitoring and control in USA. *Advances in Science and Technology 56*, 277–286.

Ng, C. & Y. Xu (2007). Semi-active control of a building complex with variable friction dampers. *Engineering Structures 29*(6), 1209–1225.

Nishitani, A. & Y. Inoue (2001). Overview of the application of active/semiactive control to building structures in Japan. *Earthquake Engineering and Structural Dynamics 30*(11), 1565–1574.

Nishitani, A., Y. Nitta, & Y. Ikeda (2003). Semiactive structural-control based on variable slip-force level dampers. *Journal of Structural Engineering 129*(7), 933–940.

Nishitani, A., Y. Nitta, A. Itoh, & Y. Ikeda (2000). Semiactive variable-friction damper control with simple algorithm. In *Proc of The American Control Conference*, Chicago, Illinois, pp. 503–507.

Ohtori, Y., R. Christenson, B. Spencer, & S. Dyke (2004). Benchmark control problems for seismically excited nonlinear buildings. *Journal of Engineering Mechanics-ASCE 130*(4), 366–385.

Pall, A. & C. Marsh (1982). Response of friction damped braced frames. *Journal of Structural Division ASCE 108*(ST6), 1313–1323.

Pall, A. & R. Pall (2004). Performance-based design using Pall friction dampers -An economical design solution. In *Proc 13th World Conference on Earthquake Engineering*, Vancouver, BC, Canada.

Parulekar, Y. & G. Reddy (2009). Passive response control systems for seismic response reduction: a state-of-the-art review. *International Journal of Structural Stability and Dynamics 9*(1), 151–177.

Pasquin, C., N. Leboeuf, & R. Pall (2002). Friction dampers for seismic rehabilitation of Eaton building, Montreal. In *Proc of the 4th Structural Specialty Conference of the Canadian Society for Civil Engineering*, Montreal, Canada.

Paz, M. (1997). *Structural dynamics: theory and computation* (4th ed.). Norwell, Massachussetts: Kluwer Academic Publishers.

PEER (2011). Pacific Earthquake Engineering Research Center, Strong Earthquake Database. http://peer.berkeley.edu/peer_ground_motion_database.

Prakash, V., G. Powell, & S. Campbell (1993). Drain-2DX: Base program description and user guide, Version 1.10. Technical Report UCB/SEMM-93/17, University of California.

Rai, N., G. Reddy, S. Ramanujam, V. Venkatraj, & P. Agrawal (2009). Seismic response control systems for structures. *Defence Science Journal 59*(3), 239–251.

Rao, R., P. Gergely, & R. White (1995). Retrofit of non-ductile reinforced concrete frames using friction dampers. Technical Report NCEER 95-0020, Cornell University.

Spencer, B. & S. Nagarajaiah (2003). State of the art of structural control. *Journal of Structural Engineering-Asce 129*(7), 845–856.

Spencer, B. & T. Soong (1999). New applications and development of active, semi-active and hybrid control techniques for seismic and non-seismic vibration in the usa. In *Proc of International Post-SMiRT Conference Seminar on Seismic Isolation, Passive Energy Dissipation and Active Control of Vibration of Structures*, Cheju, Korea.

Subbaraj, K. & M. Dokainish (1989). A survey of direct time-integration methods in computational structural dynamics II. Implicit methods. *Computers & Structures 32*(6), 1387–1401.

Symans, M., F. Charney, A. Whittaker, M. Constantinou, C. Kircher, M. Johnson, & R. McNamara (2008). Energy dissipation systems for seismic applications: Current practice and recent developments. *Journal of Structural Engineering, ASCE 134*(1), 3–21.

Symans, M. & M. Constantinou (1999). Semi-active control systems for seismic protection of structures: a state-of-the-art review. *Engineering Structures 21*(6), 469–487.

The MathWorks Inc. (2012). *Matlab version 7.14.0.739 (R2012a)*. Natick, Massachusetts: The MathWorks Inc.

Uang, C. & V. Bertero (1990). Evaluation of seismic energy in structures. *Earthquake Engineering & Structural Dynamics 19*(1), 77–90.

Unsal, M., C. Niezrecki, & C. Crane (2003). *A new semi-active piezoelectric-based friction damper*, Volume 5052 of *Proc of SPIE -The International Society for Optical Engineering*, pp. 413–420.

Xu, Y. & C. Ng (2008). Seismic protection of a building complex using variable friction damper: Experimental investigation. *Journal of Engineering Mechanics 134*(8), 637–649.

Xu, Y., W. Qu, & Z. Chen (2001). Control of wind-excited truss tower using semiactive friction damper. *Journal of Structural Engineering 127*(8), 861–868.

Yao, J. (1972). Concept of structural control. *Journal of Structural Division - ASCE 98*(ST7), 1567–1574.